NUMERICAL FLOW FIELD PREDICTION

FOR PROJECT RAM-C

By G. Widhopf, B. Kaplan and J. Jannone

Prepared for

National Aeronautics and Space Administration
Langley Research Center
Hampton, Virginia

NAS1-5519

Prepared by

General Applied Science Laboratories, Inc.
Merrick and Stewart Avenues
Westbury, L. I., New York

June 30, 1966

GASL TR-605

NASA CONTRACTOR REPORT NO. 66109

Total No. of Pages - xii & 145

Copy (81) of 110

NUMERICAL FLOW FIELD PREDICTION

FOR PROJECT RAM-C

By G. Widhopf, B. Kaplan and J. Jannone

Distribution of this report is provided
in the interest of information exchange.
Responsibility for the contents resides
in the author or organization that pre-
pared it.

Prepared for

National Aeronautics and Space Administration
Langley Research Center
Hampton, Virginia

NAS1-5519

Prepared by

General Applied Science Laboratories, Inc.
Merrick and Stewart Avenues
Westbury, L.I., New York

June 30, 1966

Approved by: _____
Antonio Ferri
President

TABLE OF CONTENTS

LIST OF TABLES

iii

LIST OF FIGURES

vi

x

NUMERICAL FLOW FIELD PREDICTION

FOR PROJECT RAM-C

By G. Widhopf, B. Kaplan, and J. Jannone

General Applied Science Laboratories, Inc.

SUMMARY

Detailed flow field calculations have been performed in order to investigate the state of the gas in the shock layer surrounding the RAM-C vehicle. Calculations were performed at altitudes of 36.8, 53.5, and 71 km. For numerical purposes the shock layer flow field was separated into an inviscid and viscous layer wherein the viscous-inviscid interaction was taken into account by a displacement thickness iteration procedure. A nonsimilar boundary layer approach was assumed to be applicable in the viscous region where edge conditions were computed by tracing non-equilibrium inviscid streamlines as they were entrained by the boundary layer. Finite rate chemistry was computed throughout the entire shock layer. Detailed plots of profiles of velocity, temperature, electron density, pressure, and species mole fractions are presented at various surface locations. The results indicate that this type of computational procedure is not valid for this configuration at the two higher altitudes.

INTRODUCTION

A series of flight experiments has been designed by the Langley Research Center in order to investigate the interference of the ionized flow field immediately surrounding a reentry vehicle with radio transmission, communications and tracking. The official designation of these flight experiments is Project Ram (Radio Attenuation Measurements). Utilizing these experiments, coupled with detailed computations, methods will be sought to eliminate the "blackout" phenomena. Also, assessments of theoretical analyses used in the prediction of flow field ionization and the associated RF signal loss will be possible, since in-flight experiments have been included to measure specific reentry observables.

Project RAM has been divided into specific flight experiments (RAM-A,B,C) where a spectrum of reentry flight conditions has been investigated. RAM-A,B have been concerned with a velocity regime of 18,000 ft/sec and below, where various measurements and experiments have been made.

The RAM-C series consists of flight experiments at a higher velocity regime ($\approx$ 25 kfps). Data from onboard sensors will be transmitted in real time and recorded onboard for playback after reentry. Tracking and telemetry data will be obtained throughout the flight. Experiments included in the RAM-C series are: onboard reflectometers, Langmuir probes, material addition schemes, thermocouples, multiple-frequency RF transmission systems and antenna measurements. The RAM-C vehicle has a payload of 200 pounds (see Fig. 1 for geometry) boosted to orbital reentry conditions by a four-stage Scout vehicle launched from Wallops Island, Virginia, in the direction of Bermuda. The reentry data period starts after the fourth stage separation at an attitude of about 350 kft and continues through the telemetry playback period which extends to below 50 kft. A beryllium heat sink nose cap will be used down to about 160 kft, then expelled, and ablation heat protection used for the remainder of reentry. A second payload using only ablation heat protection will also be tested. It is likely that Teflon will be the primary ablation material, with mass loss expected to initiate at 200 kft or below. The payload will be spin stabilized during reentry in an attempt to maintain a zero angle of attack attitude.

The purpose of the study reported herein is to provide a numerical evaluation of the state of the gas in the shock layer between the vehicle surface and the shock wave envelope extending from the nose region to the aft portion of the vehicle. This numerical investigation was carried out at the conditions specified in Table I.

Computation of the flow field about a blunted reentry vehicle of this type is a complex problem wherein the inviscid and viscous portions of the fluid field can interact to a high degree. Certain restricting assumptions must therefore be made to obtain a feasible line of approach toward a numerical solution.

Consideration must be given to the nature of the objectives to be realized. The primary objective of the RAM-C program is to determine electromagnetic-fluid dynamic interaction. Therefore the most important feature will be to determine the magnitude and spatial distribution of free-electron concentration in the flow field.

A few conditions have been outlined to define the minimum requirements needed and the general scope of the required numerical investigation. The gas in the complete shock layer flow is considered to be a multicomponent mixture of reacting air species in the continuum flow regime. Radiation is to be neglected as well as any angle of attack considerations. The surface of the vehicle is to be considered as nonablative and nonreactive, but is catalytic with respect to a non-equilibrium reacting boundary layer. The surface temperature is constant at a value of 1000°K while the flow near the surface is viscous as well as reacting. The boundary layer is to be considered a laminar region, where finite rate air chemistry, diffusion, viscosity and heat conduction effects are taken into account. Corrections should be made to account for momentum flux effects (displacement thickness) and for inviscid flow vorticity.

3

LIST OF SYMBOLS

C_p — specific heat at constant pressure, GM-CAL/GM^{o}K

$\mathcal{D}$ — specie diffusion term in energy equation

D_{ij} — specie diffusion coefficient, CM^2/sec

$\mathcal{E}^C$ — species diffusion term in energy equation

$\mathcal{E}^H$ — enthalpy diffusion term in energy equation

F — characteristic function in finite difference notation

h — static enthalpy, GM-CAL/GM

H — total enthalpy, GM-CAL/GM

K_R — surface recombination coefficient, cm/sec

k — thermal conductivity, GM-CAL/CM sec^{o}K; Boltzmann constant $= 1.38032 \times 10^{-23}$ joule ^{o}K^{-1}

L — body length, meters

m — finite difference mesh indicator

M — Mach number

n — finite difference mesh indicator

N_{e-} — electron density, particles/meter^3

p — pressure, Newtons/meter^2

Pr — Prandtl number

r — local body radius, meters

$R_{e_{L_\infty}}$ — free stream Reynolds number based on body length

R_N	nose radius, meters
Sc	Schmidt number
T	temperature, $^{\circ}$K
u	velocity component in x direction, meters/sec
v	velocity component in y direction, meters/sec
V_i	diffusion velocity at wall, meters/sec
$\dot{w}_i$	net rate of production of the ith specie, moles/cm^3 sec
X	surface coordinate, meters
Y	coordinate normal to surface, meters
α	mass fraction, $\alpha = \rho_i/\rho$
β	local bow shock angle, degrees
γ	ratio of specific heats $= c_p/c_v$
δ	nondimensional ratio $= (\gamma - 1)/(\gamma + 1)$, boundary layer thickness
ϵ	an index $\begin{cases} 0 - \text{two-dimensional flow} \\ 1 - \text{axisymmetric flow} \end{cases}$
$\zeta_{1,2}$	coordinates along and normal to body centerline
λ	Mach angle, degrees
μ	viscosity coefficient, GM/CM-sec
ν	kinematic viscosity; $\nu = \mu/\rho$, cm^2/sec
ρ	density, GM/CM^3
$\bar{\sigma}$	stability parameter for finite difference scheme
τ	shear stress, GM/CM sec^2; transformed coordinate $= 2\psi/Y^2$

$\bar{\chi}$ interaction parameter

ψ stream function, GM/sec

Subscripts

b   base

e   boundary layer edge

i i^{th} specie

sh   shock

w   wall

∞ free stream conditions

ANALYSIS

In the situation where the Reynolds number is high, viscous phenomena which occur in the flow field about a reentry vehicle could be assumed, for computational purposes, to be restricted to the boundary layer, enabling the inviscid and viscous portions of the flow field to be calculated independently. If in addition, the Prandtl* and Schmidt** numbers are on the order of one, a finite rate chemically reacting flow field can also be separated in this fashion.

Separation of a flow field into inviscid and viscous fields is dependent upon the condition that inviscid-viscous interactions can either be neglected or accounted for in a reasonable fashion. For conditions where neither of the above is true a shock layer approach is necessary, wherein the entire field is solved as a viscous region.

Viscous interaction effects can generally be accounted for by an iteration procedure (when the Reynolds number is high) whereby an apparent body is introduced to calculate the alteration of the inviscid flow due to the presence of the viscous layer. The apparent body utilized is the original body contour plus the local displacement thickness as calculated from the boundary layer flow. The entrainment of outer inviscid streamlines can be taken into account by the actual finite-rate-chemistry computation along these streamlines as they are "swallowed," and by the utilization of these computations to provide the variable boundary layer edge conditions needed to compute the viscous layer structure.

Due to the severe discontinuities in flow variables across the curved bow shock and the resulting associated high temperatures, ionization and dissociation phenomena are generally important in the entire shock layer flow. Chemical considerations are important in varying degrees in the inviscid region where streamlines have associated with them a relatively higher velocity and lower temperature (due to the decrease in curvature of the bow shock) than those swallowed in the viscous flow.

---

*Prandtl No. $\equiv$ Pr $\equiv$ $C_p \mu / k$ = viscous/thermal transports.

**Schmidt No. $\equiv$ Sc $\equiv$ $\mu / \rho D_{12}$ = viscous/diffusive transports.

Inviscid Field

The shock shape and the subsonic portion of the flow field is computed by solving the elliptic Euler equations utilizing the inverse method (Refs. 1-3). Here the body geometry in the nose region is specified, and an initial estimate of the bow shock shape is made by satisfying continuity conditions. Characteristic lines are then constructed in the transonic region (see Fig. 2) immediately downstream of the sonic line. The characteristic line which extends from the shock and terminates at the supersonic body point which is nearest to the sonic point, and subject to the condition that $\lambda \leq 1.0$, ($\lambda = \sin^{-1} \frac{1}{M}$), is chosen as a reference line. The subsonic portion of the flow field is then solved using the "inverse approach" where the governing equations in the transformed τ, y plane are (Ref. 3)

Continuity

$$\frac{\partial \psi}{\partial X} = -\frac{\rho}{\rho_\infty} \frac{vY}{u_\infty} \qquad \frac{\partial \psi}{\partial Y} = \frac{\rho}{\rho_\infty} \frac{u}{u_\infty} Y \tag{1}$$

Momentum

$$\frac{\partial}{\partial \tau} \left[\frac{u}{v} - \tau \frac{u_\infty}{u} \frac{\rho_\infty}{\rho} \right] + \frac{\delta}{2} \frac{\partial}{\partial Y} \left[\frac{Y\rho_\infty}{\rho \delta u} u_\infty \right] = 0$$

$$\frac{\partial}{\partial \tau} \left[\frac{p}{\rho_\infty u_\infty^2} + \frac{u}{u_\infty} \right] - \frac{1}{2} Y \frac{\partial}{\partial Y} \left[\frac{u}{u_\infty} Y^2 \right] = 0 \tag{2}$$

Energy

$$\left(\frac{u}{u_\infty} \right)^2 + \left(\frac{v}{u_\infty} \right)^2 + (1 + \delta) \frac{p}{u_\infty^2 \rho \delta} = 1 + [(1 - \delta)/\delta M_\infty^2] \tag{3}$$

where $\tau = \dfrac{2\psi}{Y^2}$, and $\delta = (\gamma - 1)/(\gamma + 1)$.

8

Streamline entropy conservation

$$\left[\frac{p}{\rho_\infty^2 u_\infty^2} \; \rho\delta\right]^{-\gamma} = f(\tau Y^2) \tag{4}$$

where $f(\tau Y^2)$ is an arbitrary function determined by the shape of the shock which maps into the line $\tau = 1$.

The calculated profile of the nose between the axis of symmetry and the point on the body common to the reference line is compared with the given body profile. If deviations are found the basic shock shape is automatically perturbed and the calculation procedure described above is repeated until satisfactory agreement is obtained. The gas is considered in chemical equilibrium and includes the effects of gas dissociation and vibrational excitation.

Conditions previously computed along the reference line are utilized as initial conditions for computation of the supersonic portion of the flow field. The familiar axisymmetric rotational characteristic method is used assuming a real gas in either chemical equilibrium or frozen flow. The program has the capability of detecting discontinuities in the body contour and therefore flow fields about body shapes containing reentrant or expansion corners can be computed.

One-Dimensional Inviscid Flow

Assuming that non-equilibrium effects are small perturbations on the basic equilibrium or frozen inviscid pressure distribution as obtained from the inviscid solution described previously, finite-rate chemistry can now be computed along suitable streamlines.

A one-dimensional finite rate chemistry program (Ref. 5) is used to compute the pointwise state of the fluid along streamlines wherein all initial conditions and a streamwise pressure distribution are prescribed. The analysis includes the effects of vibrational relaxation in the chemical kinetics.

The post shock conditions are solved utilizing real gas thermodynamics whereas the species are considered frozen across the shock. The governing equations are then integrated numerically along the specified streamline path utilizing these initial conditions. Up to thirteen air species can be analyzed utilizing up to thirty-nine air reactions. These reactions and their associated reaction rates are specified in Appendix I. A complete description of the analysis and the governing equations can be found in (Ref. 5).

Boundary Layer

The governing partial differential equations for the viscous flow of a multicomponent chemically reacting gas mixture are derived from the pertinent conservation laws with the classical boundary layer assumptions (Ref. 4). The transformation of the boundary layer equations to von Mises coordinates, X, ψ, is carried out to obtain a form more appropriate for numerical solution. The stream function ψ satisfies the continuity equation and eliminates the need for numerical integration of that equation. The transformation variable is defined by

$$\rho u r^\epsilon = \frac{\partial \psi}{\partial Y} \; ; \; \rho v r^\epsilon = - \frac{\partial \psi}{\partial X} \tag{5}$$

where $\epsilon = 0$ for two-dimensional flow and $\epsilon = 1$ for axisymmetric flow. The body coordinate X is retained in the equations to simplify specification of distributions of body pressure and wall conditions as well as to facilitate the tracing of inviscid flow streamlines from shock to body stations.

The conservation equations take the following form in the transformed plane:

10

Momentum

$$\frac{\partial u}{\partial X} = -\frac{1}{\rho u}\frac{dp}{dX} + r^{\epsilon}\frac{\partial \tau}{\partial \psi} \tag{6}$$

Energy

$$\frac{\partial H}{\partial X} = r^{\epsilon}\frac{\partial}{\partial \psi}(\mathcal{E}^{H} + \mathcal{E}^{C}) \tag{7}$$

Species continuity (i = 1,2,3,...N)

$$\frac{\partial \alpha_i}{\partial X} = \frac{\dot{w}_i}{\rho u} + r^{\epsilon}\frac{\partial \mathcal{D}}{\partial \psi} \tag{8}$$

where τ is the shear stress, $\mathcal{E}^{H}$ is the total enthalpy diffusion term. $\mathcal{E}^{C}$ is the energy diffusion term due to species gradients, $\mathcal{D}$ is the species diffusion term and $\dot{w}_i$ is the net rate of production of the ith specie (Ref. 4). The diffusion velocity resulting from gradients in the species distributions is assumed to be specified by Fick's law for a binary mixture and the laminar viscosity is assumed to be given by the Sutherland law. The reactions and their associated reaction rates are listed in Appendix I where the reactions included in the analysis are the first seven.

The equations are solved in the domain defined by inner boundary conditions at the wall, outer edge conditions in the inviscid flow which are unknown a priori, and the initial conditions for property distributions through the layer at an initial body station. The inner conditions at the wall and distributions of initial conditions are specified as input to the problem. The species distributions at the wall are assumed known as a function of the effectiveness of the wall participating as a catalyst or a reactant in surface chemical reactions, or are selected to be in local equilibrium.

The catalytic wall assumption is as follows:

$$- \rho(\alpha_i V_i) = K_R \rho \alpha_i \qquad (9)$$

where K_R = surface recombination coefficient and V_i = diffusion velocity at wall.

For binary mixture

$$V_i = - \frac{D_{12}}{\alpha_i} \frac{\partial \alpha_i}{\partial Y}$$

$$\therefore \frac{\partial \alpha_i}{\partial Y} = \frac{1}{K_R} \alpha_i \qquad (10)$$

For fully catalytic wall, $K_R \to \infty$ for recombination of atoms and "intermediate" molecular species. Therefore, for these species $\alpha \equiv 0$ at wall. For air there results

$$\left. \begin{array}{l} \alpha_{O_2} = (\alpha_{O_2})_\infty \\[2ex] \alpha_{N_2} = (\alpha_{N_2})_\infty \end{array} \right\} \text{ at wall} \qquad (11)$$

all other α's = 0.

The varying streamwise outer edge conditions are obtained from one-dimensional non-equilibrium chemistry calculations carried out along approximate inviscid streamlines from the shock to the body station of interest. The air ingested in the boundary layer by the swallowing of the inviscid flow is used to determine the streamtube area at the boundary layer edge (Fig. 3). Since the shock shape is specified data for this portion of the problem,* the coordinates of the shock intersection point with the free streamtube are readily determined. At that point all local post shock conditions are obtained from

---

*From the inviscid calculations, described above.

12

solutions of the shock equations with the assumption of frozen species composition across the shock. The properties along the streamlines, and thus, at the boundary layer edge, are then determined for the chemically reacting air; where it is assumed that the streamline pressure variation is of the same form as the body pressure variation. The pressure level along each streamline is uniquely defined by the post shock pressure and terminating body pressure of each streamline.

Thus the conditions for solution of the problem (in the absence of ablation) are:

$$X = X(0,\psi) \quad ; \quad u = u(Y) \quad , \quad H = H(Y) \quad , \quad \alpha_i = \alpha_i (Y)$$

$$\psi = \psi (X,0) \quad ; u = 0, \quad v = 0, \quad H = H_w(X), \quad \alpha_i = \alpha_{iw} (X) \qquad (12)$$

$$\psi = \psi (X,\psi_e) \quad ; \quad u = u_e (X) \quad , \quad H = H_\infty \quad , \quad \alpha_i = \alpha_{ie} (X)$$

The deviations from zero slope condition at the outer edge of the profiles (velocity, total enthalpy and species mass fractions) beyond specified numerical tolerances are subsequently used in the computer program to establish a call for new edge conditions, via the forenoted streamline procedure.

The set of partial differential equations is reduced to a system of algebraic equations for numerical solution utilizing an explicit finite difference technique. The finite difference form is developed by expressing the explicit difference relations for each of the dependent variables of the conservation equations (the variable here denoted by a characteristic function, F) as follows:

$$\frac{\partial F}{\partial X} = \frac{F(X+\Delta X, \psi) - F(X,\psi)}{\Delta X}$$

$$(13)$$

$$\frac{\partial F}{\partial \psi} = \frac{F(X,\psi+\Delta \psi) - F(X,\psi-\Delta \psi)}{2\Delta \psi}$$

$$\frac{\partial}{\partial \psi}\left(a\;\frac{\partial F}{\partial \psi}\right) = [a(X,\psi + \tfrac{1}{2}\Delta\psi)\{F(X,\psi + \Delta\psi) - F(X,\psi)\} -$$

$$- a(X,\psi - \tfrac{1}{2}\Delta\psi)\{F(X,\psi) - F(X,\psi - \Delta\psi)\}]\;\frac{1}{(\Delta\psi)^2} \tag{14}$$
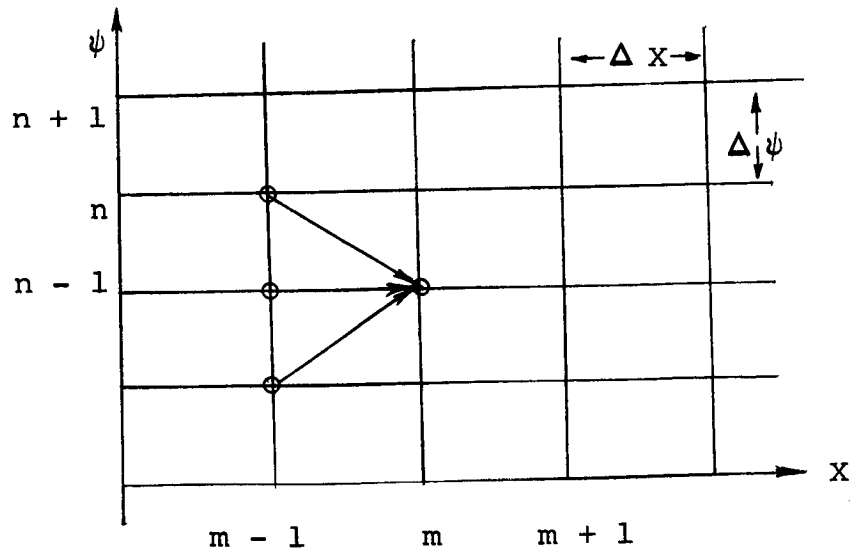
where

$$a(X,\psi \pm \tfrac{1}{2}\Delta\psi) = \tfrac{1}{2}[a(X,\psi) + a(X,\psi \pm \Delta\psi)]$$

The resulting difference equations are of the form

$$F(X+\Delta X,\psi) = A_n + B_n\,F(X,\psi) + C_n\,F(X,\psi + \Delta\psi) + D_n\,F(X,\psi - \Delta\psi) \tag{15}$$

in which A, B, C, and D depend upon the equation (n index), the ψ coordinate, and the various air species.

The X, ψ plane is divided into a finite mesh with grid spacing of Δ X and Δ ψ, with nodal points denoted by intersections of lines m - 1, m, m + 1, and n - 1, n, n + 1, shown in sketch.

Solutions are obtained for the variables along line m + 1, corresponding to X + Δ X, on each line n by stepping off from line m subject to the known conditions at nodal points (m, n) and (m, n $\pm$ 1) corresponding to (X, ψ) and (X, $\psi \pm \Delta \psi$).

The system of algebraic equations which results from the explicit finite difference method is subject to stability conditions that impose restrictions on the permissible relative grid dimensions. A general analytical method for determination of stability requirements of a nonlinear system of equations considered here is not known. However stability estimates can be formulated analytically for a linear system which can be applied to the present problem by linearizing the equations to develop locally constant coefficients. The analytical estimate of the stability condition for the present problem is given by

$$\bar{\sigma} \le \frac{1}{2} \frac{(\Delta \psi)^2}{\Delta X} \qquad (16)$$

where the parameter $\bar{\sigma}$ must be determined for each equation at every grid point. The $\bar{\sigma}$ expressions for the momentum, energy and the i species equations, respectively, are as follows:

$$\bar{\sigma} = r^{2\epsilon} \rho u \, \mu$$

$$\bar{\sigma}_H = r^{2\epsilon} \rho u \, \frac{\mu}{Pr} \qquad (17)$$

$$\bar{\sigma}_{c_i} = r^{2\epsilon} \rho u \, \frac{\mu}{Sc} \quad (i = 1, 2, \ldots)$$

(where the Schmidt number is the ratio of Prandtl to Lewis numbers, or Sc = $\rho D / \mu$).

Transformation of the boundary layer momentum equation by the von Mises stream function coordinate, ψ, results in singularities at the wall where the velocity vanishes. It has been shown that a series solution $\sim \psi^{n/2}$ satisfies the incompressible flow boundary layer equations; the extension to compressible flow with the species conservation equations coupled with the coefficients of the series for u from the momentum equation has been shown (Ref. 4).

METHOD OF CALCULATION

Described herein is the computational technique utilized to investigate conditions at the three altitudes of interest. The methods used in order of application are:

(a) The inviscid flow field is computed for the basic RAM-C configuration assuming equilibrium flow at the two lower altitudes and frozen flow at the higher altitude. The analysis, and the IBM 7094 program utilized, is described in Refs. 1 and 2 and in the ANALYSIS SECTION of this report. Results of this program include the shock shape, and the tracing of inviscid streamlines.

(b) The resulting shock shape and pressure distribution serve as input to the non-equilibrium, reacting boundary layer program detailed in Ref. 4 and in the ANALYSIS SECTION of this report. Here the viscous region is computed utilizing non-equilibrium chemistry and accounts for "swallowing" of vortical inviscid streamlines. Among the parameters computed, the displacement thickness is of immediate importance.

(c) Utilizing the resulting displacement thickness computed from (b) a "corrected" body inviscid flow field is computed (where the "corrected" body is the original shape plus the displacement thickness). The resulting body pressure distribution is then compared to that pressure distribution which was used in the previous boundary layer calculation. If there is serious disagreement, step (b) is repeated. Steps (b) and (c) are repeated until agreement in the pressure distribution is reached. We then proceed to step (d).

(d) Non-equilibrium chemistry along streamlines in the inviscid flow field is computed using the analysis described in Ref. 5. Here the chemistry package utilizes 11 species and 22 reactions accounting for vibrational relaxation where the species are considered to be frozen across the bow shock.

16

RESULTS

Detailed plots of the results obtained are shown in
Figs. 4-112. Profiles of velocity, temperature, pressure,
electron density and specie mole fraction have been plotted
at various stations along the body surface. Contour plots
of electron density, temperature and pressure are also in-
cluded for each altitude of interest. The results have
been divided into sections, according to altitude, with a
separate cover sheet describing in detail the nomenclature
utilized on the enclosed figures.

The complete profiles in the shock layer are depicted by
solid or dashed lines while the points illustrated by symbols
pertain only to the inviscid field calculations. The curves
represent computed values where no interpretation has been
impressed on the graphical presentation.

It is noted that the various chemical species are shown
approaching their respective free stream values which is con-
sistent with the concept of a thin shock (i.e., frozen species
across the shock). Thermodynamic and fluid mechanical quan-
tities approach values which are very near perfect-gas shock
theory. This occurs because the streamline chemistry program
accounts for finite vibrational relaxation times, and immed-
iately behind the shock the vibrational mode has not been fully
excited, hence the near perfect-gas results.

Examination of the results poses some interesting questions
as to the feasibility of the approach utilized and interpreta-
tion of the results. It is therefore necessary to investigate
the assumptions and procedure used.

In order to obtain a feasible approach to a numerical
solution of the state of the shock layer flow certain initial
assumptions were necessary. A boundary layer approach was
taken to be feasible if modifications were made to compute
variable edge conditions and account for viscous interaction.
An iteration procedure was utilized whereby the viscous and
inviscid flows were perturbed until agreement was reached on
the body pressure distribution. The validity of this assump-
tion is contingent upon the degree of these interactions. The

17

interaction parameter $\bar{\chi}$ (Ref. 6) is indicative of pressure and viscous interaction, where

$$\bar{\chi} = \frac{M_\infty}{\left(\dfrac{r_b}{L}\right)^2 Re_{L_\infty}^{\frac{1}{2}}} \tag{18}$$

For altitudes of 71, 53,5, and 36.8 km, $\bar{\chi}$ has the values 2.17, 0.53, and 0.19 respectively. Values of $\chi \sim 0(1)$ represent conditions where strong interaction effects should be taken into account.

It would be expected, then, that the results of the lower altitude calculations would be acceptable whereas the results of the two higher altitude cases would be open to doubt. This situation was, in fact, borne out by the results. The results of the 53.5 km case were marginal and those of the highest altitude case (71 km) were completely unrealistic.

Results of the 36.8 km case are presented in Figs. 4-48. The match between the two solutions is reasonable. The curves shown for this case represent the type of results attainable from this type of computational procedure.

The mismatches between the viscous and the inviscid results at the boundary layer edge (for any streamwise station) are due largely to the arbitrariness associated with picking an edge streamline. At any given station an edge streamline – and thereby the complete state at the edge of that station – is chosen by matching the mass flow in the boundary layer with an inviscid streamtube in the free stream; i.e. the radius of the inviscid streamtube, $\zeta_{2\,sh}$, is chosen so that the mass flow matches that in the boundary layer.

$$\zeta_2 = \left[\frac{2}{\rho_\infty u_\infty} \int_0^\delta \rho u r(X) \, dY \right]^{\frac{1}{2}} \tag{19}$$

The arbitrariness comes, of course, in the choice of δ, wherein the resultant streamline (defined by $\zeta_{2\,sh}$ may be relatively hot or cool depending at what portion of the curved bow shock it originated. Therefore computation of the edge conditions is

18

dependent upon this edge definition as well as the approximate technique used to trace the swallowed streamlines. The displacement thickness is also dependent upon this edge definition.

The iteration procedure used to perturb the inviscid flow becomes questionable when the displacement thickness is large, since a fundamental assumption involved in the utilization of this technique is that the boundary layer is only a small perturbation on the inviscid field. For the two higher altitude cases the displacement thicknesses are large and thus the mismatching between the inviscid and viscous solutions becomes worse with increasing altitude.

Results of the 53.5 km case are presented in Figs. 49-81 where the streamline locations for the initial and final iterations have been indicated. Successive iterations for the 71 km case resulted in boundary layer thicknesses larger than the shock layer thickness and these results have been included for the sake of completeness only, in Figs. 82-112.

At the higher altitudes the concept of a boundary layer is no longer a realistic representation of the viscous layer about the RAM-C vehicle. The classic assumption of a "thin" viscous layer, fundamental in the derivation of the boundary layer equations, is not valid and therefore the structure of the viscous region as a boundary layer type flow is subject to question. An approach whereby the entire shock layer is considered to be viscous must therefore be utilized to adequately investigate the flow field properties at these reentry conditions. This type of shock layer formulation, where non-equilibrium chemistry is considered, is an interesting problem and should be given future consideration.

APPENDIX

SUMMARY OF CHEMICAL REACTIONS

AND THEIR RATE CONSTANTS

This appendix summarizes a large number of chemical reactions which are significant at the high temperatures of reentry into the earth's atmosphere at hypersonic speeds.

The presentation here includes two classes of units, namely cm, sec, particle (used in Ref. 12) and meter, sec, kg mole (required for the present analysis). The tables are self-explanatory, though a word of caution is in order for the ionization reactions 10 through 15. The rate constants for these reactions are tabulated as the forward (i.e. to the right) values, which is contrary to the remainder of the appendix.

20

SUMMARY OF CHEMICAL REACTIONS AND RATE CONSTANTS

NO. j	REACTION	CATALYST X	n	REVERSE RATE CONSTANT AT EQUILIBRIUM $(k_j^x)_e$	
				$\dfrac{kg\ moles}{m^3\ sec}\left(\dfrac{m^3}{kg\ mole}\right)^n$	$\dfrac{particles}{cm^3\ sec}\left(\dfrac{cm^3}{particle}\right)^n$
1	$O_2 + X + 5.1\ ev = 2O + X$	O	3	$2.3 \times 10^{14}\ T^{-3/2}$	$6.2 \times 10^{-28}\ T^{-3/2}$
		O_2		$8.0 \times 10^{13}\ T^{-3/2}$	$2.2 \times 10^{-28}\ T^{-3/2}$
		N_2		$6.2 \times 10^{9}\ T^{-1/2}$	$1.7 \times 10^{-32}\ T^{-1/2}$
		all other		$3.0 \times 10^{9}\ T^{-1/2}$	$8.3 \times 10^{-33}\ T^{-1/2}$
2	$N_2 + X + 9.8\ ev = 2N + X$	N	3	$2.4 \times 10^{15}\ T^{-3/2}$	$6.5 \times 10^{-27}\ T^{-3/2}$
		N_2		$2.8 \times 10^{10}\ T^{-1/2}$	$7.6 \times 10^{-32}\ T^{-1/2}$
		all other		$1.1 \times 10^{10}\ T^{-1/2}$	$3.0 \times 10^{-32}\ T^{-1/2}$
3	$NO + X + 6.5\ ev = N + O + X$	A		$1.7 \times 10^{14}\ T^{-3/2}$	$4.66 \times 10^{-28}\ T^{-3/2}$
		NO		$2.0 \times 10^{15}\ T^{-3/2}$	$5.5 \times 10^{-27}\ T^{-3/2}$
		all other		$1.0 \times 10^{14}\ T^{-3/2}$	$2.8 \times 10^{-28}\ T^{-3/2}$
4	$O + N_2 + 3.3\ ev = NO + N$		2	1.6×10^{10}	2.7×10^{-11}

SUMMARY OF CHEMICAL REACTIONS AND RATE CONSTANTS

NO. j	REACTION	CATALYST X	n	REVERSE RATE CONSTANT AT EQUILIBRIUM $(k_{j-}^x)_e$	
				* $\dfrac{kg\ moles}{m^3\ sec}\left(\dfrac{m^3}{kg\ mole}\right)^n$	** $\dfrac{particles}{cm^3\ sec}\left(\dfrac{cm^3}{particle}\right)^n$
5	$NO+O\ 1.4\ ev = N + O_2$		2	$1.3 \times 10^7\ T\ exp\left(-\dfrac{3560}{T}\right)$	$2.2 \times 10^{-1/4}\ T\ exp\left(-\dfrac{3560}{T}\right)$
6	$N_2 + O_2 + 1.9\ ev = 2NO$		2	$2.4 \times 10^{20}\ T^{-5/2}\ exp\left(-\dfrac{43,000}{T}\right)$	$0.4 \times T^{-5/2}\ exp\left(-\dfrac{43,000}{T}\right)$
7	$N+O+2.8\ ev = NO^+ + e^-$		2	$1.8 \times 10^{18}\ T^{-3/2}$	$3 \times 10^{-3}\ T^{-3/2}$
8	$2N+5.8\ ev = N_2^+ + e^-$		2	$3.01 \times 10^{16}\ T^{-3/4}$	$5.0 \times 10^{-5}\ T^{-3/4}$
9	$2O+6.9\ ev = O_2^+ + e^-$		2	$1.2 \times 10^{18}\ T^{-3/2}$	$2 \times 10^{-3}\ T^{-3/2}$

* = upper content of brace

** = lower content of brace

22

SUMMARY OF CHEMICAL REACTIONS AND RATE CONSTANTS

NO. j	REACTION	CATALYST X	n	FORWARD RATE CONSTANT AT EQUILIBRIUM $(k_j^x)_e$
				$*\ \dfrac{kg\ moles}{m^3\ sec}\left(\dfrac{m^3}{kg\ mole}\right)^n$ $**\ \dfrac{particles}{cm^3\ sec}\left(\dfrac{cm^3}{particle}\right)^n$
10	$X+NO+9.3\ ev = X+NO^+ + e^-$	all species	2	$\left.\begin{matrix}2.7\times10^{-4}\\4.5\times10^{-26}\end{matrix}\right\}\ T^{5/2}\ (1+3\times10^{-5}T)\exp\left(-\dfrac{107,900}{T}\right)$
11	$N_2+O_2+11.2\ ev = NO+NO^+ + e^-$		2	$\left.\begin{matrix}2.7\times10^{-4}\\4.5\times10^{-26}\end{matrix}\right\}\ T^{5/2}\ (1+3\times10^{-5}T)\exp\left(-\dfrac{141,000}{T}\right)$

* = upper content of brace   ** = lower content of brace

23

SUMMARY OF CHEMICAL REACTIONS AND RATE CONSTANTS

NO. j	REACTION	CATALYST X	n	FORWARD RATE CONSTANT AT EQUILIBRIUM $(k_j^x)_e$ $*\ \dfrac{kg\ moles}{m^3\ sec}\left(\dfrac{m^3}{kg\ mole}\right)^n$ $**\ \dfrac{particles}{cm^3\ sec}\left(\dfrac{cm^3}{particle}\right)^n$
12	$X+O_2+12.1\ ev = X+O_2^+ + e^-$	N_2	2	$\left.\begin{array}{l} *\ 2.7\times10^{-4} \\ **\ 4.5\times10^{-25}\end{array}\right\} T^{5/2}(1+3\times10^{-5}\,T)\exp\left(-\dfrac{141{,}000}{T}\right)$
		O_2	2	$\left.\begin{array}{l} *\ 6.6\times10^{-13} \\ **\ 1.1\times10^{-33}\end{array}\right\} T^{9/2}(1+4\times10^{-5}\,T)\exp\left(-\dfrac{141{,}000}{T}\right)$
		all other	2	use value for N_2
13	$X+O+13.6\ ev = X+O^+ + e^-$	all species	2	$\left.\begin{array}{l} *\ 2.7\times10^{-4} \\ **\ 4.5\times10^{-25}\end{array}\right\} T^{5/2}(1+3\times10^{-5}\,T)\exp\left(-\dfrac{157{,}000}{T}\right)$
14	$X+N+14.6\ ev = X+N^+ + e^-$	all species	2	$\left.\begin{array}{l} *\ 2.7\times10^{-4} \\ **\ 4.5\times10^{-25}\end{array}\right\} T^{5/2}(1+3\times10^{-5}\,T)\exp\left(-\dfrac{169{,}400}{T}\right)$
15	$X+N_2+15.6\ ev = X+N_2^+ + e^-$	N_2 and all other	2	$\left.\begin{array}{l} *\ 1.7\times10^{-7} \\ **\ 2.8\times10^{-28}\end{array}\right\} T^{7/2}(1+3\times10^{-5}\,T)\exp\left(-\dfrac{181{,}000}{T}\right)$

* = upper content of brace

** = lower content of brace

SUMMARY OF CHEMICAL REACTIONS AND RATE CONSTANTS

NO. j	REACTION	CATALYST X		REVERSE RATE CONSTANT AT EQUILIBRIUM $(k^x_{j-})_e$	
			n	$\dfrac{\text{kg moles}}{\text{m}^3 \text{ sec}}\left(\dfrac{\text{m}^3}{\text{kg mole}}\right)^n$	$\dfrac{\text{particles}}{\text{cm}^3 \text{ sec}}\left(\dfrac{\text{cm}^3}{\text{particle}}\right)^n$
			2	$7.8\times10^8\ T^{1/2}$	$1.3\times10^{-12}\ T^{1/2}$
				for all reactions on this page	
16	$N+O_2^+ +0.2\ ev = O^+ +NO$				
17	$NO+NO^+ +0.9\ ev = N_2 +O_2^+$				
18	$N+O^+ +0.9\ ev = N^+ +O$				
19	$N_2 +N^+ +1.0\ ev = N_2^+ +N$				
20	$NO^+ +N+1.1\ ev = N_2 +O^+$				
21	$O+O_2^+ +1.6\ ev = O^+ +O_2$				
22	$N_2 +O^+ +2.0\ ev = N_2^+ +O$				
23	$O+N_2^+ +2.2\ ev = N^+ +NO$				
24	$NO+O^+ +2.3\ ev = O_2 +N^+$				
25	$N+O_2^+ +2.5\ ev = N^+ +O_2$				

25

SUMMARY OF CHEMICAL REACTIONS AND RATE CONSTANTS

NO. j	REACTION	CATALYST X	n	REVERSE RATE CONSTANT AT EQUILIBRIUM $(k_j^x-)_e$	
				$\dfrac{kg\ moles}{m^3\ sec}\left(\dfrac{m^3}{kg\ mole}\right)^n$	$\dfrac{particles}{cm^3\ sec}\left(\dfrac{cm^3}{particle}\right)^n$
26	$O_2 + NO^+ + 2.8\ ev = O_2^+ + NO$		2	$7.8 \times 10^8\ T^{1/2}$	$1.3 \times 10^{-12}\ T^{1/2}$
27	$NO^+ + N + 3.1\ ev = N_2^+ + O$				
28	$N_2 + O_2^+ + 3.5\ ev = N_2^+ + O_2$				
29	$NO^+ + O + 4.2\ ev = O_2^+ + N$			for all reactions on this page	
30	$N_2 + O^+ + 4.2\ ev = NO + N^+$				
31	$O + NO^+ + 4.4\ ev = O^+ + NO$				
32	$NO + NO^+ + 4.5\ ev = N_2^+ + O_2$				
33	$N + NO^+ + 5.3\ ev = N^+ + NO$				
34	$N_2 + NO^+ + 6.3\ ev = N_2^+ + NO$				
35	$NO^+ + O + 6.7\ ev = O_2 + N^+$				

SUMMARY OF CHEMICAL REACTIONS AND RATE CONSTANTS

NO. j	REACTION	CATALYST X	n	REVERSE RATE CONSTANT AT EQUILIBRIUM $(k_{-j}^{x})_e$ $\dfrac{\text{kg moles}}{\text{m}^3 \text{ sec}}\left(\dfrac{\text{m}^3}{\text{kg mole}}\right)^n$	$\dfrac{\text{particles}}{\text{cm}^3 \text{ sec}}\left(\dfrac{\text{cm}^3}{\text{particle}}\right)^n$
36	$X+O^-+1.465\ ev = X+O+e^-$	all species	3	$1.1\times10^{13}\ T^{-1}$	$3.03\times10^{-29}\ T^{-1}$
37	$X+O_2^-+0.46\ ev = X+O_2+e^-$	O_2	3	10^{12}	2.75×10^{-30}
		all other		$7.6\times10^{10}\ T^{-1}$	$2.1\times10^{-29}\ T^{-1}$
38	$NO+O+7.835\ ev = O^-+NO^+$		2	$1.0\times10^{15}\ T^{-1/2}$	$1.7\times10^{-6}\ T^{-1/2}$
39	$NO+O_2+8.84\ ev = O_2^-+NO^+$		2	$1.0\times10^{15}\ T^{-1/2}$	$1.7\times10^{-6}\ T^{-1/2}$

REFERENCES

1. Lieberman, E., Computer Programs and Analysis for Flow Fields About Bodies in Hypersonic Flight - Air in Chemical Equilibrium and Frozen Flow Chemistry, GASL TR-460, September 1964.

2. Lieberman, E., Input Formats and Operating Instructions for IBM 709/90/94 Computer Programs to Calculate Inviscid Flow Fields, GASL TR-460A, September 1964.

3. Vaglio-Laurin, R. and Ferri, A., Theoretical Investigation of the Flow Field About Blunt Nosed Bodies in Supersonic Flight, JAS, Vol. 25, pp. 761-770, December 1958.

4. Galowin, L. S. and Gould, H., A Finite Difference Method Solution of Non-similar Equilibrium and Non-equilibrium Air, Boundary Layer Equations with Laminar and Turbulent Viscosity Models, Part I - Analysis, Part II - Computer Program and Supplement, Part III - Input Manual, GASL TR-501, February 1965.

5. Gavril, B. D., Generalized One-Dimensional Chemically Reacting Flows with Molecular Vibrational Relaxation, GASL TR-426, January 1964.

6. Lees, L., Recent Developments in Hypersonic Flow, Jet Propulsion, Vol. 27, pp. 1162-1178, November 1957.

7. Lin, S. C. and Teare, J. D., Rate of Ionization Behind Shock Waves in Air, II - Theoretical Interpretations, The Physics of Fluids, Vol. 6, No. 3, March 1963.

8. Whitten, R. C. and Poppoff, I. G., Ion Kinetics in the Lower Ionosphere, J. Atmos. Sci., Vol. 21, No. 2.

9. Eschenroeder, A. Q., Daiber, J. W., Golian, T. C., and Hertzberg, A., Shock Tunnel Studies of High-Enthalpy Ionized Airflows, Cornell Aeronautical Laboratory Report No. AF-1500-A-1, July 1962.

10. Zeiberg, S. L., Oxygen-Electron Attachment in Hypersonic Wakes, AIAA Journal, Vol. 2, No. 6, pp. 1151-1152, June 1964.

11. Lees, L., Hypersonic Wakes and Trails, Presented at 17th
     Annual Meeting of the American Rocket Society, ARS
     Reprint No. 2662-62, November 1962.

12. Steiger, M.H., On the Chemistry of Air at High Temperatures,
     GASL TR-357, June 1963.

TABLE I

RAM-C FLIGHT CONDITIONS

Conditions	Case Number		
	I	II	III
Geometric Altitude			
m	71,000	53,500	36,800
ft	232,900	175,500	120,700
Relative Velocity			
m/sec	7913	7864	7425
ft/sec	25,960	25,800	24,360
Ambient Conditions			
Pressure			
N/m^2	4.735	51.63	445.5
lbs/ft^2	.0989	1.078	9.305
Temperature			
$^\circ K$	215.8	268.5	241.5
$^\circ R$	388.4	483.3	434.7
Density			
kg/m^3	7.644×10^{-5}	6.697×10^{-4}	6.427×10^{-3}
lbs/ft^3	4.772×10^{-6}	4.181×10^{-5}	4.012×10^{-4}
Velocity of Sound			
m/sec	294.5	328.5	311.5
ft/sec	966.2	1000.8	1022.0

The ambient conditions used for these cases are those found in the following document: Anon.: U.S. Standard Atmosphere, 1962. NASA, U.S. Air Force, and U.S. Weather Bureau, December 1962. SI Units are shown, followed by the corresponding English Units.

30
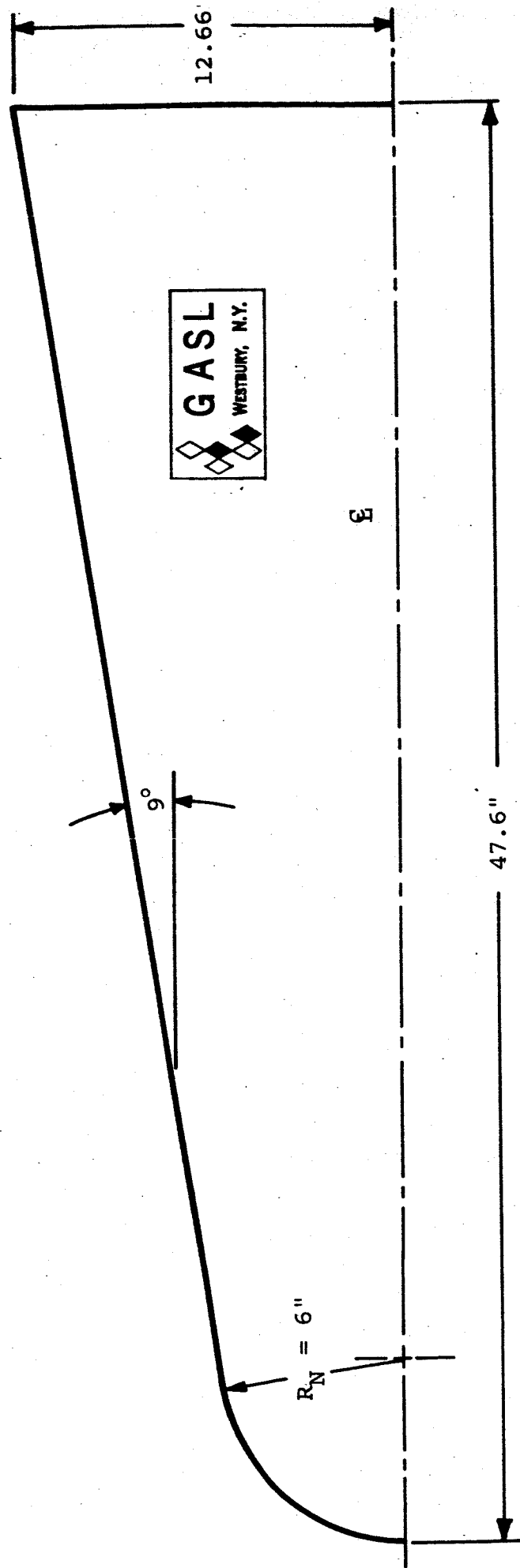
FIG. 1. RAM-C VEHICLE GEOMETRY

31

Detached Shock, $x = F(y)$

Body Profile

Transonic Region

Sonic Line

Axis of Symmetry

Reference
Line

Subsonic
Region

GASL
WESTBURY, N.Y.
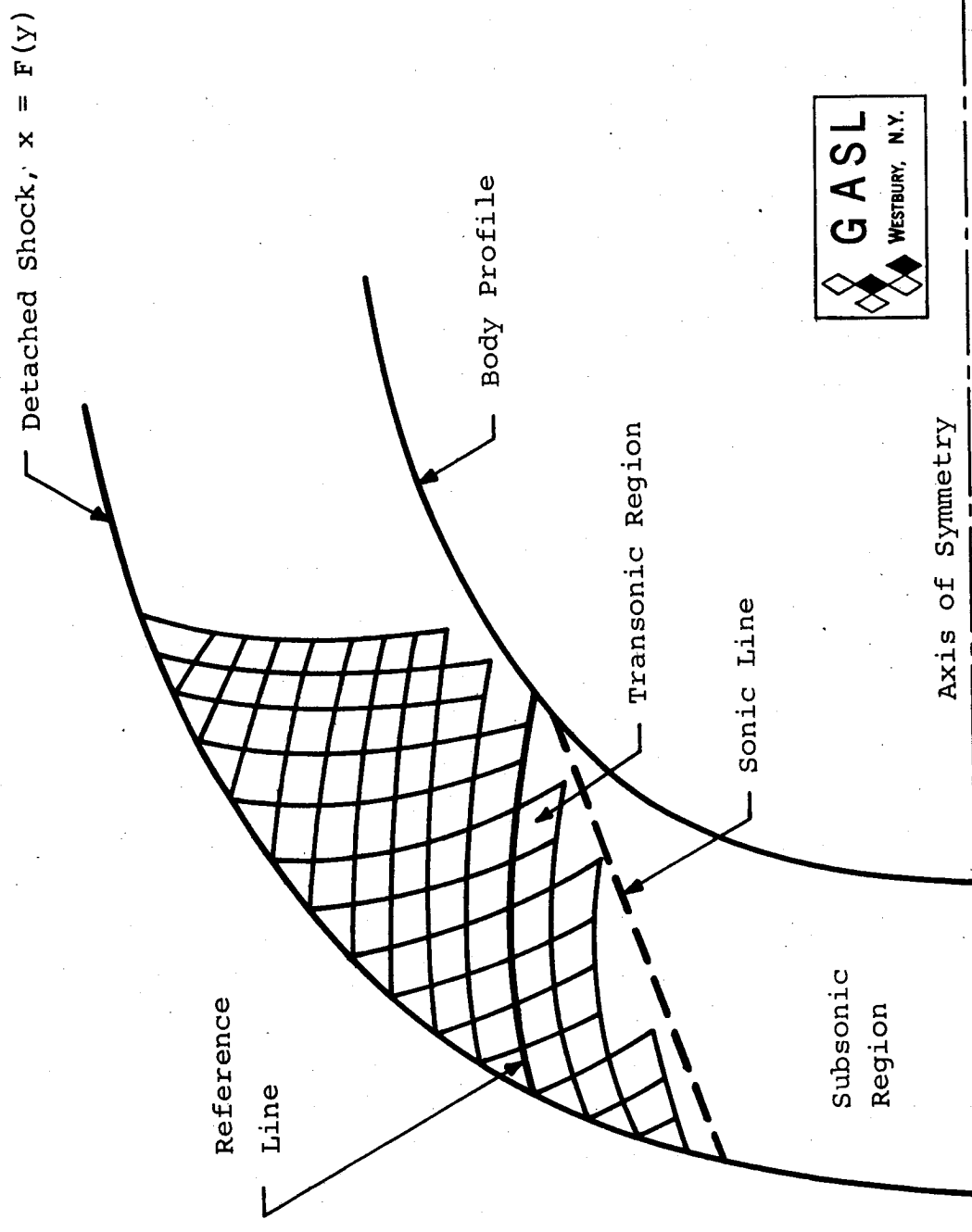
FIG. 2. SCHEMATIC OF SUBSONIC AND SUPERSONIC FLOW FIELD REGIONS
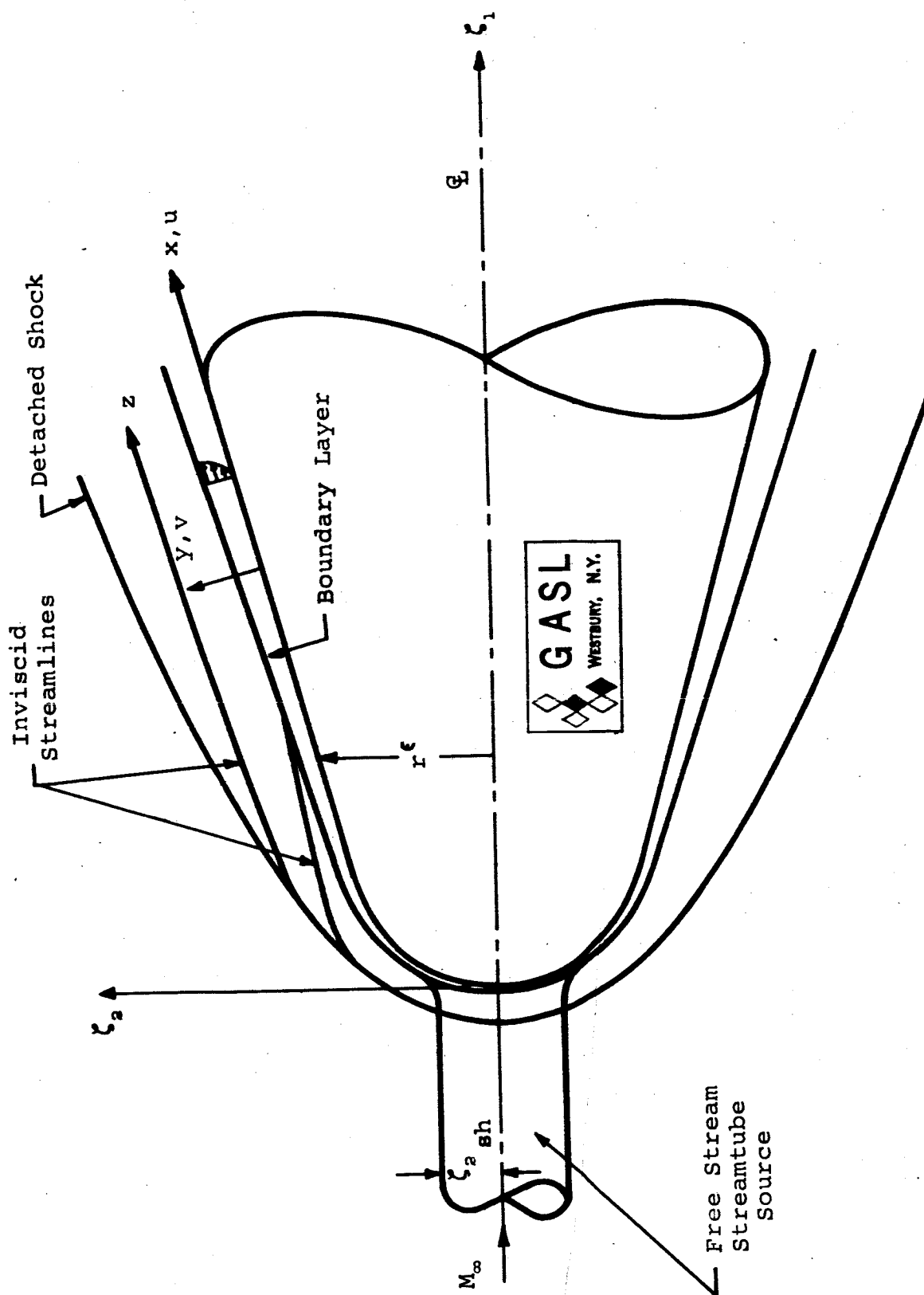
FIG. 3. FLOW FIELD SCHEMATIC

NOMENCLATURE

ALTITUDE = 36,800 METERS

The shock locations for each profile are indicated by the short solid lines drawn along the normal coordinate. Since the shock layer thickness increases with increasing surface coordinate location, their identification is therefore self-explanatory.

The data points indicate the results of streamline calculations where the code utilized for each station is indicated on each figure. The symbol β indicates the post bow shock entry angle of the streamline considered.
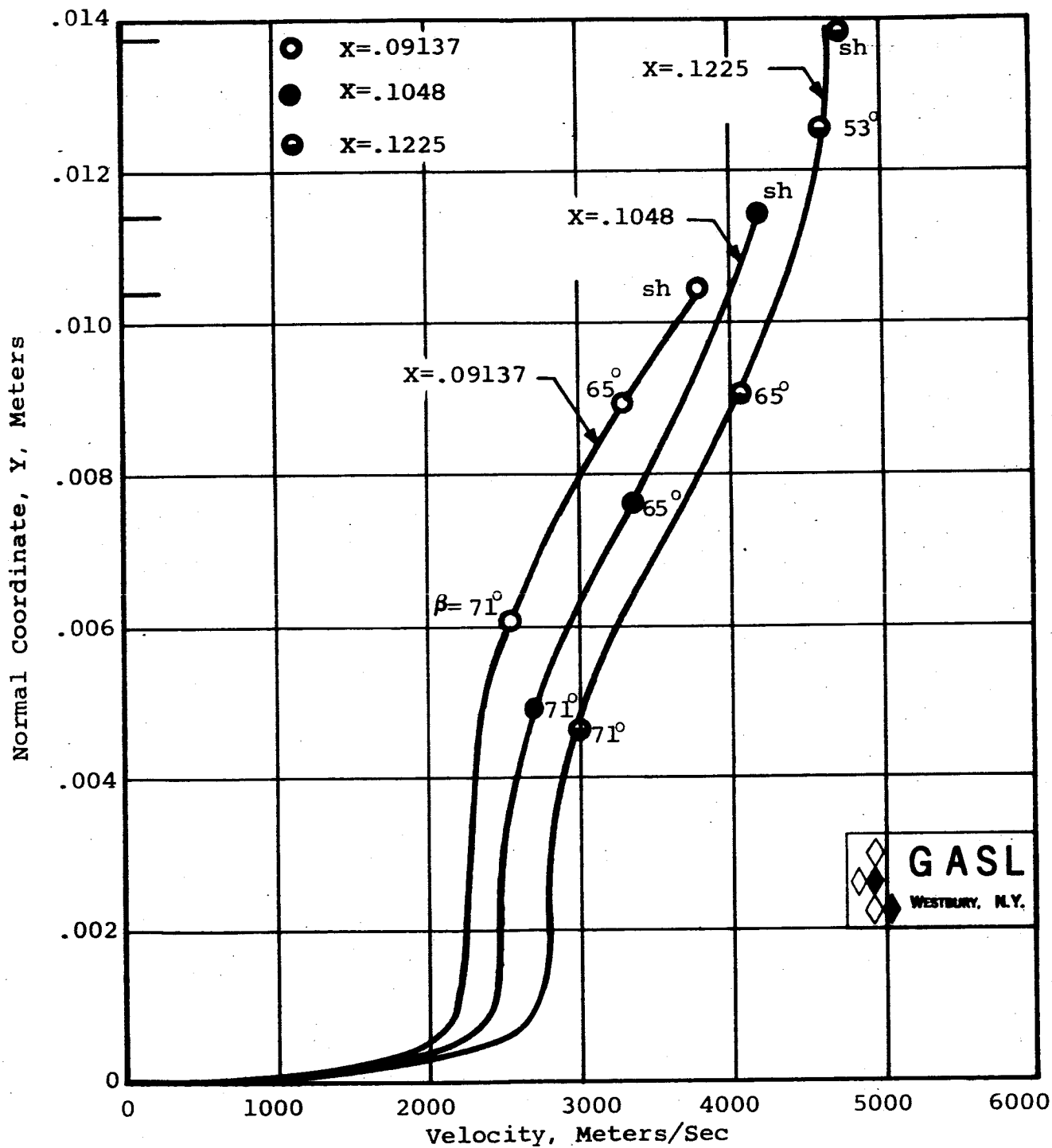
FIG. 4. VELOCITY AT SURFACE COORDINATE LOCATIONS X=.09137, X=.1048, AND X=.1225 METERS, ALTITUDE = 36,800 METERS
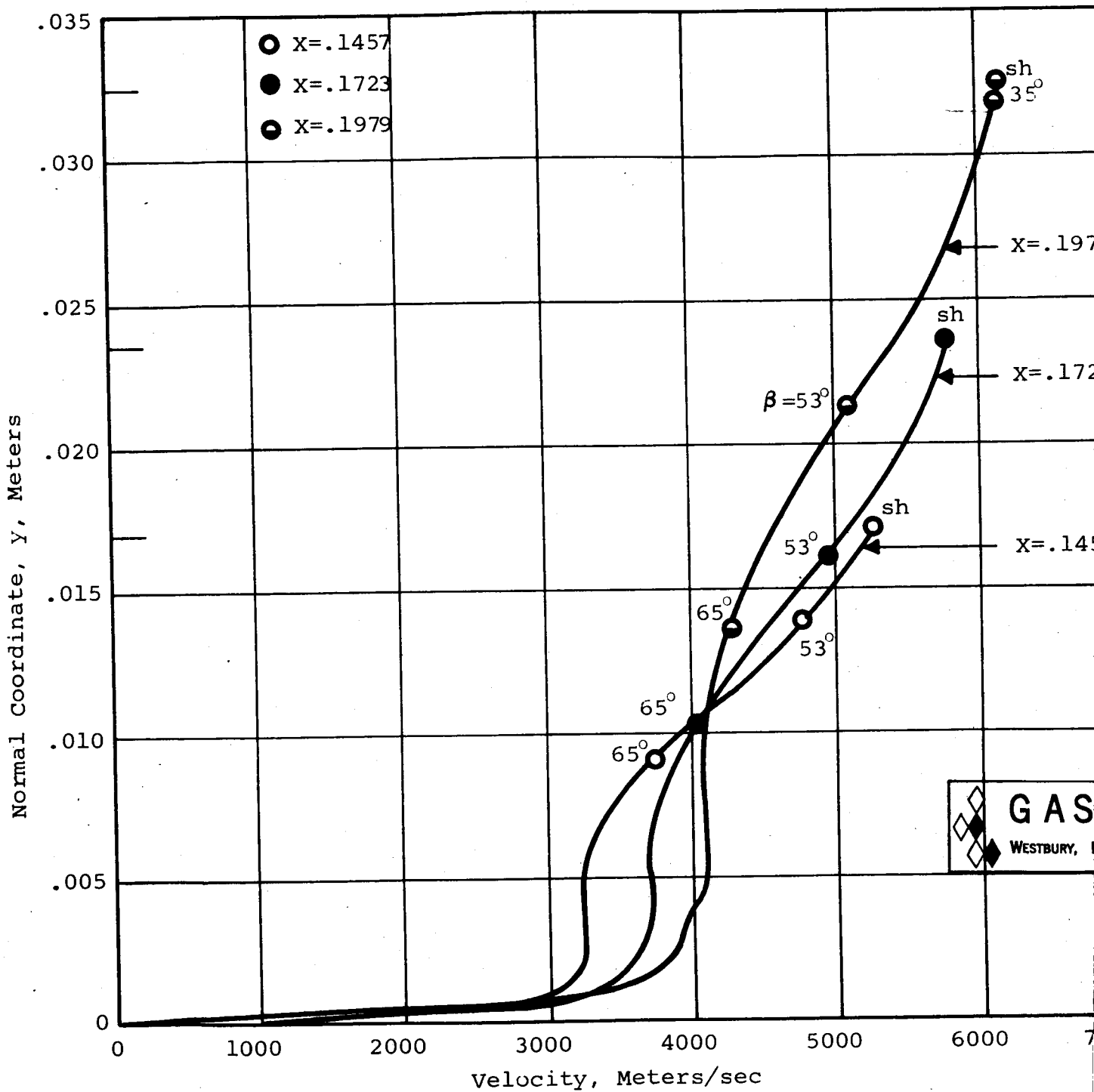
FIG. 5.   VELOCITY AT SURFACE COORDINATE LOCATIONS X=.1457, X=.1723,
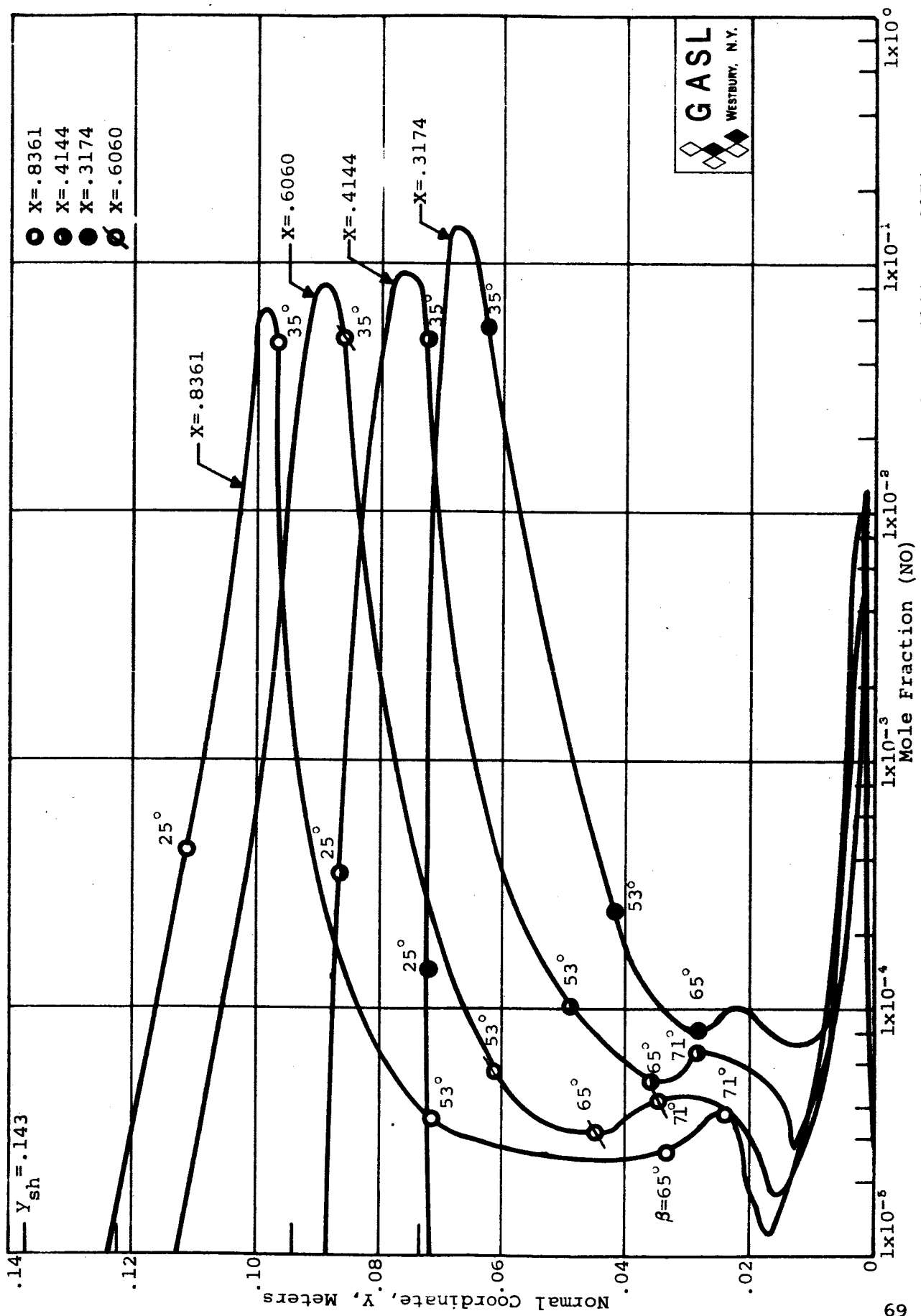AND X=.1979 METERS, ALTITUDE = 36,800 METERS

36
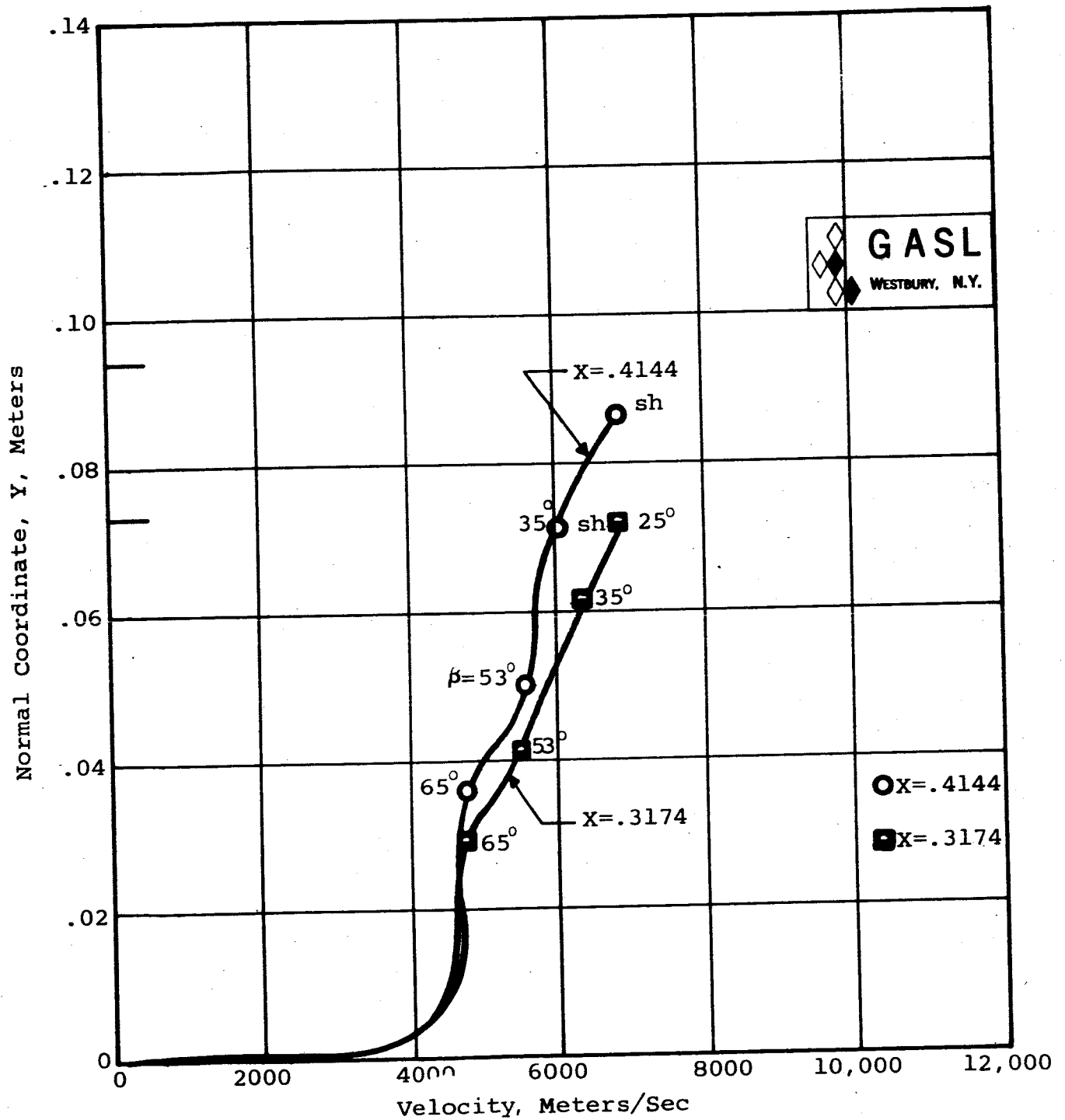
FIG. 6. VELOCITY AT SURFACE COORDINATE LOCATIONS X=.4144
AND X=.3174 METERS, ALTITUDE = 36,800 METERS
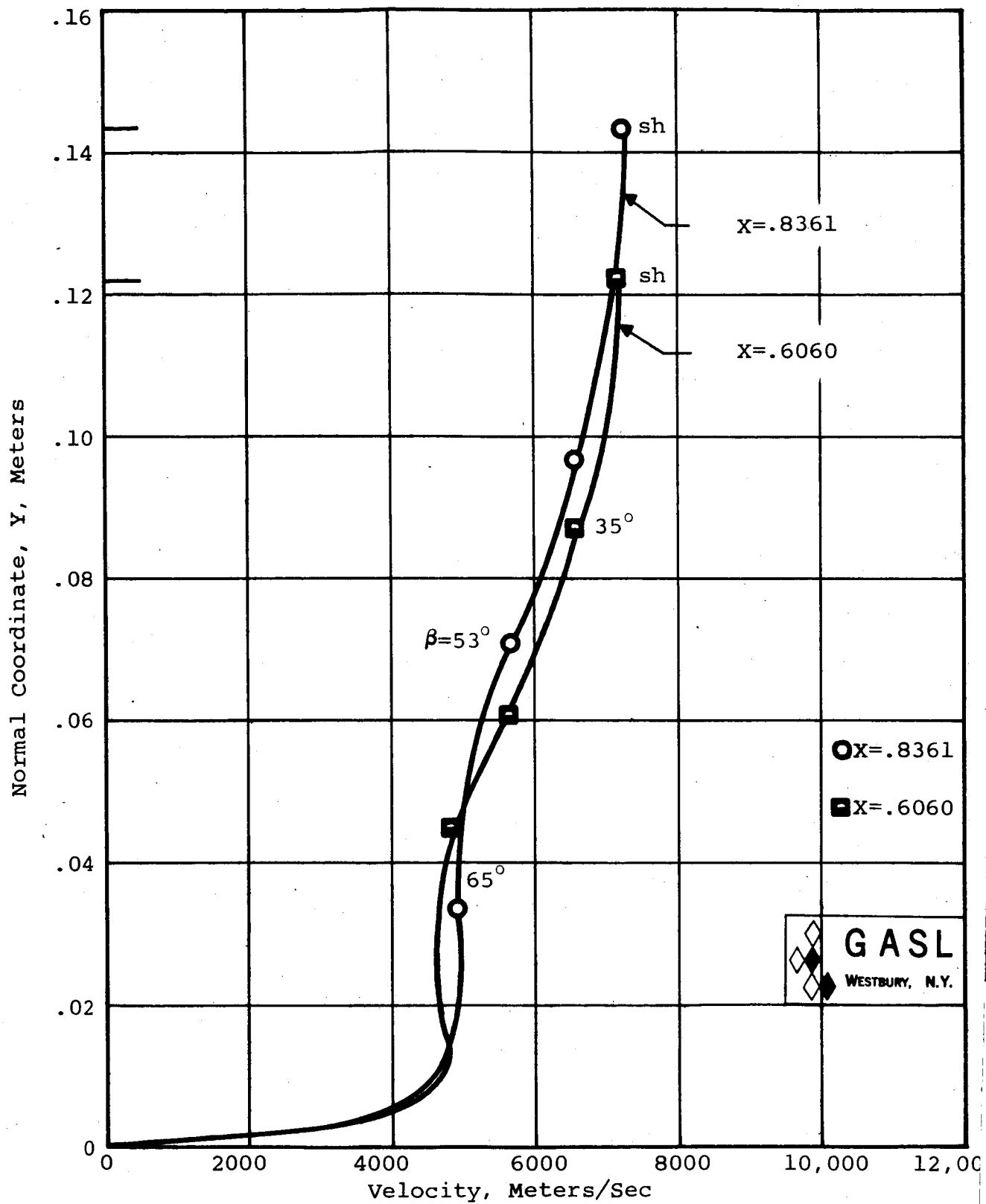
FIG. 7. VELOCITY AT SURFACE COORDINATE LOCATIONS X=.8361
AND X=.6060 METERS, ALTITUDE = 36,800 METERS
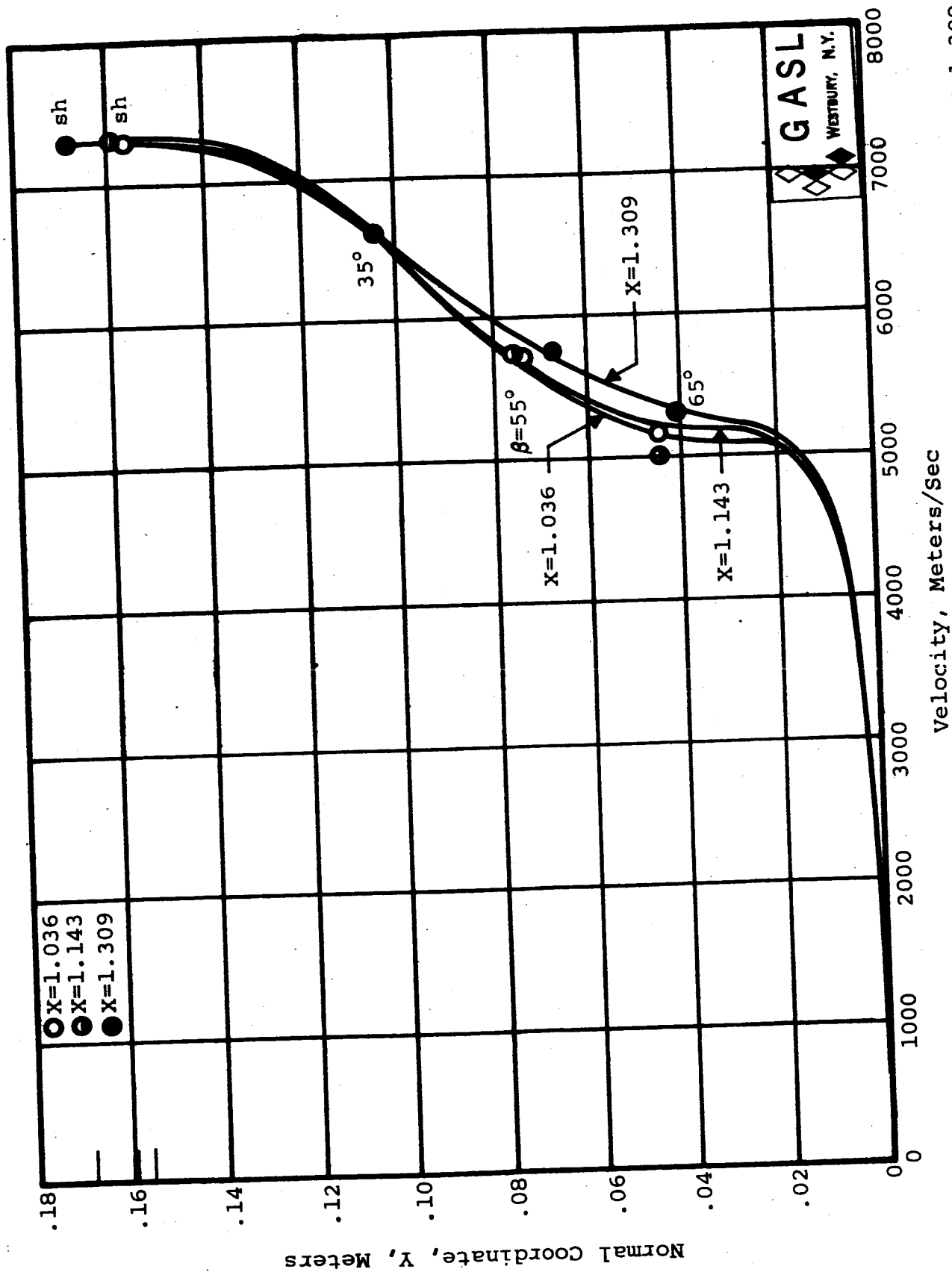
FIG. 8. VELOCITY AT SURFACE COORDINATE LOCATIONS X=1.036, X=1.143, AND X=1.309 METERS, ALTITUDE = 36,800 METERS

39
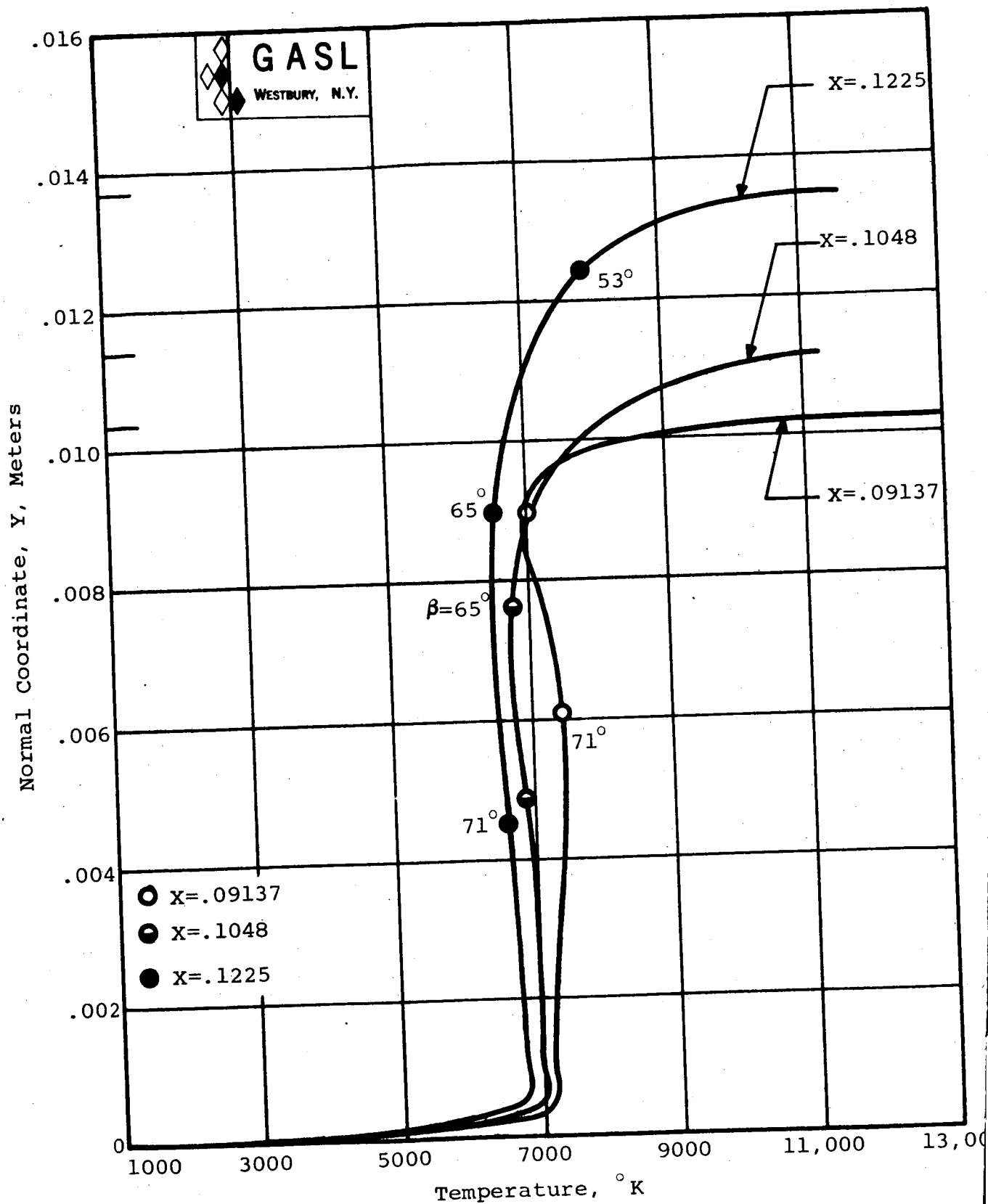
FIG. 9.   TEMPERATURE AT SURFACE COORDINATE LOCATIONS X=.0913
X=.1048, AND X=.1225 METERS, ALTITUDE = 36,800 METE
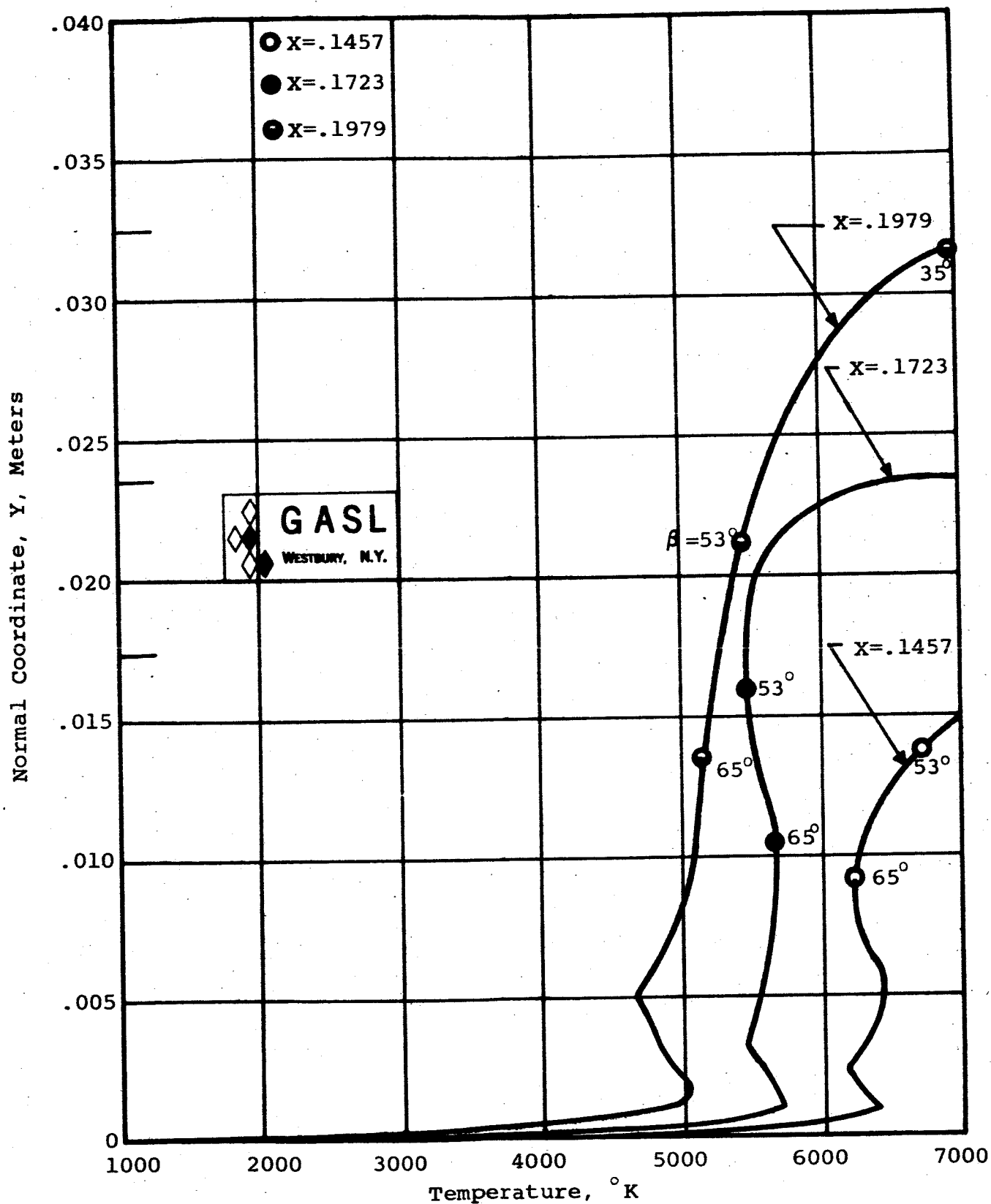
FIG. 10.   TEMPERATURE AT SURFACE COORDINATE LOCATIONS X=.1457, X=.1723, AND x=.1979 METERS, ALTITUDE = 36,800 METERS
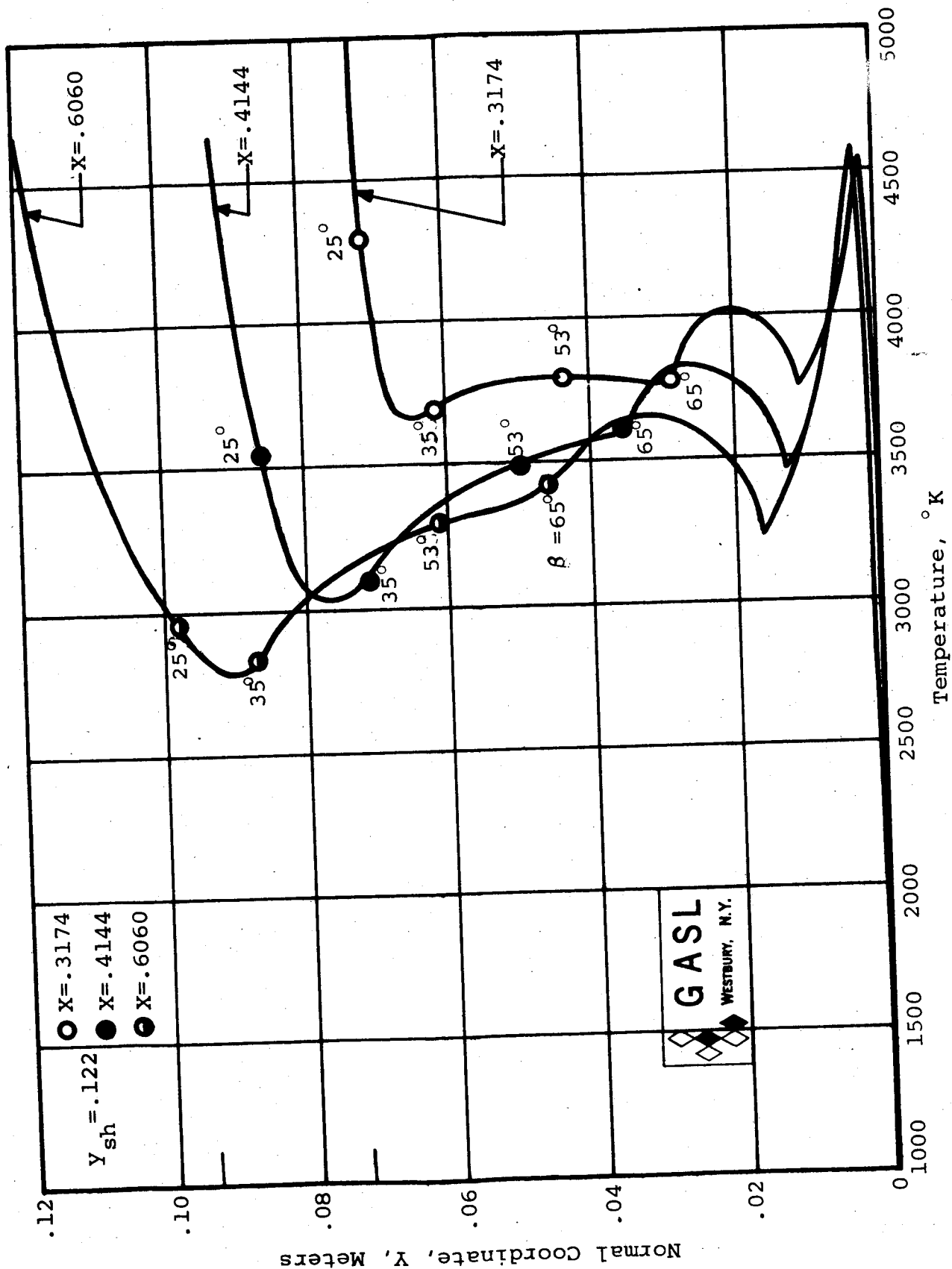
FIG. 11. TEMPERATURE AT SURFACE COORDINATE LOCATIONS X=.3174, X=.4144, AND X=.6060 METERS, ALTITUDE = 36,800 METERS

42
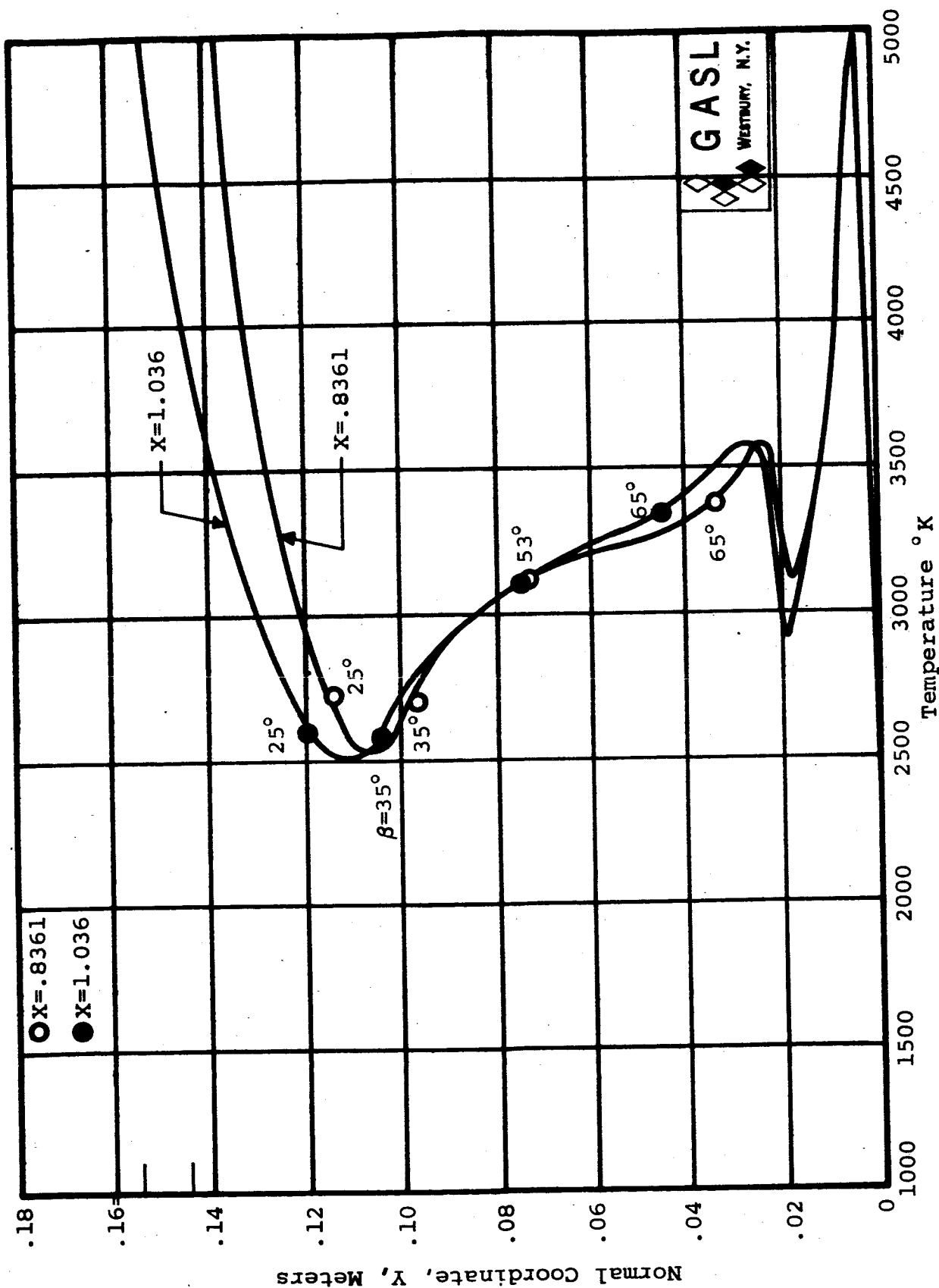
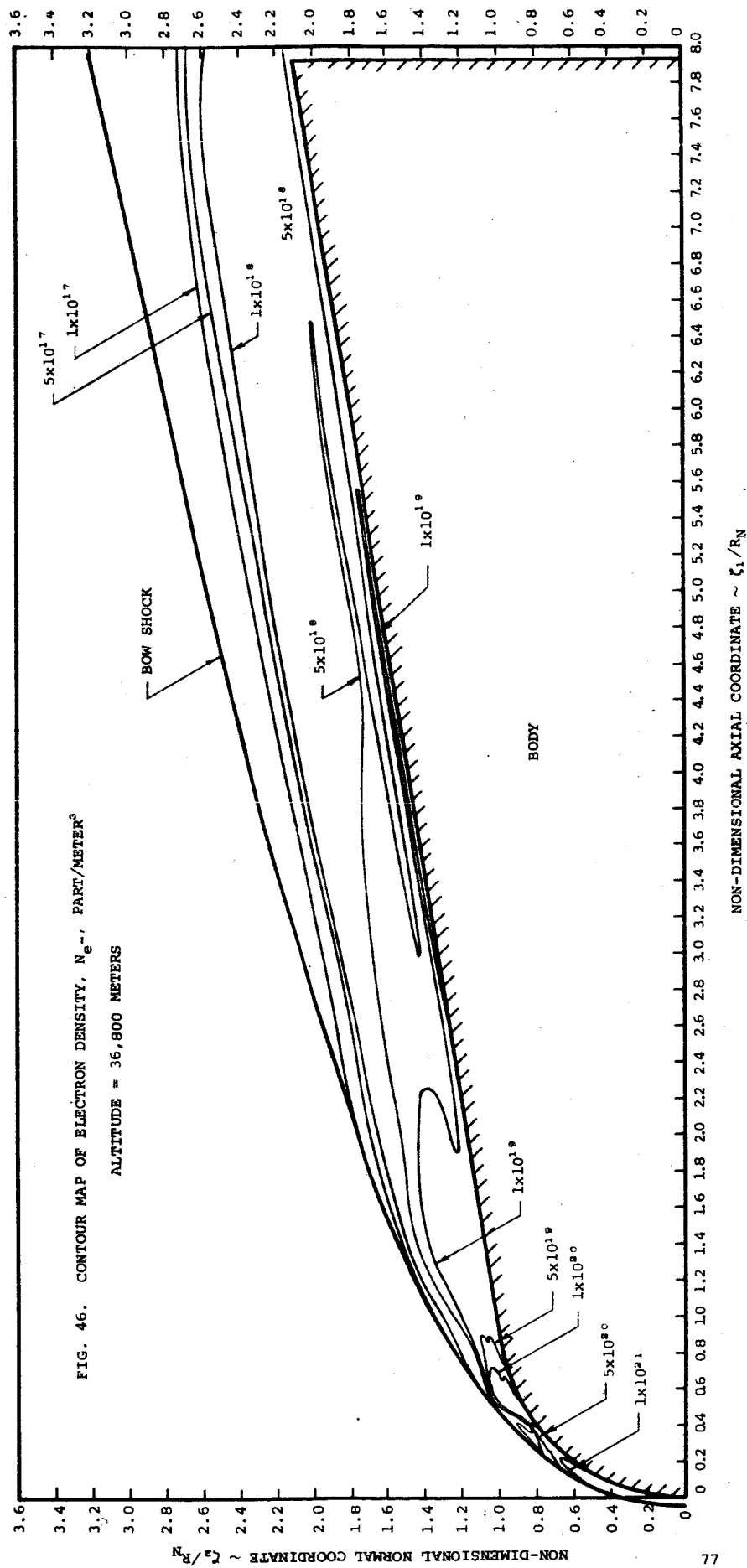FIG. 12. TEMPERATURE AT SURFACE COORDINATE LOCATIONS X=.8361 AND X=1.036 METERS, ALTITUDE = 36,800 METERS

43
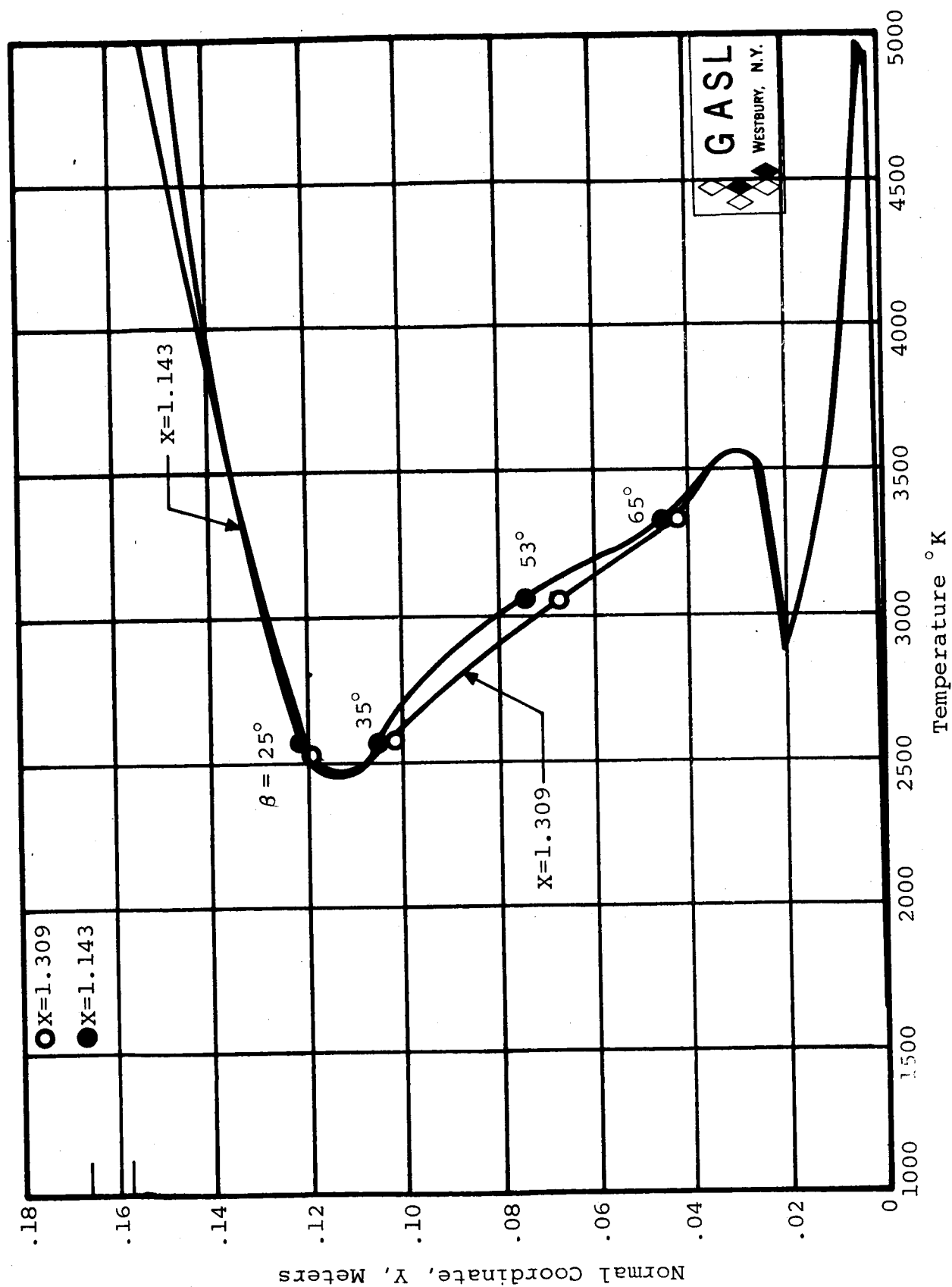
FIG. 13. TEMPERATURE AT SURFACE COORDINATE LOCATIONS X=1.309 AND X=1.143 METERS, ALTITUDE = 36,800 METERS

44
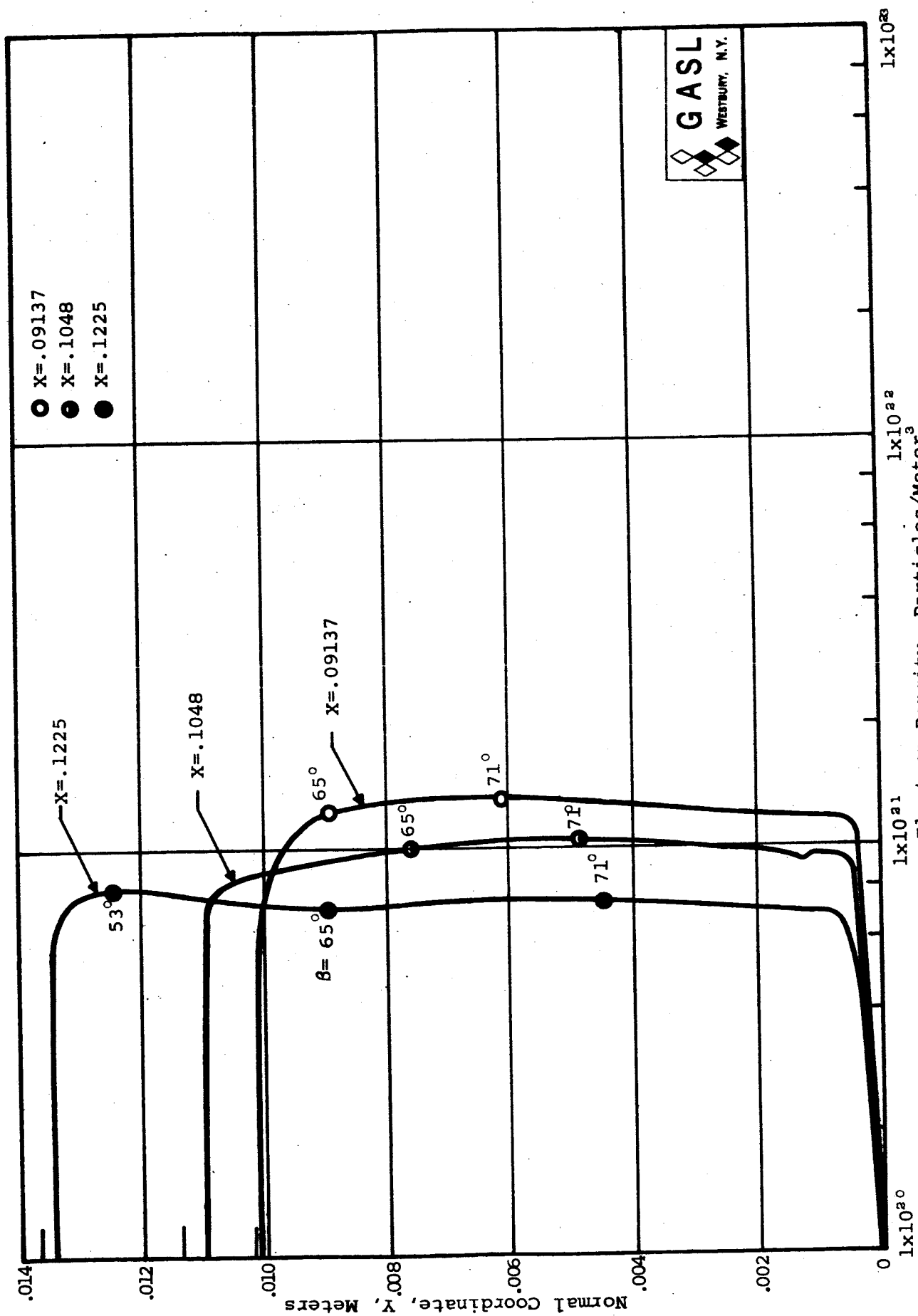
FIG. 14. ELECTRON DENSITY AT SURFACE COORDINATE LOCATIONS X=.09137, X=.1048, AND X=.1225 METERS, ALTITUDE = 36,800 METERS

45
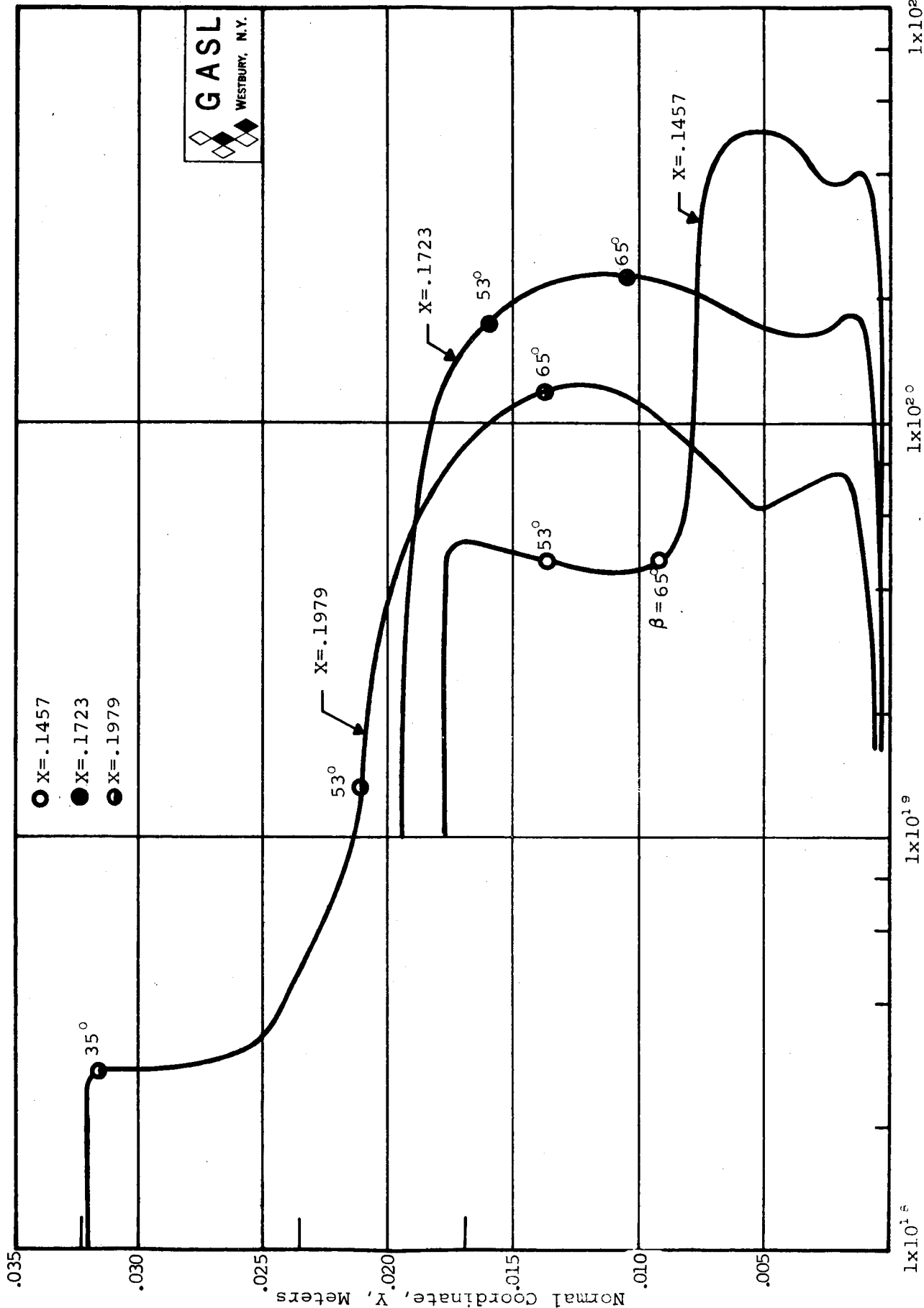
FIG. 15. ELECTRON DENSITY AT SURFACE COORDINATE LOCATIONS X=.1457, X=.1723, AND X=.1979 METERS,

46
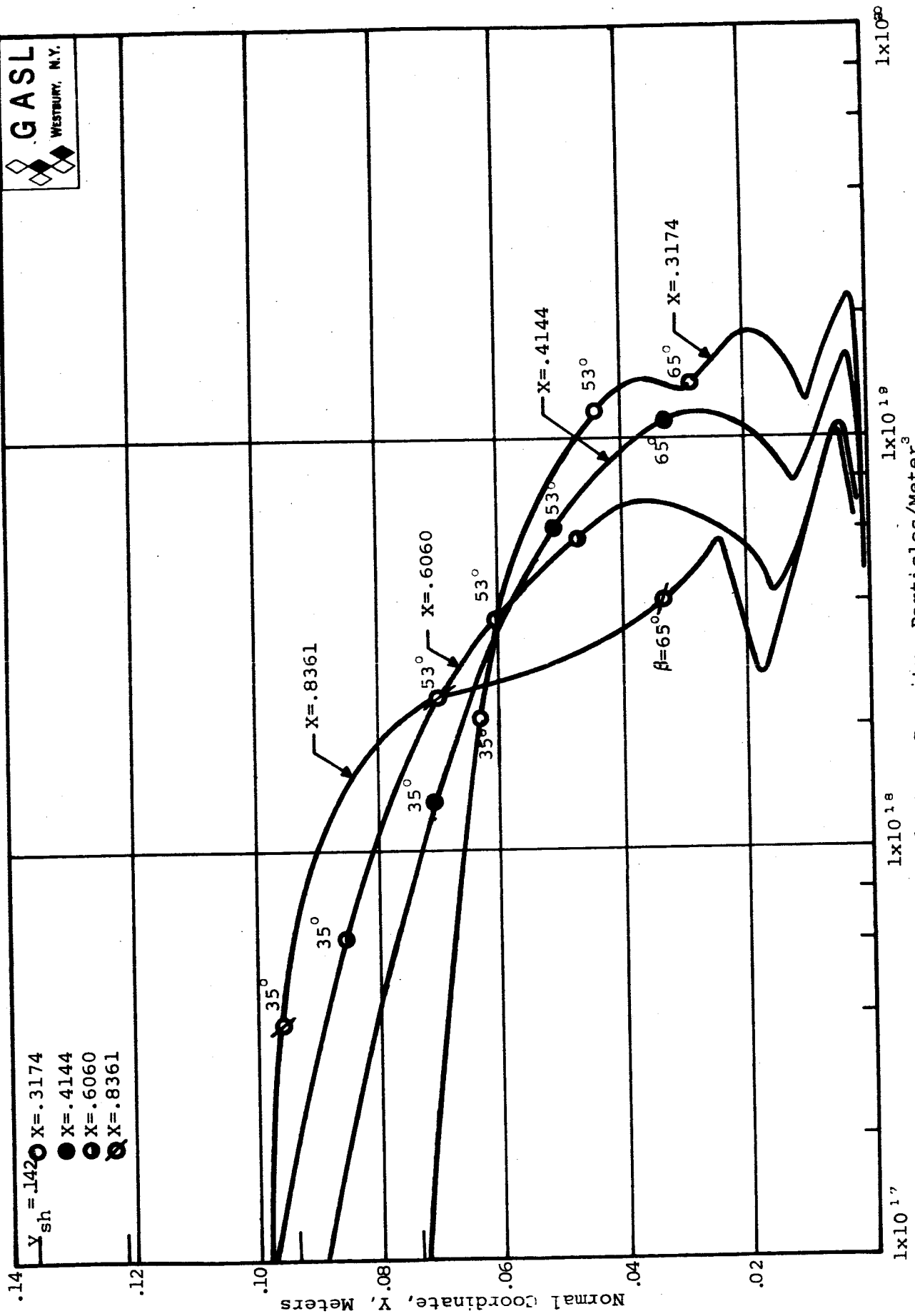
FIG. 16. ELECTRON DENSITY AT SURFACE COORDINATE LOCATIONS X=.3174, X=.4144, X=.6060, AND X=.8361 METERS, ALTITUDE = 36,800 METERS

47
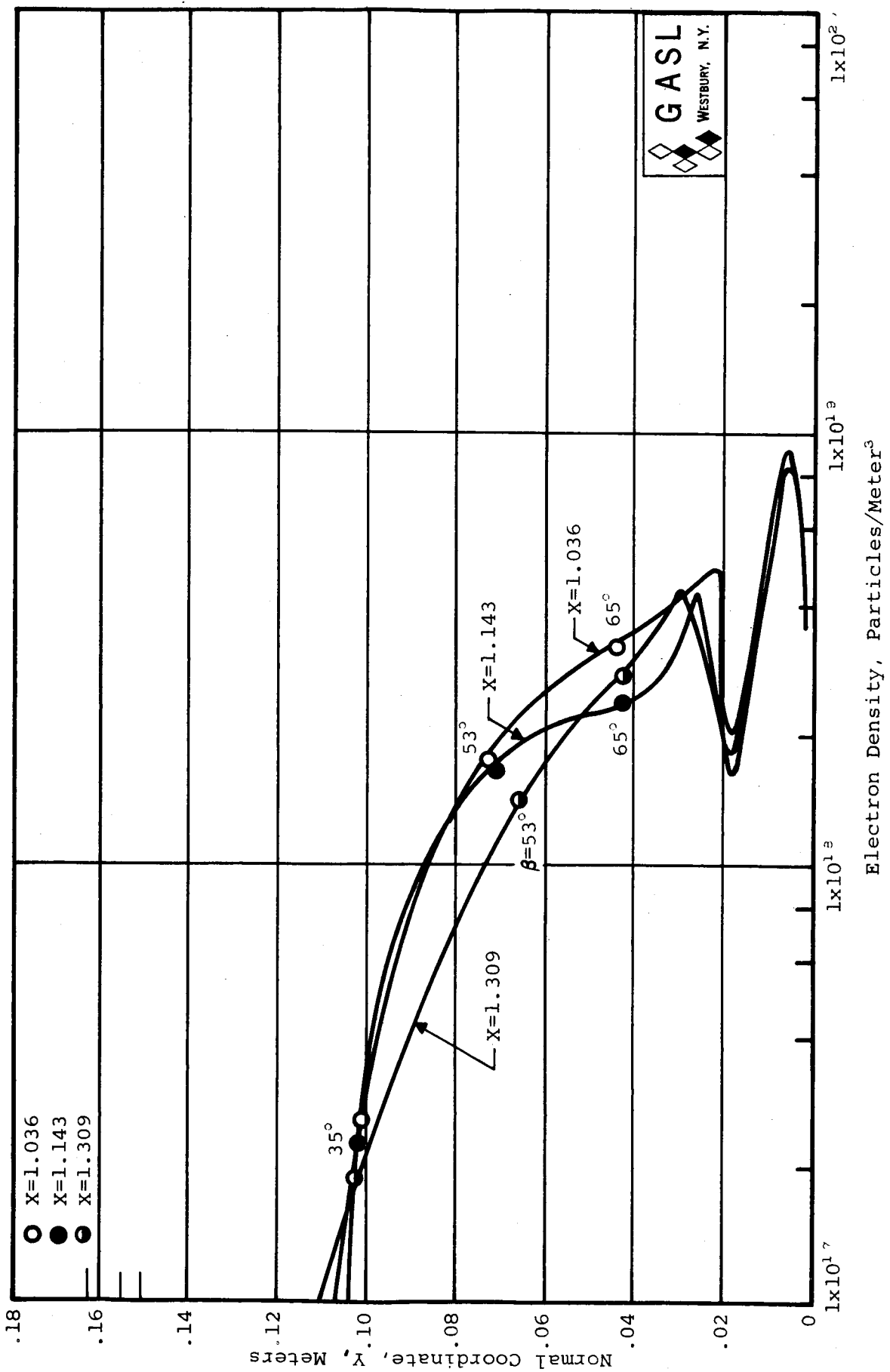
FIG. 17. ELECTRON DENSITY AT SURFACE COORDINATE LOCATIONS X=1.036, X=1.143, AND X=1.309 METERS, ALTITUDE = 36,800 METERS
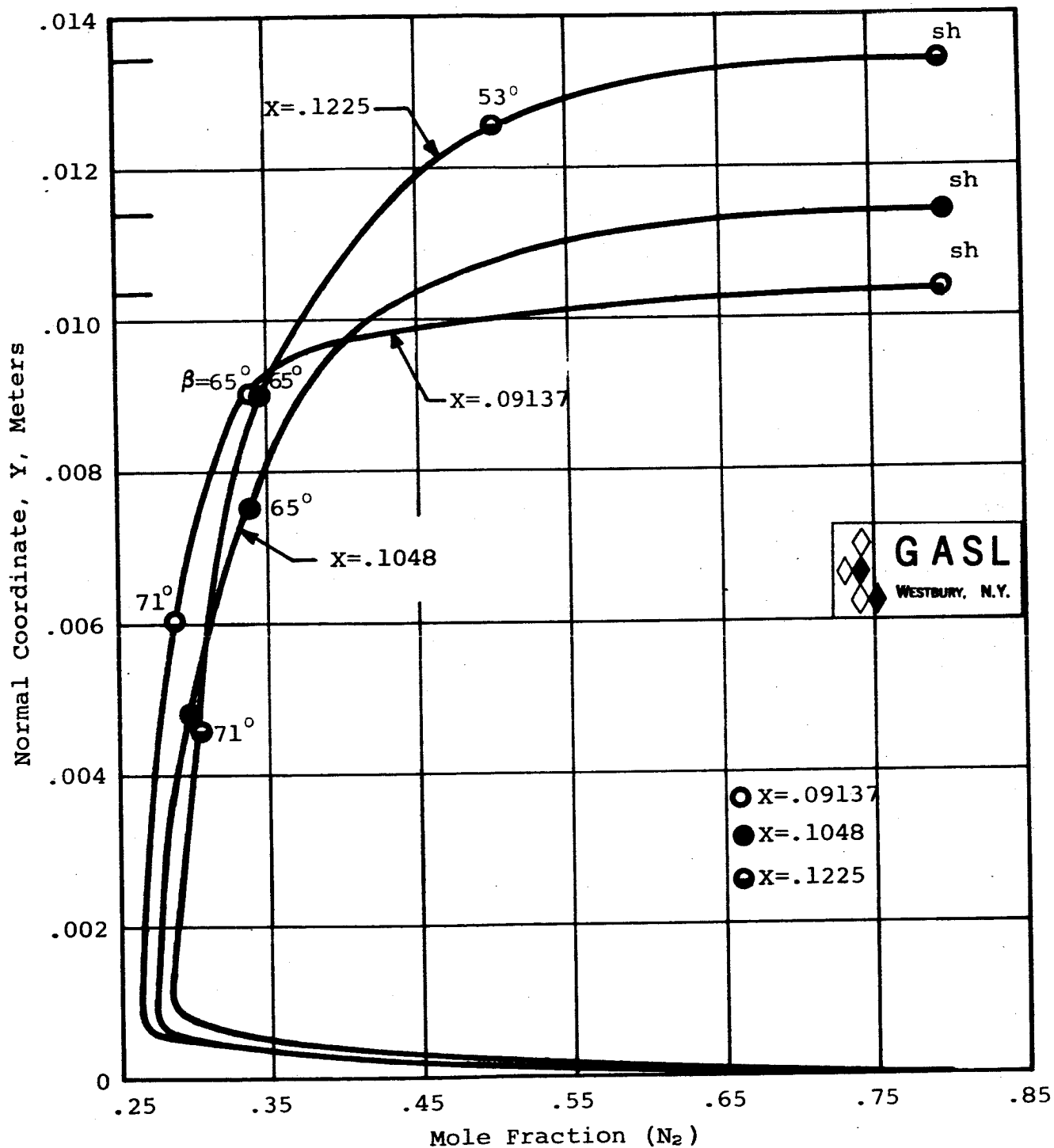
FIG. 18. SPECIE PROFILES (N_2) AT SURFACE COORDINATE
LOCATIONS X=.09137, X=.1048, AND X=.1225 METERS,
ALTITUDE = 36,800 METERS
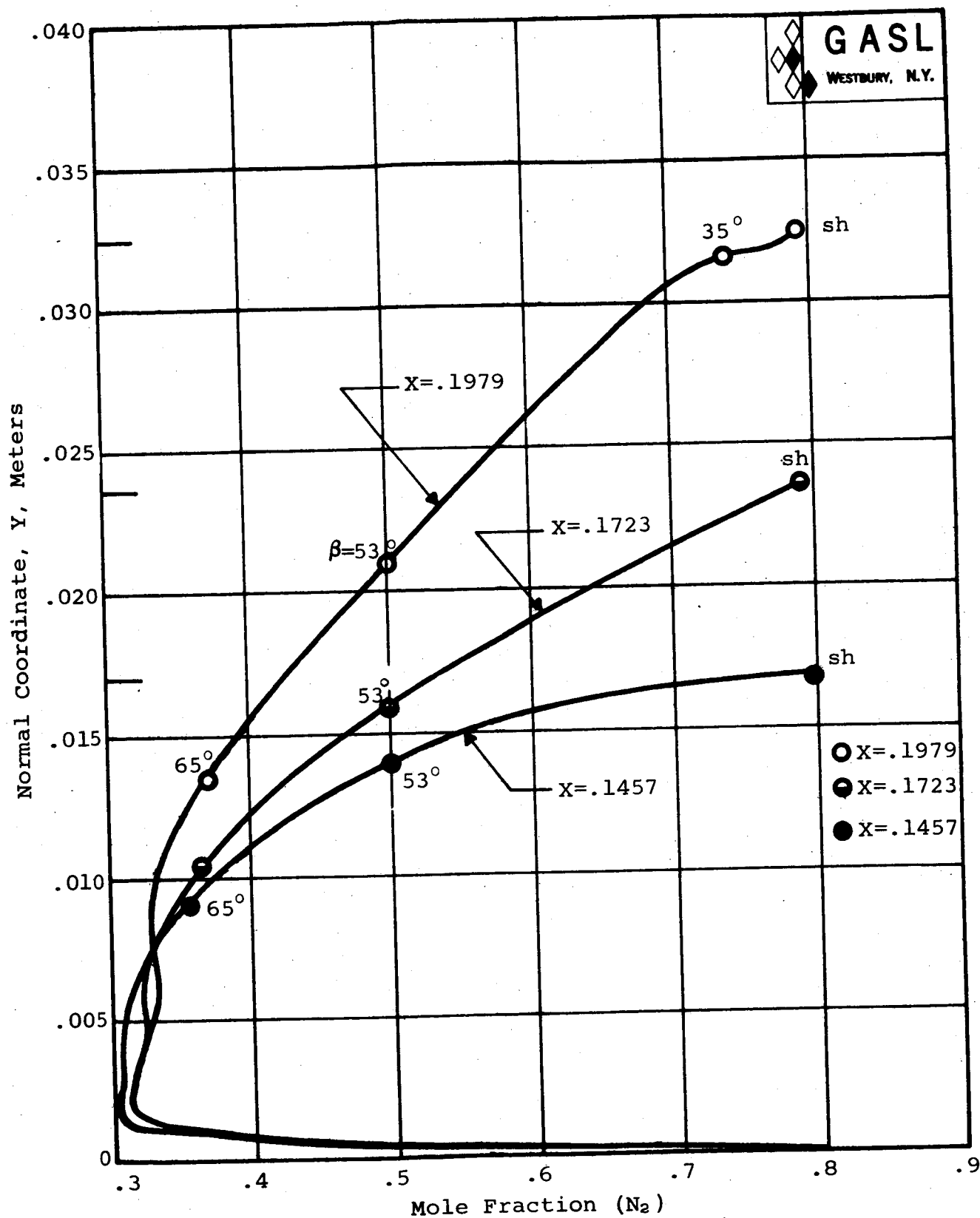
FIG. 19. SPECIE PROFILES (N_2) AT SURFACE COORDINATE LOCATIONS X=.1979, X=.1723, AND X=.1457 METERS, ALTITUDE = 36,800 METTERS
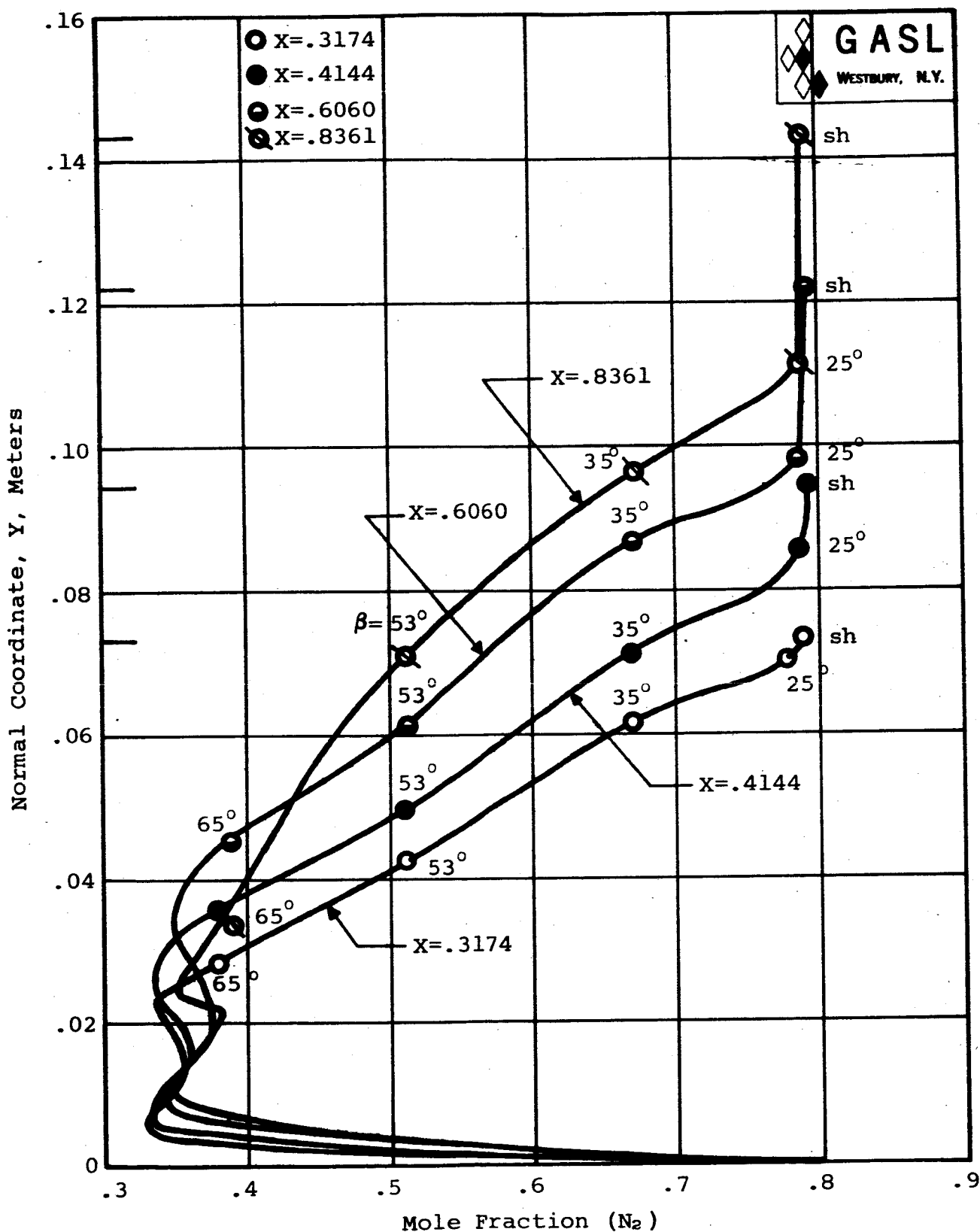
FIG. 20. SPECIE PROFILES (N_2) AT SURFACE COORDINATE
LOCATIONS X=.3174, X=.4144, X=.6060, AND
X=.8361 METERS, ALTITUDE = 36,800 METERS

51
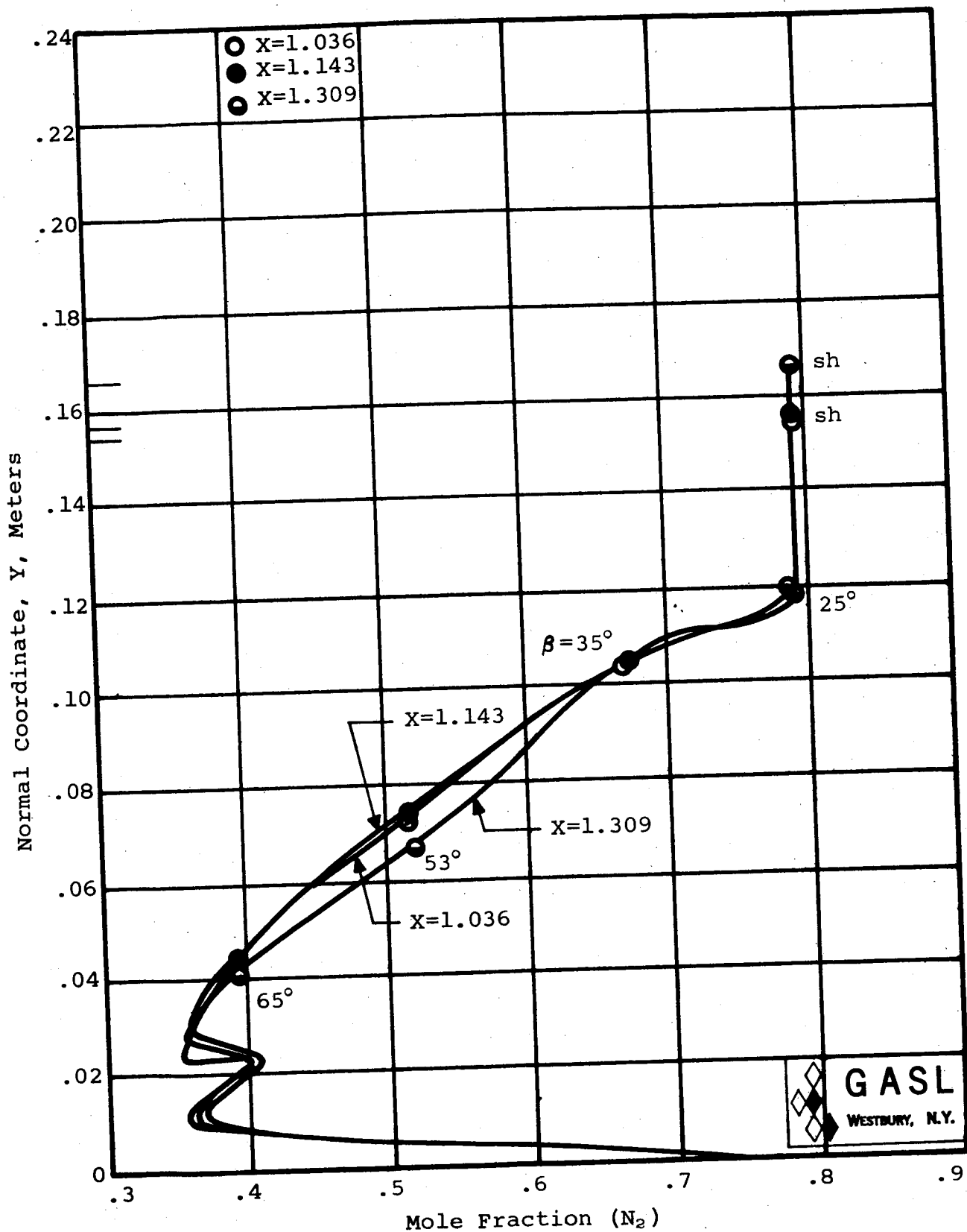
FIG. 21. SPECIE PROFILES (N_2) AT SURFACE COORDINATE
LOCATIONS X=1.036, X=1.143, AND X=1.309 METERS,
ALTITUDE = 36,800 METERS
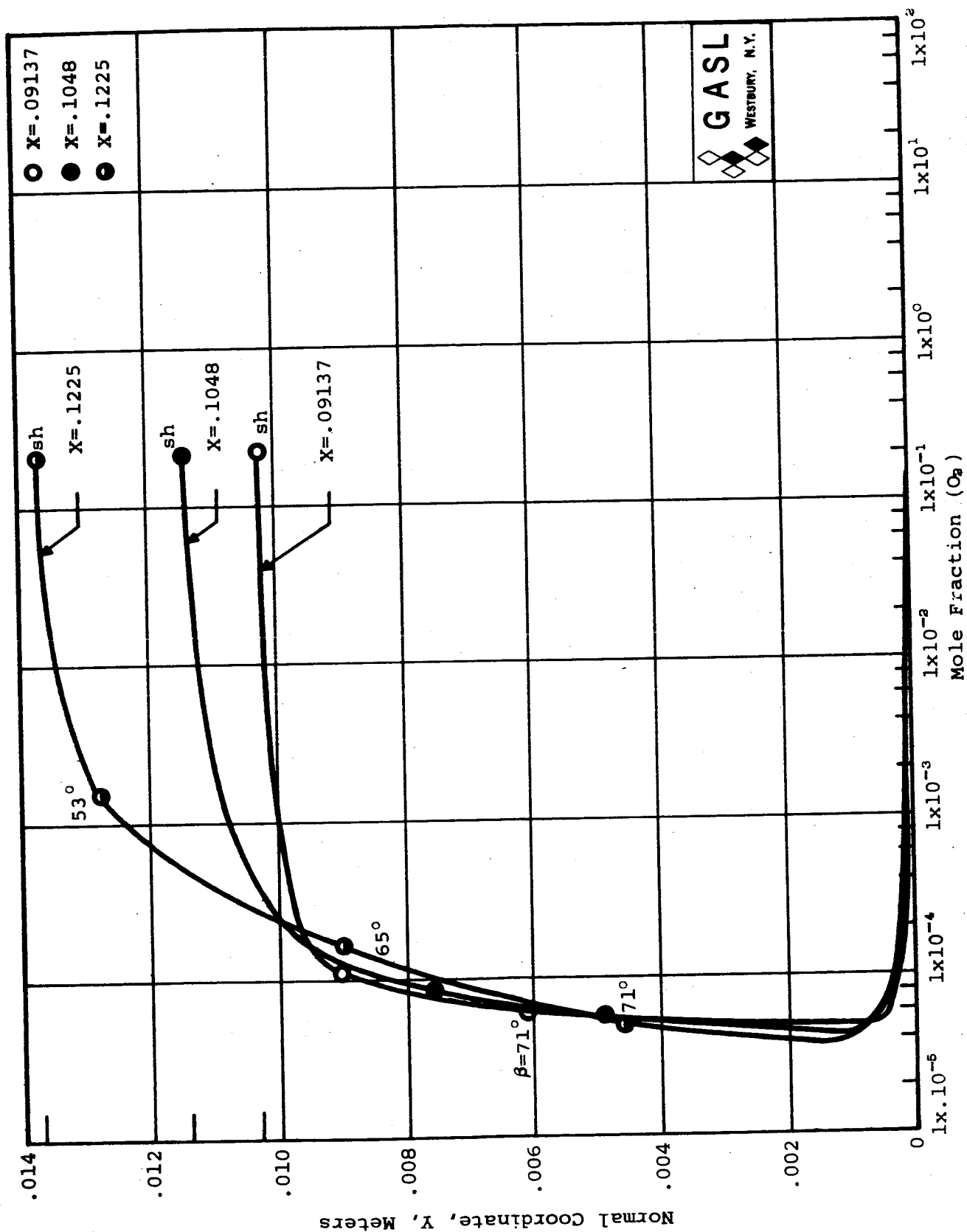
FIG. 22. SPECIE PROFILES (O_2) AT SURFACE COORDINATE LOCATIONS X=.09137, X=.1048, AND X=.1225 METERS, ALTITUDE = 36,800 METERS
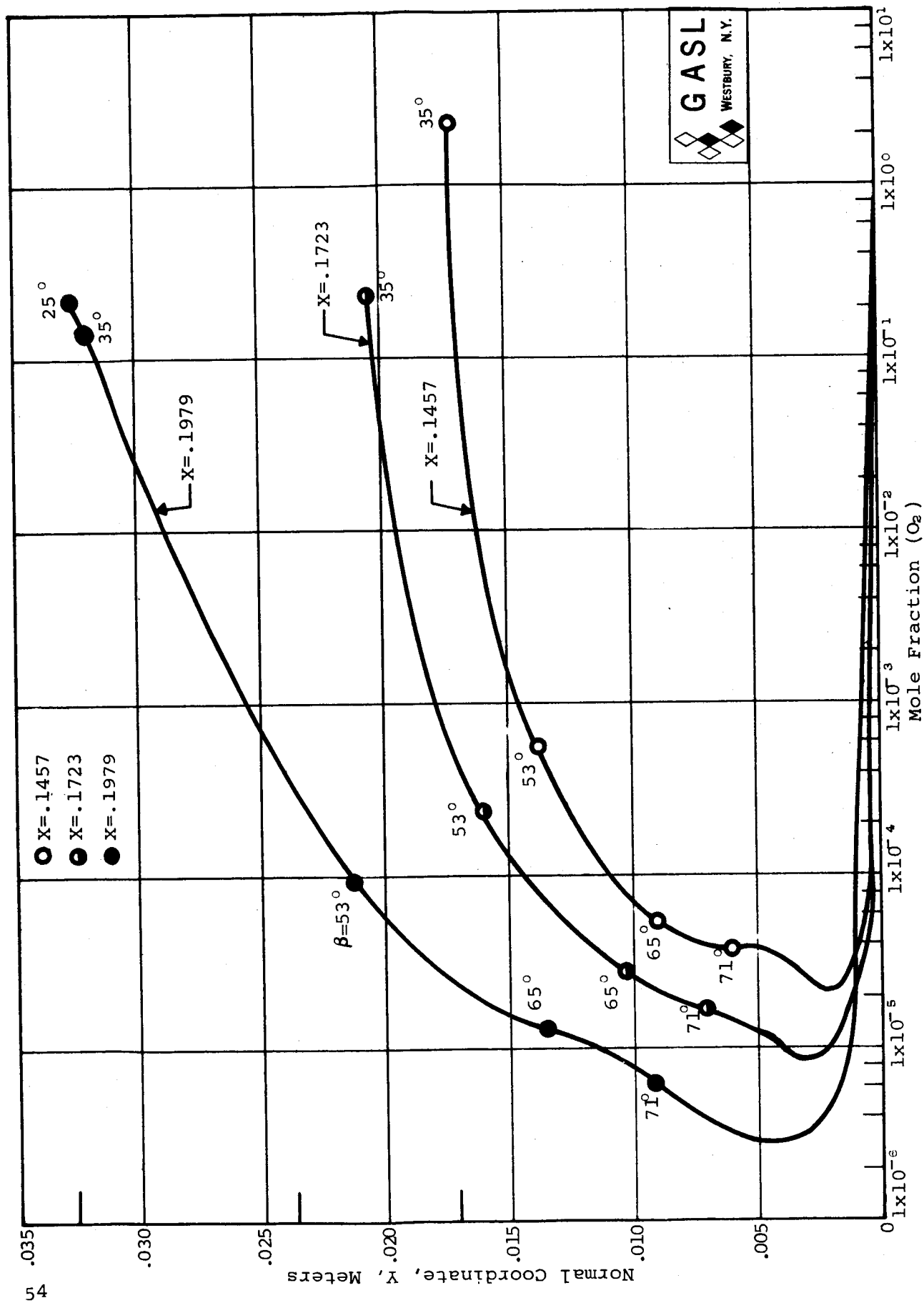
FIG. 23. SPECIE PROFILES (O_2) AT SURFACE COORDINATE LOCATIONS X=.1457, X=.1723, AND X=.1979 METERS, ALTITUDE = 36,800 METERS.

54
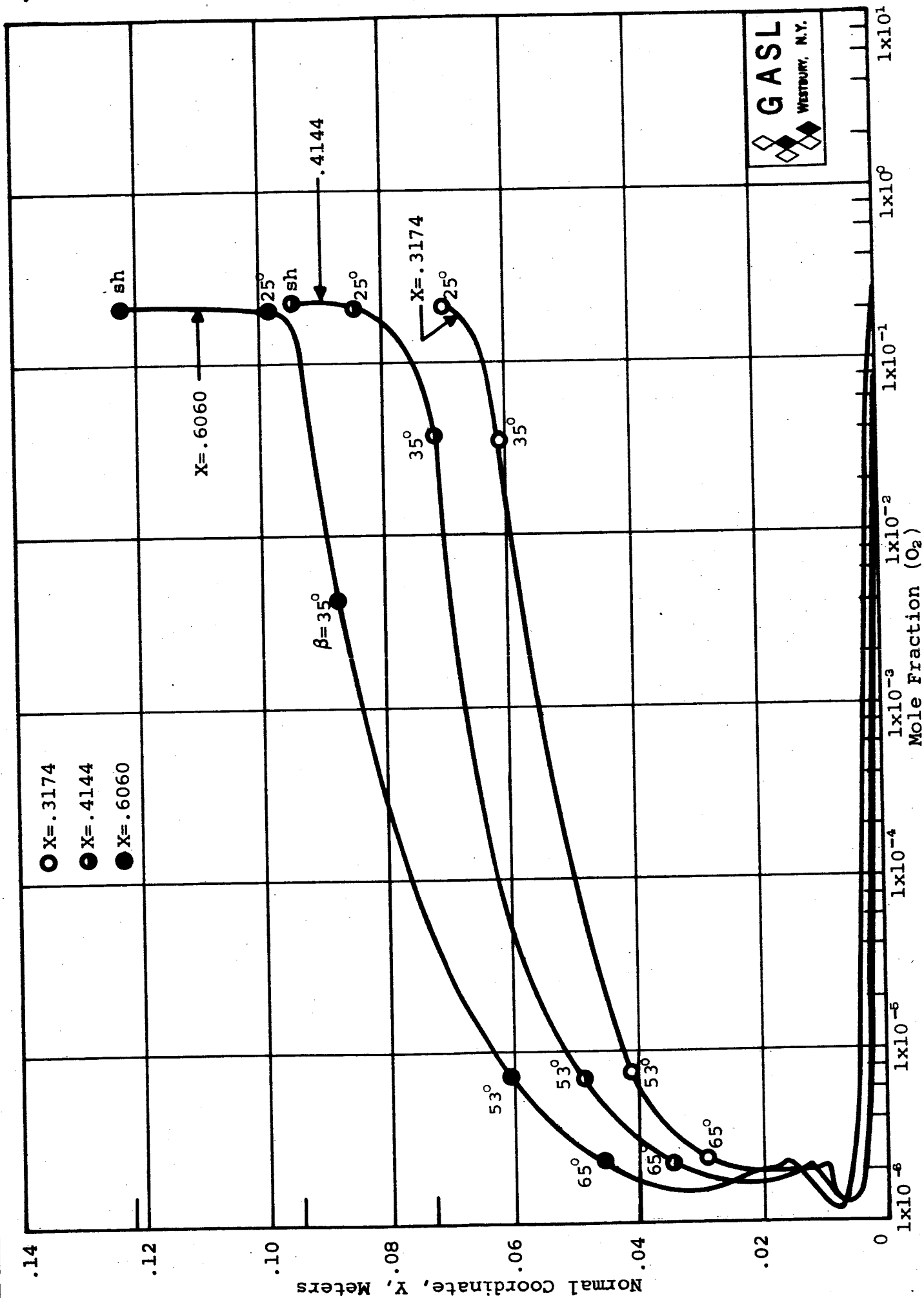
FIG. 24. SPECIE PROFILES (O_2) AT SURFACE COORDINATE LOCATIONS X=.3174, X=.4144, AND X=.6060 METERS, ALTITUDE = 36,800 METERS

55
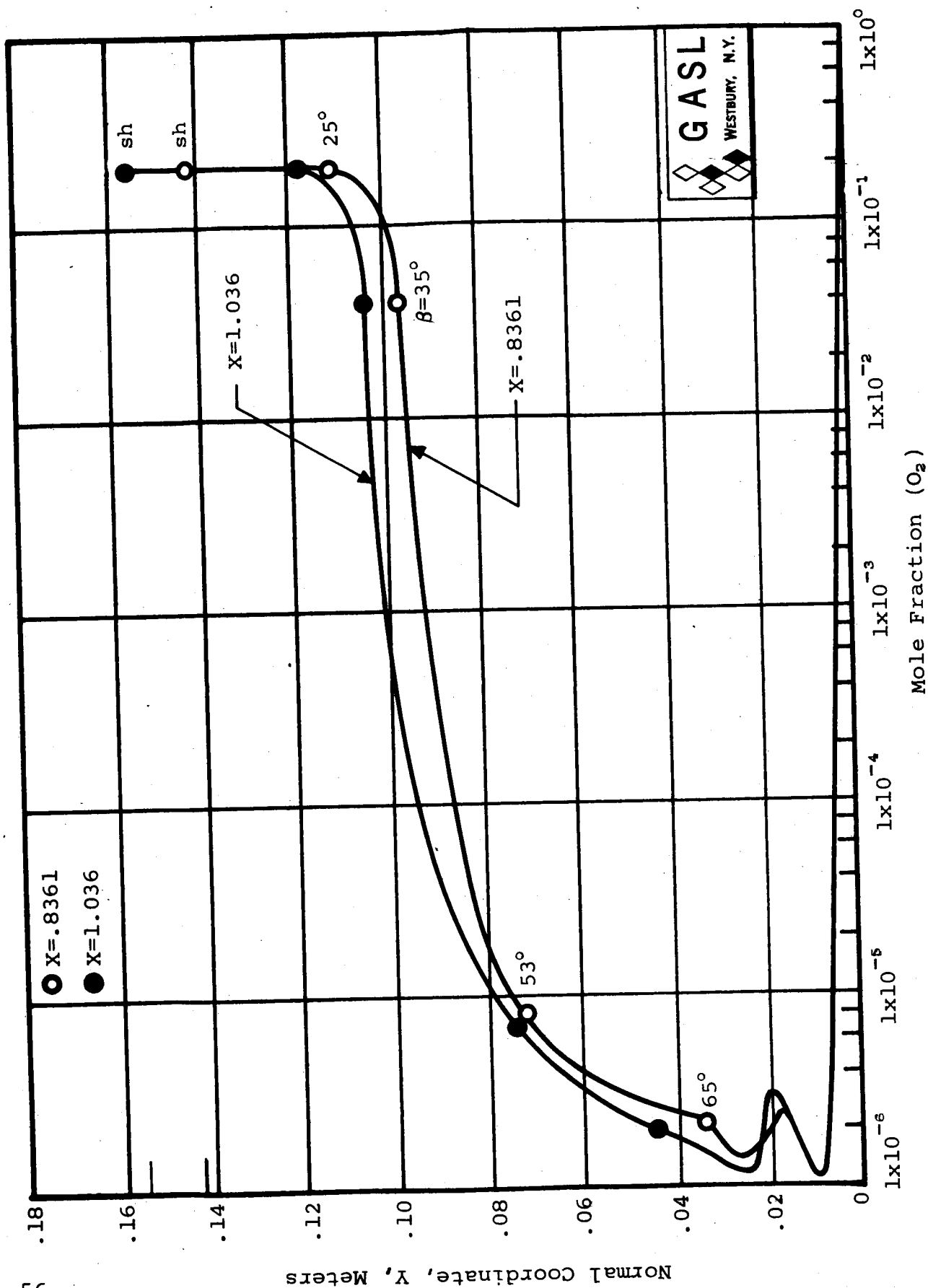
FIG. 25. SPECIE PROFILES (O_2) AT SURFACE COORDINATE LOCATIONS X=.8361, AND X=1.036 METERS, ALTITUDE = 36,800 METERS

56
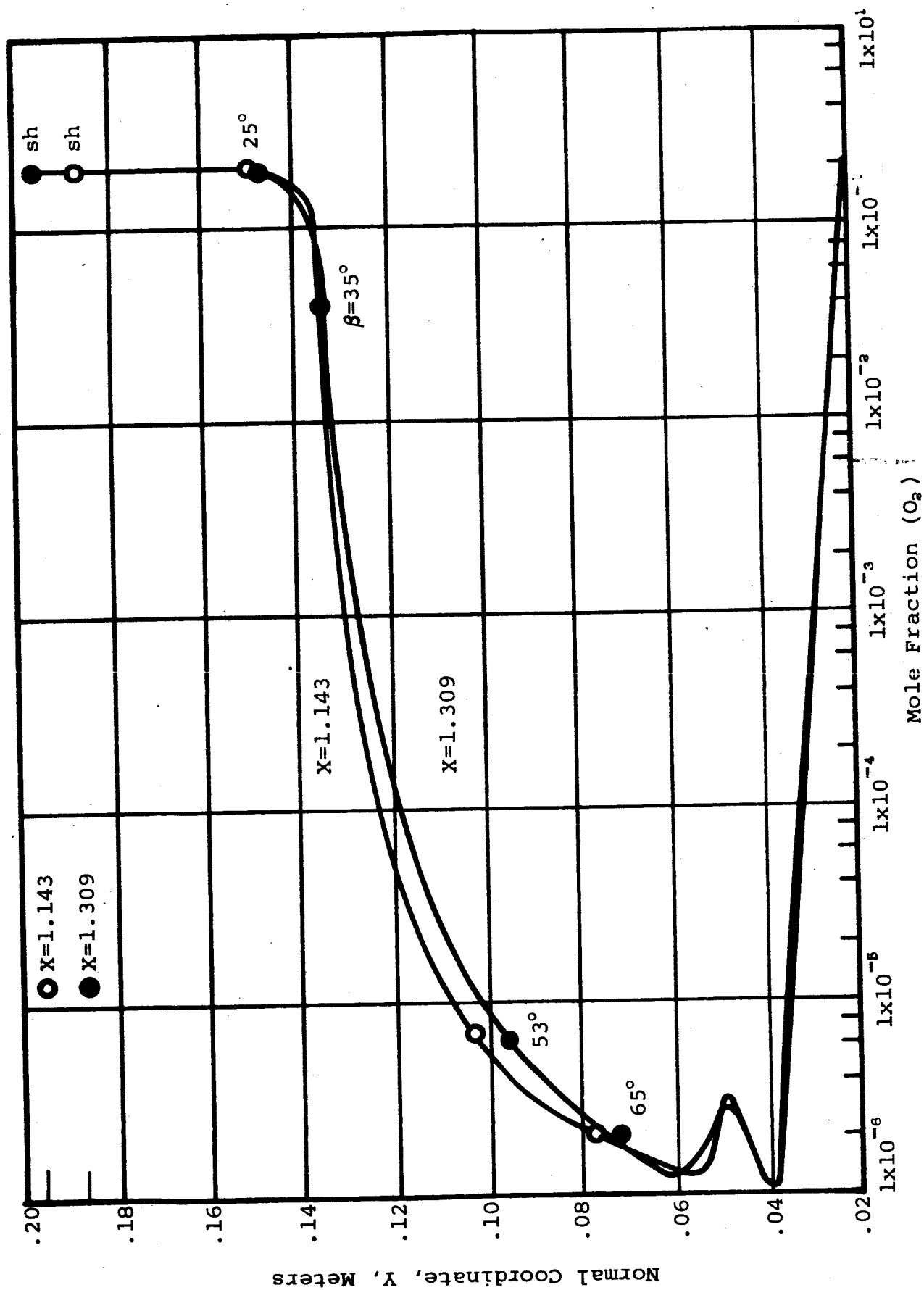
FIG. 26. SPECIE PROFILES (O_2) AT SURFACE COORDINATE LOCATIONS X=1.143 AND X=1.309 METERS, ALTITUDE = 36,800 METERS

57
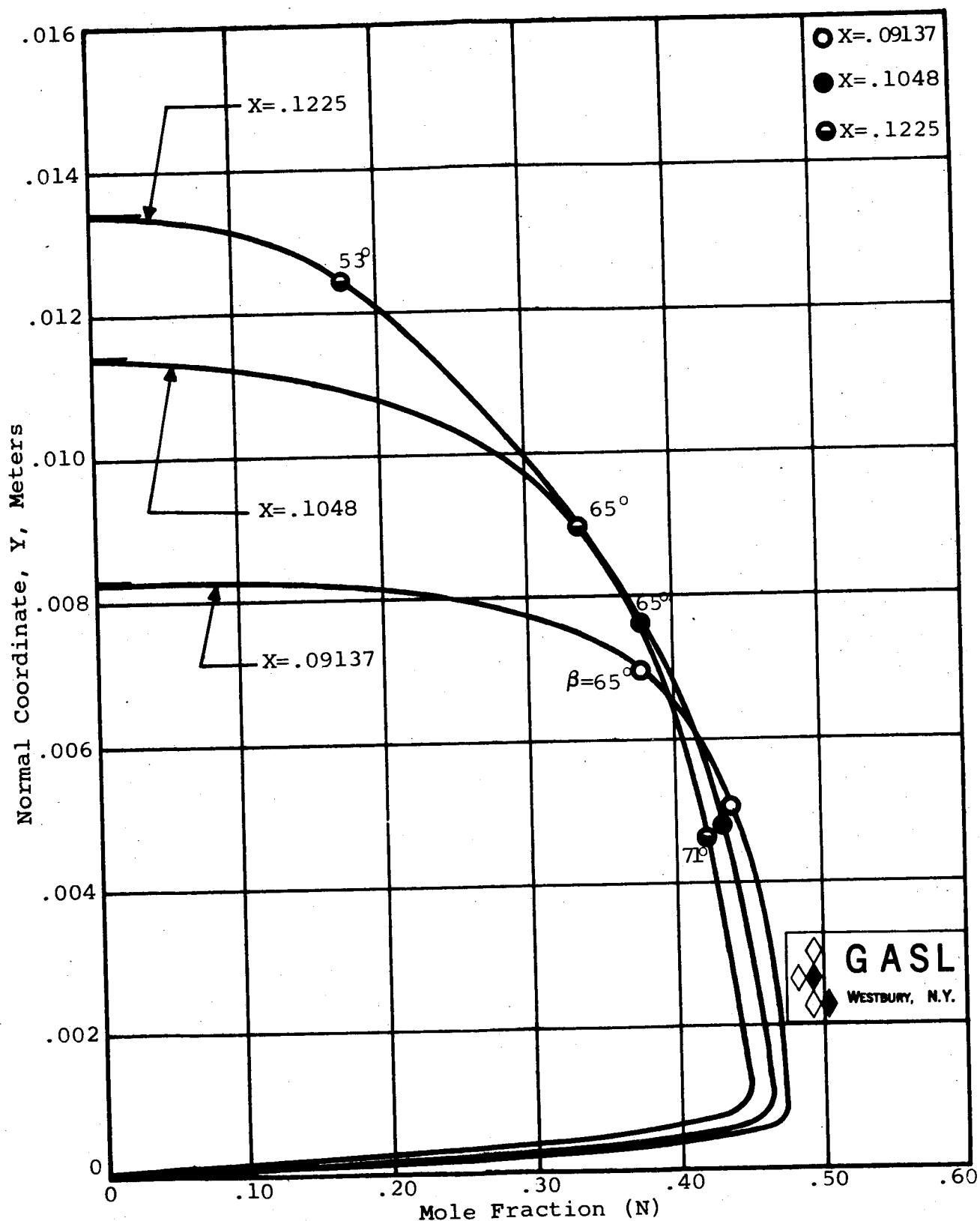
FIG. 27. SPECIE PROFILES (N) AT SURFACE COORDINATE
LOCATIONS X=.09137, X=.1048, AND X=.1225
METERS, ALTITUDE = 36,800 METERS
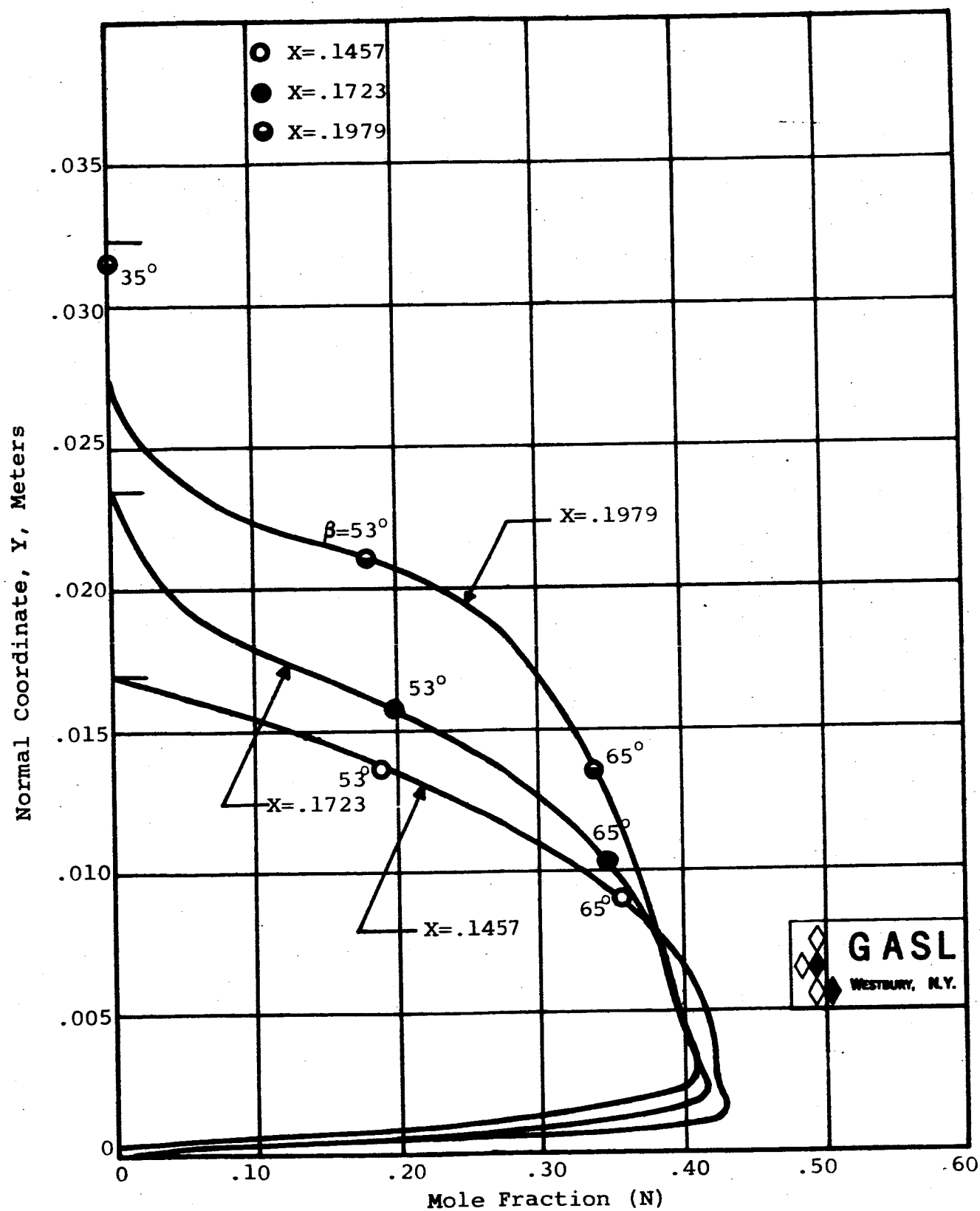
FIG. 28. SPECIE PROFILES (N) AT SURFACE COORDINATE
LOCATIONS X=.1457, X=.1723, AND X=.1979
METERS, ALTITUDE = 36,800 METERS

59
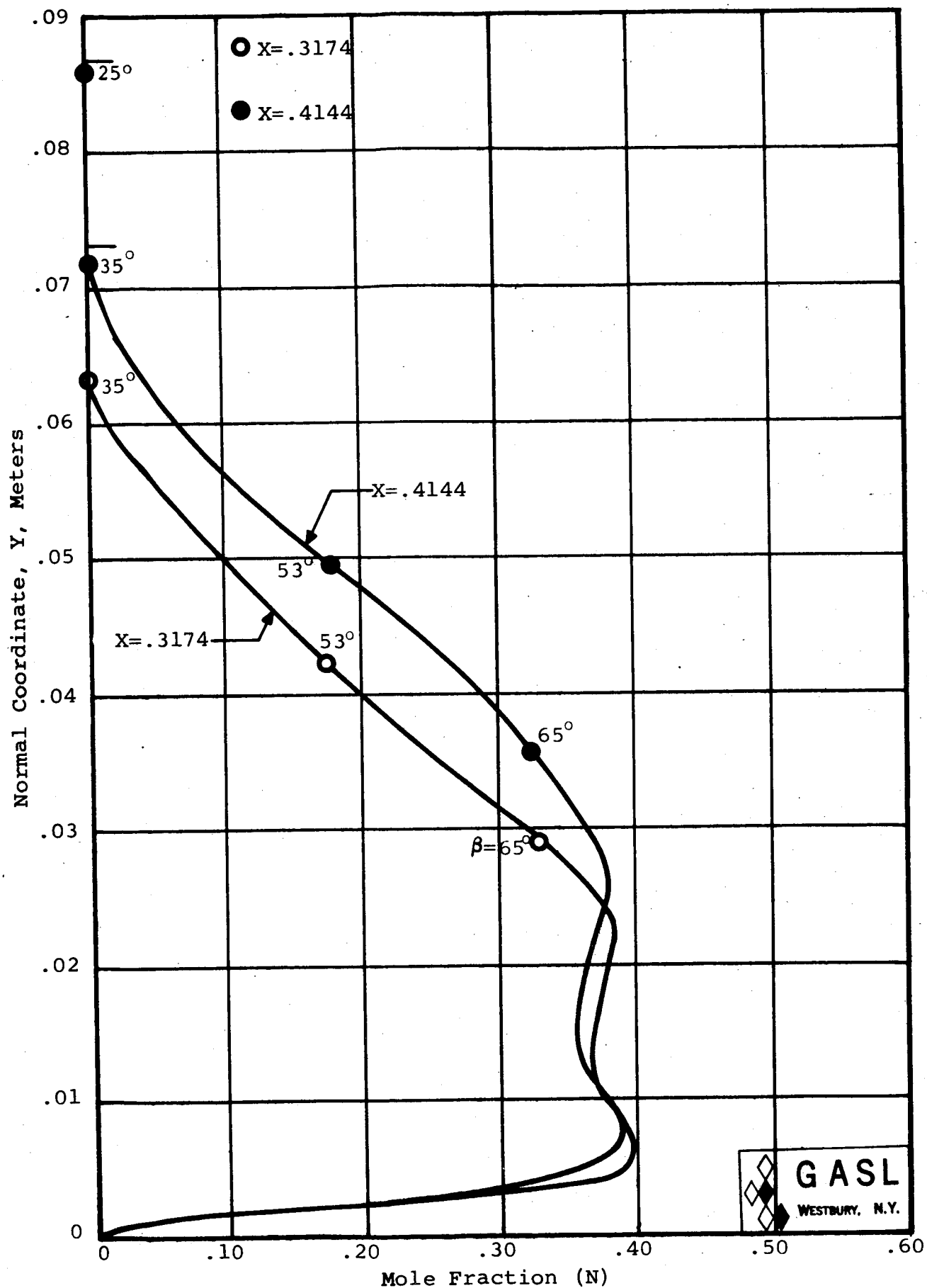
FIG. 29. SPECIE PROFILES (N) AT SURFACE COORDINATE
LOCATIONS X=.3174 AND X=.4144 METERS,
ALTITUDE = 36,800 METERS

60
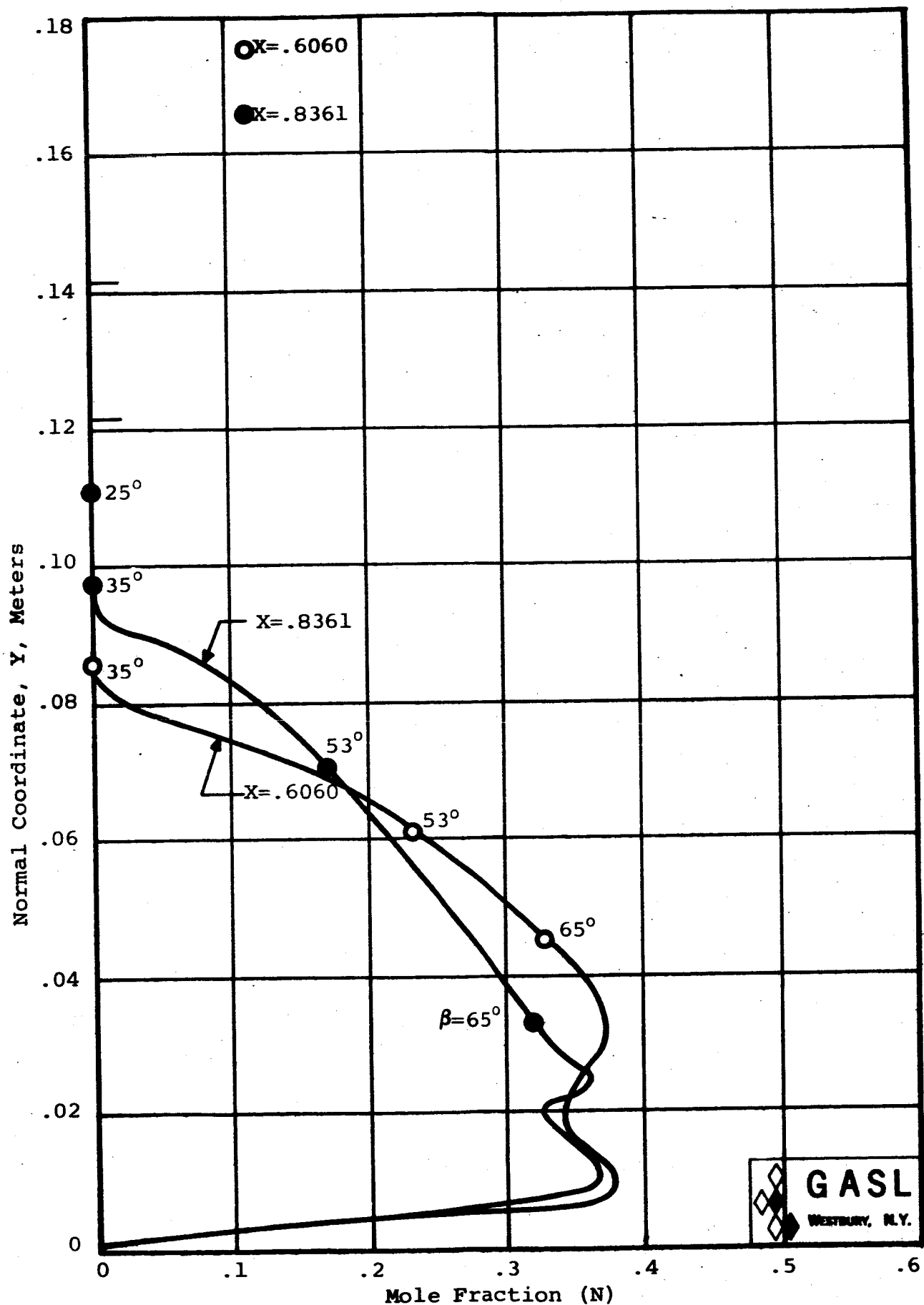
FIG. 30. SPECIE PROFILES (N) AT SURFACE COORDINATE
LOCATIONS X=.6060 AND X=.8361 METERS,
ALTITUDE = 36,800 METERS

61
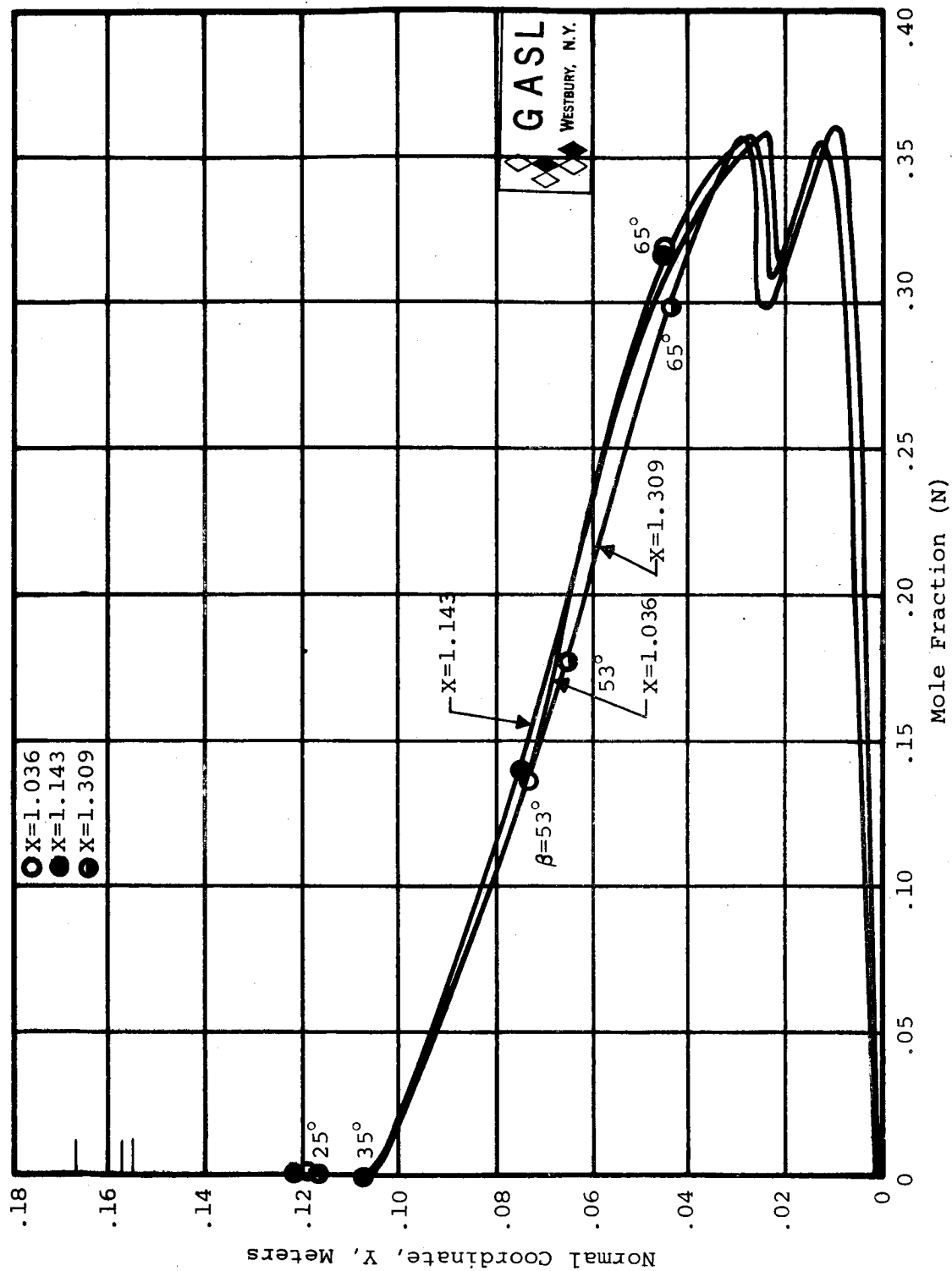
FIG. 31. SPECIE PROFILES (N) AT SURFACE COORDINATE LOCATIONS X=1.036, X=1.143, AND X=1.309 METERS, ALTITUDE = 36,800 METERS

62
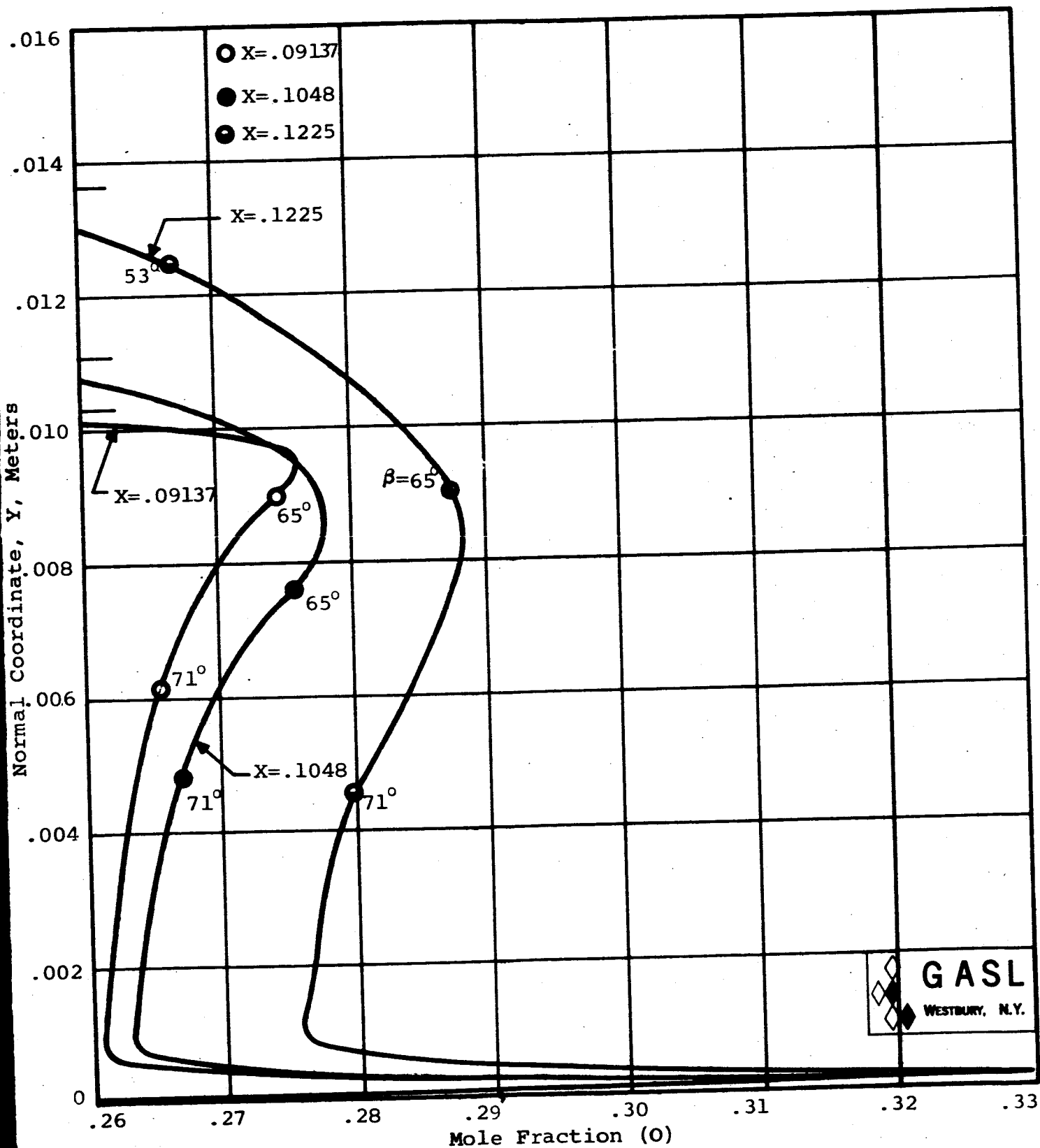
FIG. 32. SPECIE PROFILES (O) AT SURFACE COORDINATE
LOCATIONS X=.09137, X=.1048, AND X=.1225
METERS, ALTITUDE = 36,800 METERS
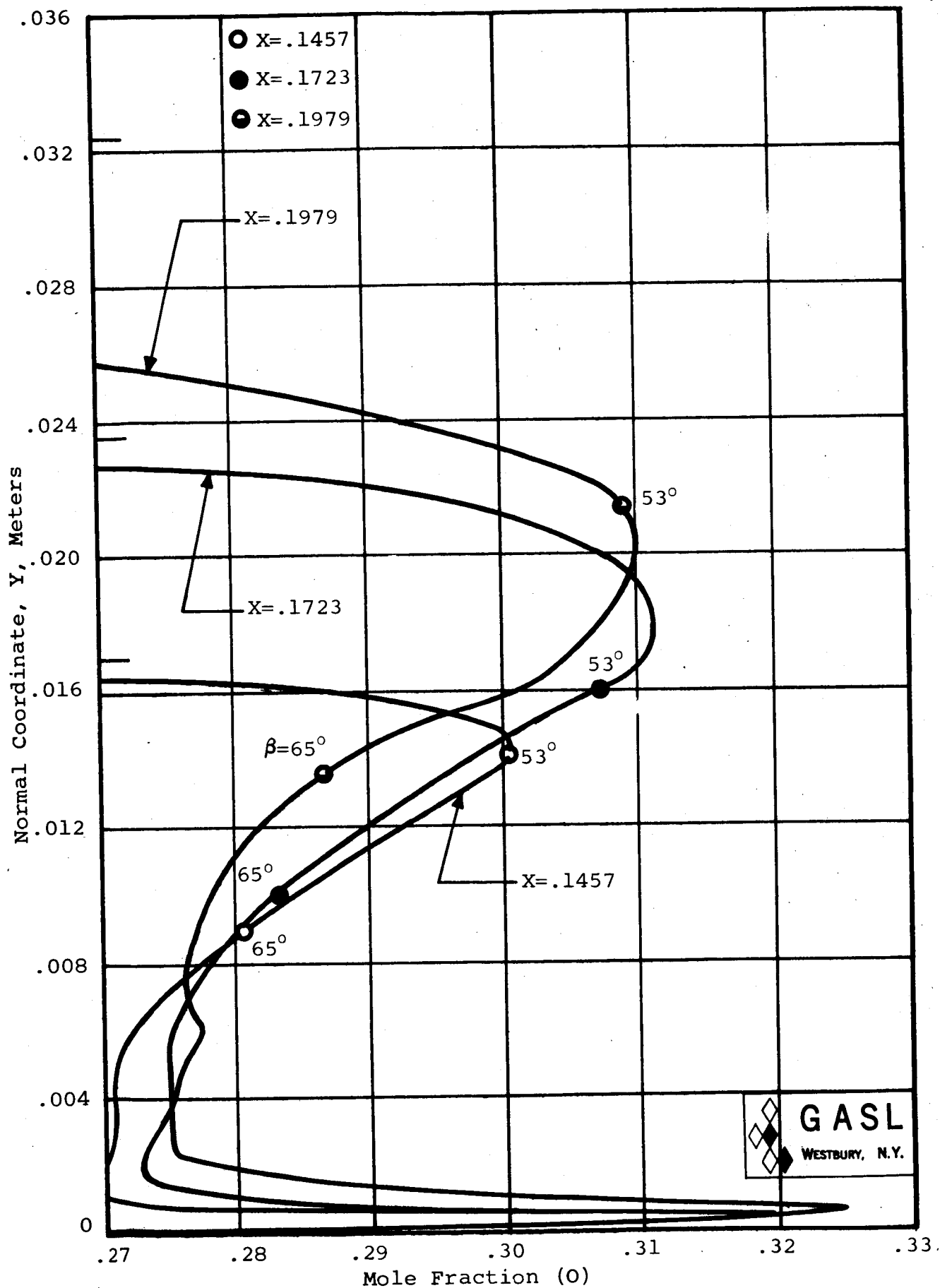
FIG. 33. SPECIE PROFILES (O) AT SURFACE COORDINATE
LOCATIONS X=.1457, X=.1723, AND X=.1979
METERS, ALTITUDE = 36,800 METERS
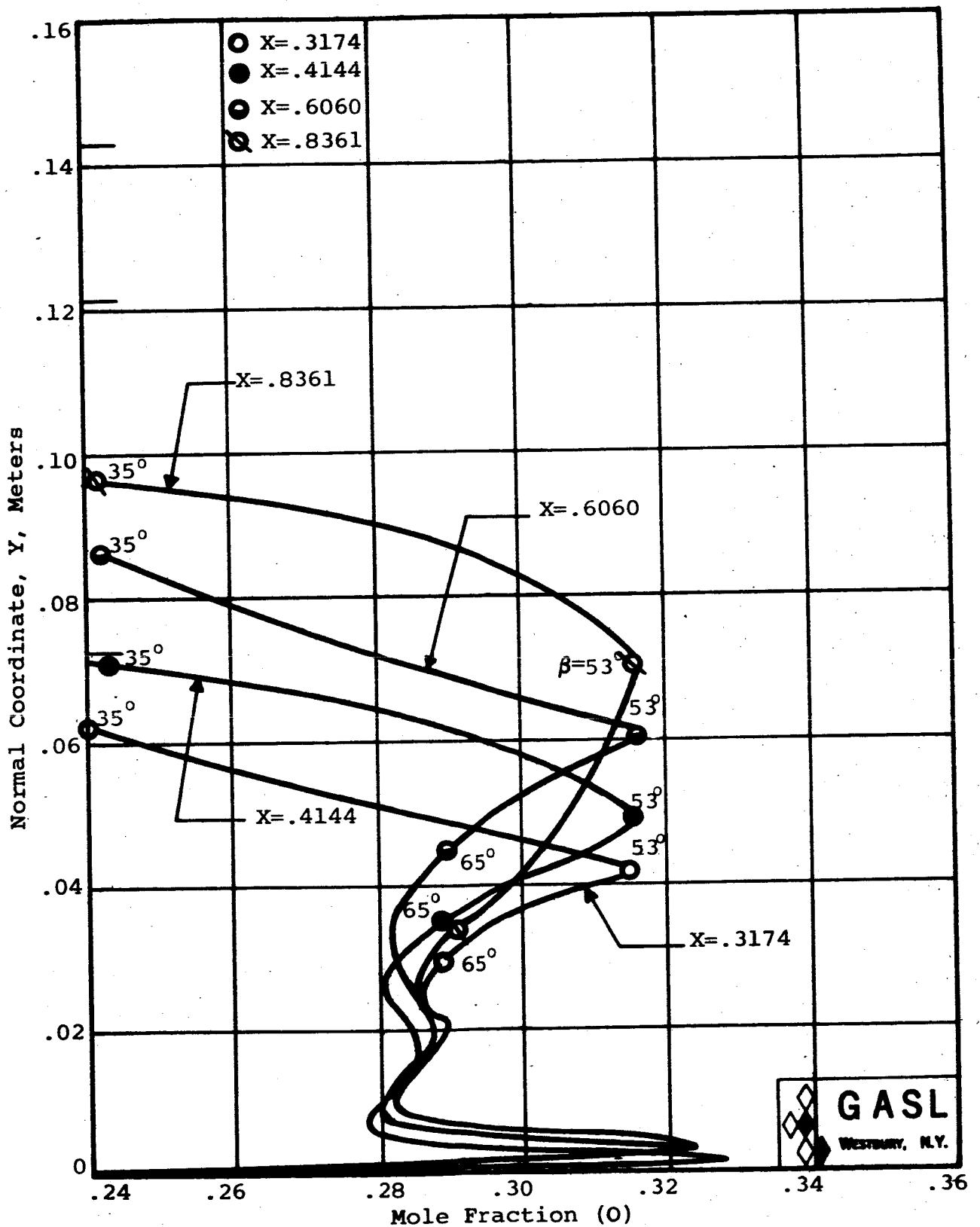
FIG. 34. SPECIES PROFILES (O) AT SURFACE COORDINATE
LOCATIONS X=.3174, X=.4144, X=.6060, AND
X=.8361 METERS, ALTITUDE = 36,800 METERS

65
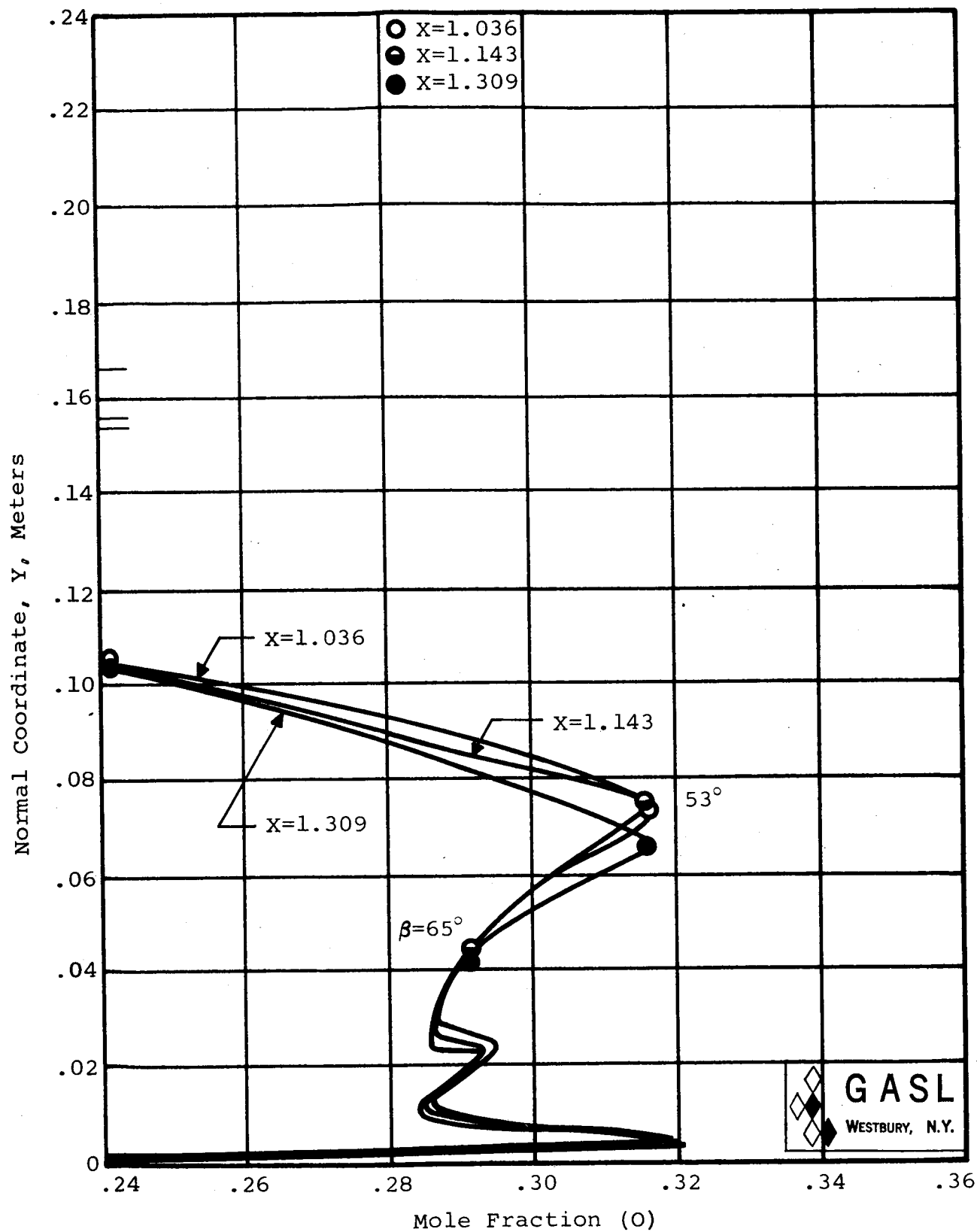
FIG. 35. SPECIE PROFILES (O) AT SURFACE COORDINATE LOCATIONS X=1.036, X=1.143 AND X=1.309 METERS, ALTITUDE = 36,800 METERS
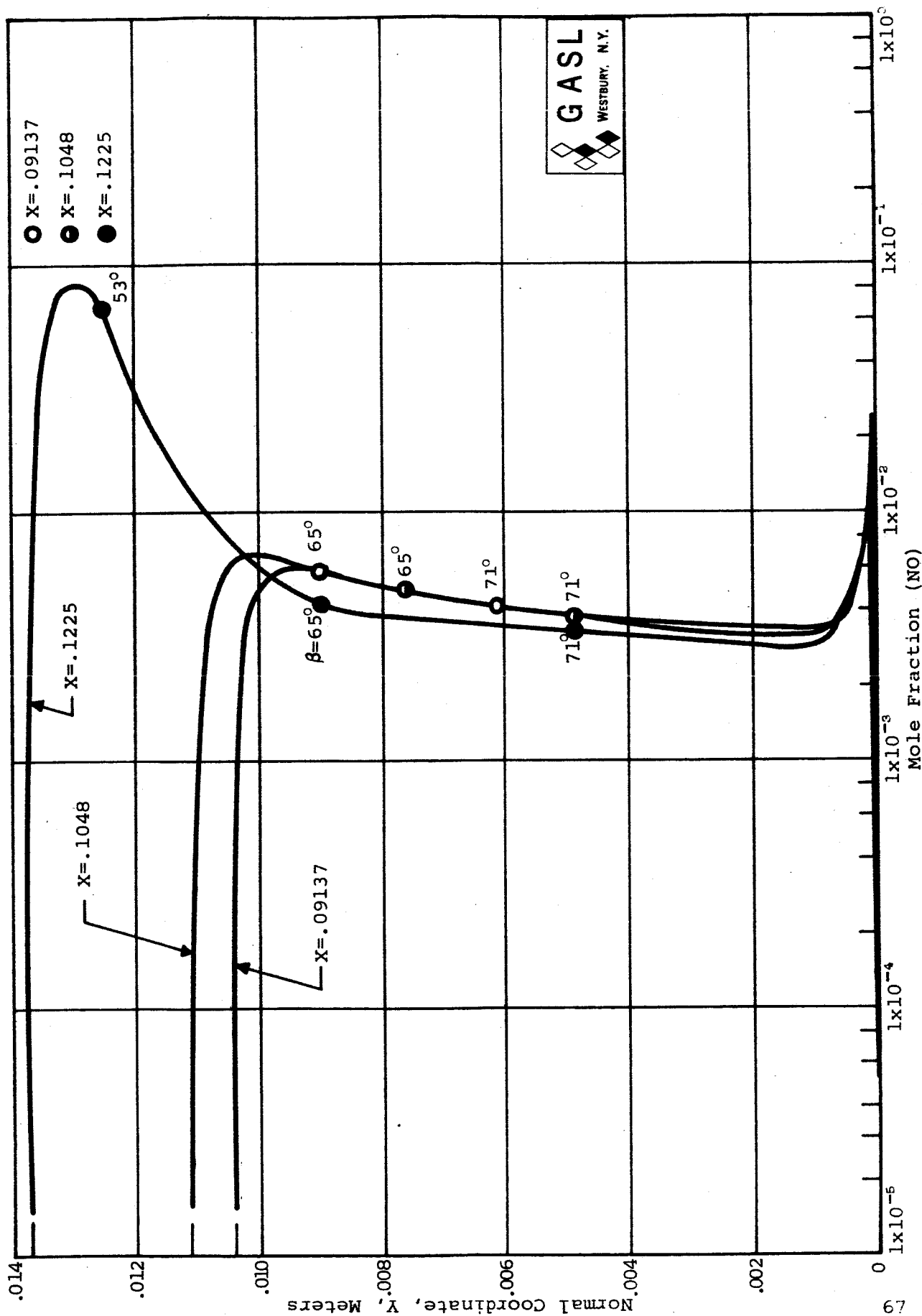
FIG. 36.   SPECIE PROFILES (NO) AT SURFACE COORDINATE LOCATIONS X=.09137, X=.1048, AND X=.1225
METERS, ALTITUDE = 36,800 METERS

67
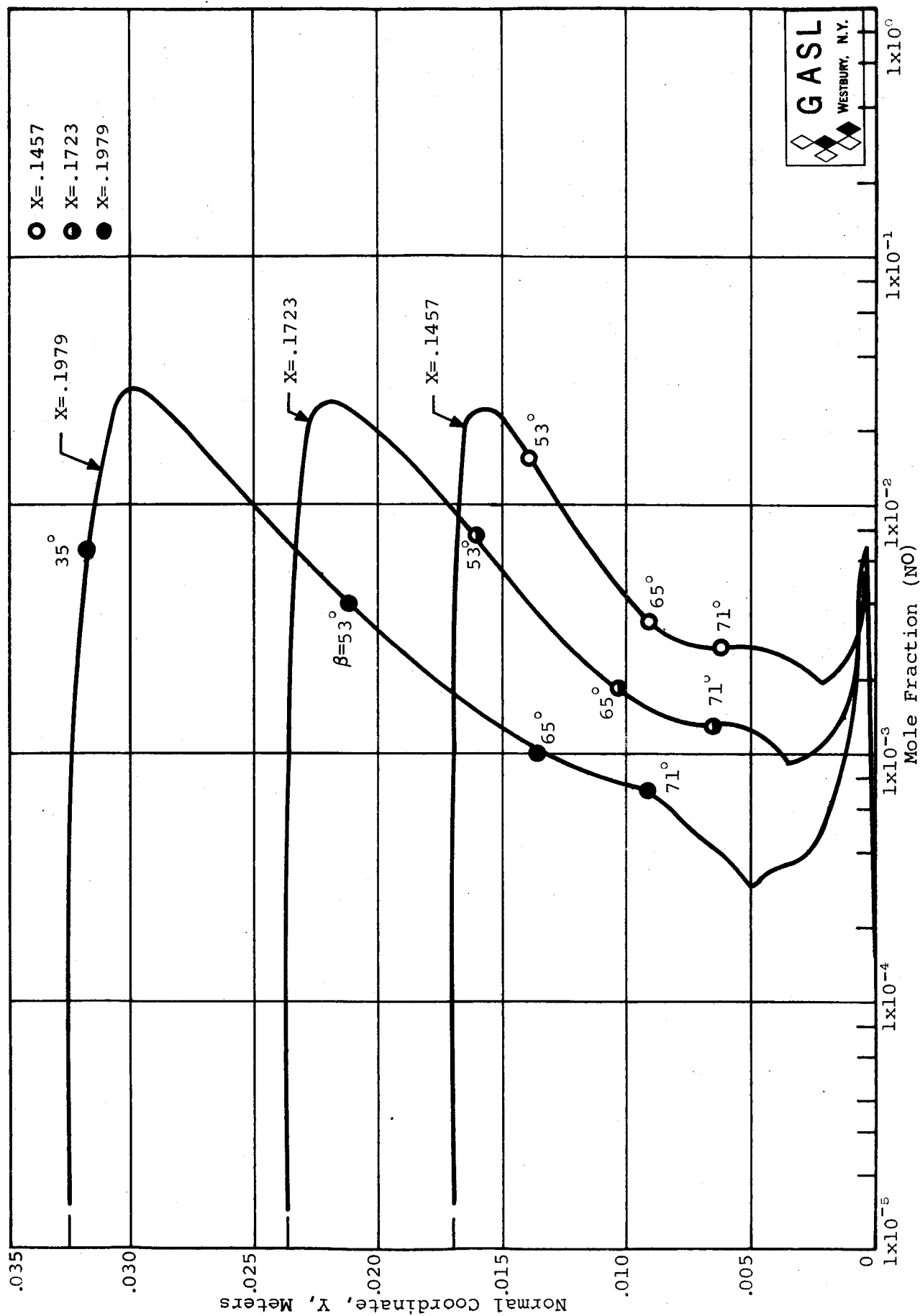
FIG. 37. SPECIE PROFILES (NO) AT SURFACE COORDINATE LOCATIONS X=.1457, X=.1723
X=.1979 METERS, ALTITUDE = 36,800 METERS

68

FIG. 38. SPECIE PROFILES (NO) AT SURFACE COORDINATE LOCATIONS X=.8361, X=.4144, X=.3174, AND X=.6060 METERS, ALTITUDE = 36,800 METERS

69
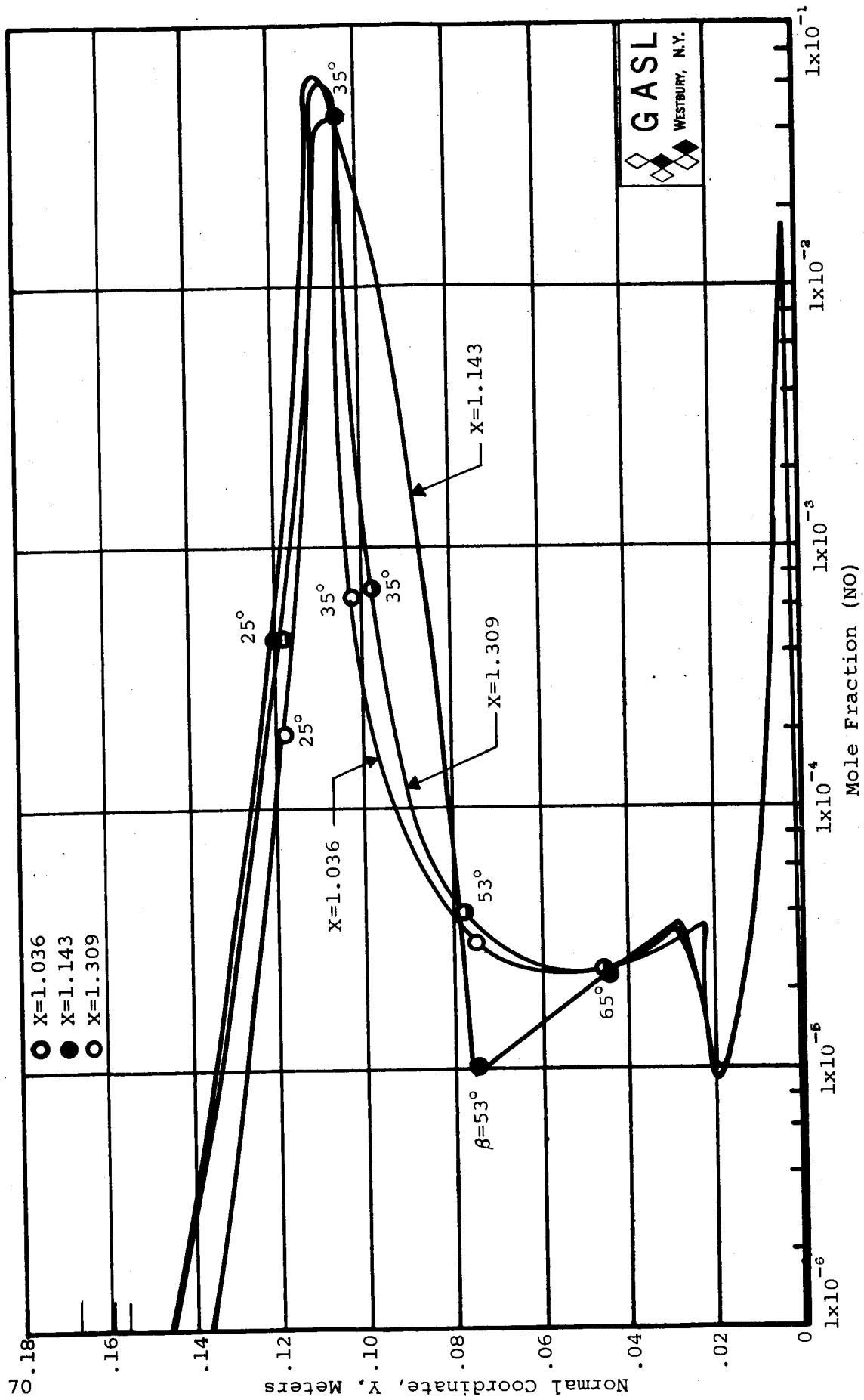
FIG. 39. SPECIE PROFILES (NO) AT SURFACE COORDINATE LOCATIONS X=1.036, X=1.143, AND X=1.309 METERS, ALTITUDE = 36,800 METERS

70
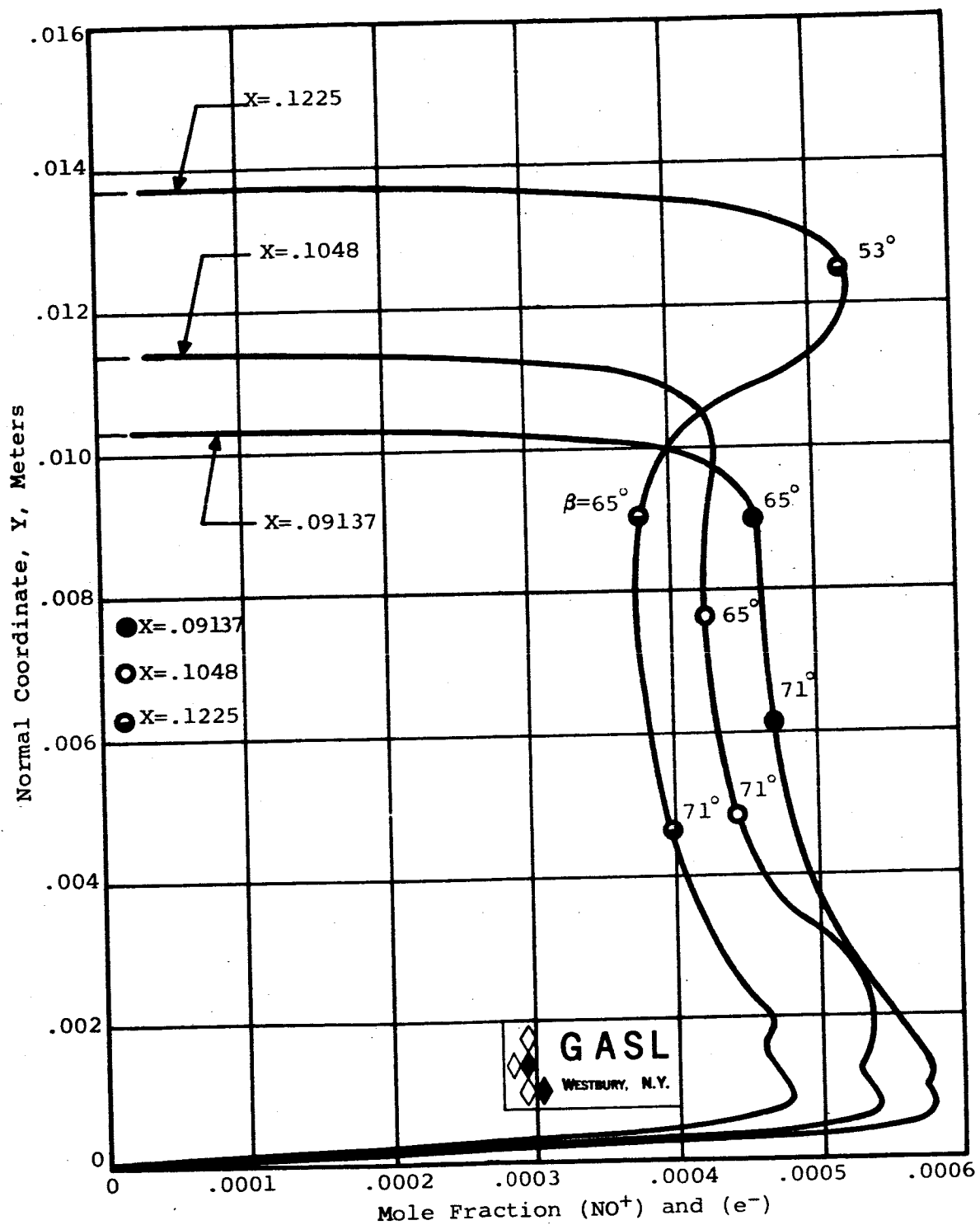
FIG. 40. SPECIE PROFILES (NO⁺) AND (e⁻) AT SURFACE
COORDINATE LOCATIONS X=.09137, X=.1048,
AND X=.1225 METERS, ALTITUDE = 36,800 METERS   71
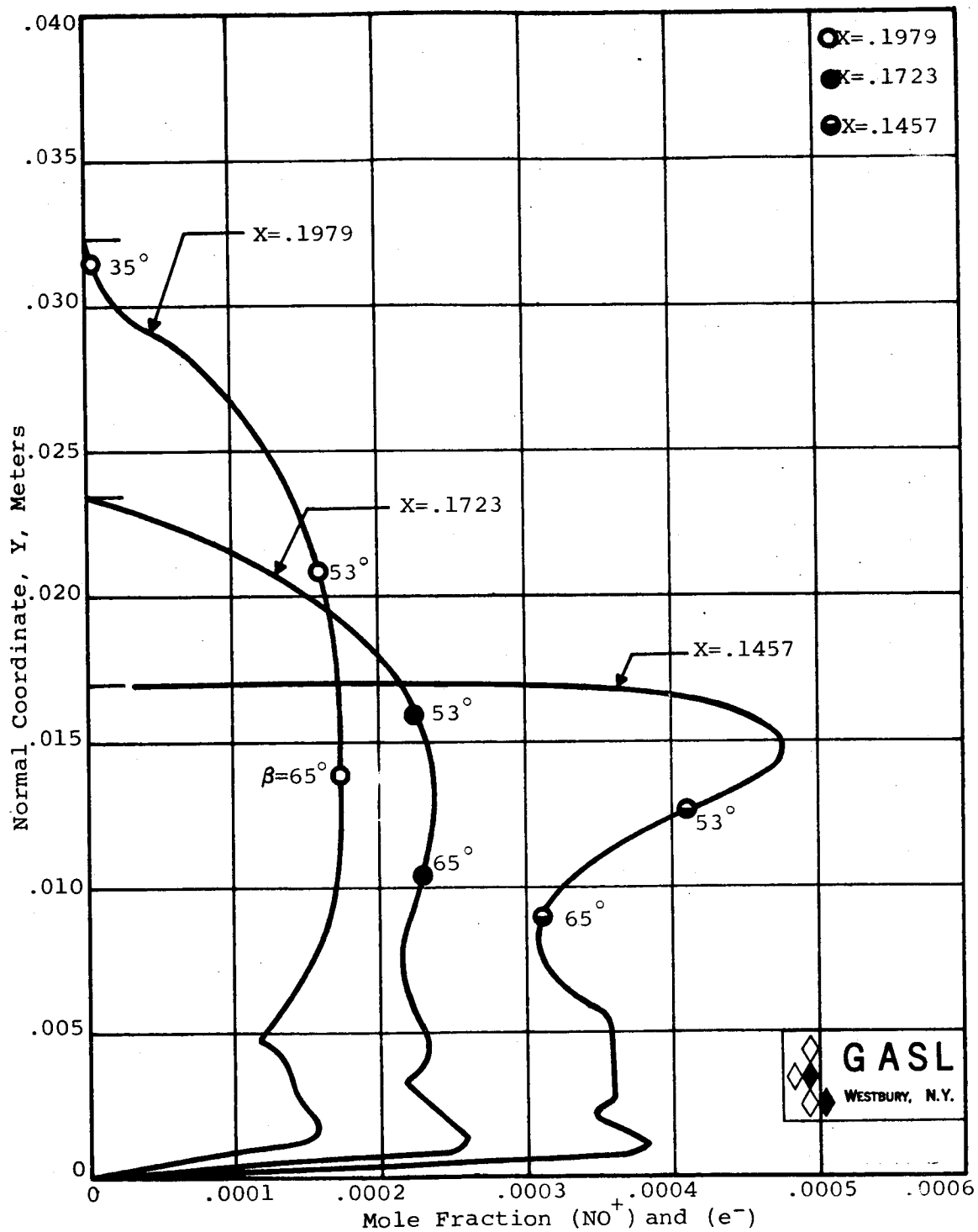
FIG. 41. SPECIE PROFILES (NO⁺) AND (e⁻) AT SURFACE
COORDINATE LOCATIONS X=.1979, X=.1723, AND
X=.1457 METERS, ALTITUDE = 36,000 METERS

72
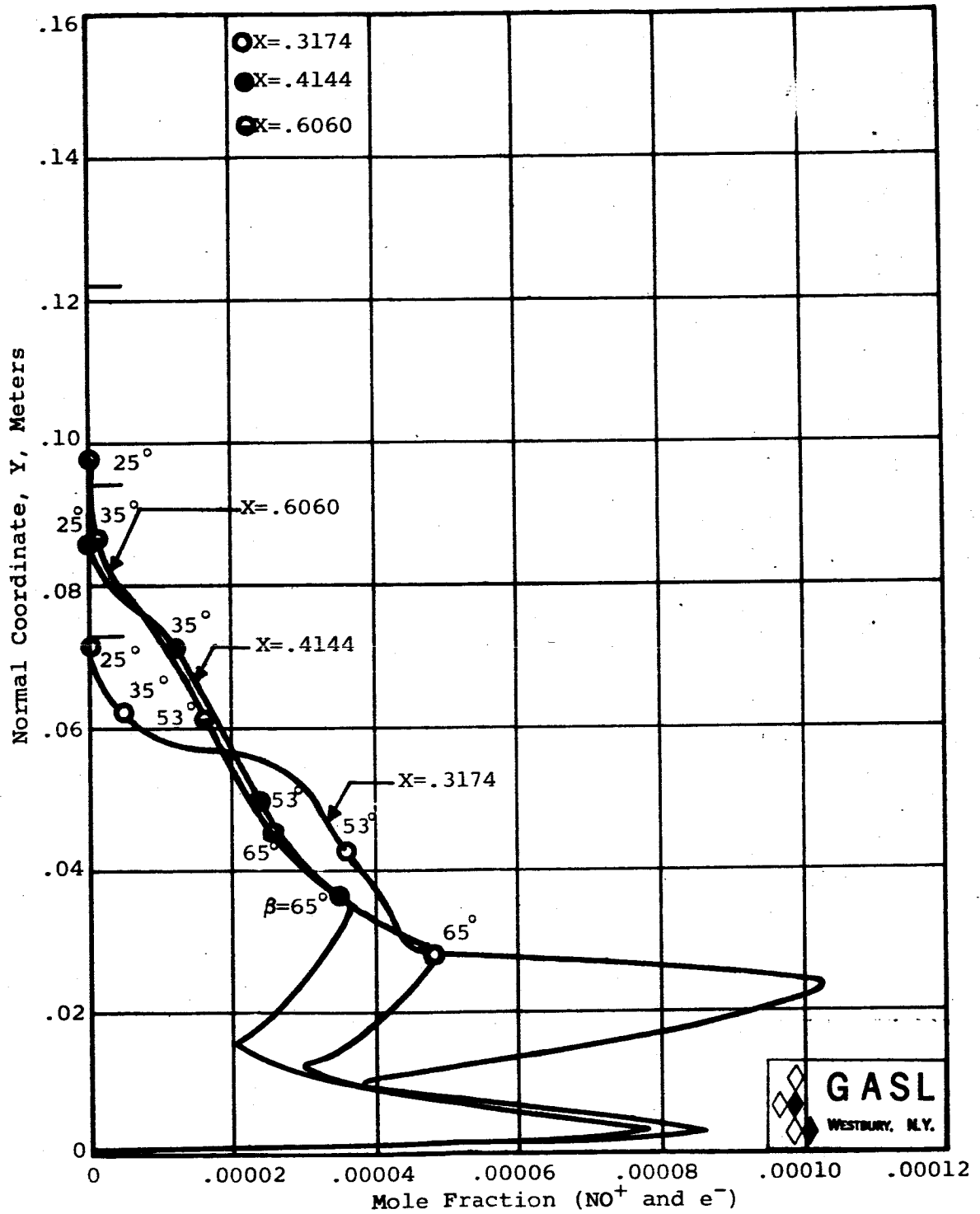
FIG. 42. SPECIE PROFILES (NO$^+$ AND e$^-$) AT SURFACE COORDINATE LOCATIONS X=.3174, X=.4144, AND X=.6060 METERS, ALTITUDE = 36,800 METERS

73
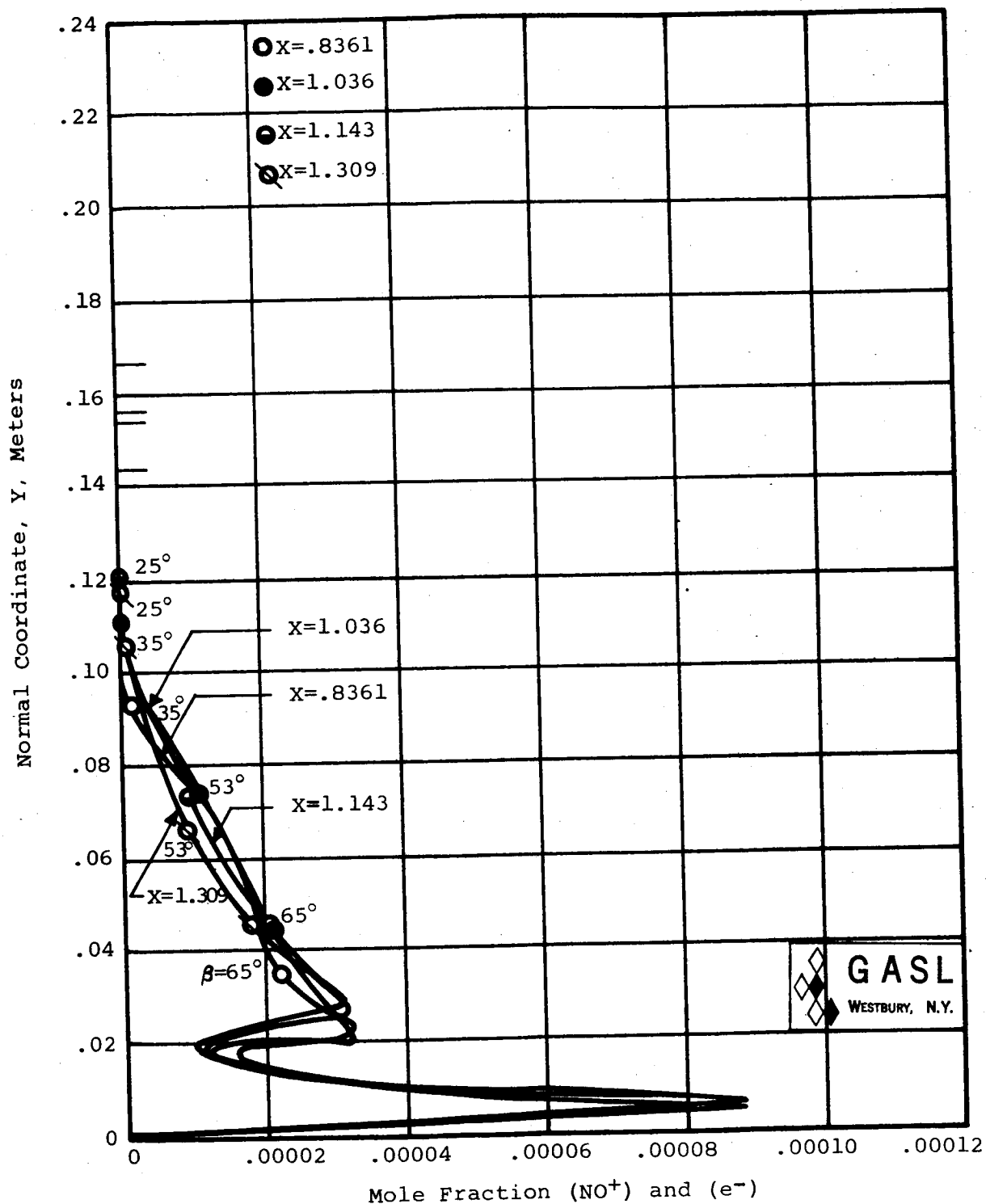
FIG. 43. SPECIE PROFILES (NO+) AND (e−) AT SURFACE
COORDINATE LOCATIONS X=.8361, X=1.036,
X=1.143, AND X=1.309 METERS,
ALTITUDE = 36,800 METERS

FIG. 44. CONTOUR MAP OF PRESSURE, p, NEWTONS/METER^2

ALTITUDE = 36,800 METERS

BOW SHOCK

BODY

NON-DIMENSIONAL AXIAL COORDINATE ~ ζ_1/R_N

NON-DIMENSIONAL NORMAL COORDINATE ~ ζ_3/R_N

6,893

7,539

8,617

9,694

12,925

17,233

21,542

43,083

129,249

107,708

89,397

67,209

150,790

172,332

193,874

215,415

256,957

FIG. 45. CONTOUR MAP OF TEMPERATURE, T, °K
ALTITUDE - 36,800 METERS

76

FIG. 46. CONTOUR MAP OF ELECTRON DENSITY, $N_e \sim$, PART/METER^3

ALTITUDE = 36,800 METERS

NON-DIMENSIONAL AXIAL COORDINATE $\sim \zeta_1/R_N$

NON-DIMENSIONAL NORMAL COORDINATE $\sim \zeta_3/R_N$

77

FIG. 47. PRESSURE PROFILES AT SURFACE COORDINATE LOCATIONS
X=.09137, X=.1048, X=.1225, X=.1457, X=.1723, AND
X=.1979 METERS, ALTITUDE = 36,800 METERS
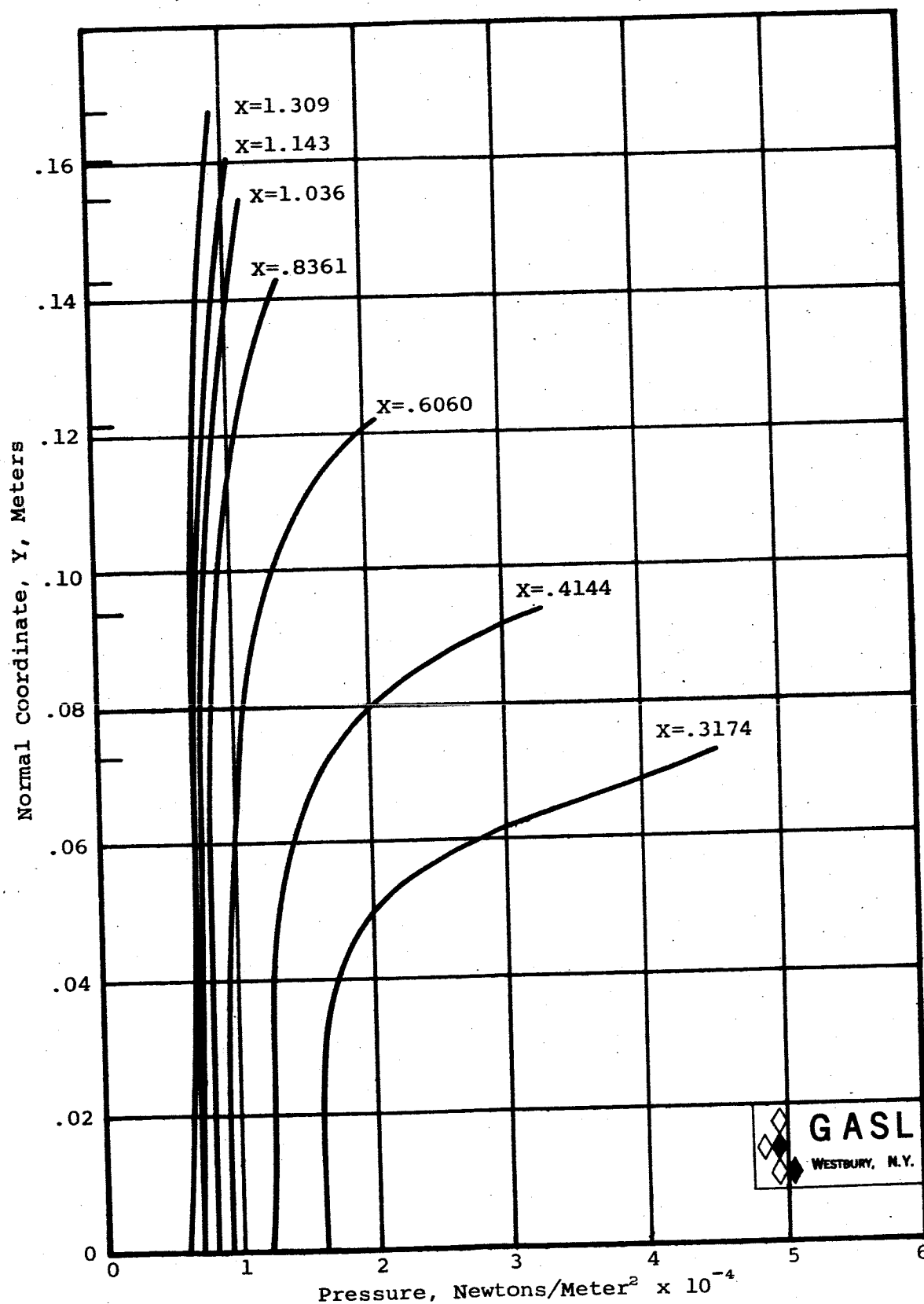
FIG. 48. PRESSURE PROFILES AT SURFACE COORDINATE LOCATIONS
X=.3174, X=.4144, X=.6060, X=.8361, X=1.036, X=1.143
AND X=1.309 METERS, ALTITUDE = 36,800 METERS

NOMENCLATURE

ALTITUDE = 53,500 METERS

The shock locations for each profile are indicated by
the short solid lines drawn along the normal coordinate.
Since the shock layer thickness increases with increasing
surface coordinate location, their identification is there-
fore self-explanatory.

The data points indicate the results of streamline calcu-
lations where the code utilized for each station is indicated
on each figure. The symbol β indicates the post bow shock
entry angle of the streamline considered.

The initial and final iterated streamline locations are
indicated on the figures; where the squares indicate the initial
locations.
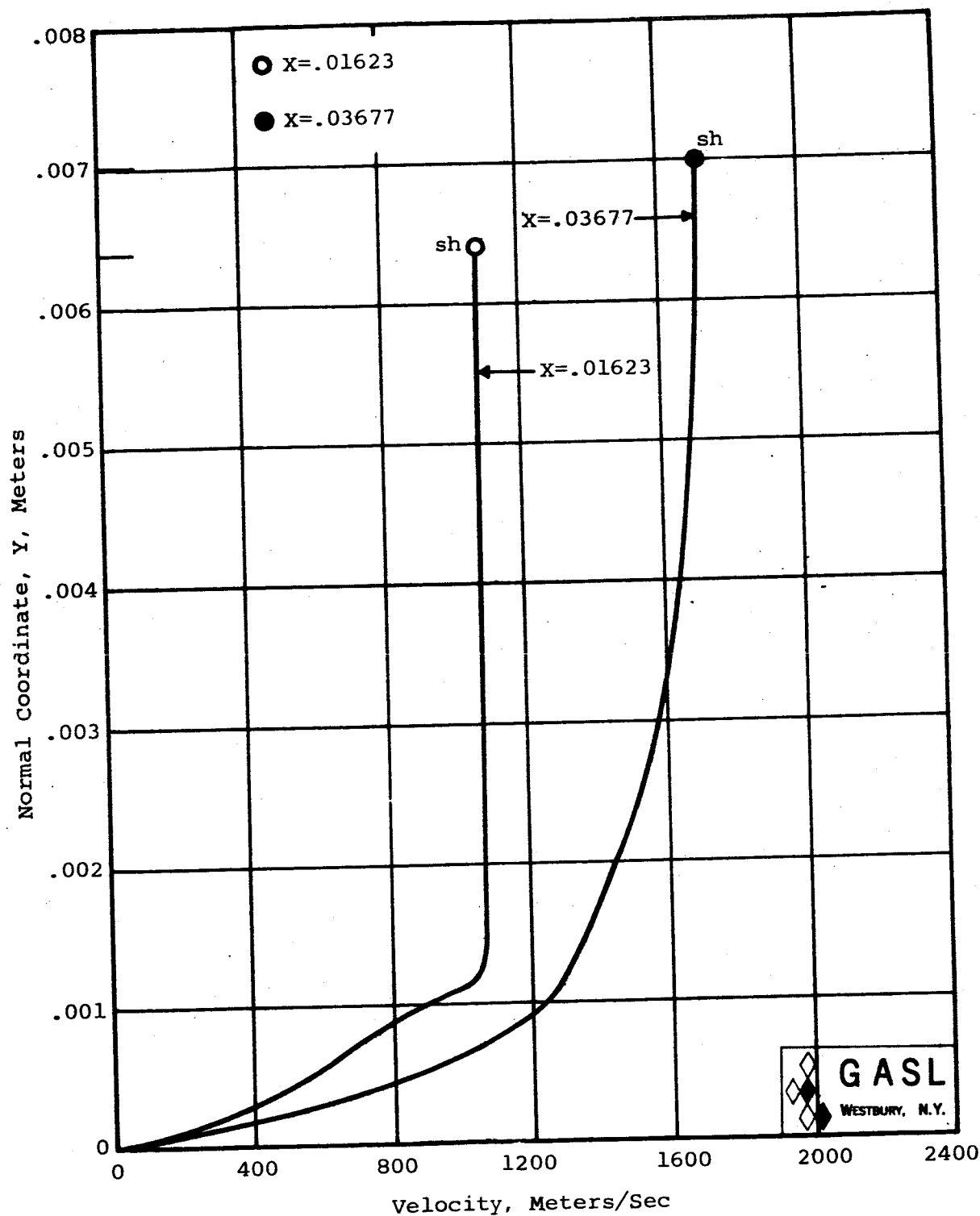
FIG. 49. VELOCITY AT SURFACE COORDINATE LOCATIONS X=.01623
AND X=.03677 METERS, ALTITUDE = 53,500 METERS
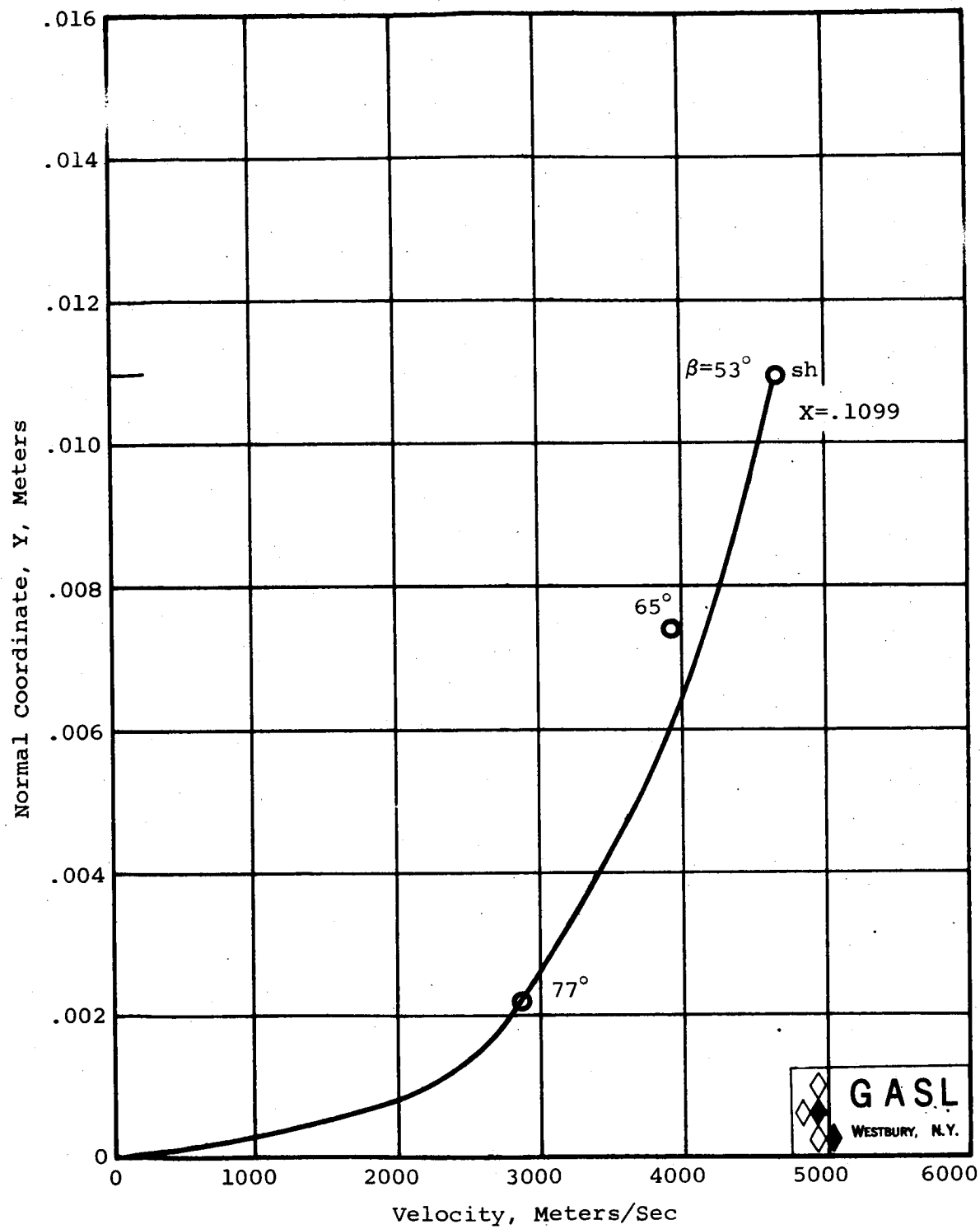
FIG. 50.   VELOCITY AT SURFACE COORDINATE LOCATION   X=.1099
            METERS, ALTITUDE = 53,500 METERS
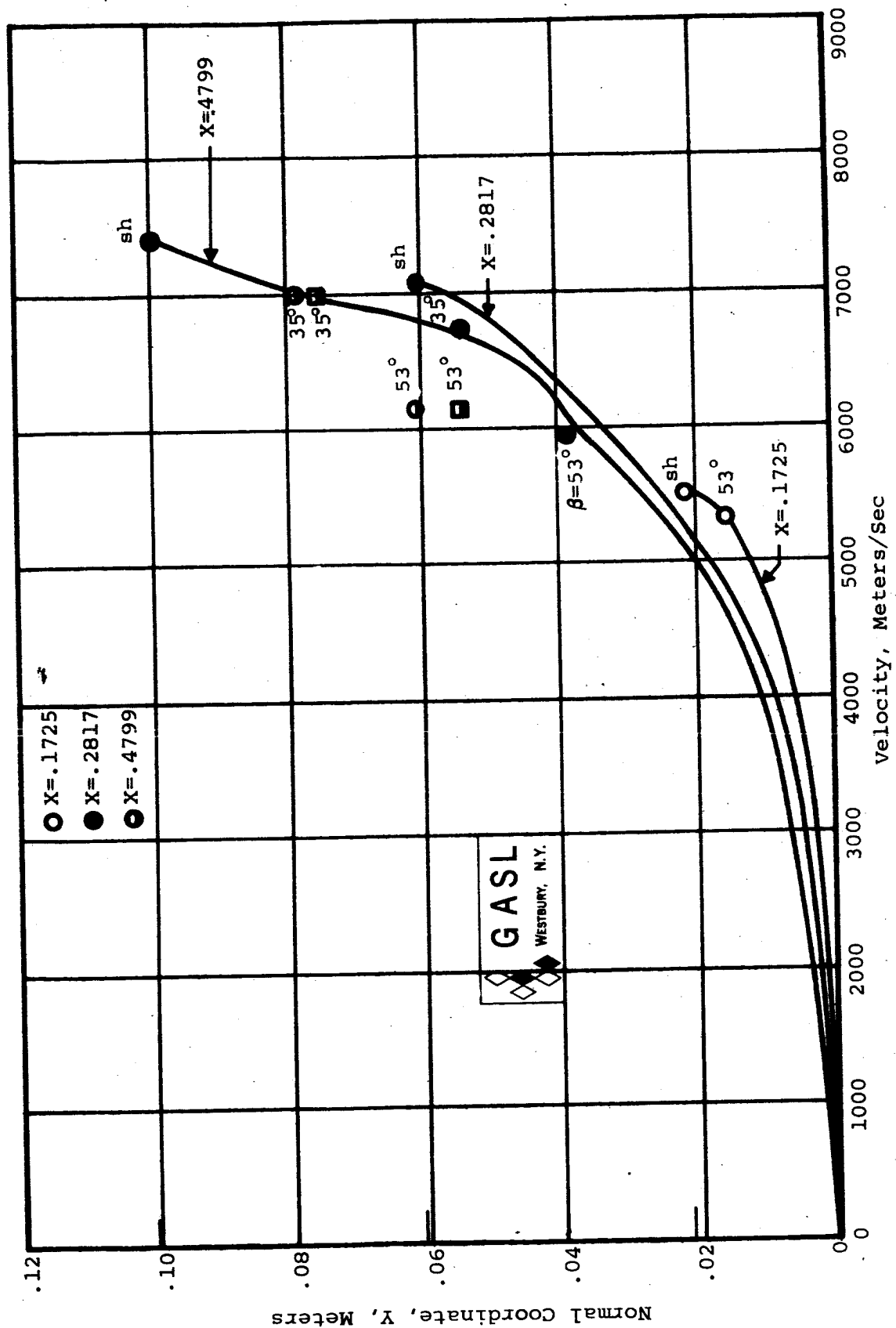
FIG. 51. VELOCITY AT SURFACE COORDINATE LOCATIONS X=.1725, X=.2817, AND X=.4799 METERS, ALTITUDE = 53,500 METERS
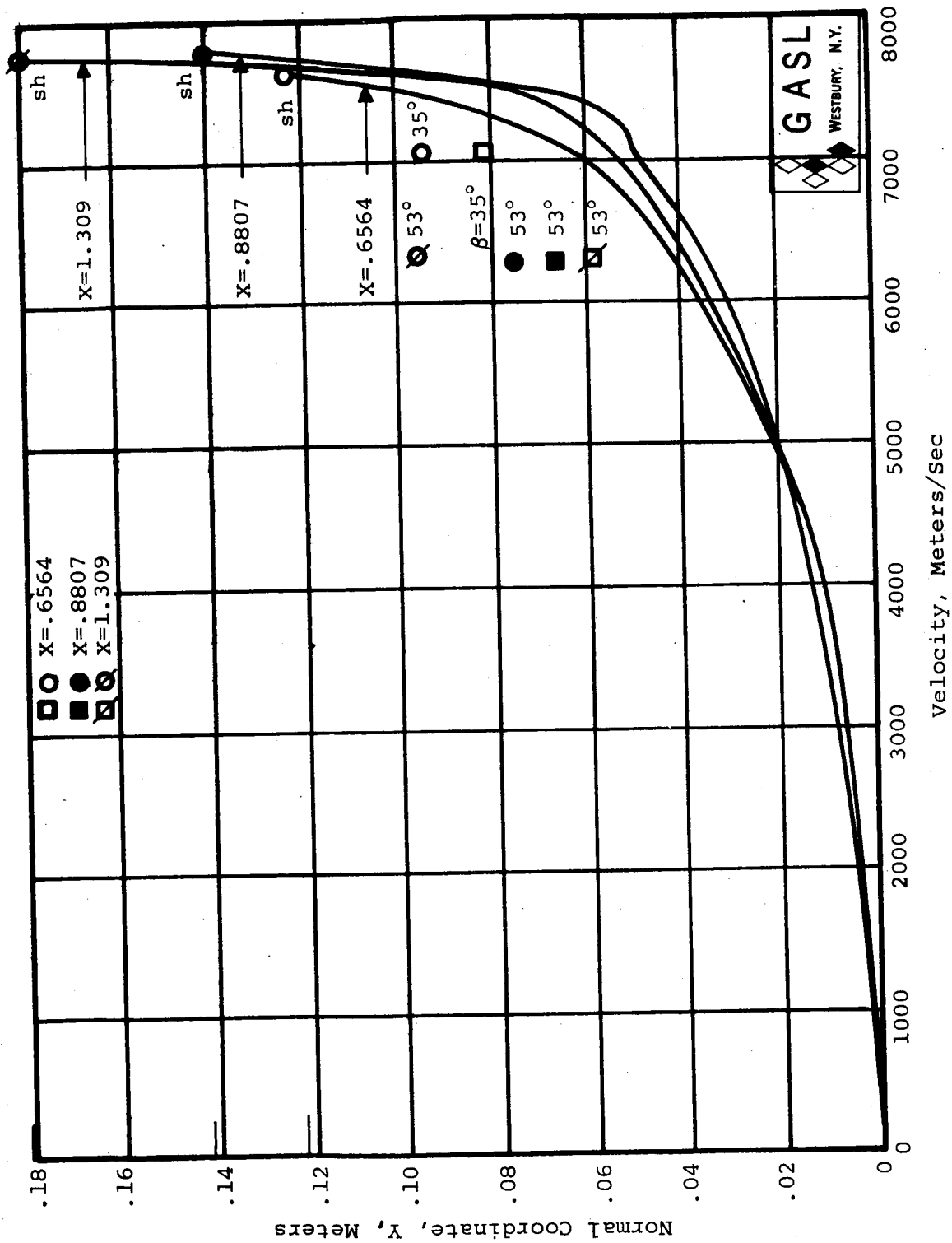
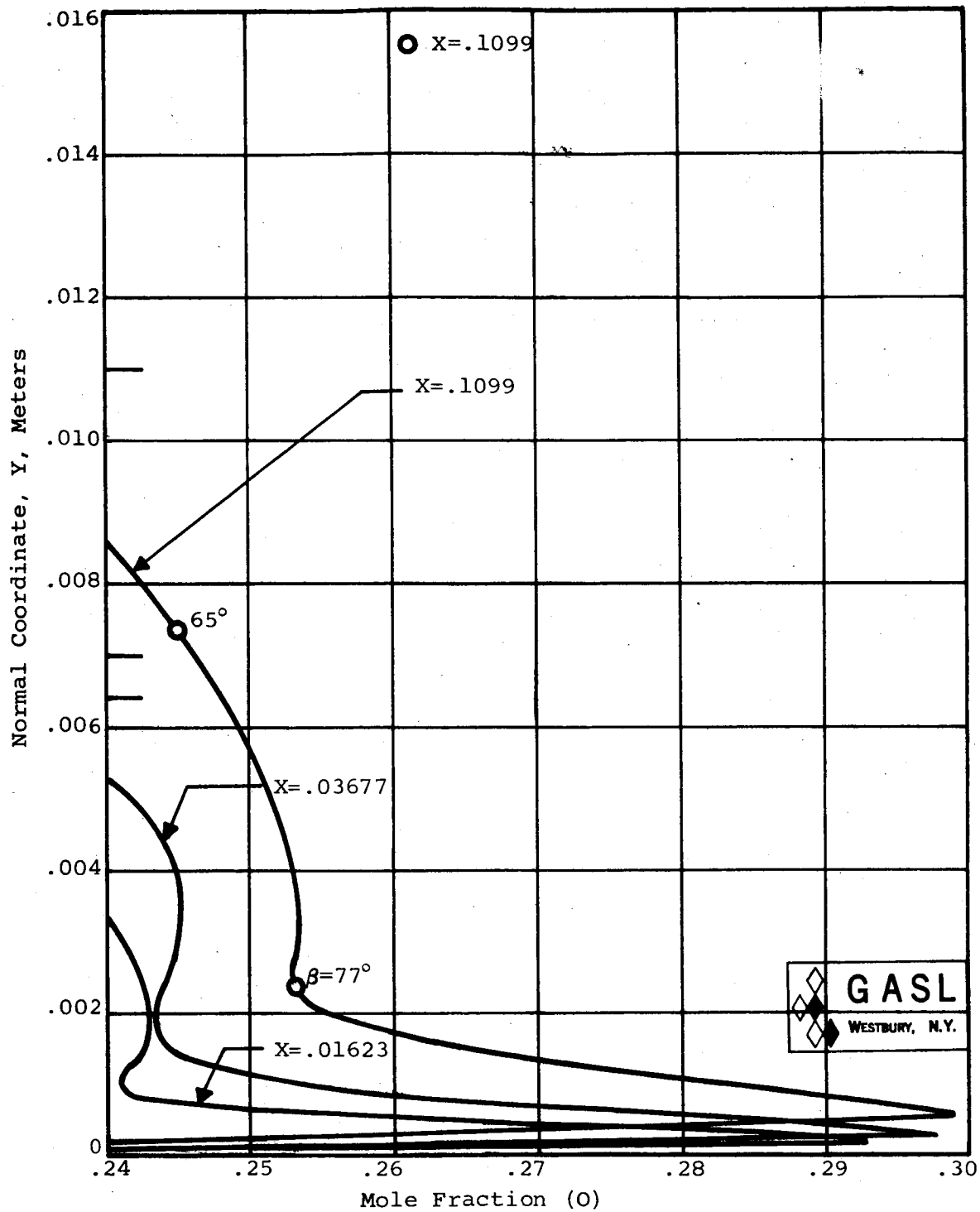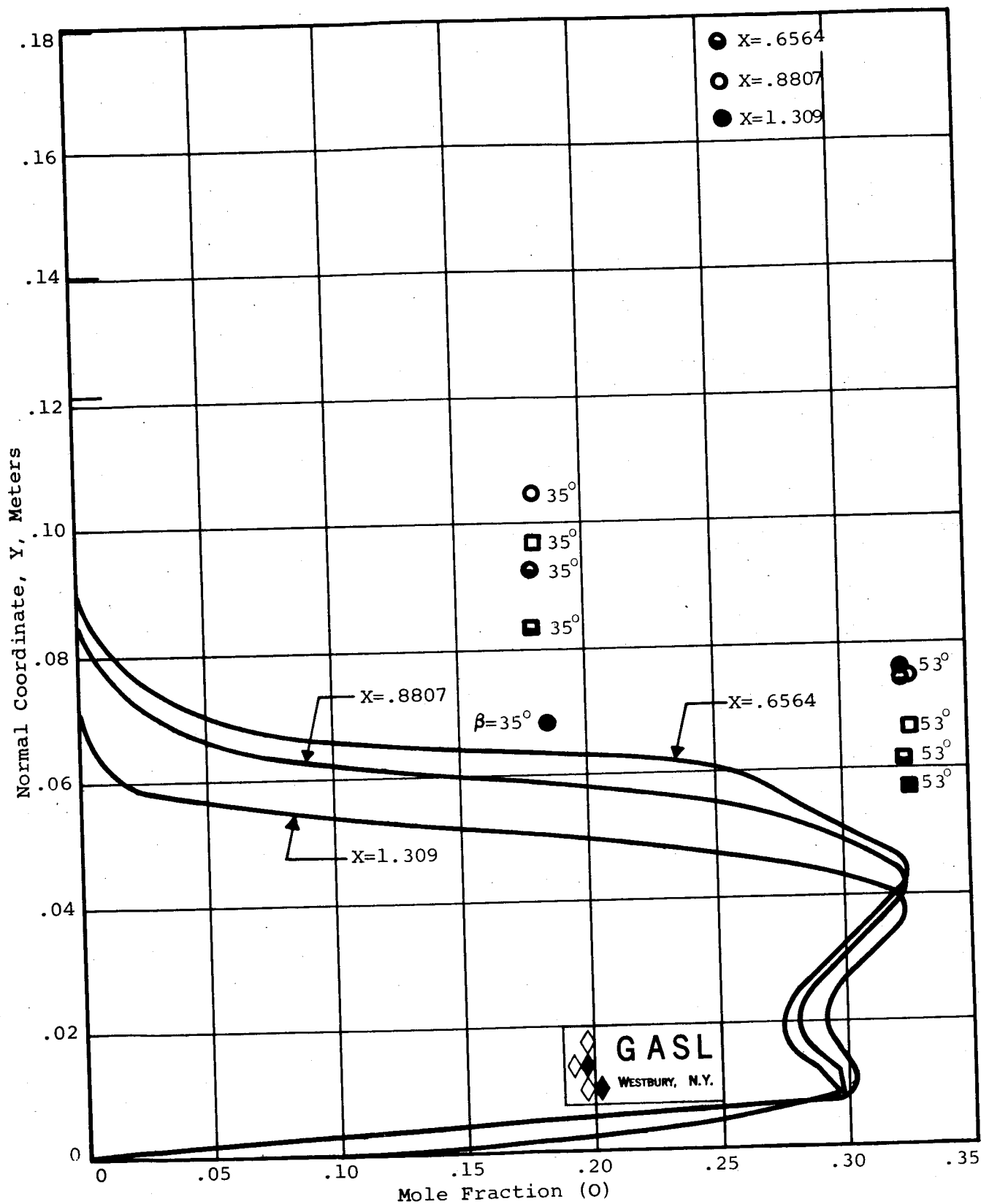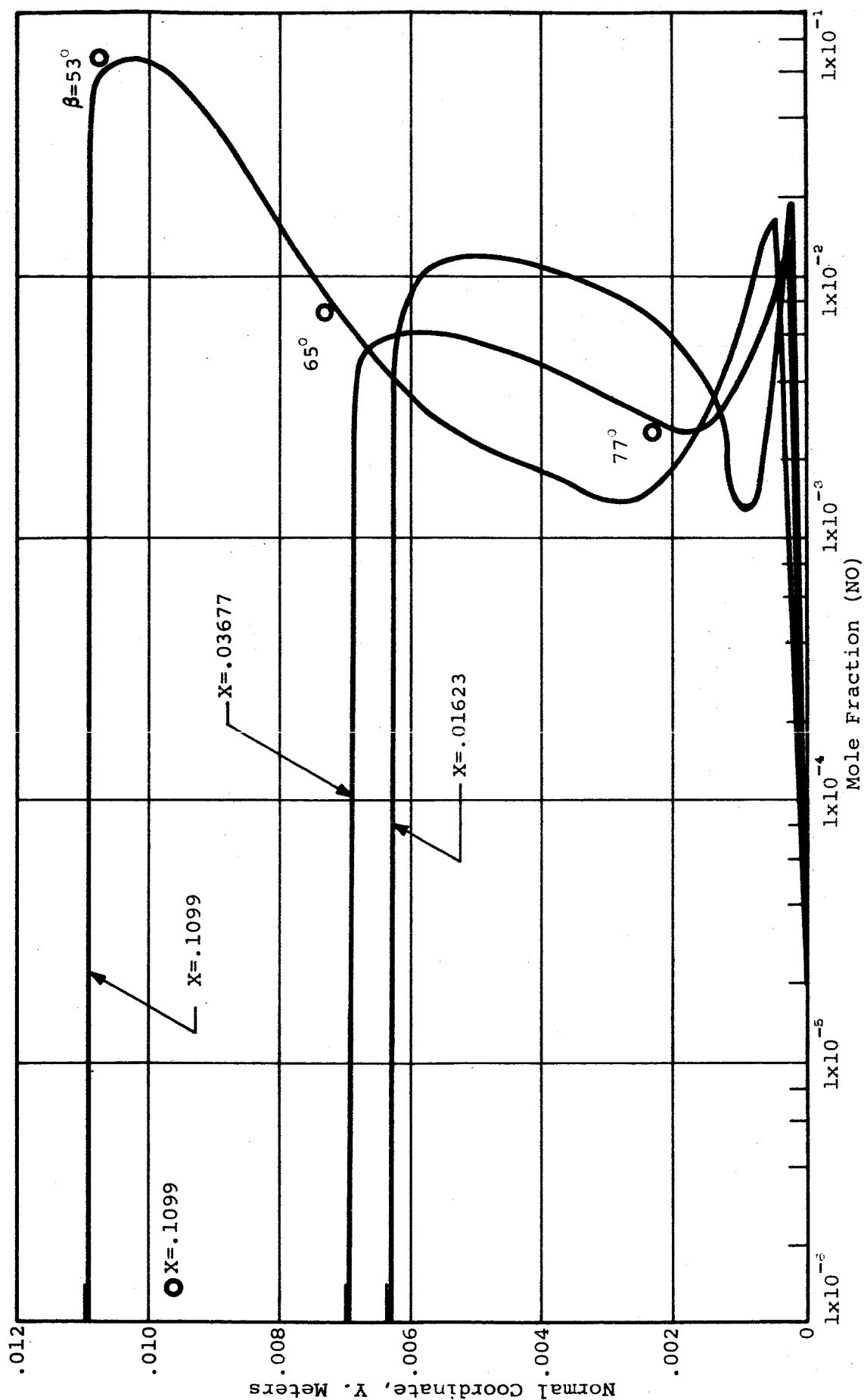FIG. 52. VELOCITY AT SURFACE COORDINATE LOCATIONS X=.6564, X=.8807, AND X=1.309 METERS, ALTITUDE = 53,500 METERS

84
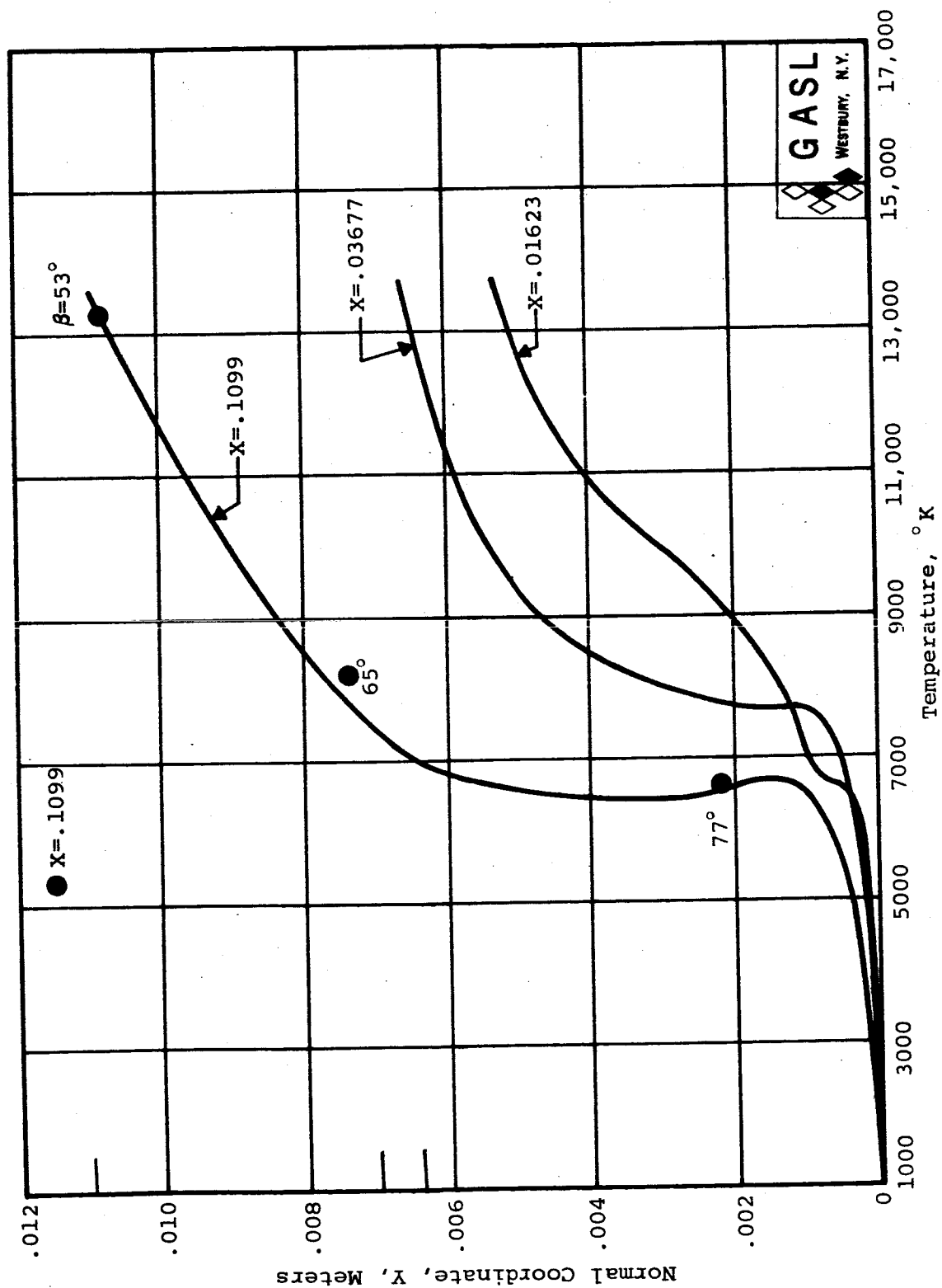
FIG. 53.   TEMPERATURE AT SURFACE COORDINATE LOCATIONS X=.1099, X=.03677, AND
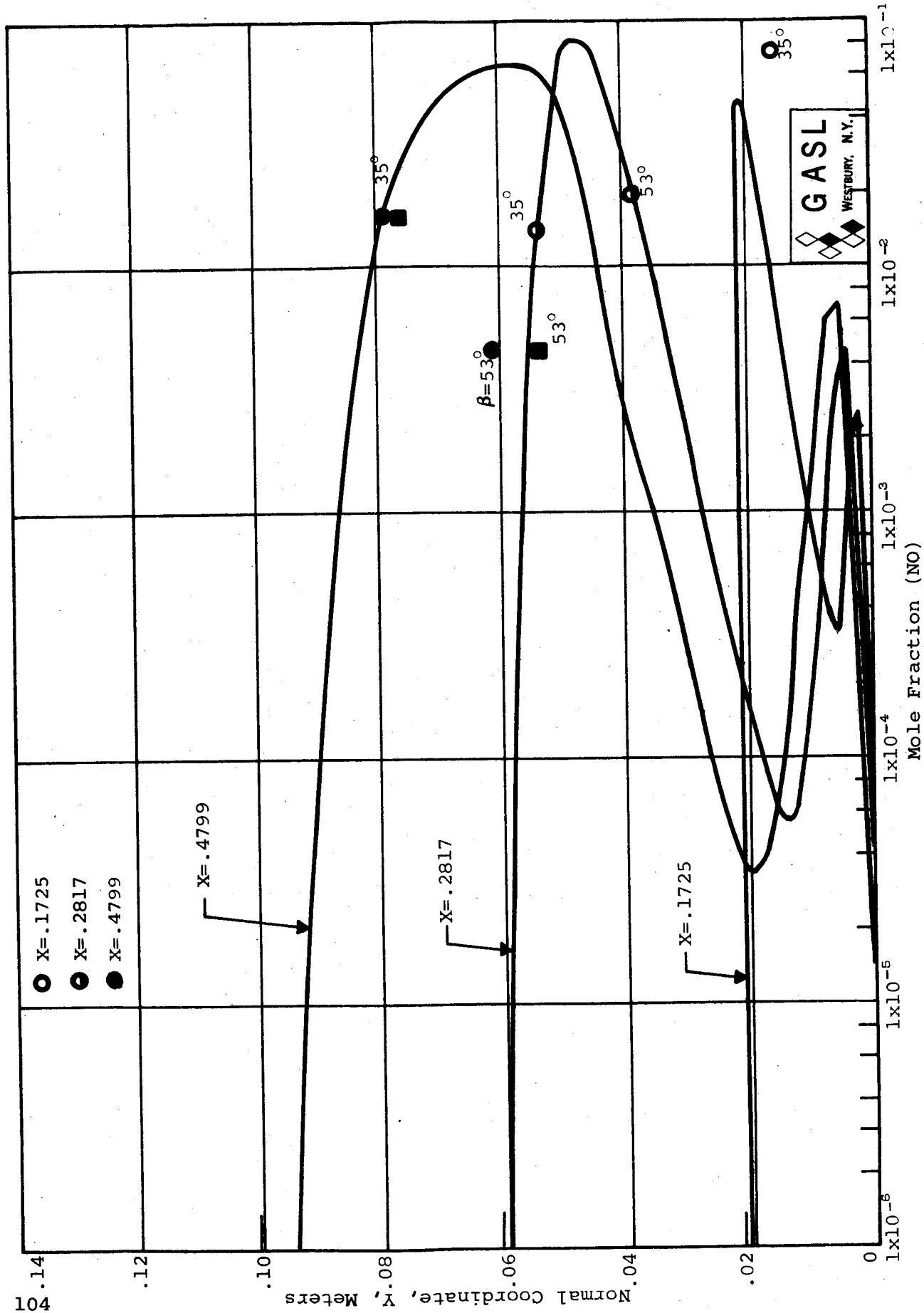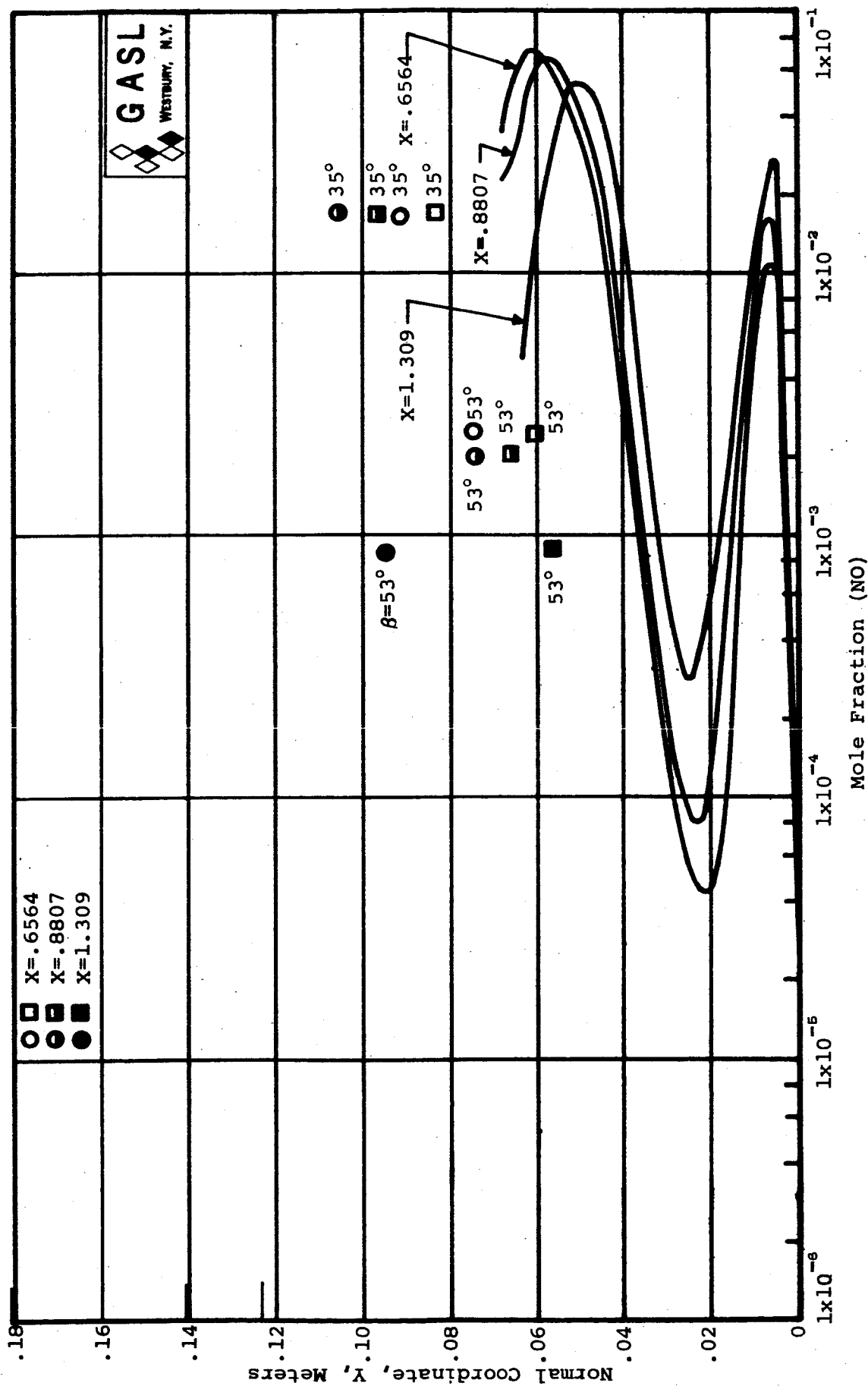X=.01623 METERS, ALTITUDE = 53,500 METERS

85
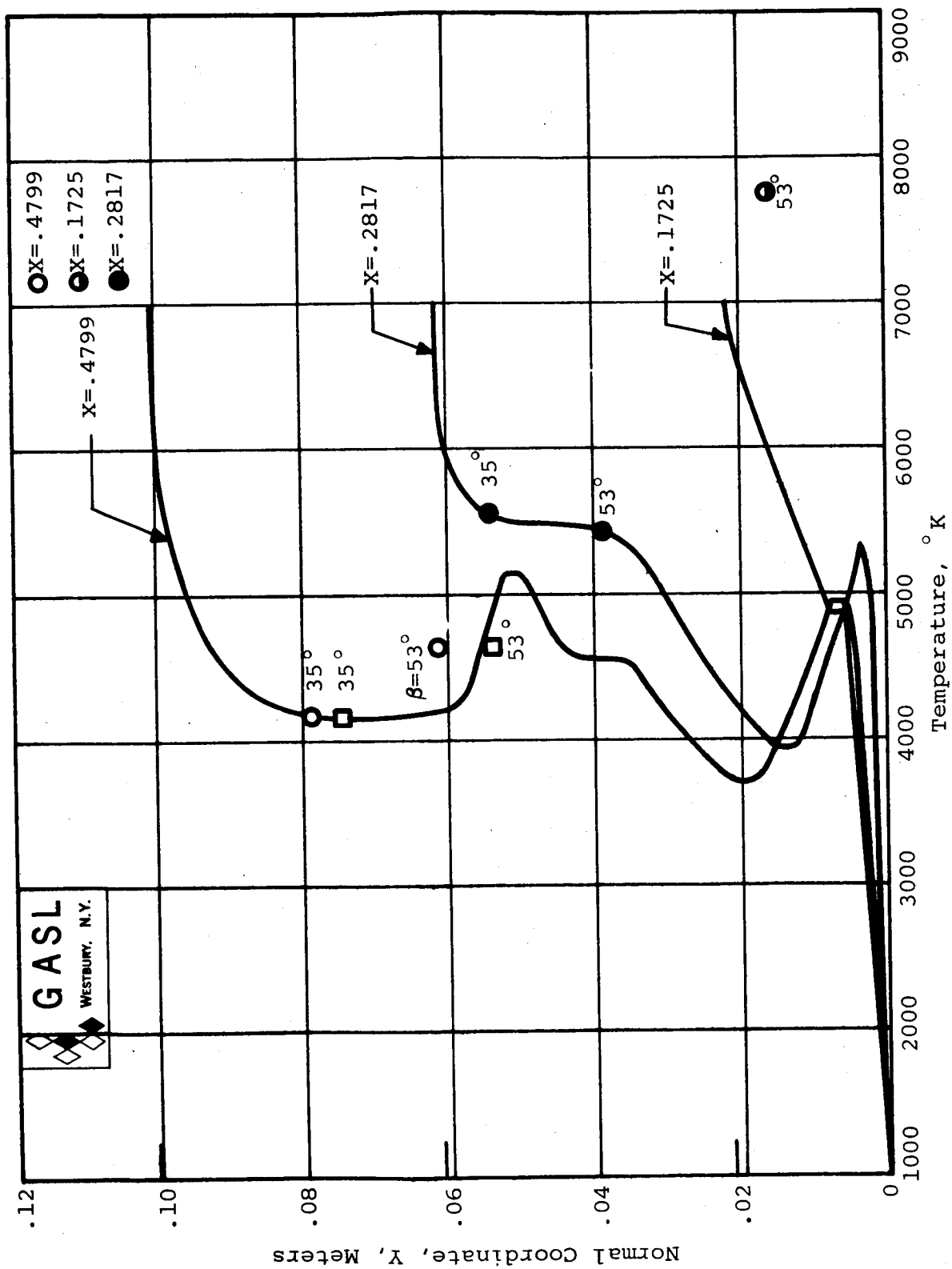
FIG. 54. TEMPERATURE AT SURFACE COORDINATE LOCATIONS X=.4799, X=.1725, AND X=.2817 METERS, ALTITUDE = 53,500 METERS
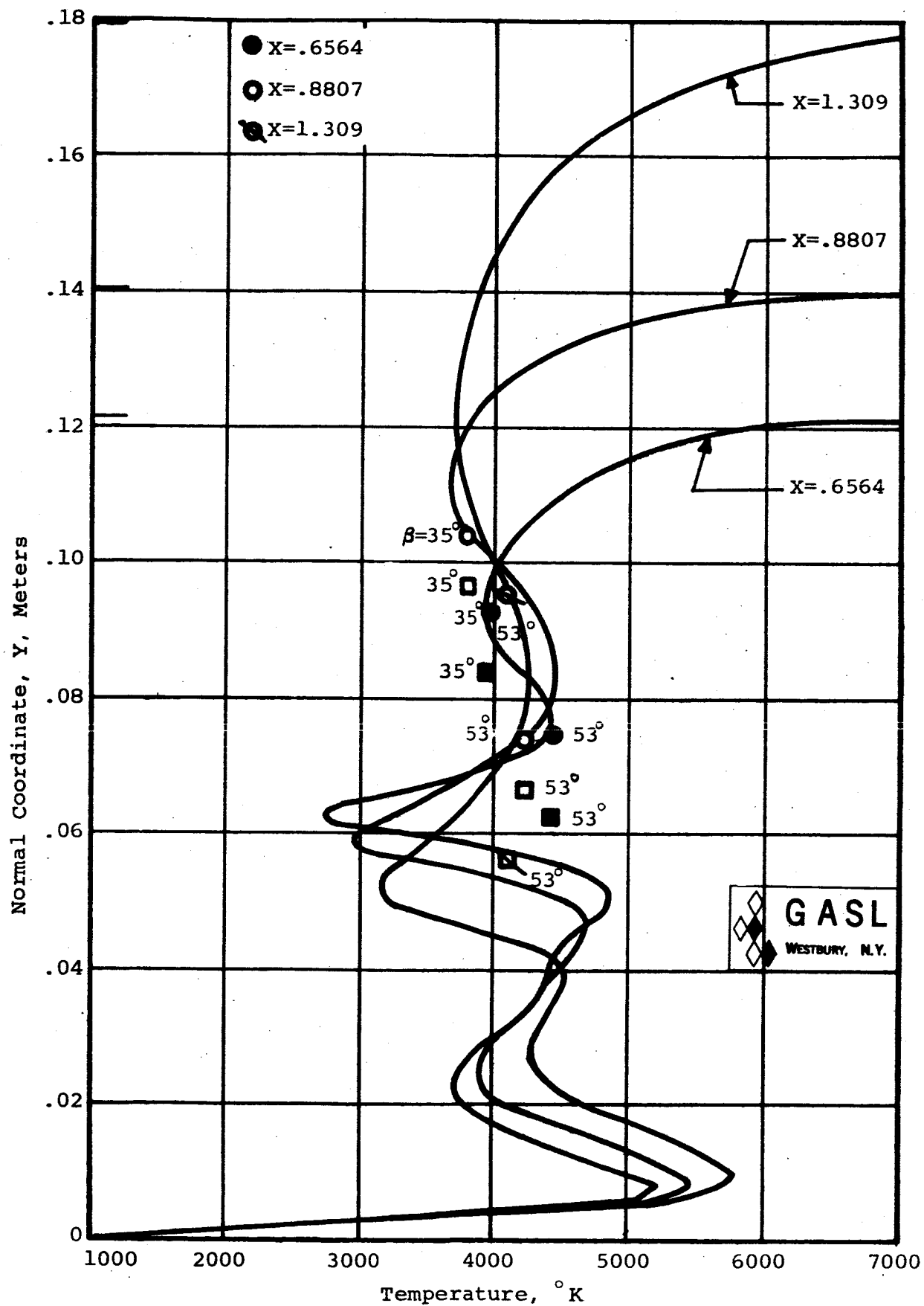
FIG. 55. TEMPERATURE AT SURFACE COORDINATE LOCATIONS X=.6564, X=.8807, AND X=1.309 METERS, ALTITUDE = 53,500 METERS

87
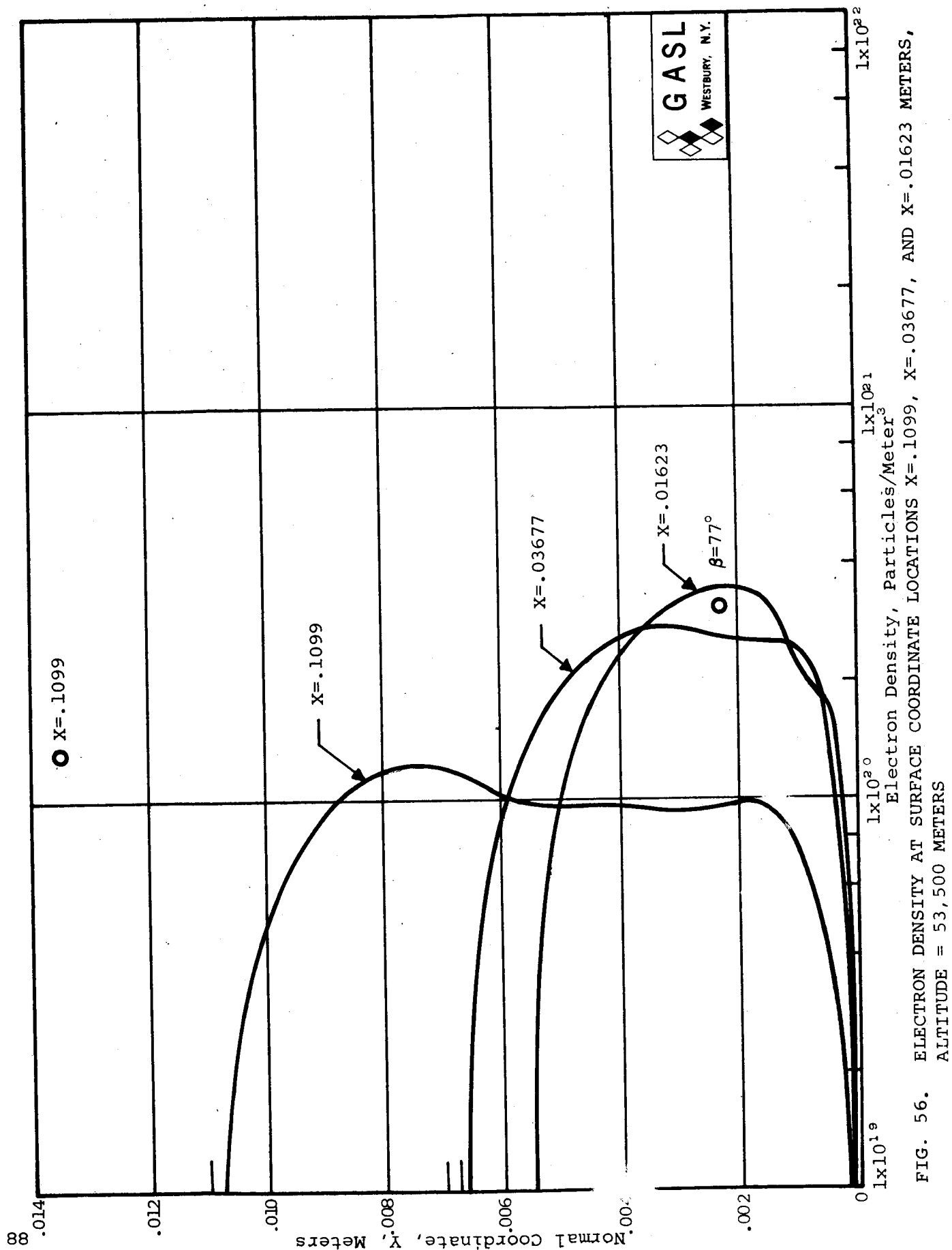
FIG. 56. ELECTRON DENSITY AT SURFACE COORDINATE LOCATIONS X=.1099, X=.03677, AND X=.01623 METERS, ALTITUDE = 53,500 METERS
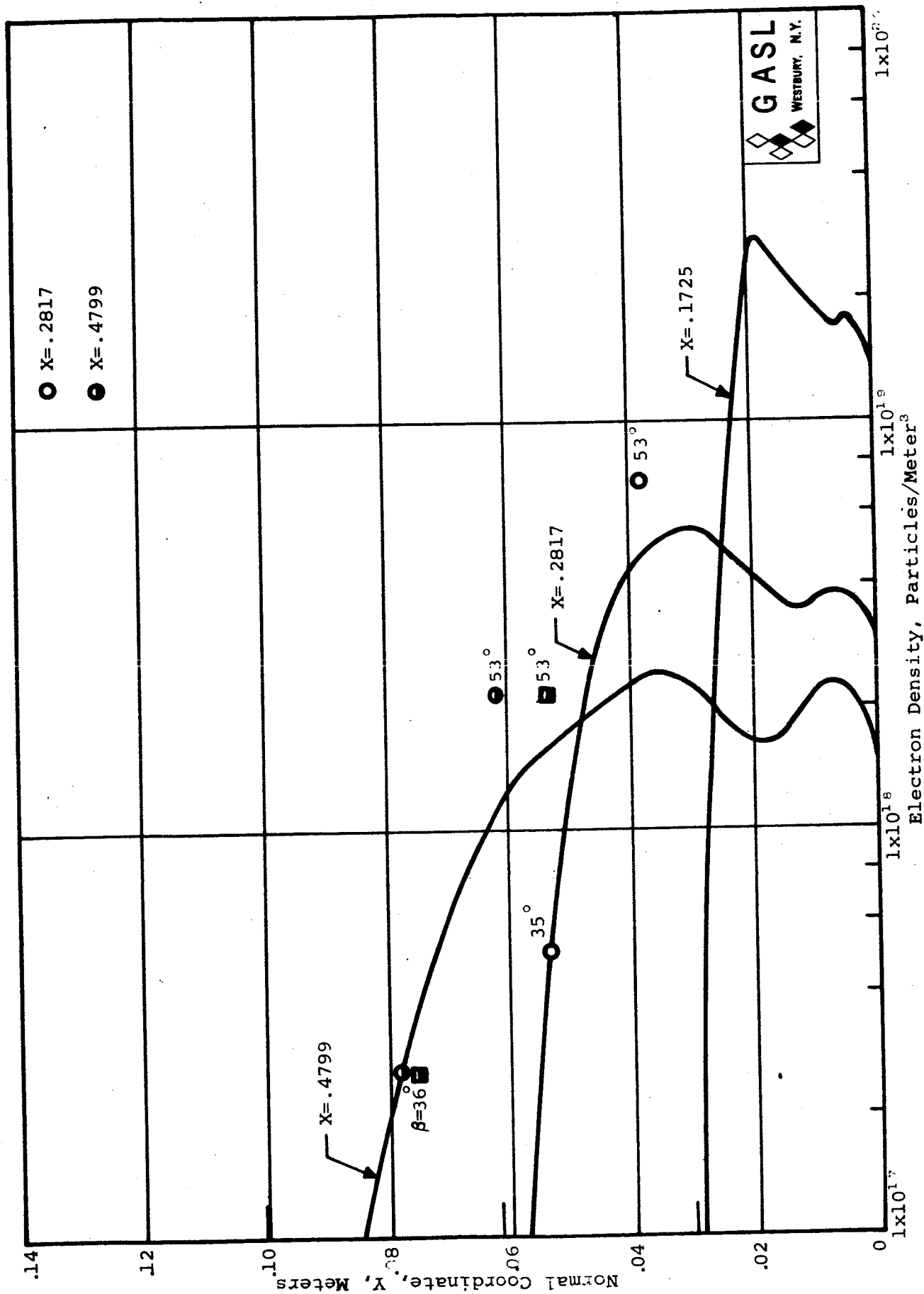
FIG. 57. ELECTRON DENSITY AT SURFACE COORDINATE LOCATIONS X=.2817, X=.1725, AND X=.4799 METERS, ALTITUDE = 53,500 METERS
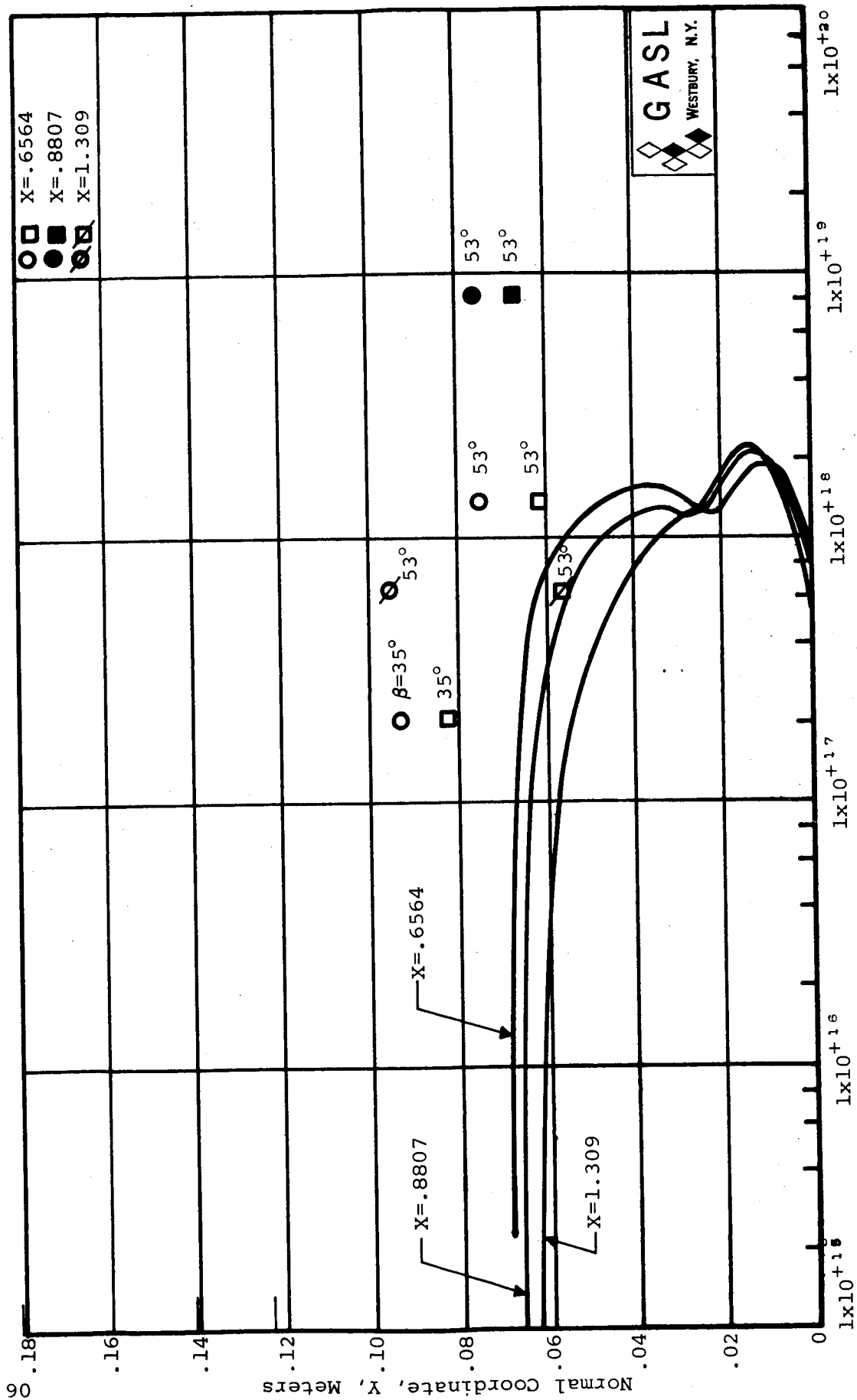
FIG. 58. ELECTRON DENSITY AT SURFACE COORDINATE LOCATIONS X=.6564, X=.8807, AND X=1.309 METERS, ALTITUDE = 53,500 METERS

90
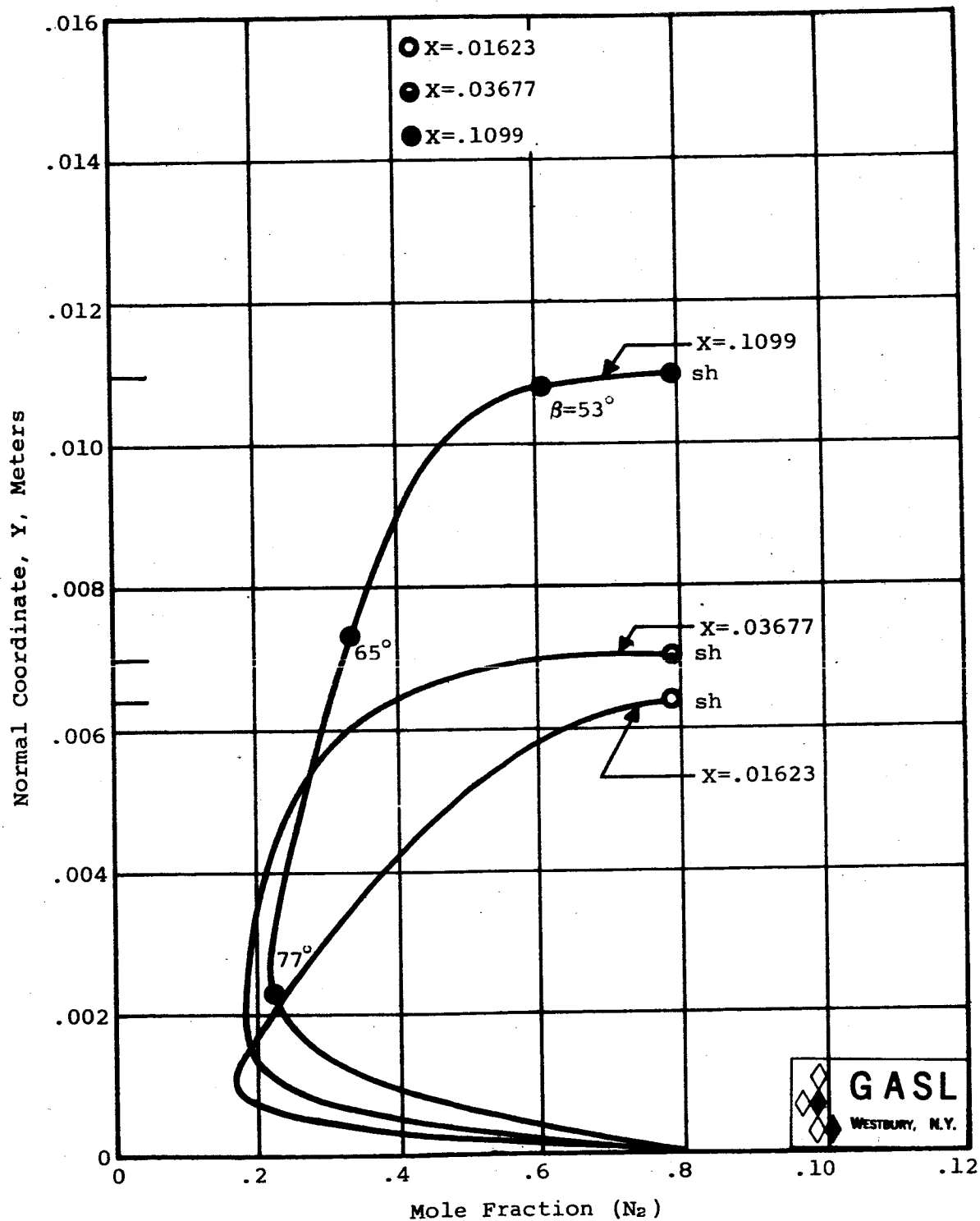
FIG. 59. SPECIE PROFILES (N₂) AT SURFACE COORDINATE
LOCATIONS X=.01623, X=.03677, AND X=.1099 METERS,
ALTITUDE = 53,500 METERS
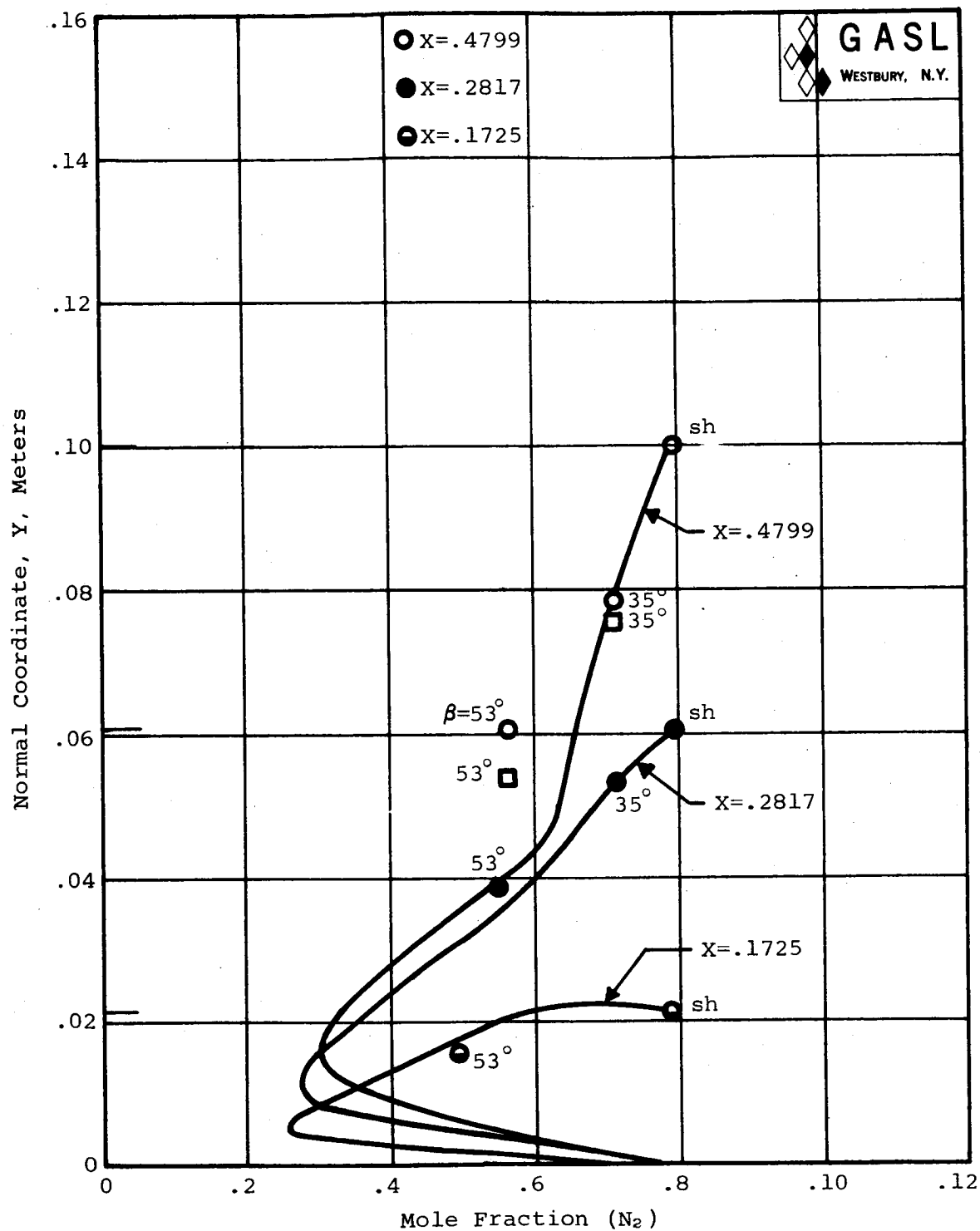
FIG. 60. SPECIE PROFILES (N_2) AT SURFACE COORDINATE
LOCATIONS X=.4799, X=.2817, AND X=.1725 METERS,
ALTITUDE = 53,500 METERS

92
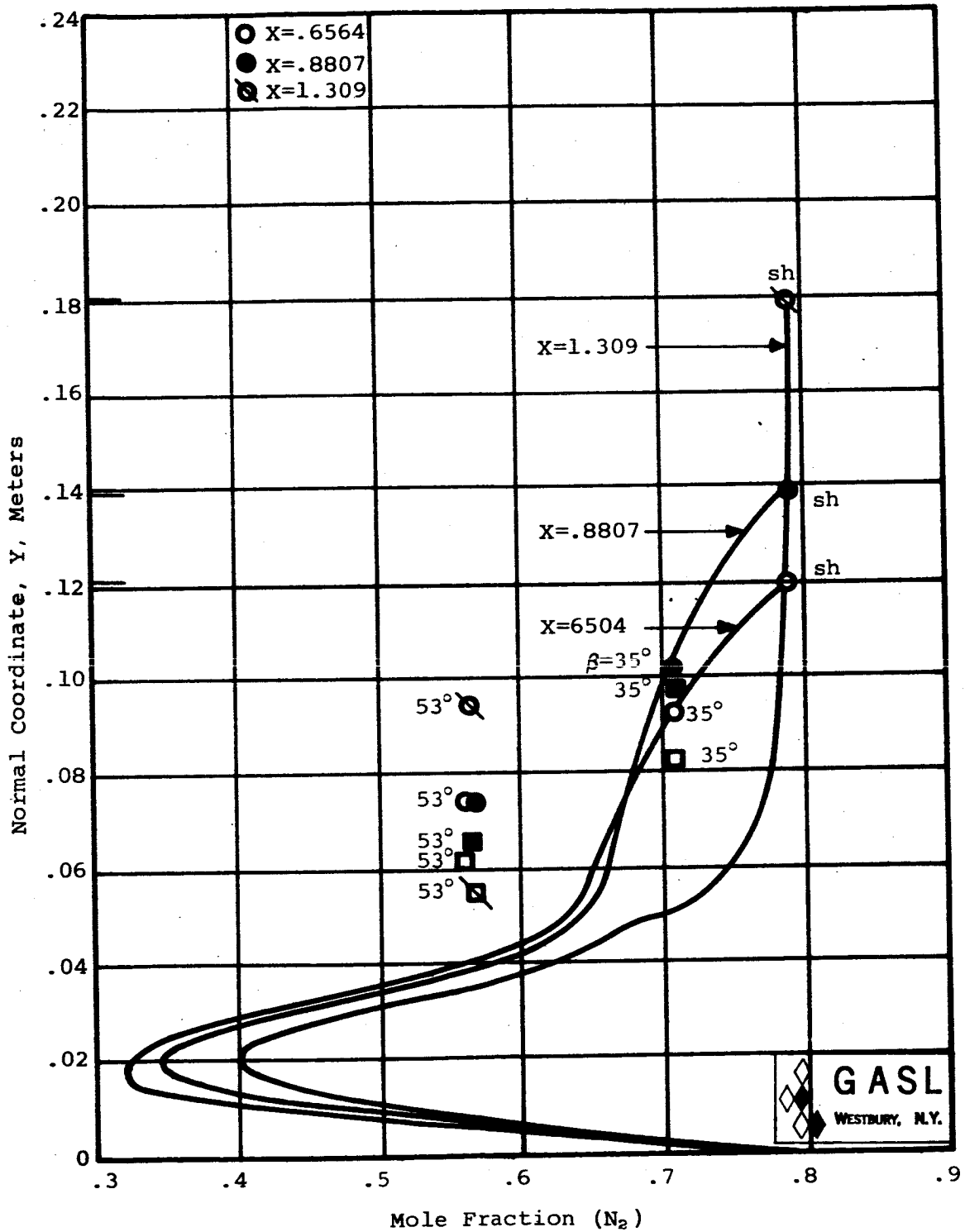
FIG. 61.   SPECIE PROFILES (N_2) AT SURFACE COORDINATE LOCATIONS
X=.6564, X=.8807, AND X=1.309 METERS,
ALTITUDE = 53,500 METERS
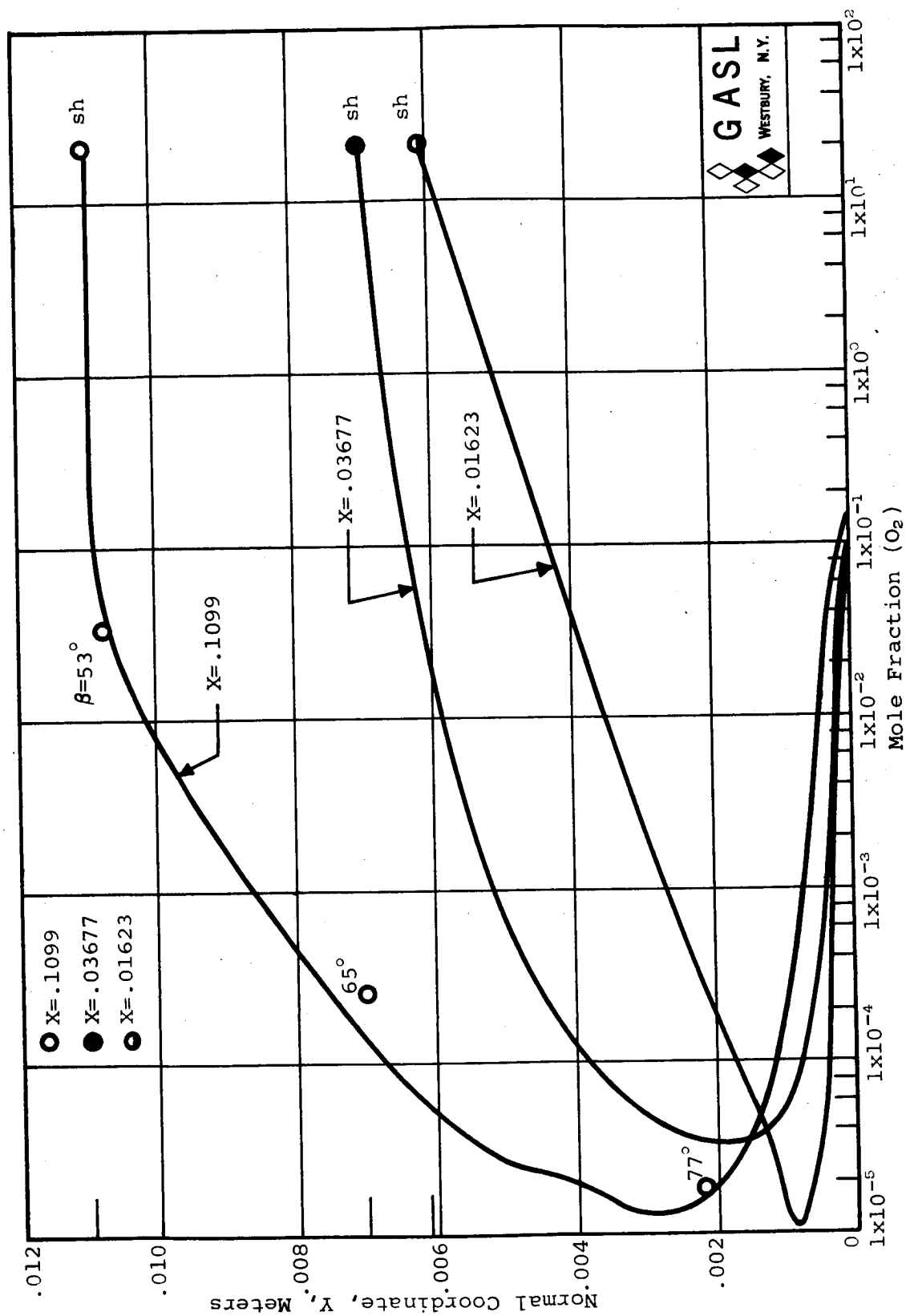
FIG. 62. SPECIE PROFILES (O_2) AT SURFACE COORDINATE LOCATIONS X=.1099, X=.03677, AND X=.01623 METERS, ALTITUDE = 53,500 METERS
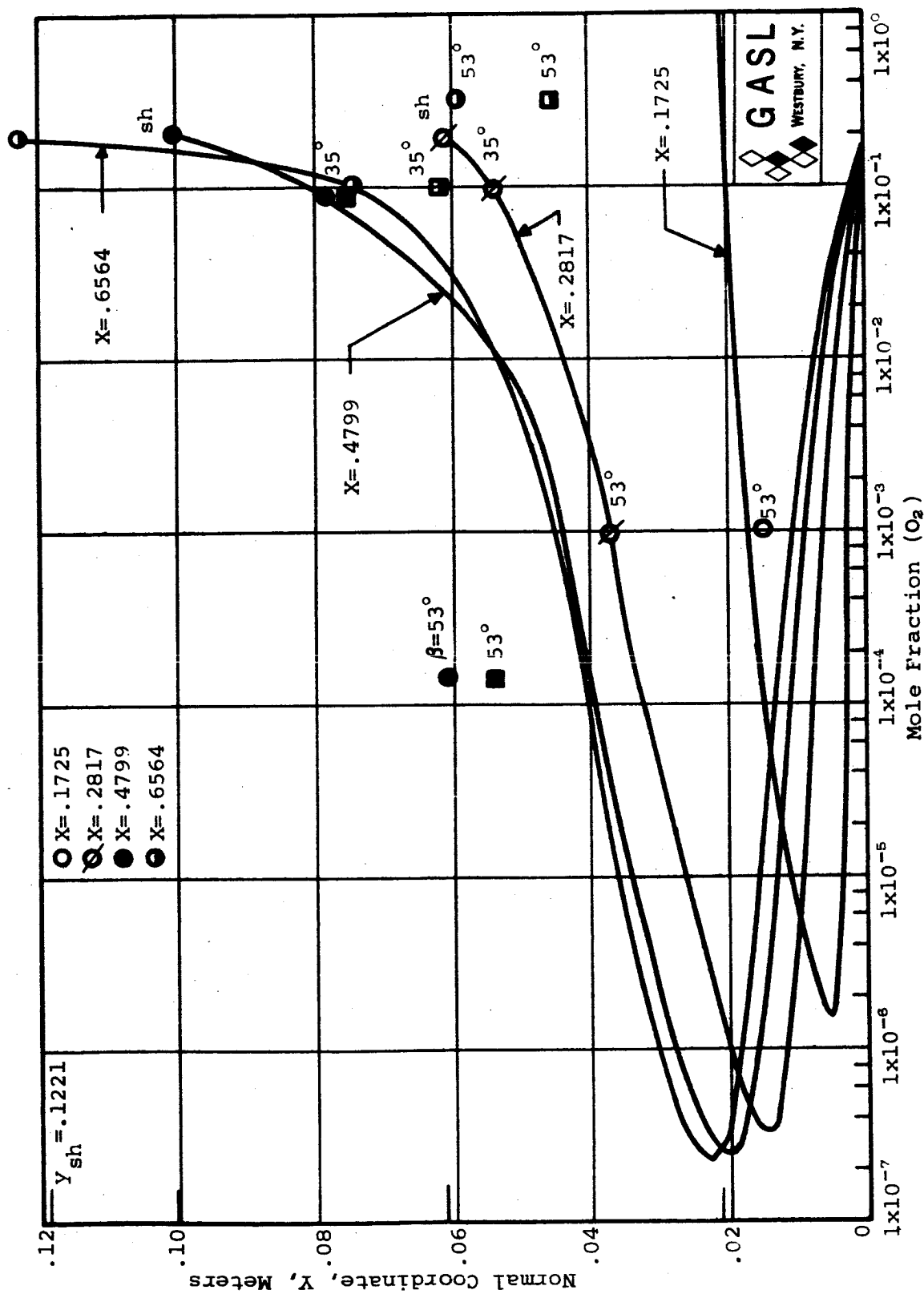
FIG. 63. SPECIE PROFILES (O_2) AT SURFACE COORDINATE LOCATIONS
X=.1725, X=.2817, X=.4799, AND X=.6564 METERS,
ALTITUDE = 53,500 METERS
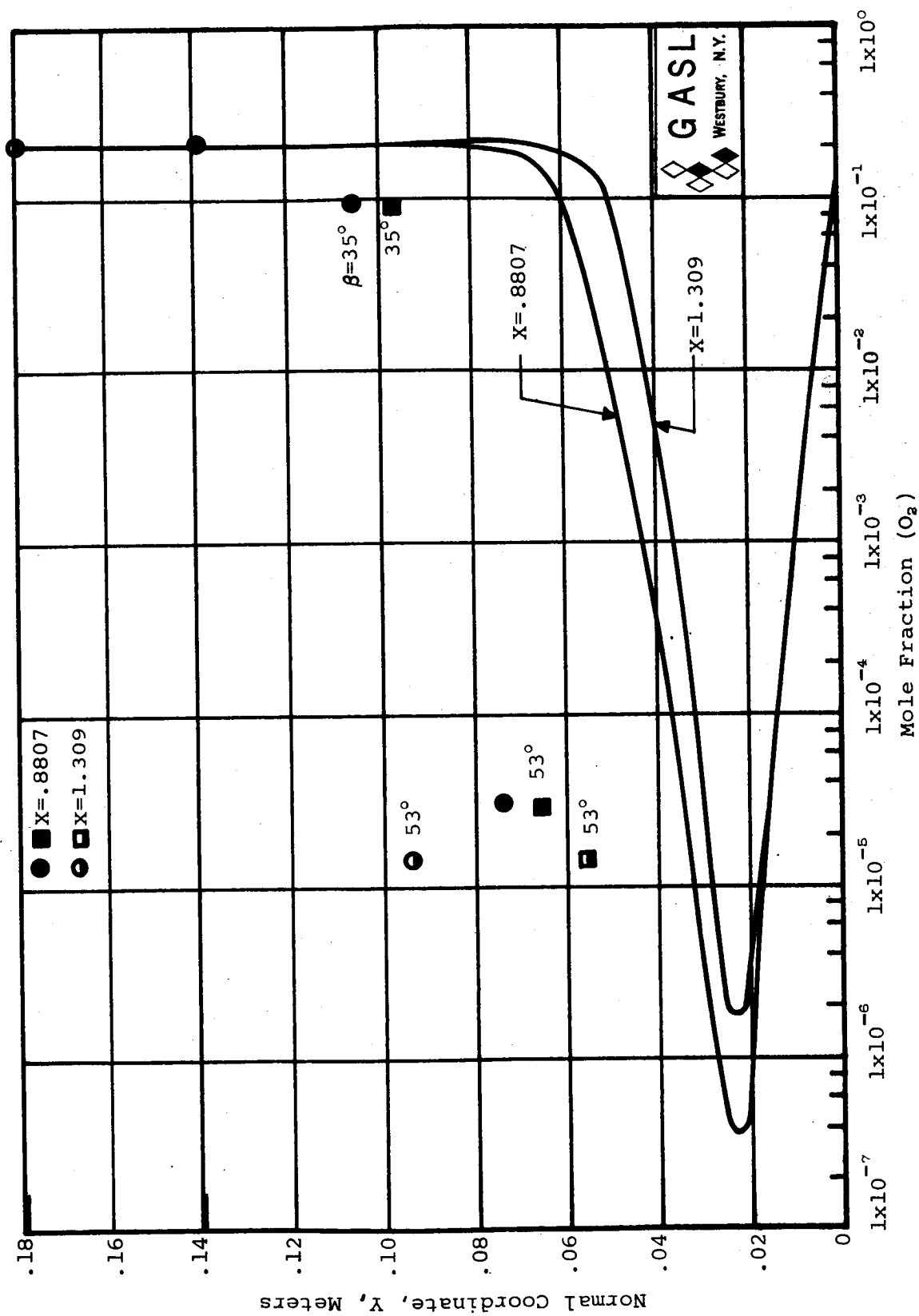
FIG. 64. SPECIES PROFILES (O_2) AT SURFACE COORDINATE LOCATIONS X=.8807 AND X=1.309 METERS, ALTITUDE = 53,500 METERS

96
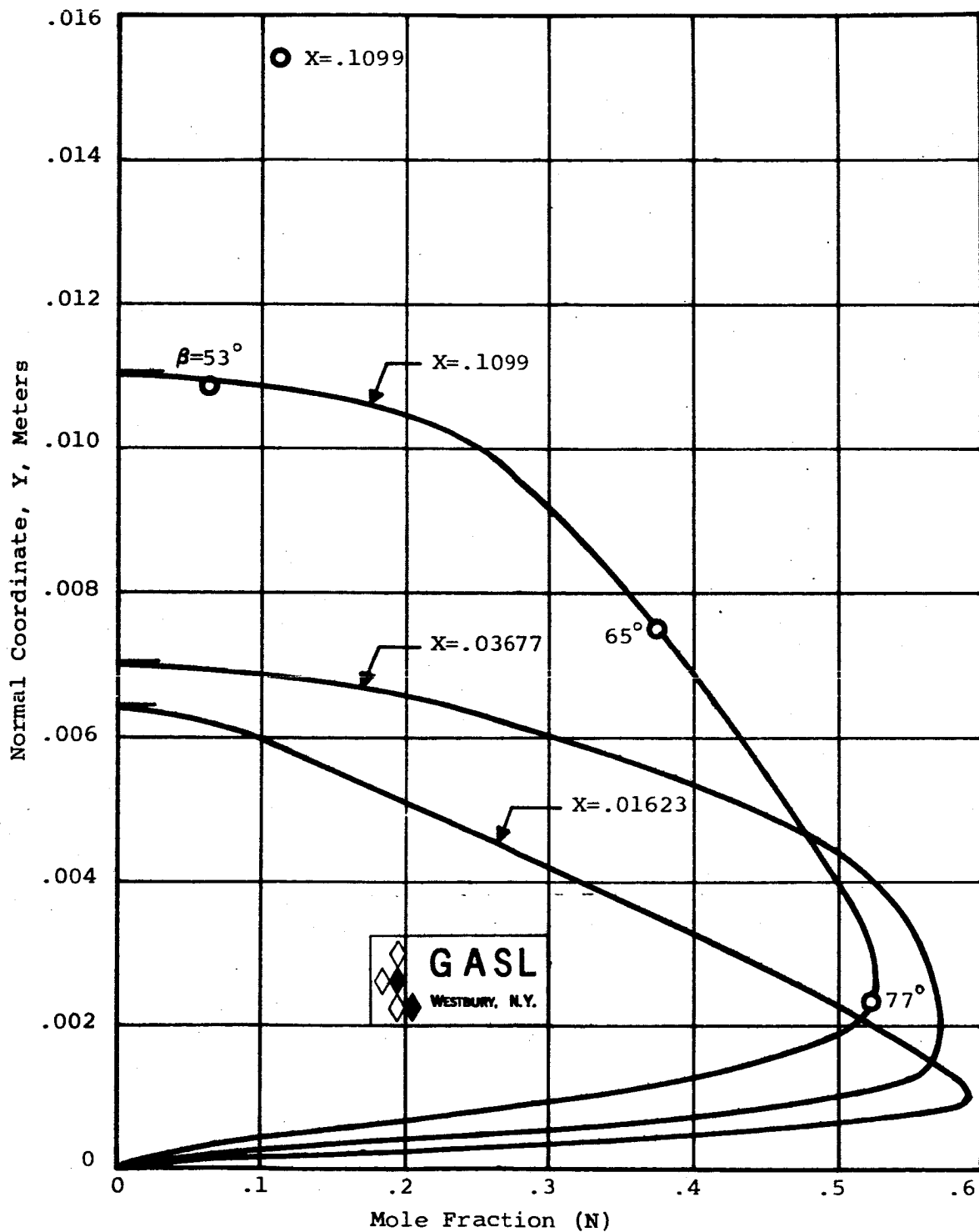
FIG. 65. SPECIE PROFILES (N) AT SURFACE COORDINATE
LOCATIONS X=.1099, X=.03677, AND X=.01623 METERS,
ALTITUDE = 53,500 METERS

97
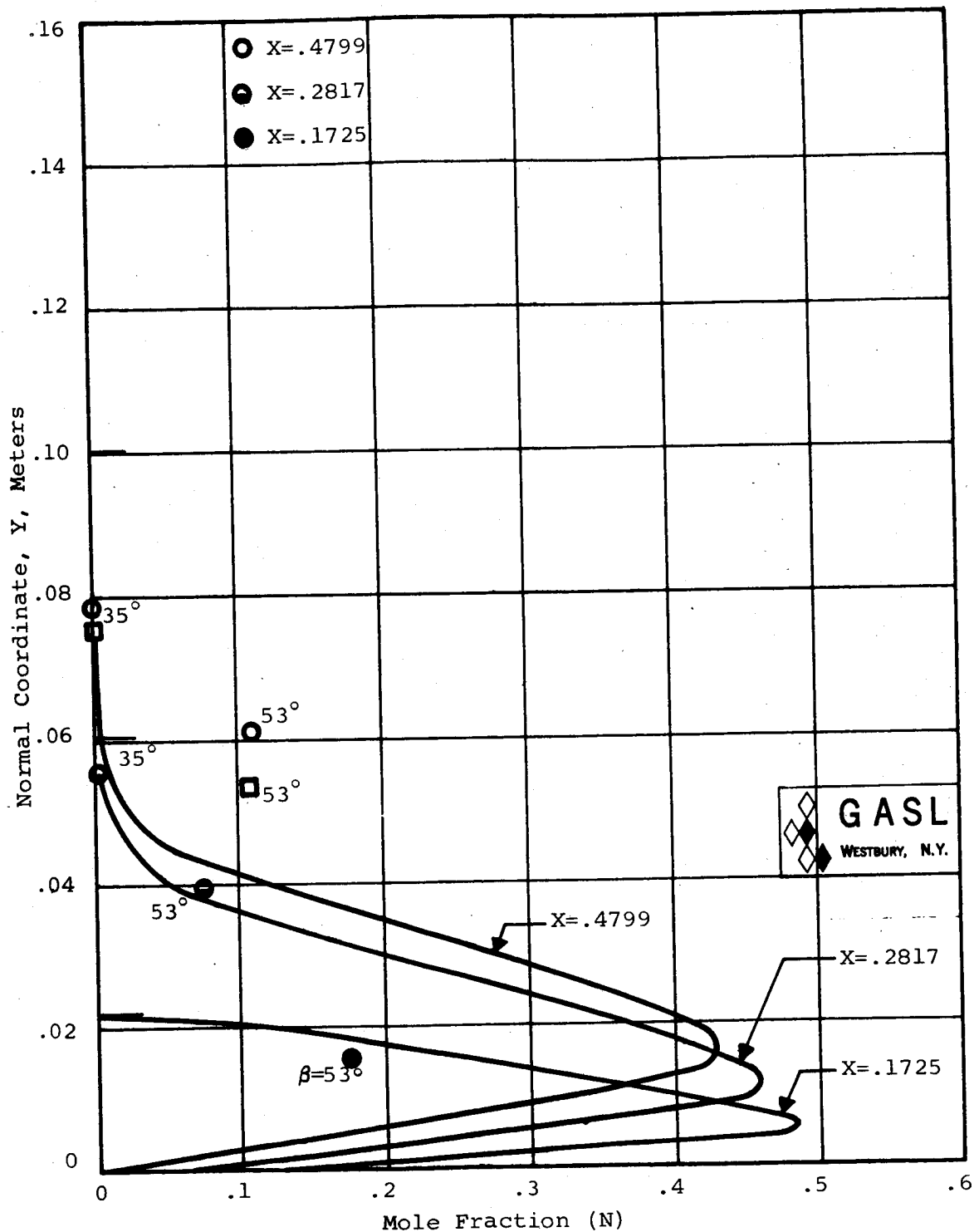
FIG. 66.   SPECIE PROFILES (N) AT SURFACE COORDINATE
            LOCATIONS X=.4799, X=.2817, AND X=.1725
            METERS, ALTITUDE = 53,500 METERS
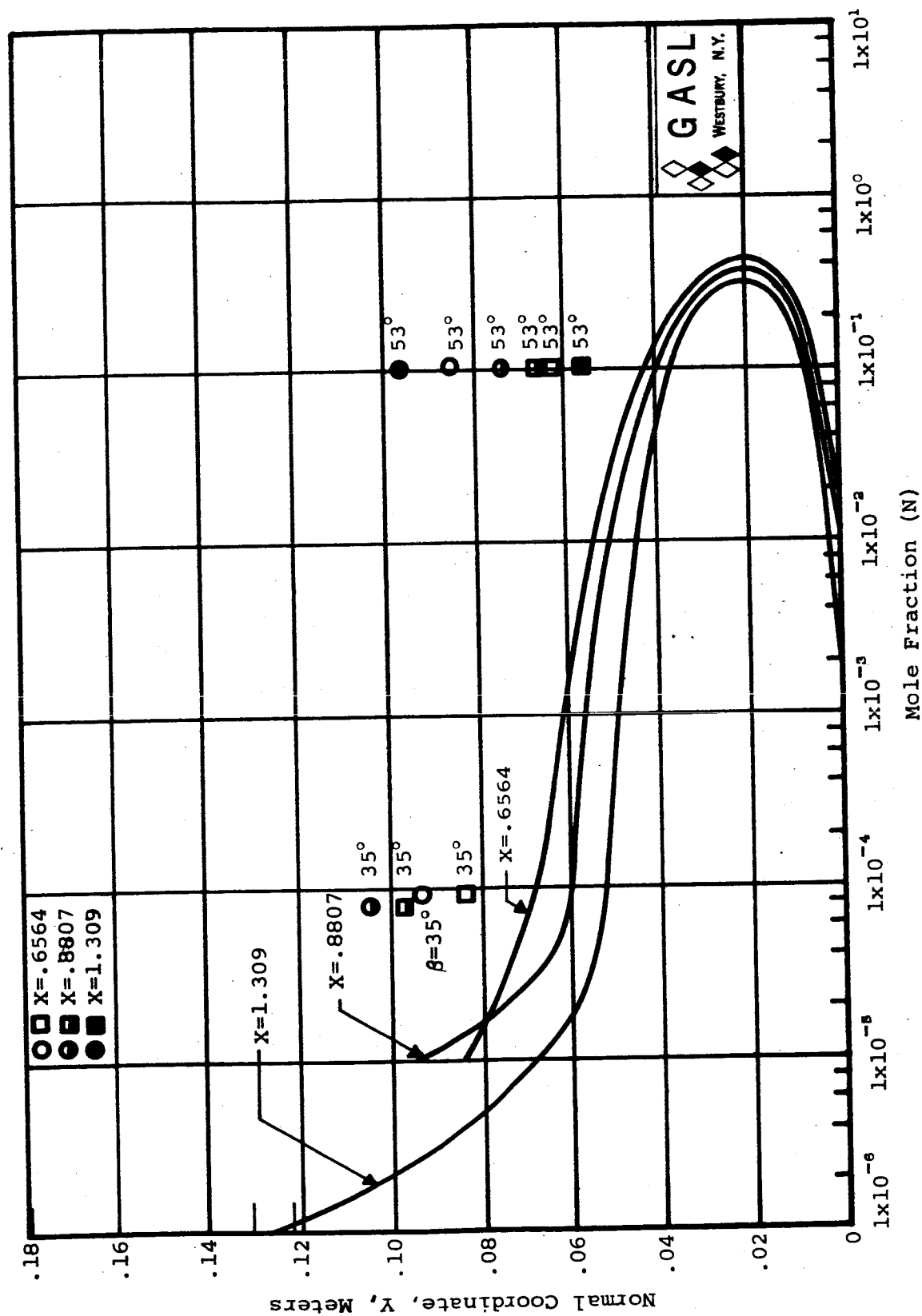
FIG. 67. SPECIE PROFILES (N) AT SURFACE COORDINATE X=.6564, X=.8807, AND X=1.309 METERS, ALTITUDE = 53,500 METERS

99

FIG. 68. SPECIE PROFILES (O) AT SURFACE COORDINATE
LOCATIONS X=.1099, X=.03677, AND X=.01623
METERS, ALTITUDE = 53,500 METERS
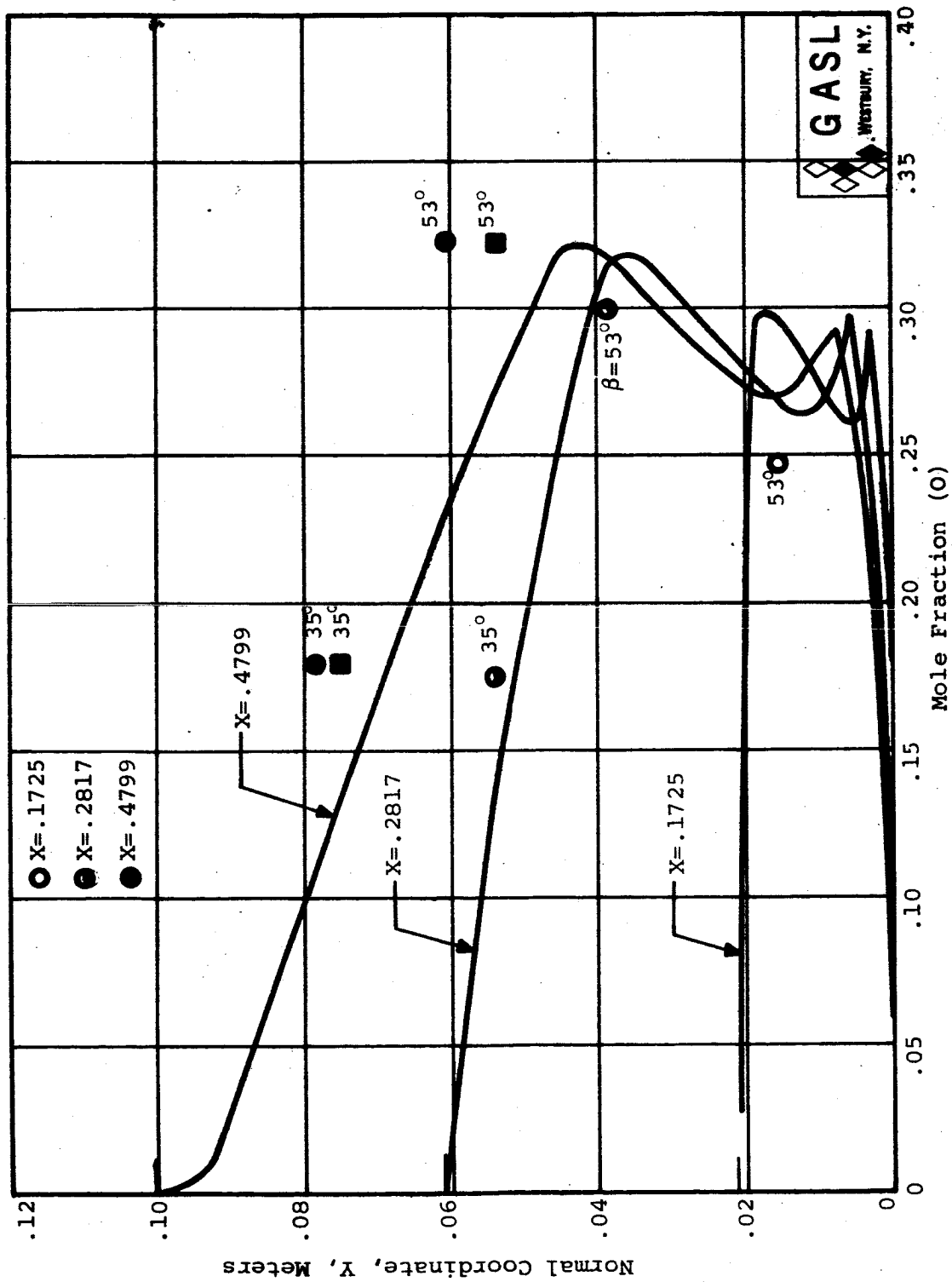
FIG. 69. SPECIE PROFILES (O) AT SURFACE COORDINATE
LOCATIONS X=.1725, X=.2817, AND X=.4799
METERS, ALTITUDE = 53,500 METERS

FIG. 70. SPECIE PROFILES (O) AT SURFACE COORDINATE
LOCATIONS X=.6564, X=.8807, AND X=1.309
METERS, ALTITUDE = 53,500 METERS

FIG. 71. SPECIE PROFILES (NO) AT SURFACE COORDINATE LOCATIONS X=.1099, X=.03677, AND X=.01623 METERS, ALTITUDE = 53,500 METERS

103

FIG. 72. SPECIE PROFILES (NO) AT SURFACE COORDINATE LOCATIONS X=.1725,
X=.2817, AND X=.4799 METERS, ALTITUDE = 53,500 METERS

FIG. 73. SPECIE PROFILES (NO) AT SURFACE COORDINATE LOCATIONS X=.6564, X=.8807, AND X=1.309
METERS, ALTITUDE = 53,500 METERS

105
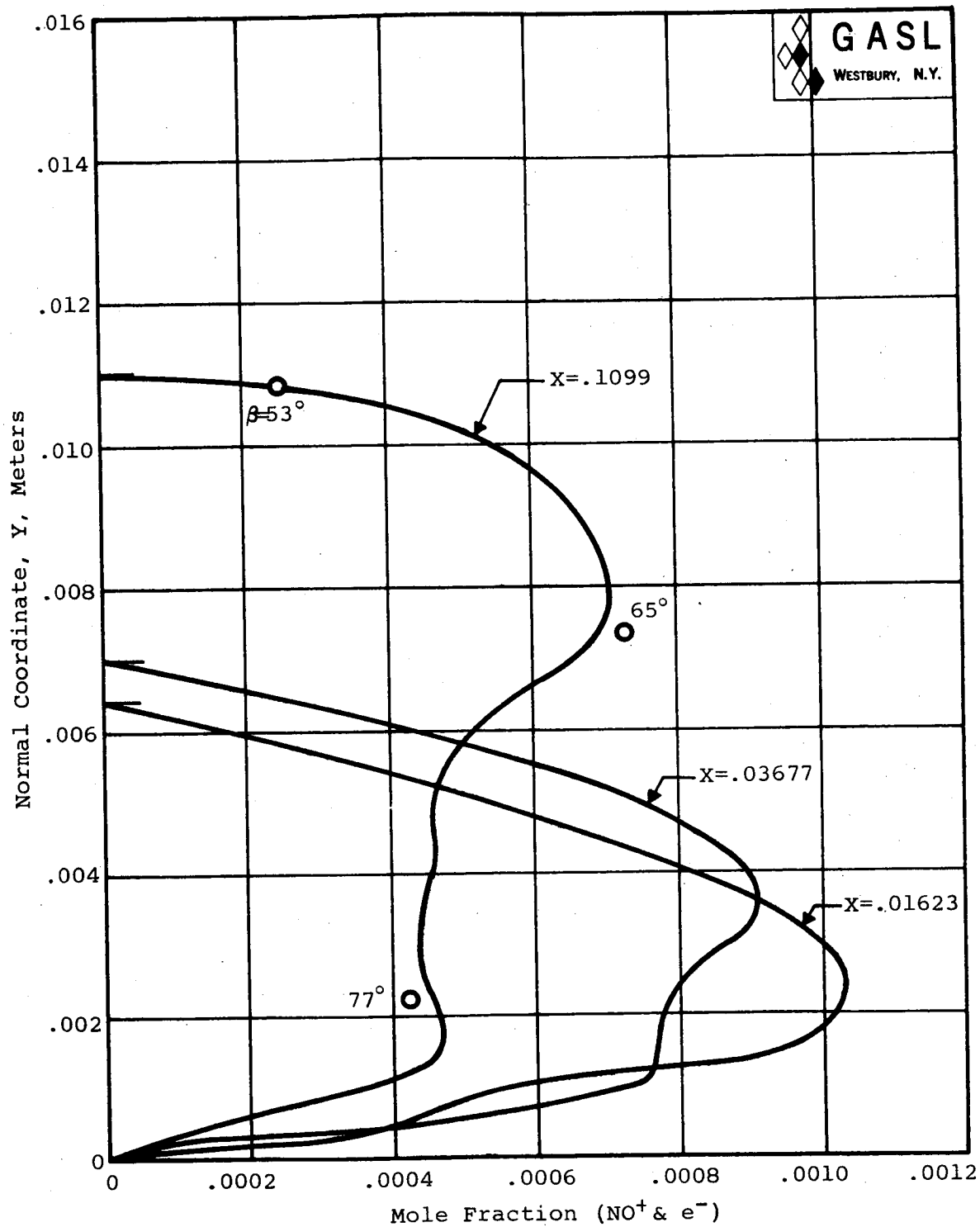
FIG. 74. SPECIE PROFILES (NO⁺) AT SURFACE COORDINATE
LOCATIONS X=.1099, X=.03677, AND X=.01623 METERS,
ALTITUDE = 53,500 METERS

106
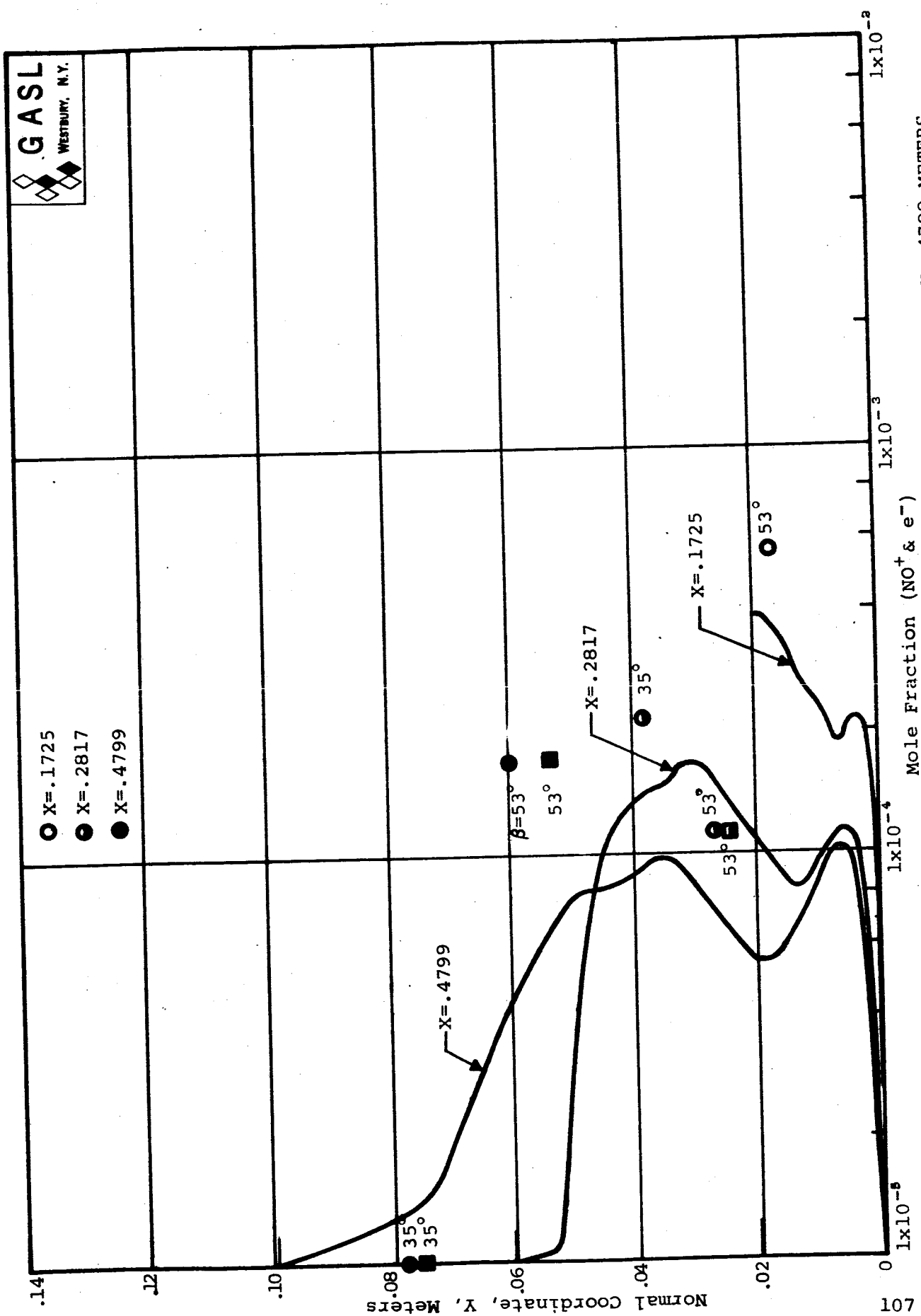
FIG. 75. SPECIE PROFILES (NO⁺) AT SURFACE COORDINATE LOCATIONS X=.1725, X=.2817, AND X=.4799 METERS, ALTITUDE = 53,500 METERS

FIG. 76. SPECIE PROFILES (NO+ AND e−) AT SURFACE COORDINATE LOCATIONS X=.6564,
X=.8807, AND X=1.309 METERS, ALTITUDE = 53,500 METERS

FIG. 77. CONTOUR MAP OF PRESSURE, p, NEWTONS/METER²

ALTITUDE = 53,500 METERS

109

FIG. 78. CONTOUR MAP OF TEMPERATURE, T, °K

ALTITUDE = 53,500 METERS

BOW SHOCK

NON-DIMENSIONAL AXIAL COORDINATE ~ ζ_1/R_N

NON-DIMENSIONAL NORMAL COORDINATE ~ ζ_2/R_N

BODY

110

FIG. 79. CONTOUR MAP OF ELECTRON DENSITY, N_e-, PART/METERS^3

ALTITUDE = 53,500 METERS

NON-DIMENSIONAL AXIAL COORDINATE ~ ζ_1/R_N

NON-DIMENSIONAL NORMAL COORDINATE ~ ζ_3/R_N

111
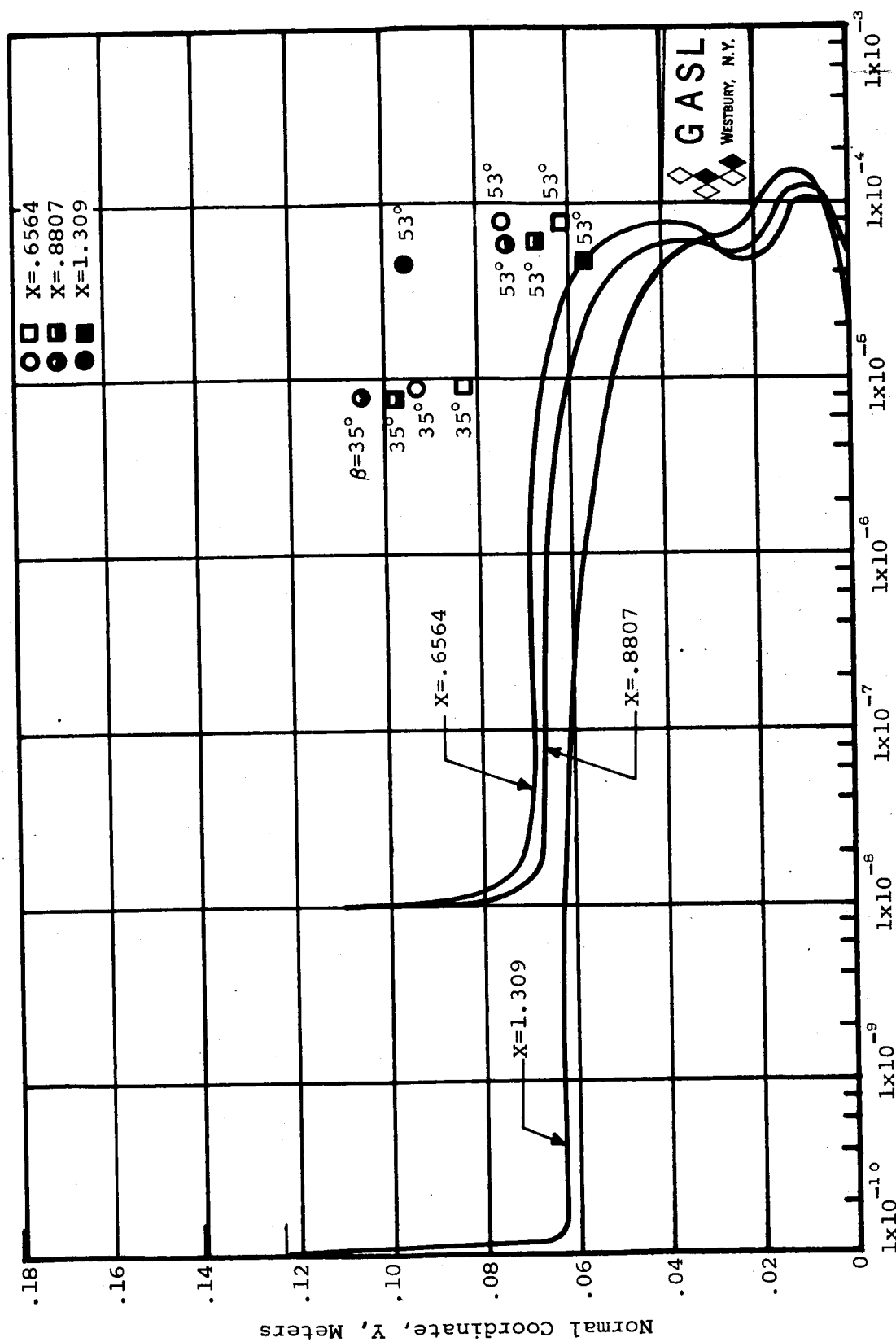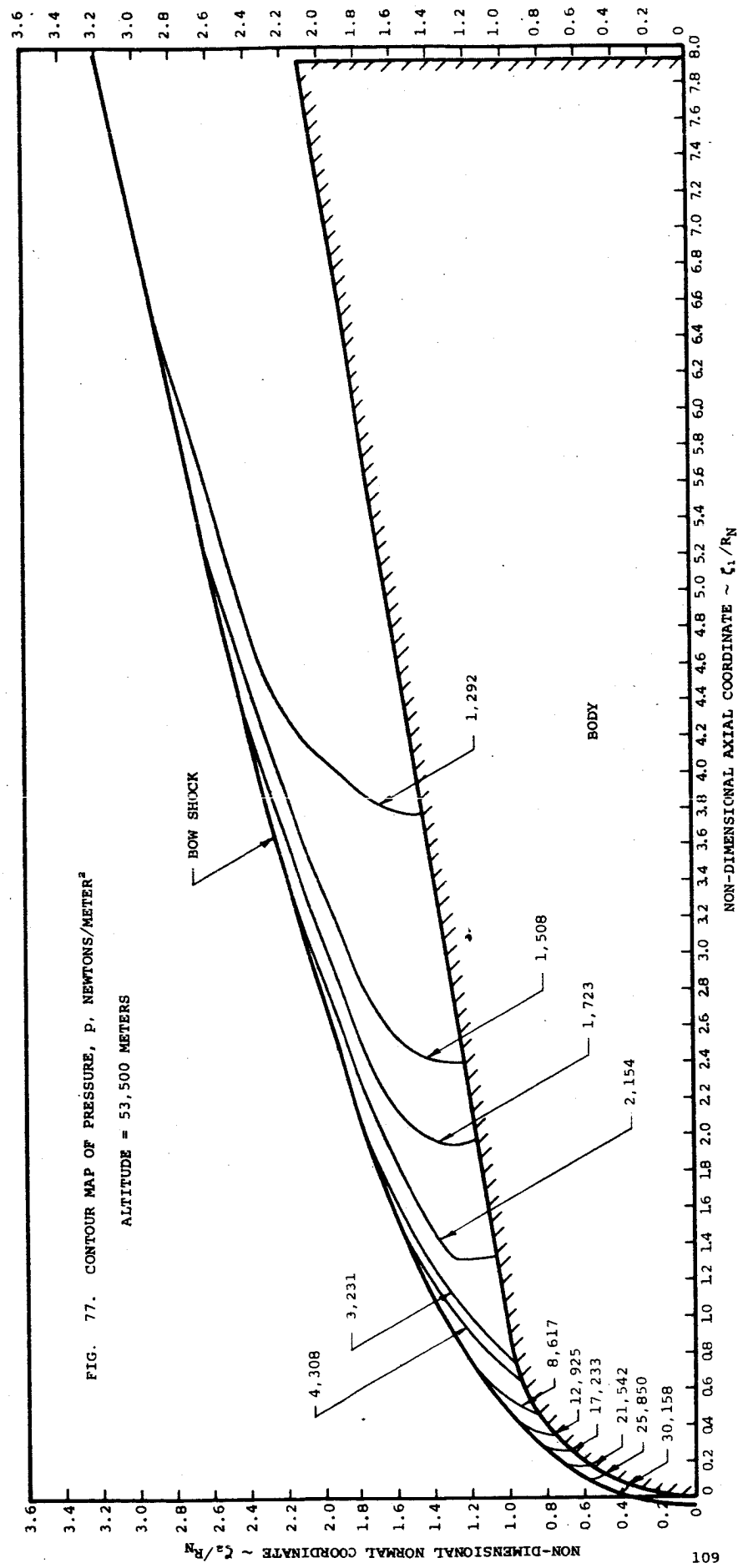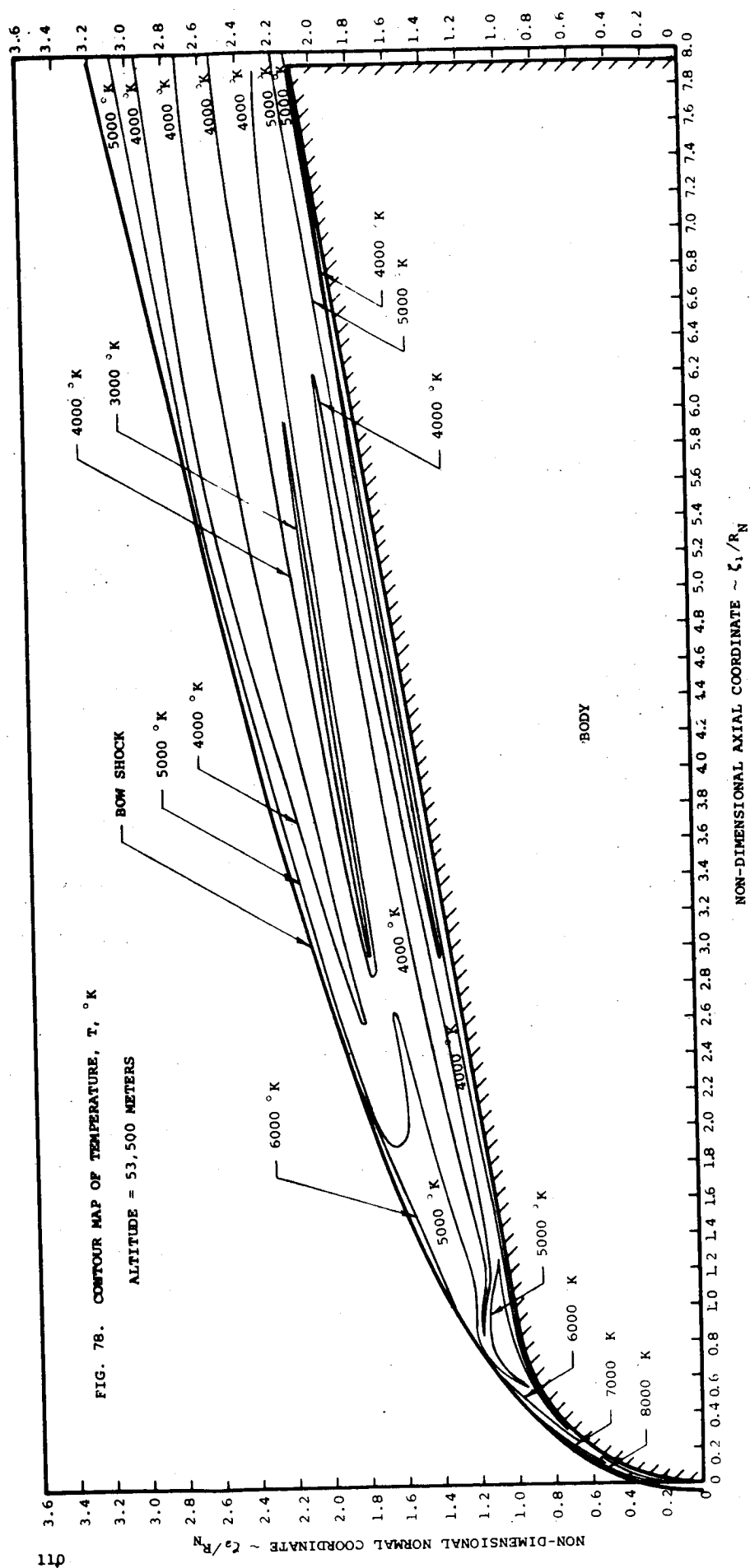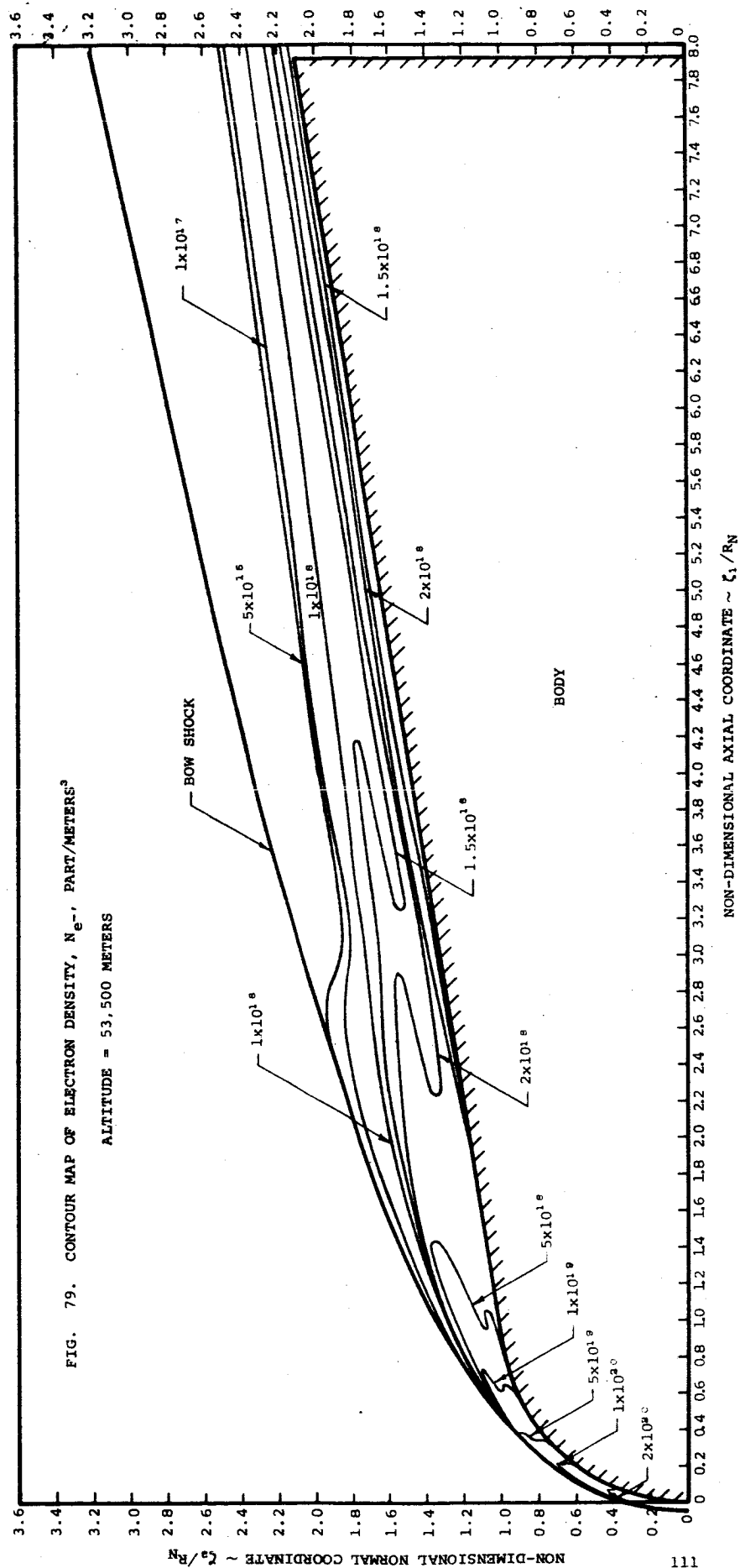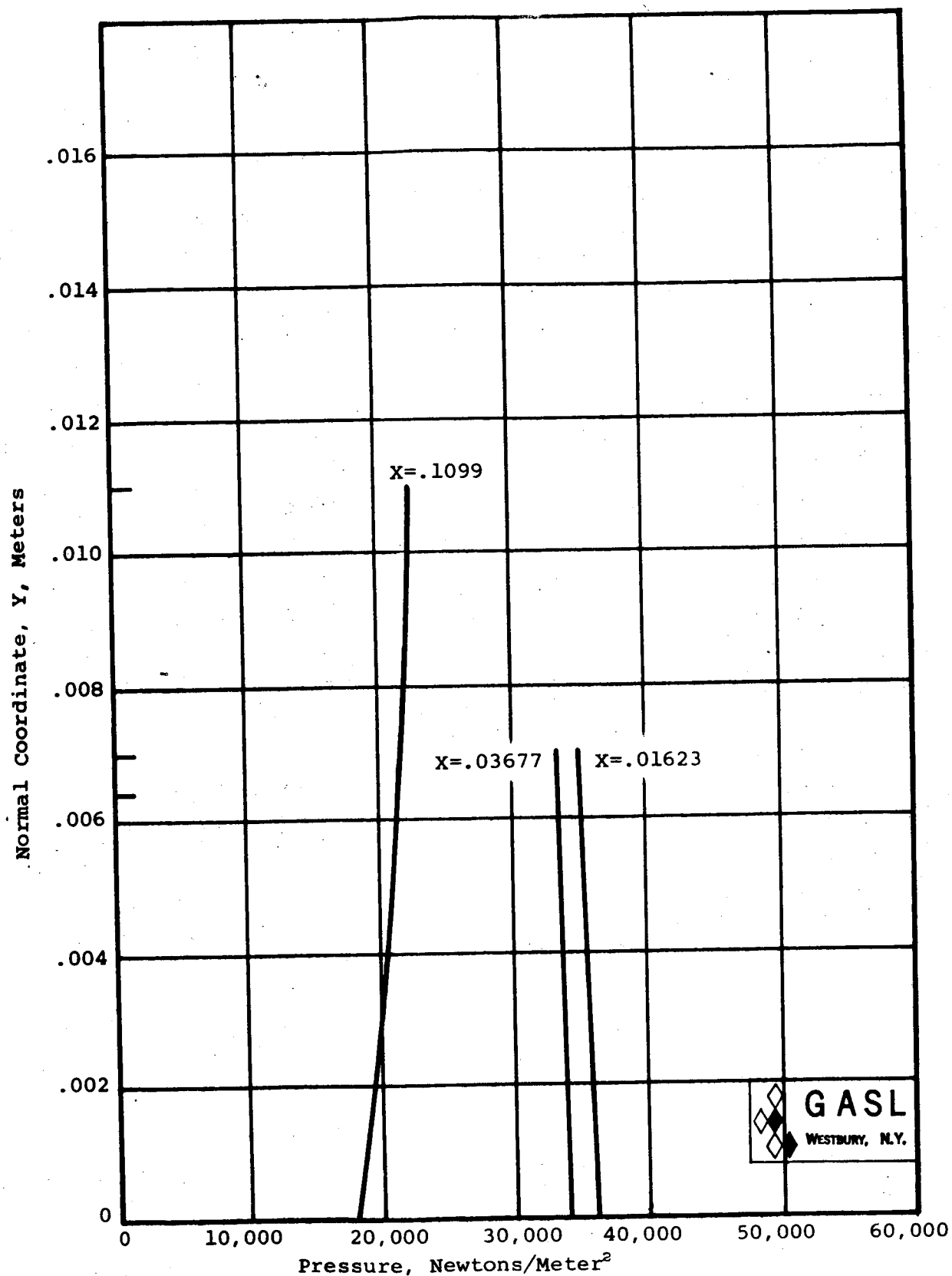
FIG. 80. PRESSURE PROFILES AT SURFACE COORDINATE LOCATIONS
X=.01623, X=.03677, AND X=.1099 METERS,
ALTITUDE = 53,500 METERS
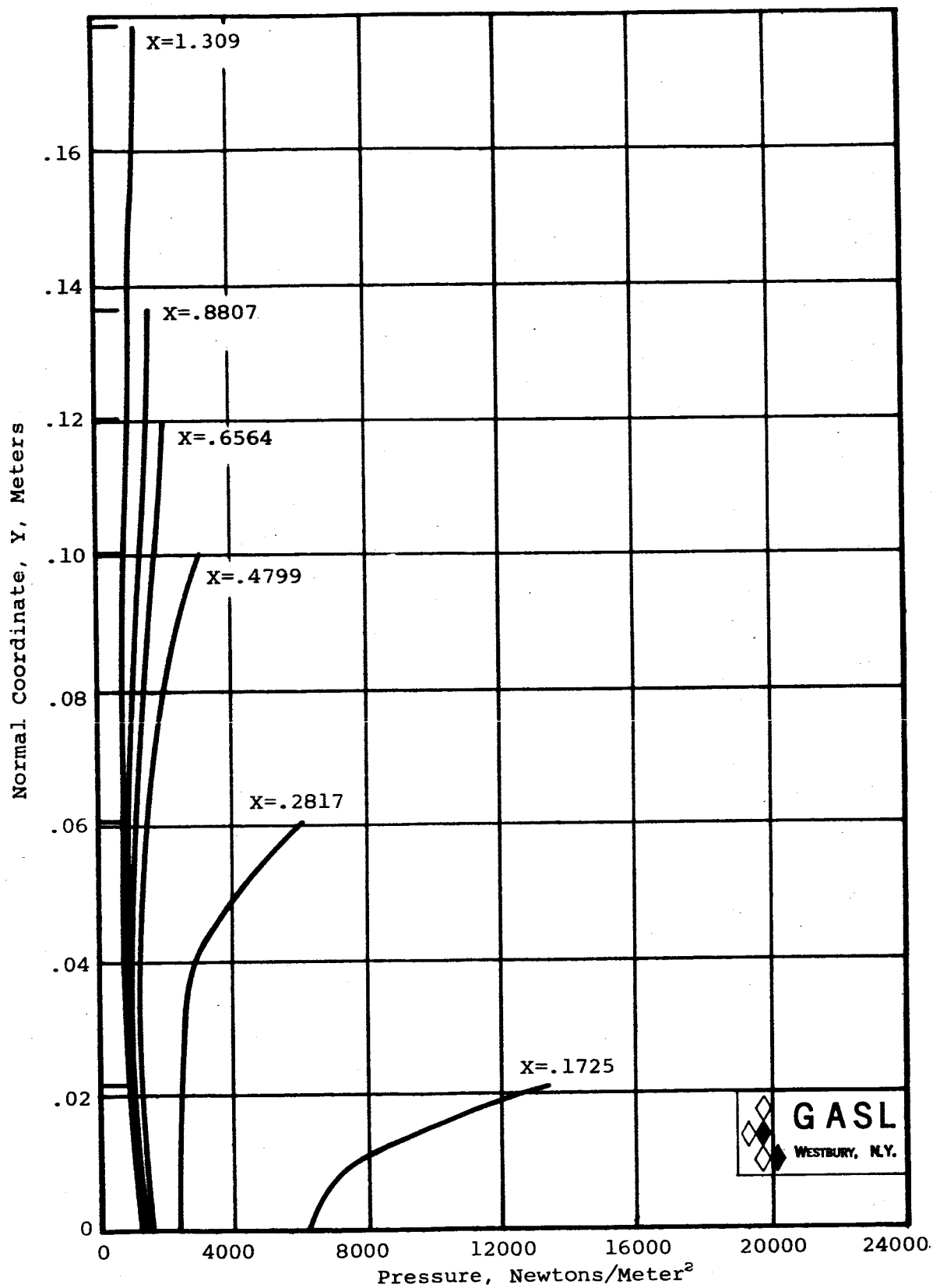
FIG. 81. PRESSURE PROFILES AT SURFACE COORDINATE LOCATIONS
X=.1725, X=.2817, X=.4799, X=.6564, X=.8807, AND
X=1.309 METERS, ALTITUDE = 53,500 METERS

113

ALTITUDE = 71,000 METERS

These results have been included for completeness only. The shock locations for each profile are indicated by the short solid lines drawn along the normal coordinate. Since the shock layer thickness increases with increasing surface coordinate location, their identification is therefore self-explanatory.

The data points indicate the results of streamline calculations where the code utilized for each station is indicated on each figure. The symbol β indicates the post bow shock entry angle of the streamline considered.

The solid lines on the enclosed curves represent the final iterated boundary layer results. These profiles have been cut off at the shock. The dashed lines represent profiles drawn through the results of the inviscid calculations.
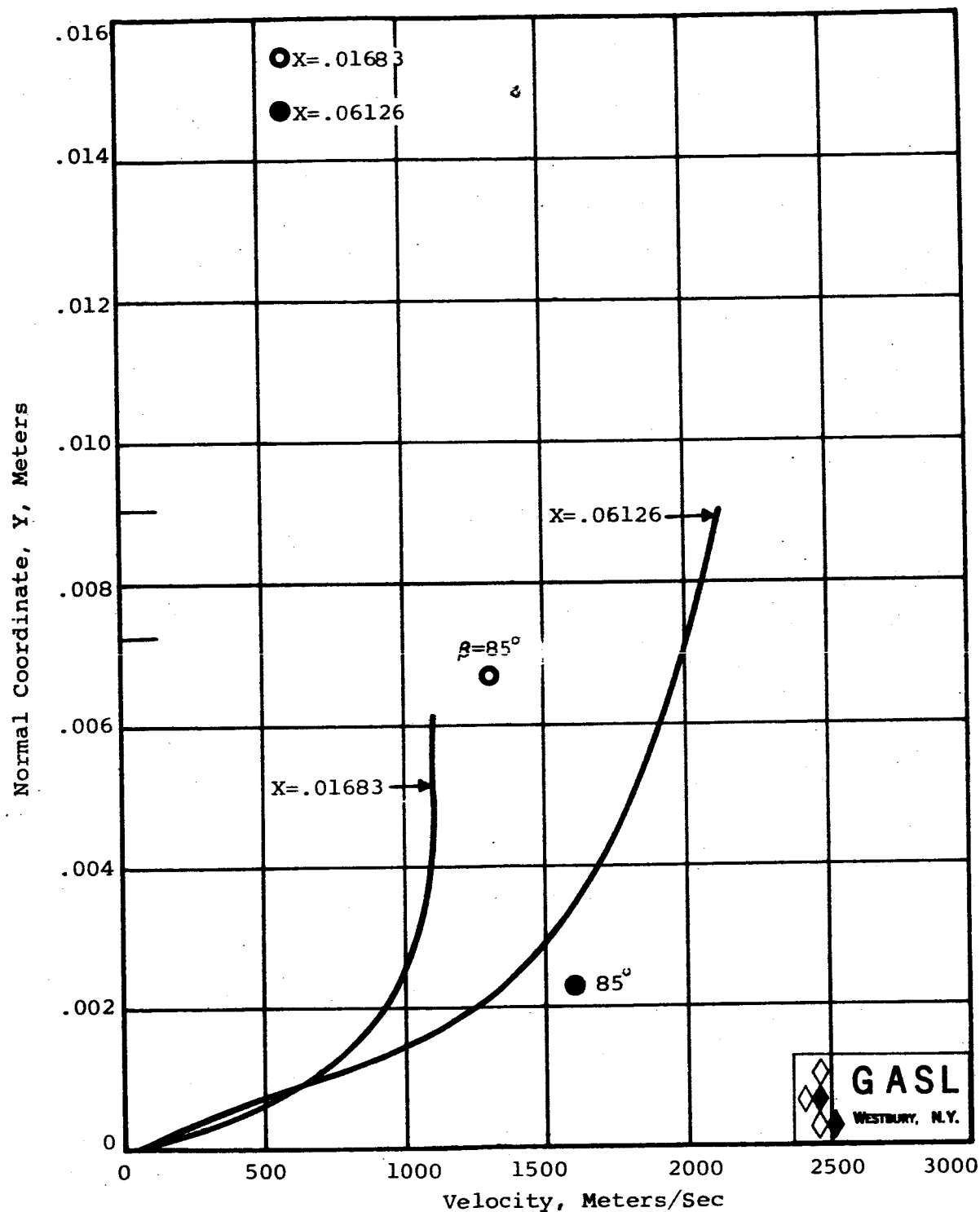
FIG. 82. VELOCITY AT SURFACE COORDINATE LOCATIONS
X=.01683 AND X=.06126 METERS,
ALTITUDE = 71,000 METERS

115
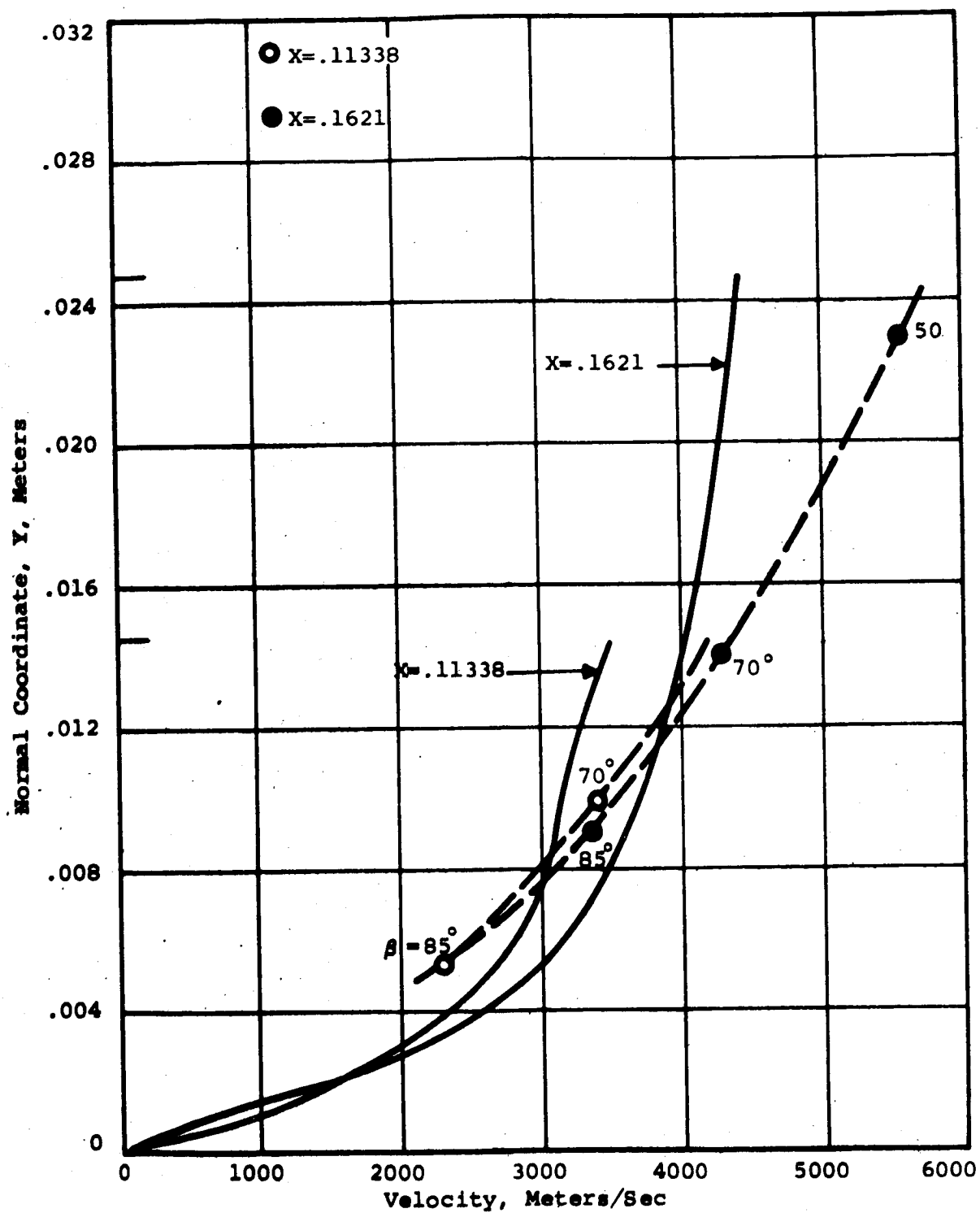
FIG. 83. VELOCITY AT SURFACE COORDINATE LOCATIONS X=.11338 AND X=.1621 METERS, ALTITUDE = 71,000 METERS
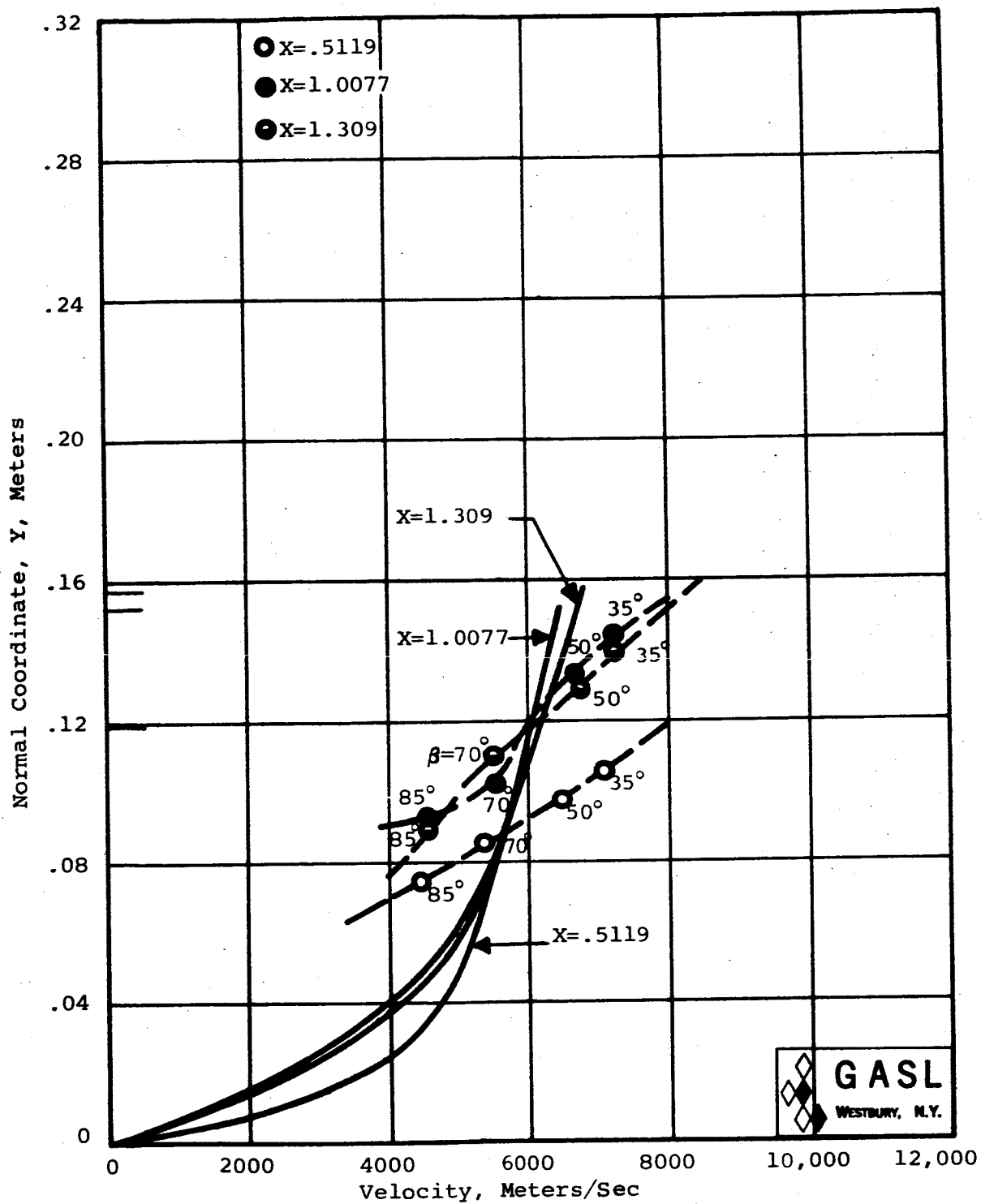
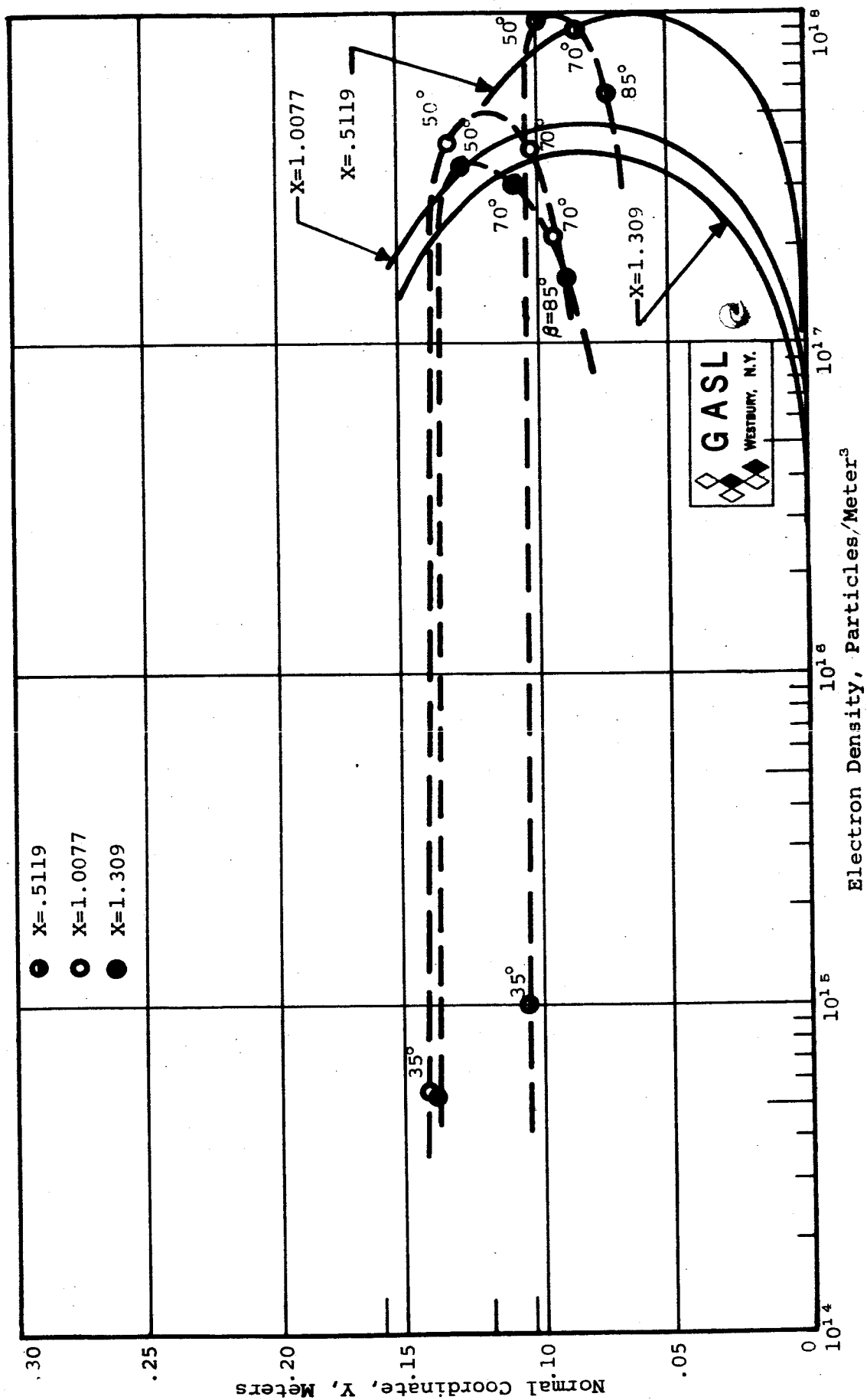FIG. 84. VELOCITY AT SURFACE COORDINATE LOCATIONS
X=.5119, X=1.0077, AND X=1.309 METERS,
ALTITUDE = 71,000 METERS

117
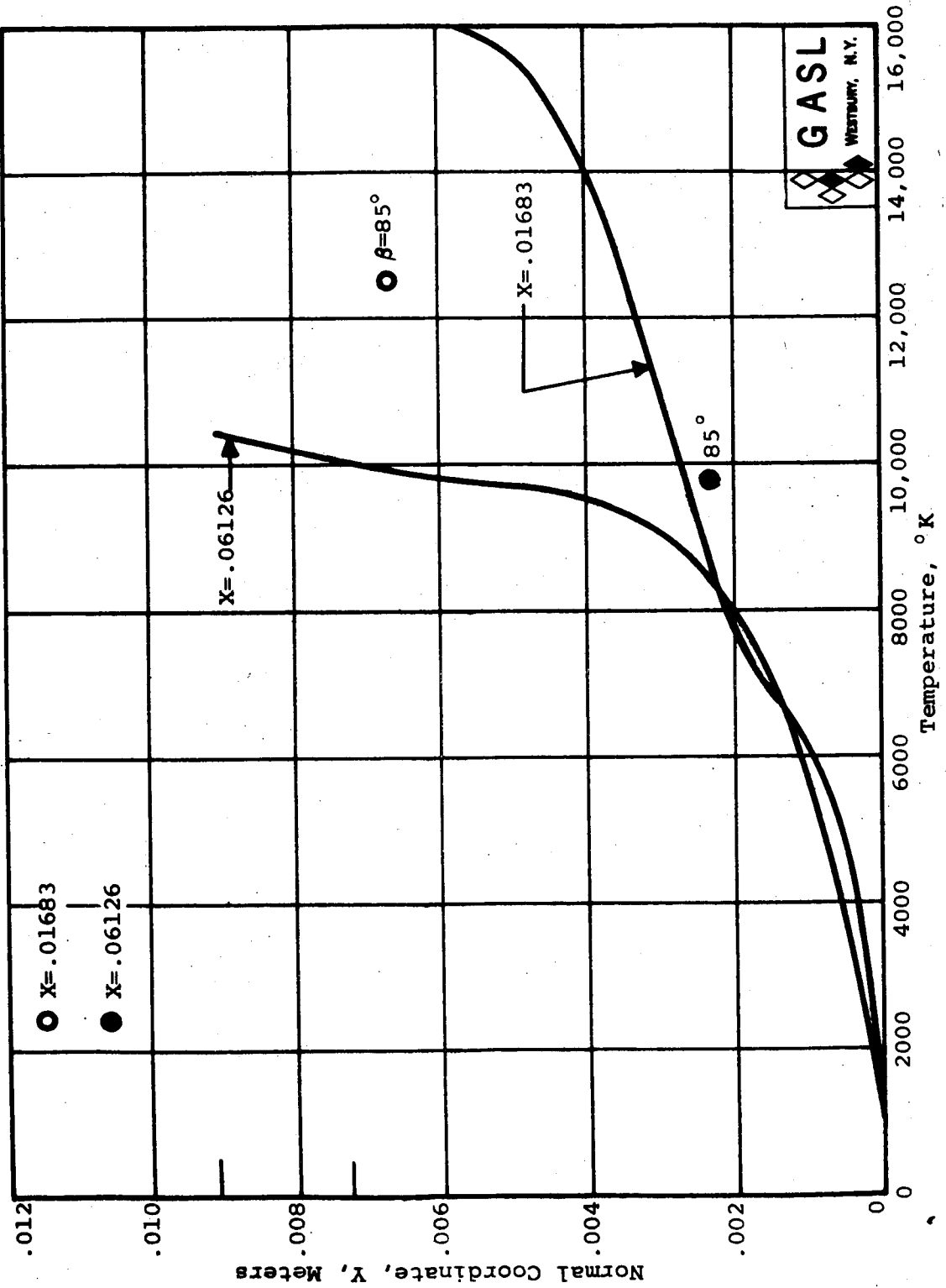
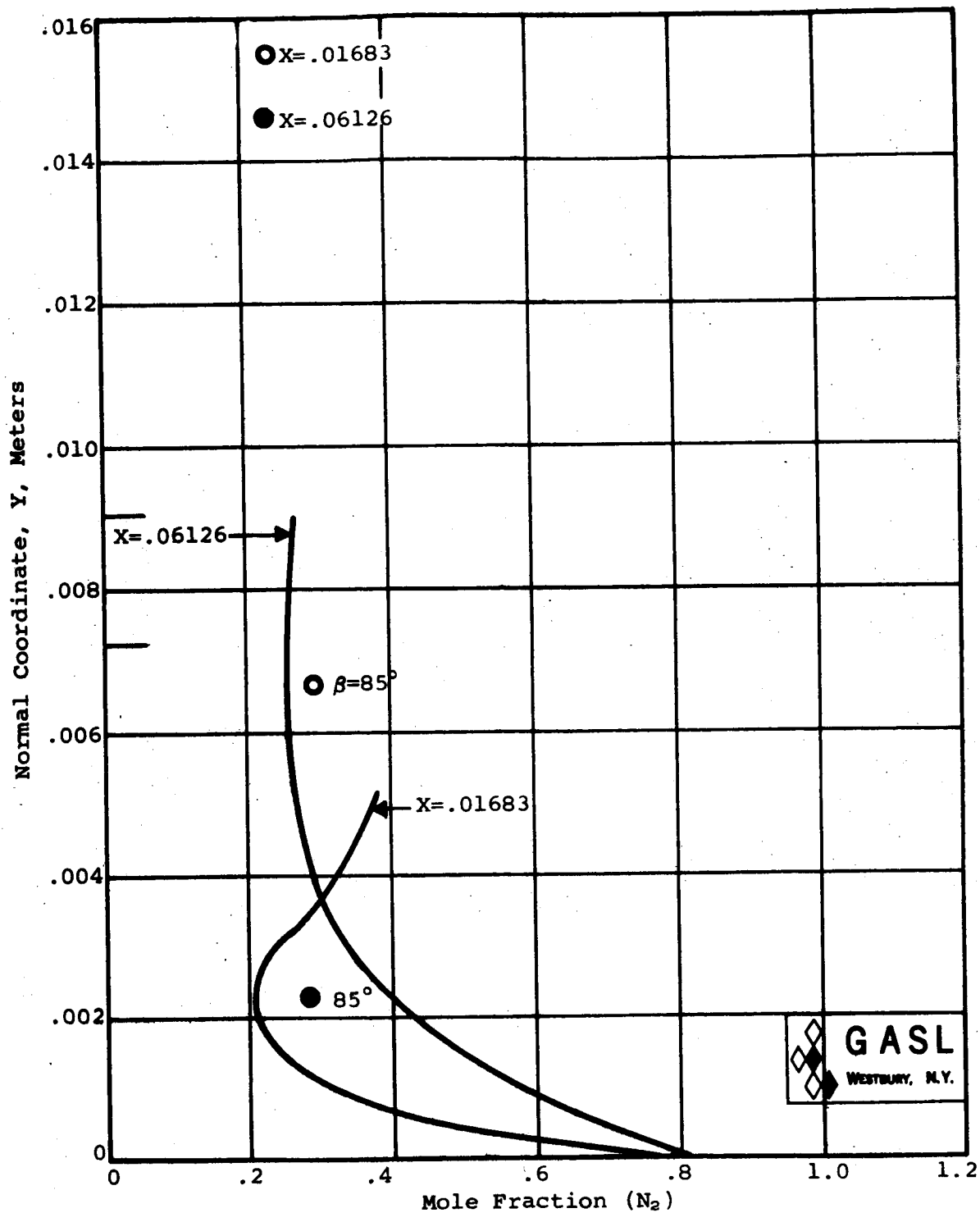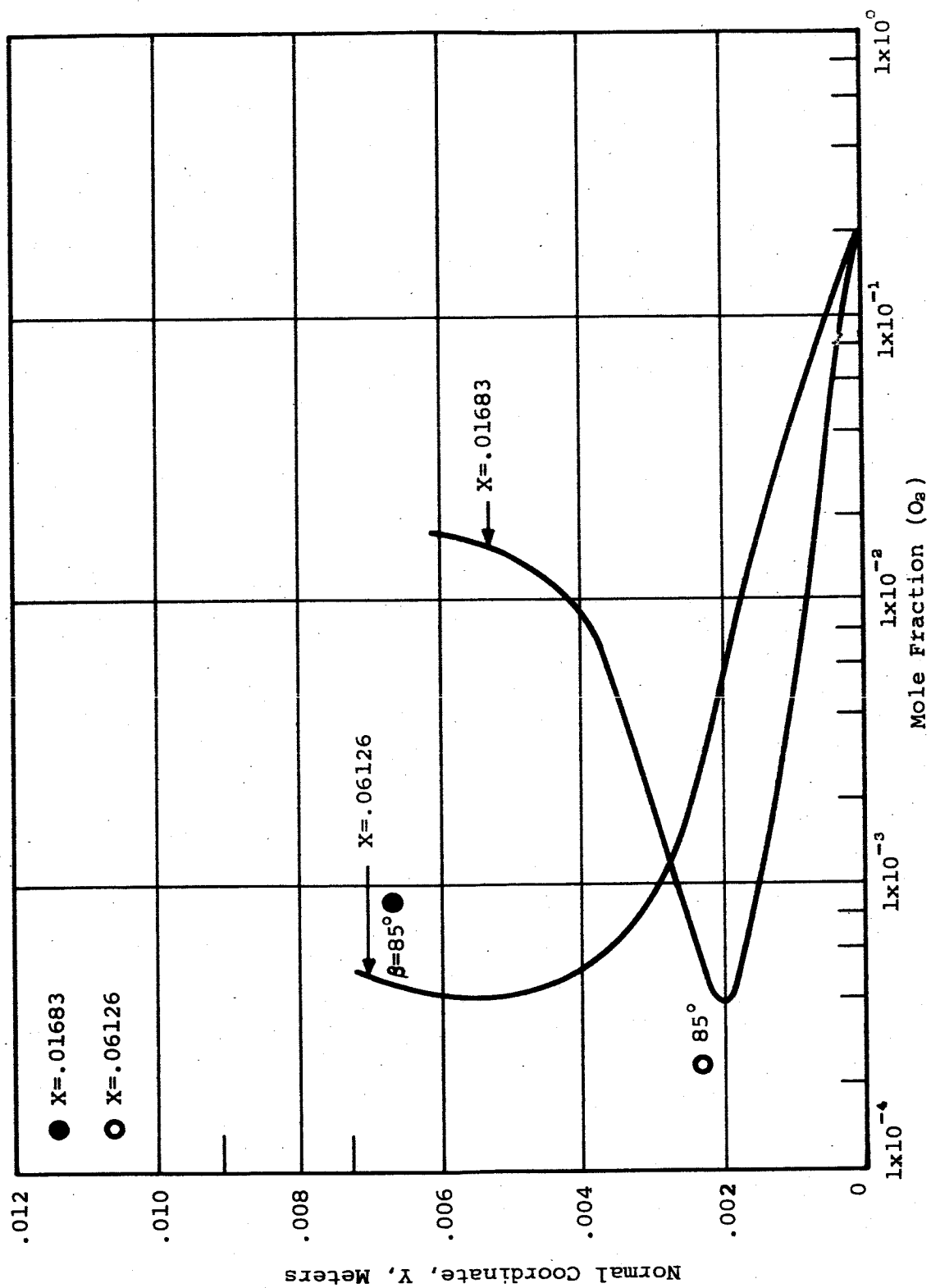FIG. 85. TEMPERATURE AT SURFACE COORDINATE LOCATION X=.01683
AND X=.06126 METERS, ALTITUDE = 71,000 METERS

118
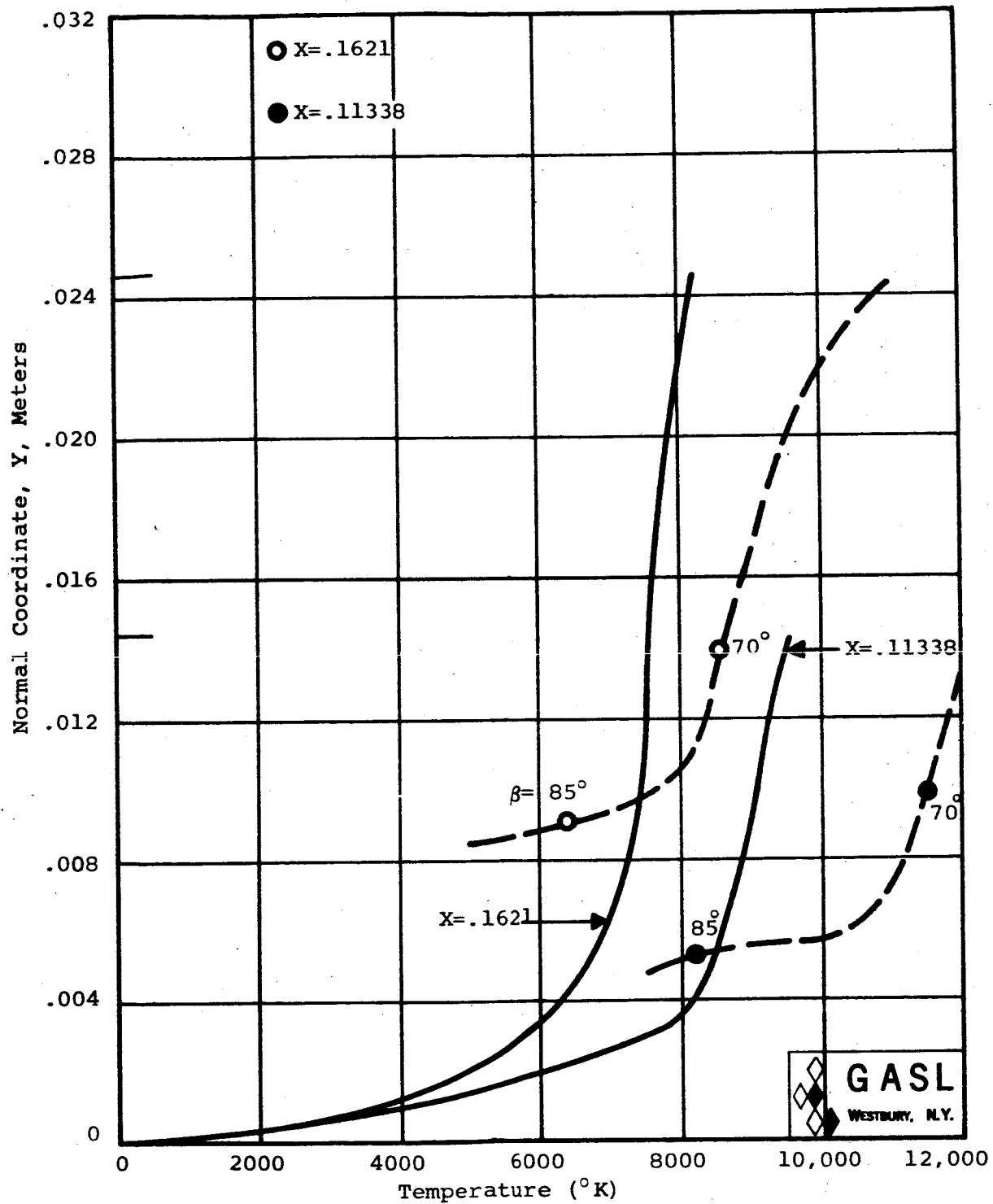
FIG. 86. TEMPERATURE AT SURFACE COORDINATE
LOCATIONS X=.1621 AND X=.11338
METERS, ALTITUDE = 71,000 METERS
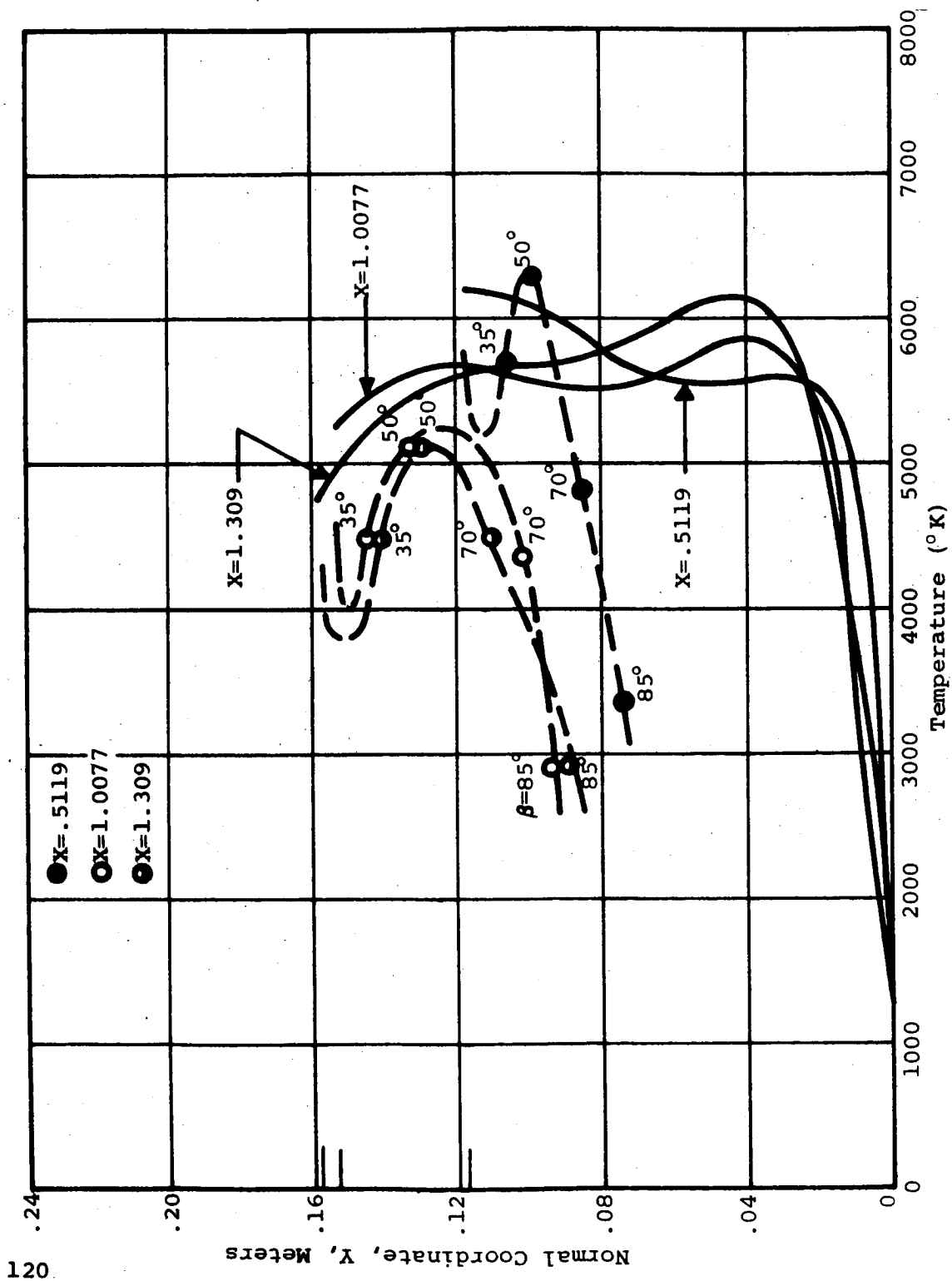
FIG. 87. TEMPERATURE AT SURFACE COORDINATE LOCATIONS
X=.5119, X = 1.0077, AND X=1.309 METERS,
ALTITUDE = 71,000 METERS

120

FIG. 88. ELECTRON DENSITY AT SURFACE COORDINATE LOCATIONS X=.01683
AND X=.06126 METERS, ALTITUDE = 71,000 METERS

121

Electron Density, Particles/Meter³
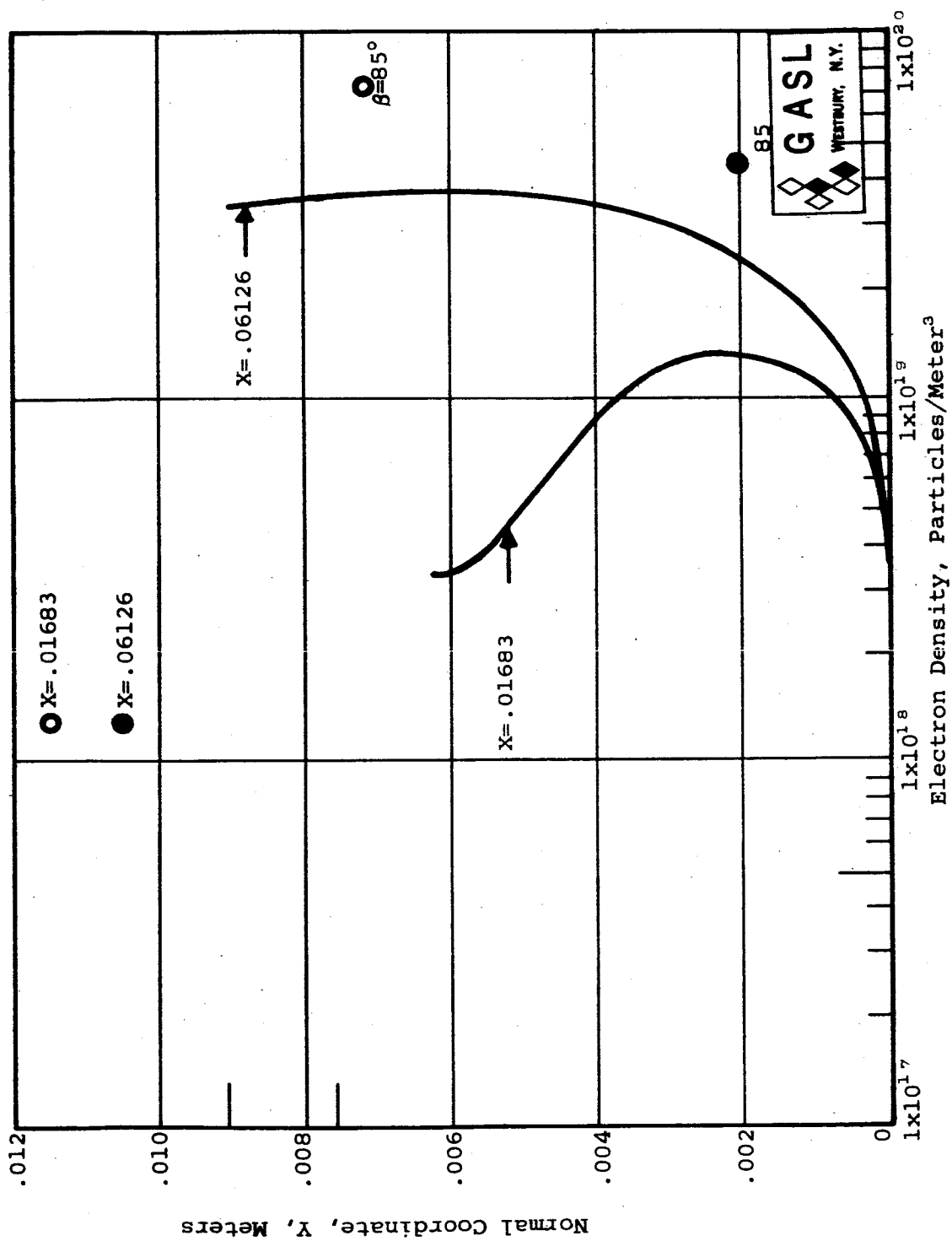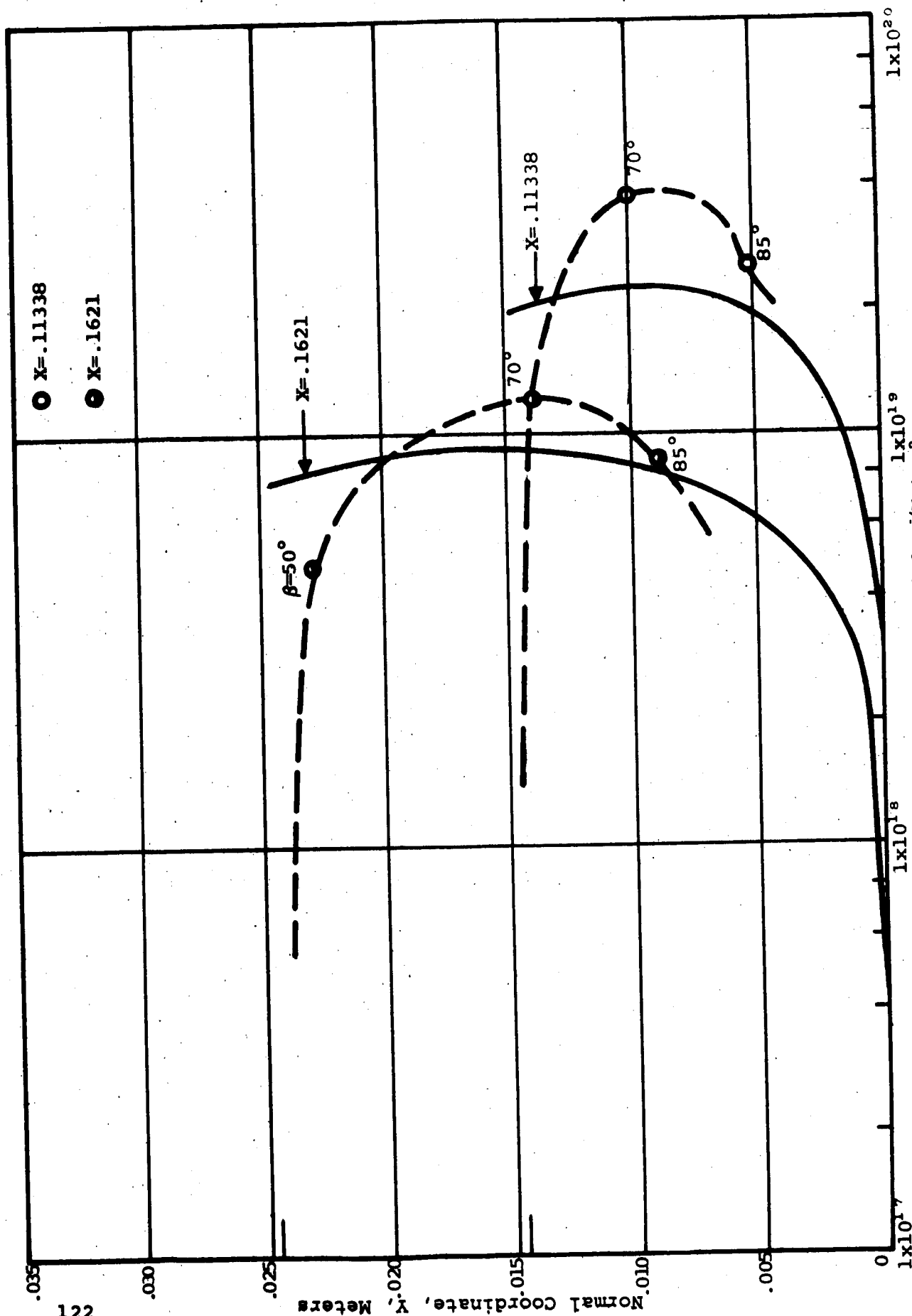
FIG. 89. ELECTRON DENSITY AT SURFACE COORDINATE LOCATIONS X=.11338 AND
X=.1621 METERS, ALTITUDE = 71,000 METERS

122

FIG. 90. ELECTRON DENSITY AT SURFACE COORDINATE LOCATIONS X=.5119, X=1.0077, AND X=1.309 METERS, ALTITUDE = 71,000 METERS

123

FIG. 91. SPECIE PROFILES (N₂) AT SURFACE
COORDINATE LOCATIONS X=.01683 AND
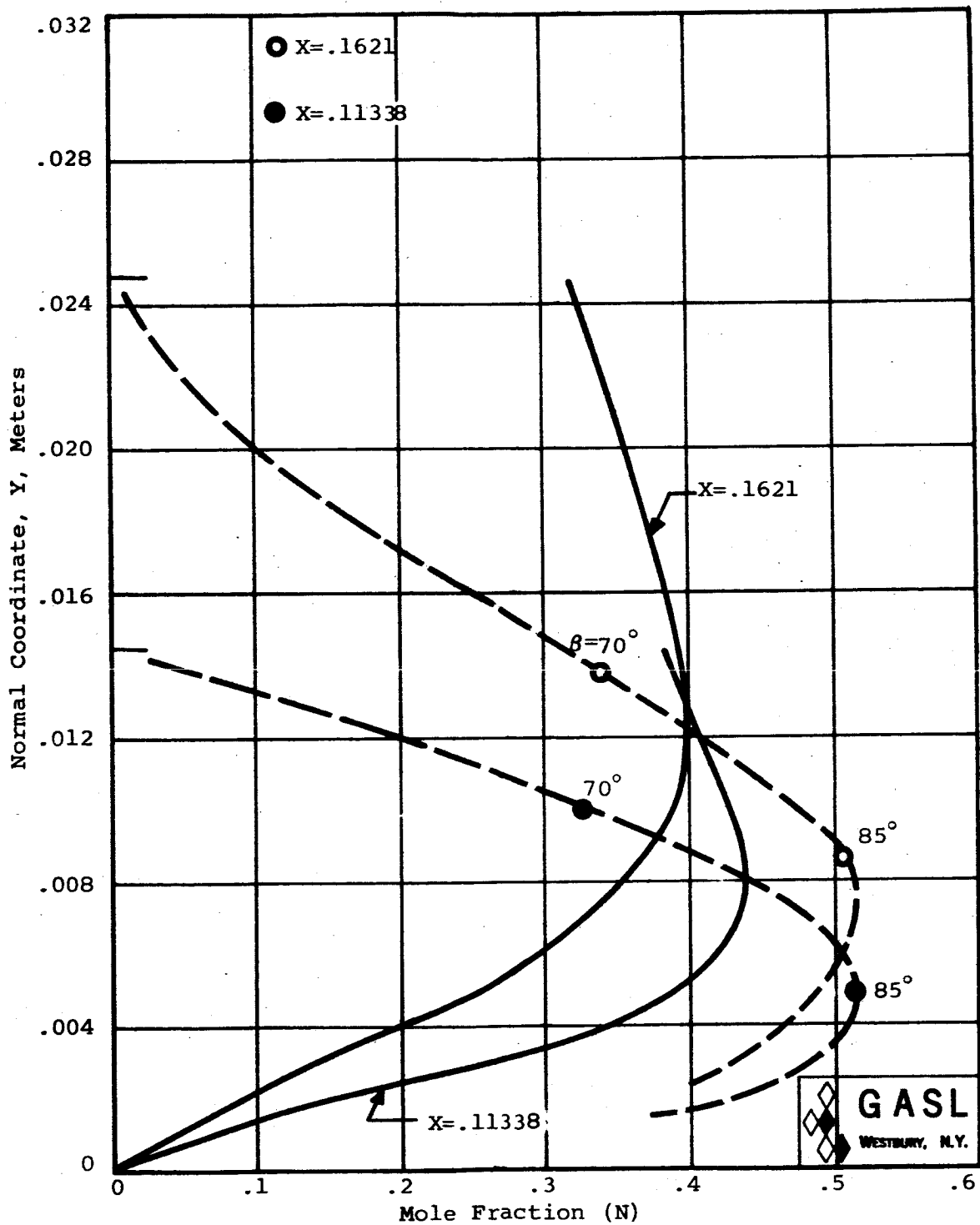X=.06126 METERS, ALTITUDE = 71,000
METERS

124
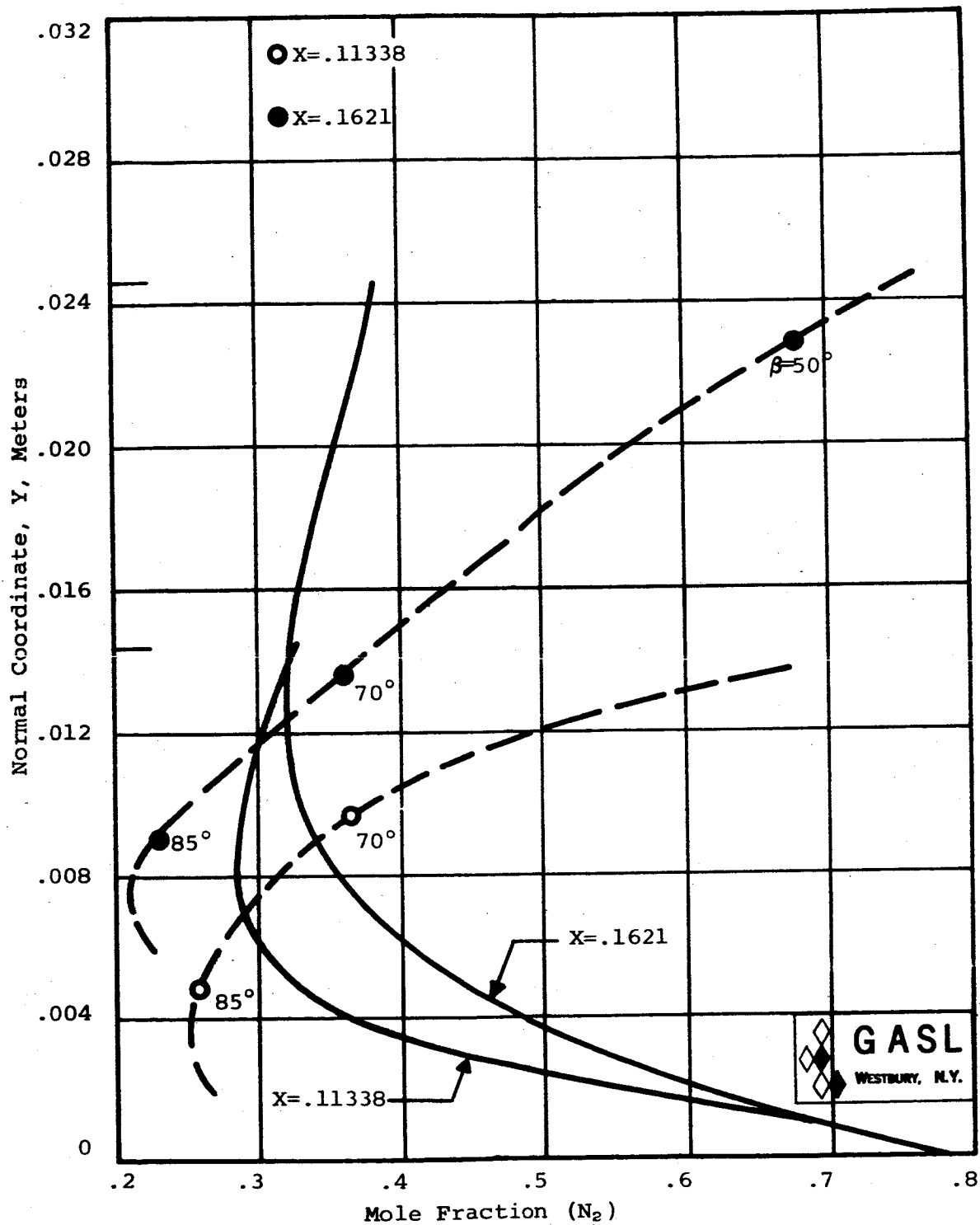
FIG. 92. SPECIES PROFILES (N₂) AT SURFACE
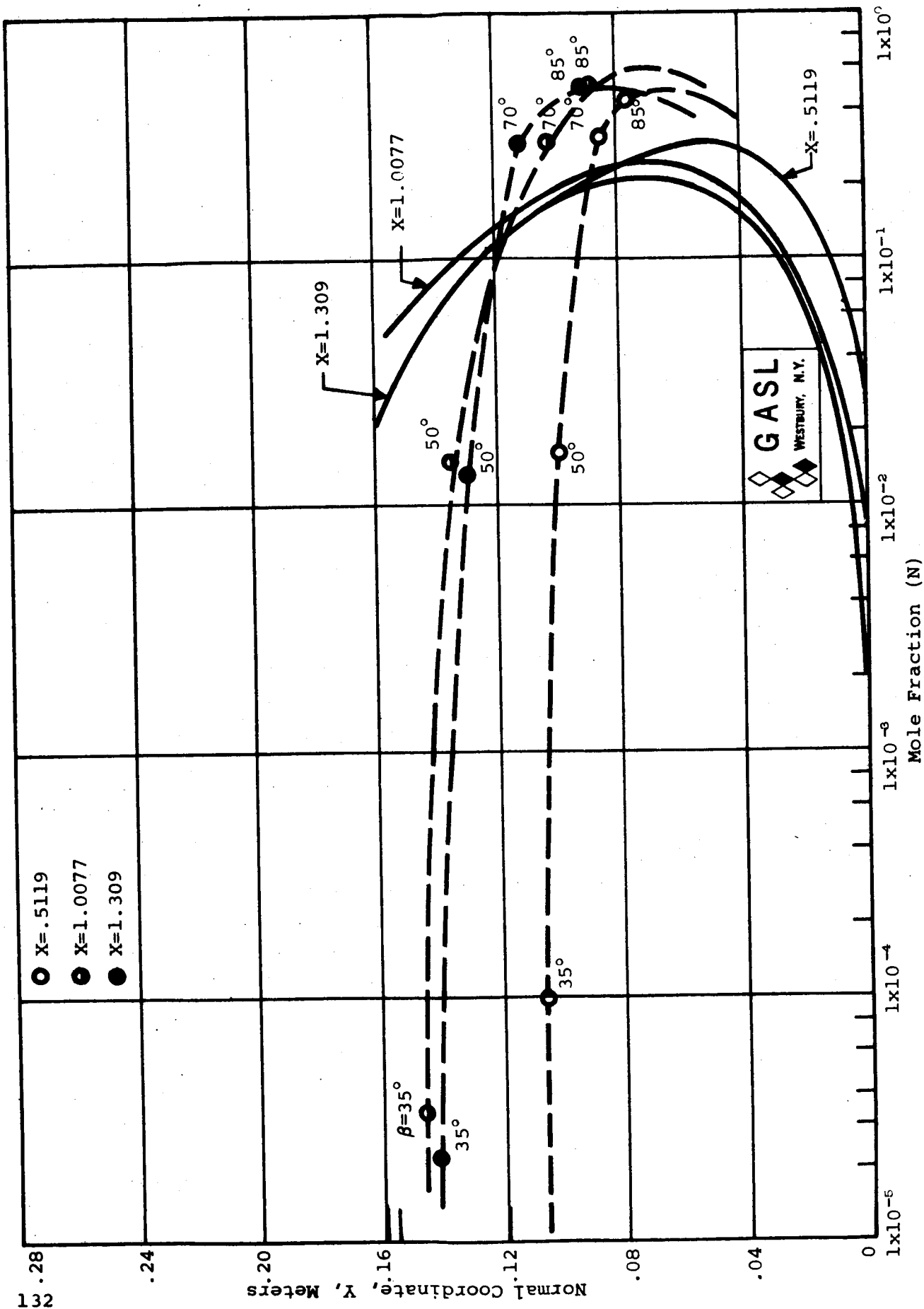COORDINATE LOCATIONS X=.11338 AND
X=.1621 METERS, ALTITUDE = 71,000 METERS
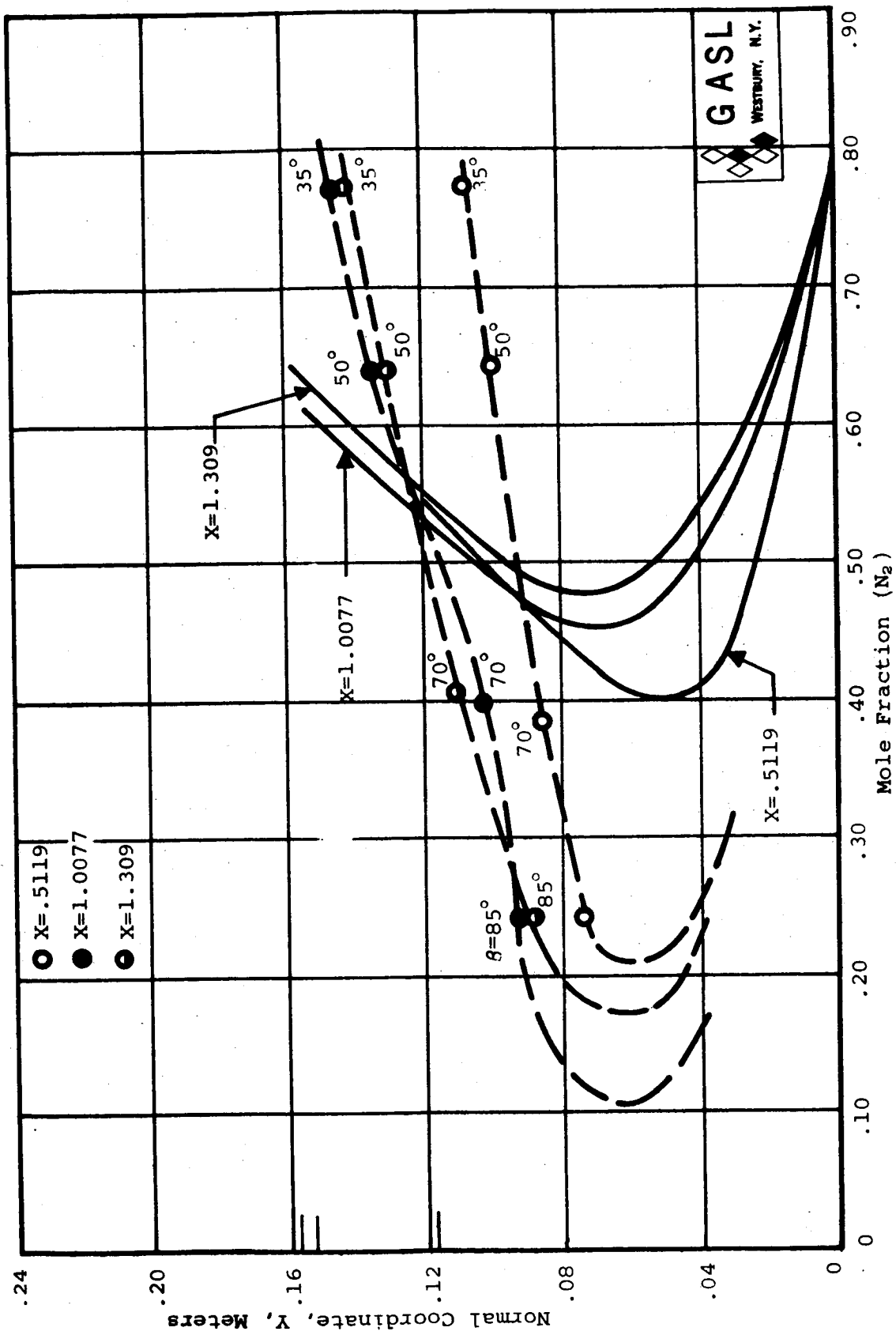
FIG. 93. SPECIE PROFILES (N_2) AT SURFACE COORDINATE LOCATIONS X=.5119, X=1.0077, AND X=1.309 **METERS, ALTITUDE = 71,000 METERS**
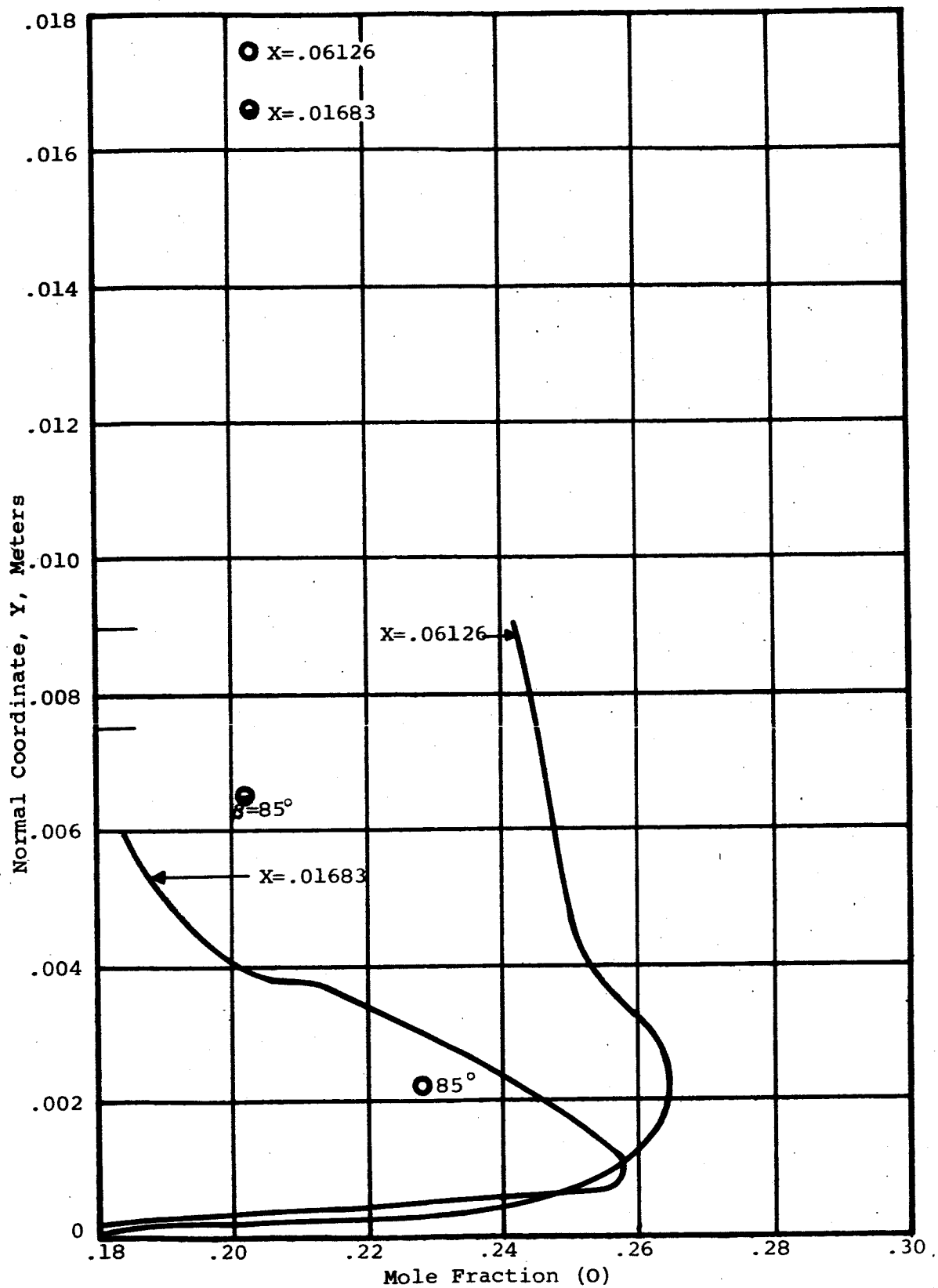
126

FIG. 94.   SPECIE PROFILES (O₂) AT SURFACE COORDINATE LOCATIONS X=.01683
AND X=.06126 METERS, ALTITUDE = 71,000 METERS

127
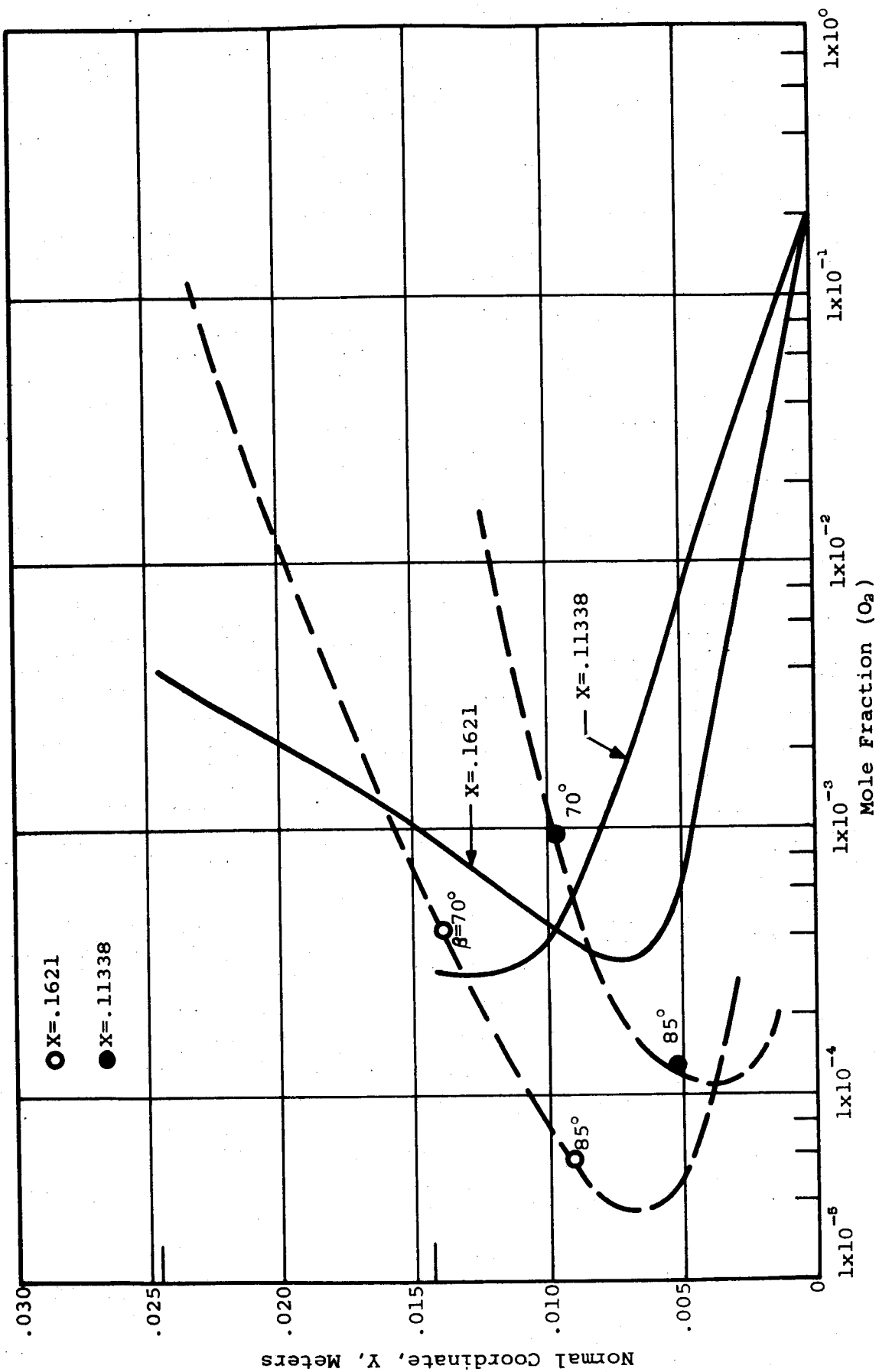
FIG. 95. SPECIE PROFILES (O_2) AT SURFACE COORDINATE LOCATIONS X=.1621 AND X=.11338 METERS, ALTITUDE 71,000 METERS

128
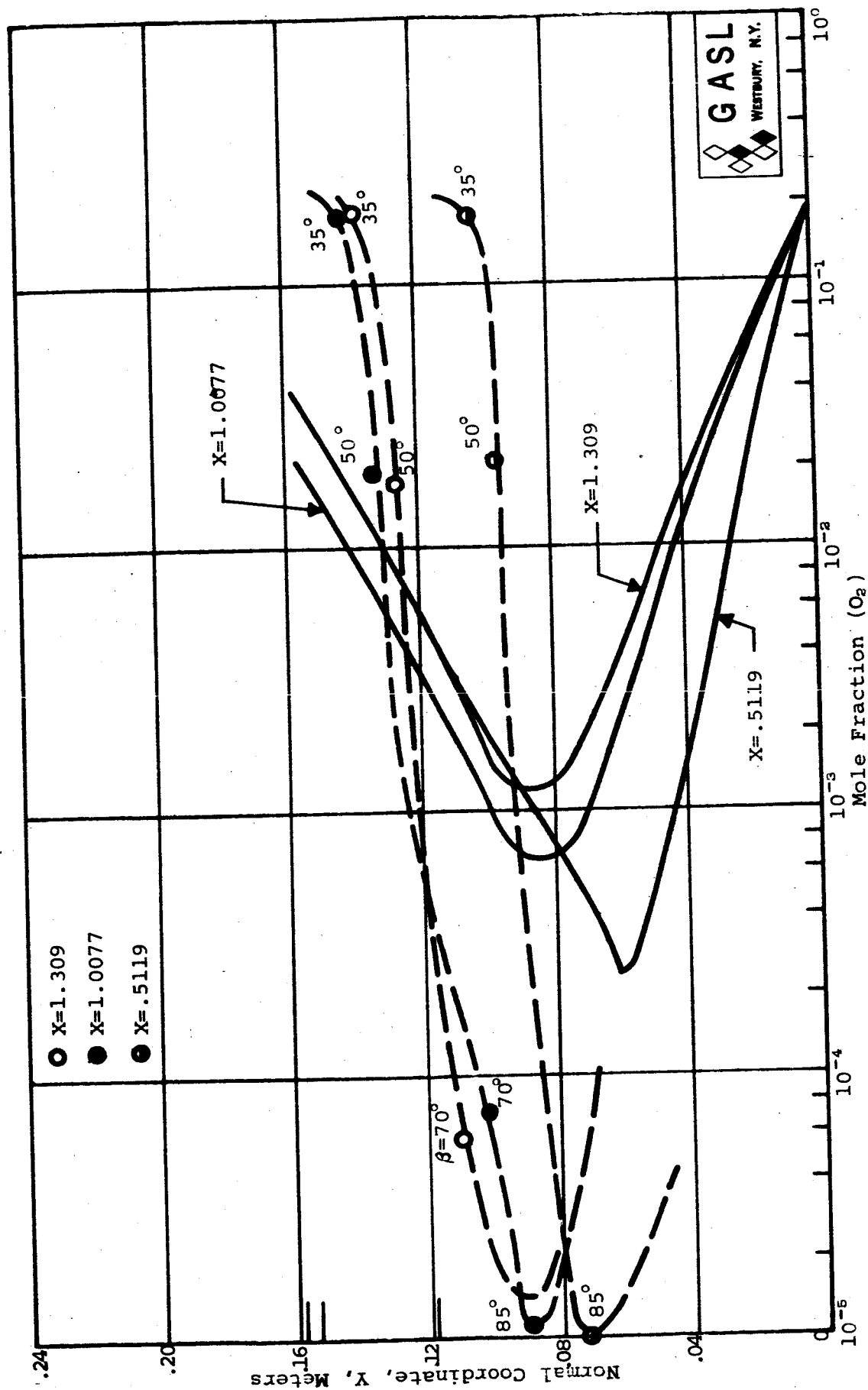
FIG. 96. SPECIE PROFILES (O_2) AT SURFACE COORDINATE LOCATIONS X=1.309, X=1.0077, AND X=.5119 METERS, ALTITUDE = 71,000 METERS

129
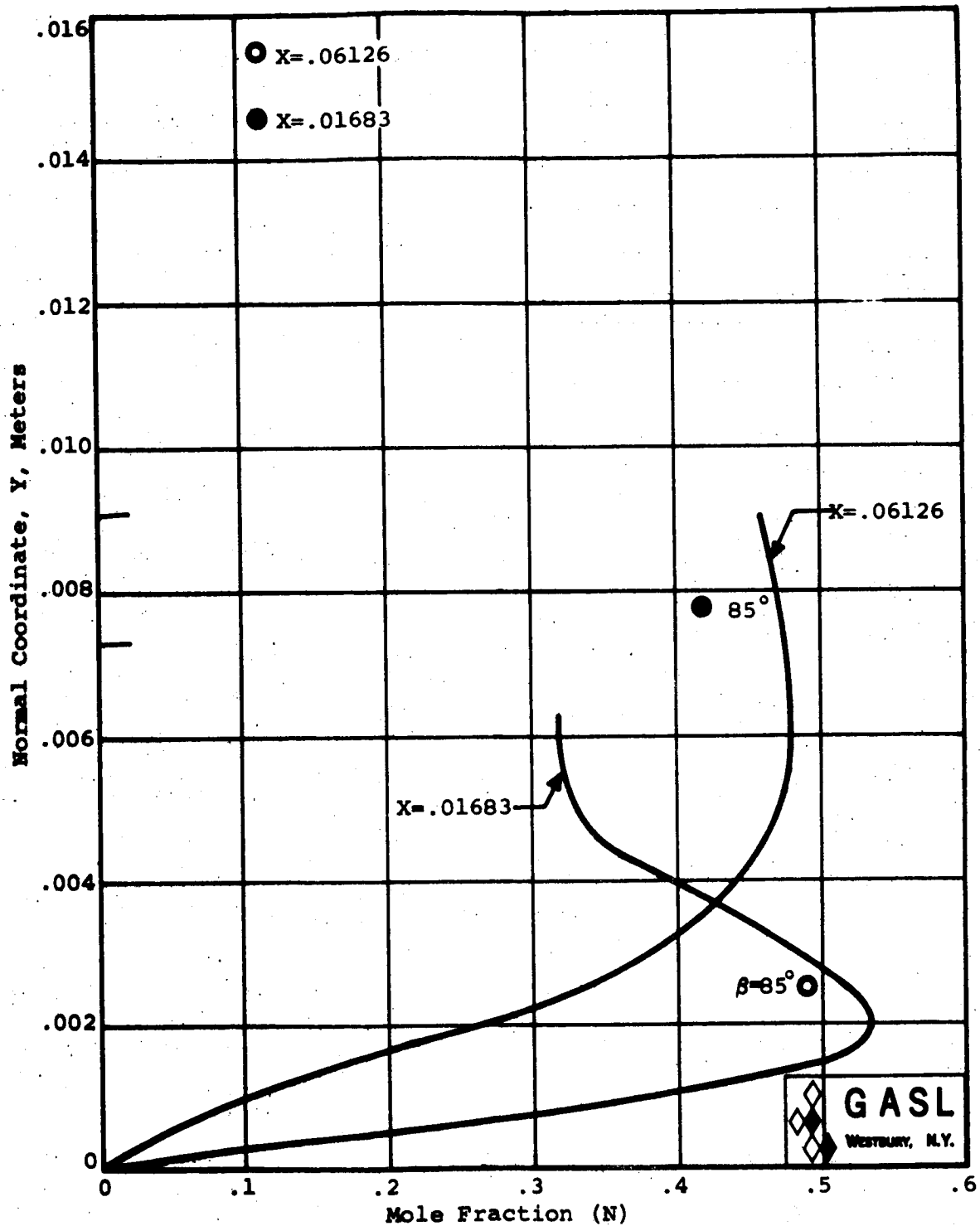
FIG. 97. SPECIE PROFILES (N) AT SURFACE COORDINATE
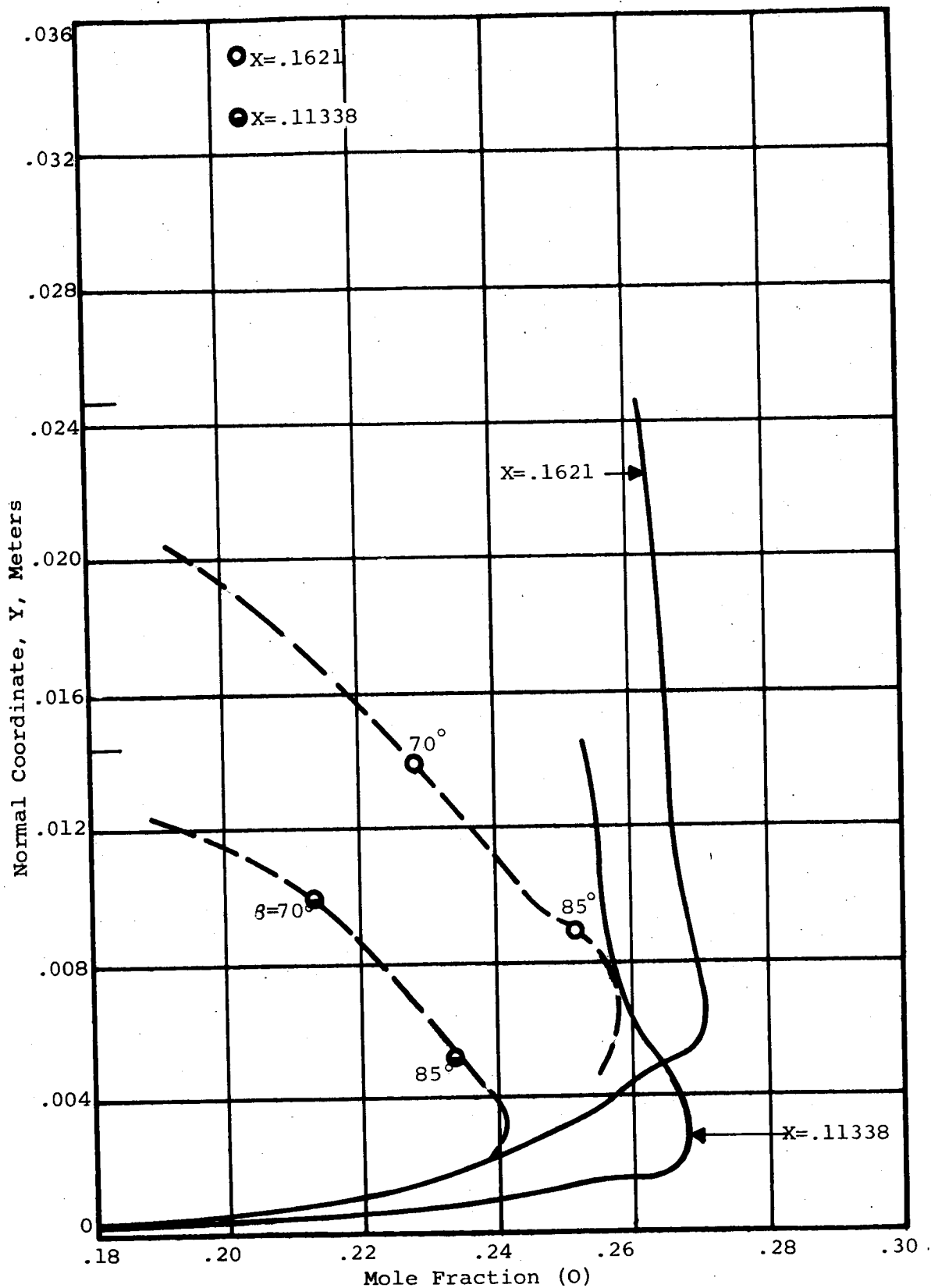X=.06126 AND X=.01683 METERS,
ALTITUDE = 71,000 METERS

FIG. 98. SPECIE PROFILES (N) AT SURFACE COORDINATE
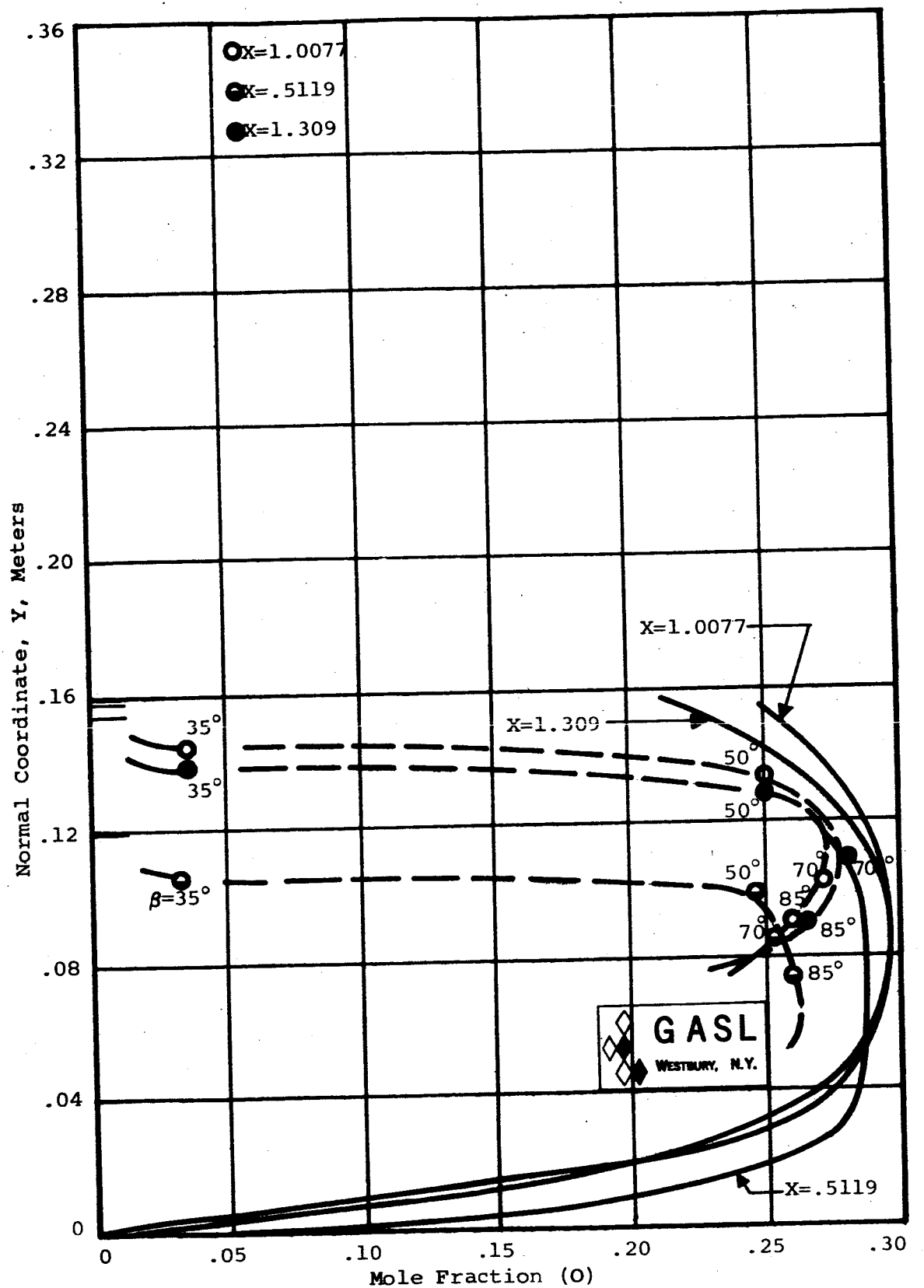LOCATION X=.1621 AND X=.11338 METERS,
ALTITUDE = 71,000 METERS

131

FIG. 99. SPECIE PROFILES (N) AT SURFACE COORDINATE LOCATION X=.5119, X=1.0077, AND X=1.309 METERS, ALTITUDE = 71,000 METERS

FIG. 100. SPECIE PROFILE (O) AT SURFACE COORDINATE
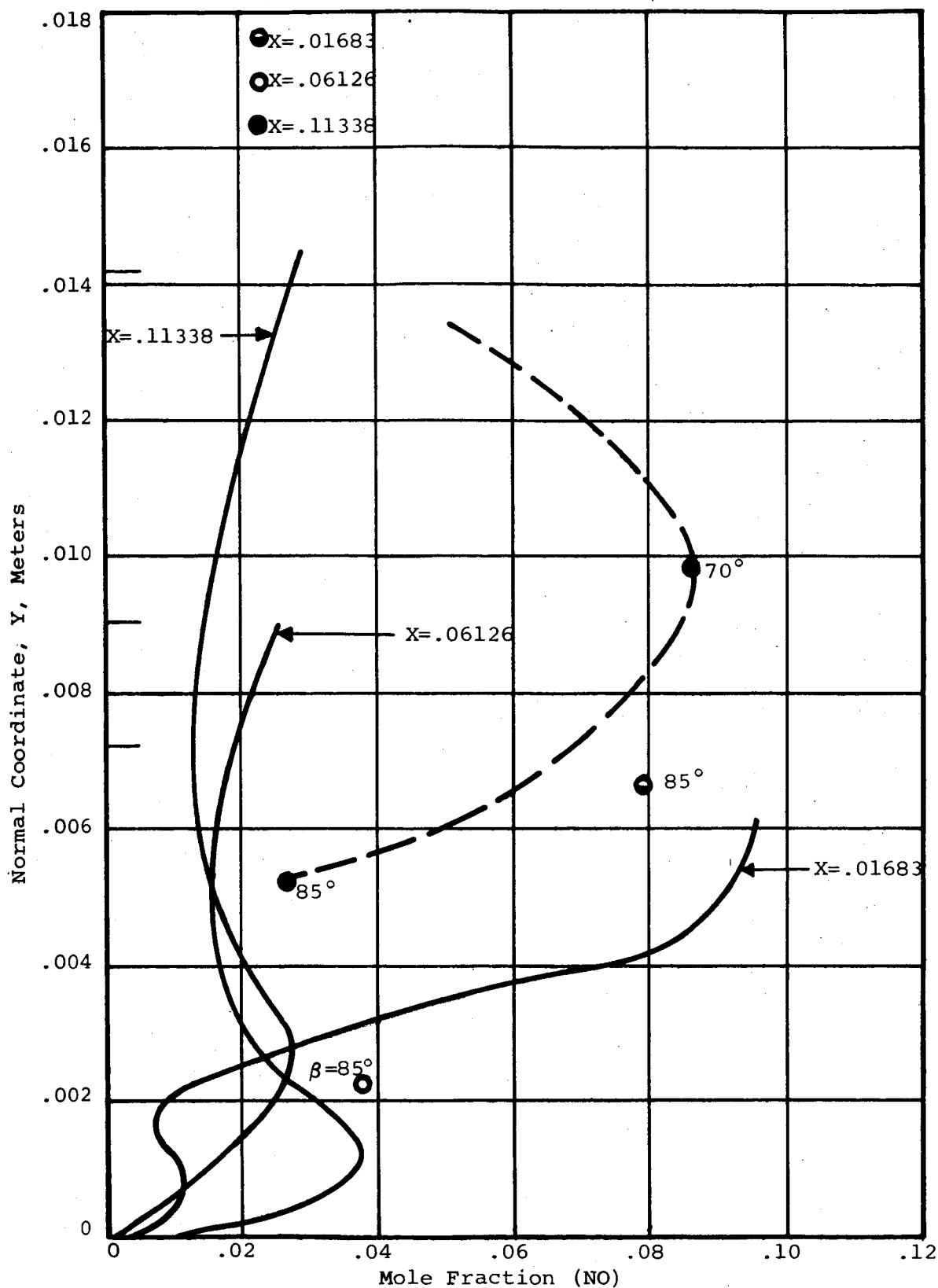LOCATION X=.06126 AND X=.01683 METERS,
ALTITUDE = 71,000 METERS

133

FIG. 101.   SPECIE PROFILES (O) AT SURFACE COORDINATE
LOCATION X=.1621 AND X=.11338 METERS,
ALTITUDE = 71,000 METERS

FIG. 102. SPECIE PROFILES (O) AT SURFACE
COORDINATE LOCATION X=1.0077, X=.5119,
AND X=1.309 METERS, ALTITUDE = 71,000
METERS

135

FIG. 103. SPECIE PROFILES (NO) AT SURFACE COORDINATE
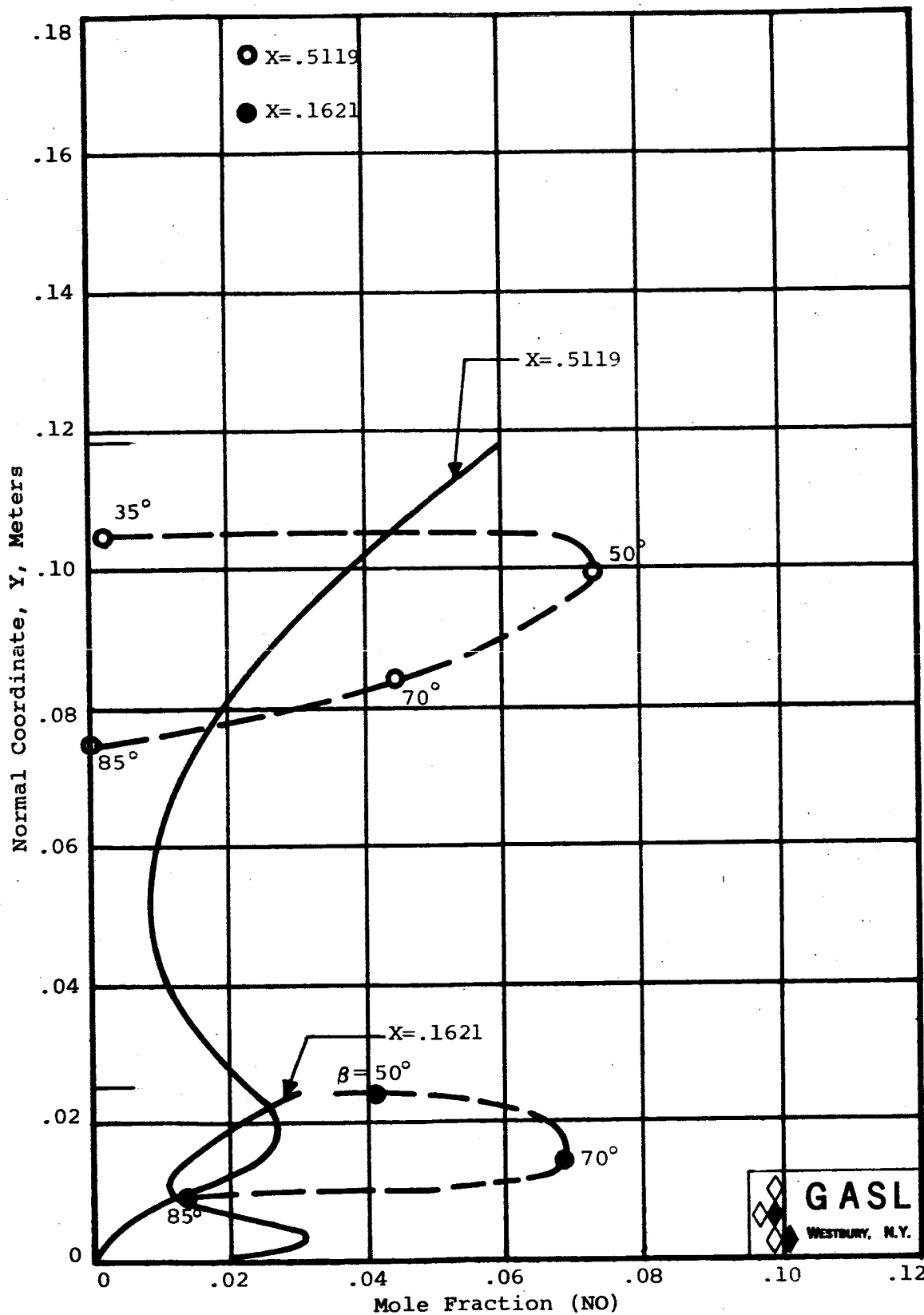LOCATION X=.01683, X=.06126, AND X=.11338
METERS, ALTITUDE = 71,000 METERS

136

FIG. 104. SPECIE PROFILES (NO) AT SURFACE COORDINATE
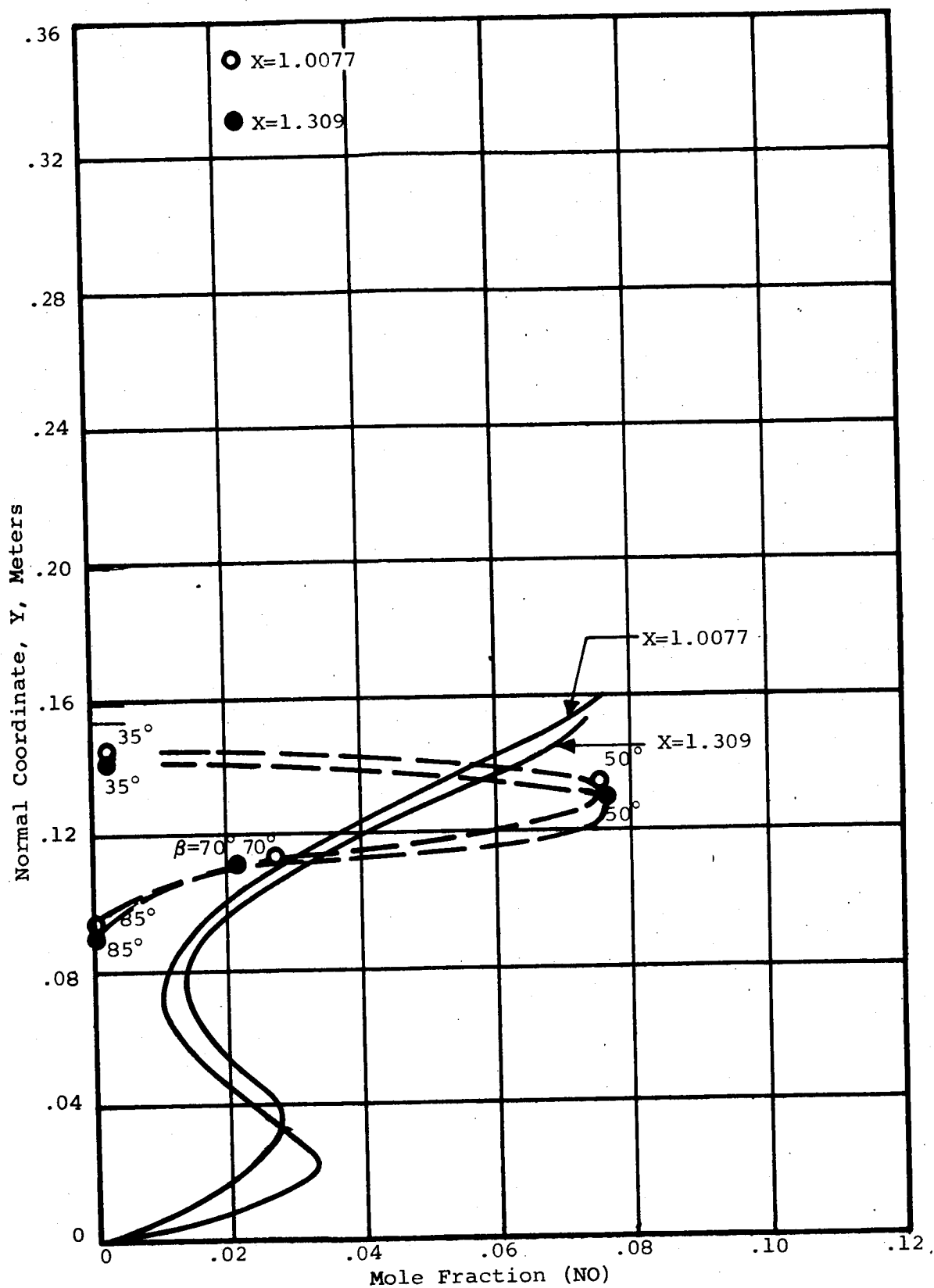LOCATIONS X=.5119 AND X=.1621 METERS,
ALTITUDE = 71,000 METERS

137

FIG. 105. SPECIE PROFILES (NO) AT SURFACE
COORDINATE LOCATION X=1.0077 AND
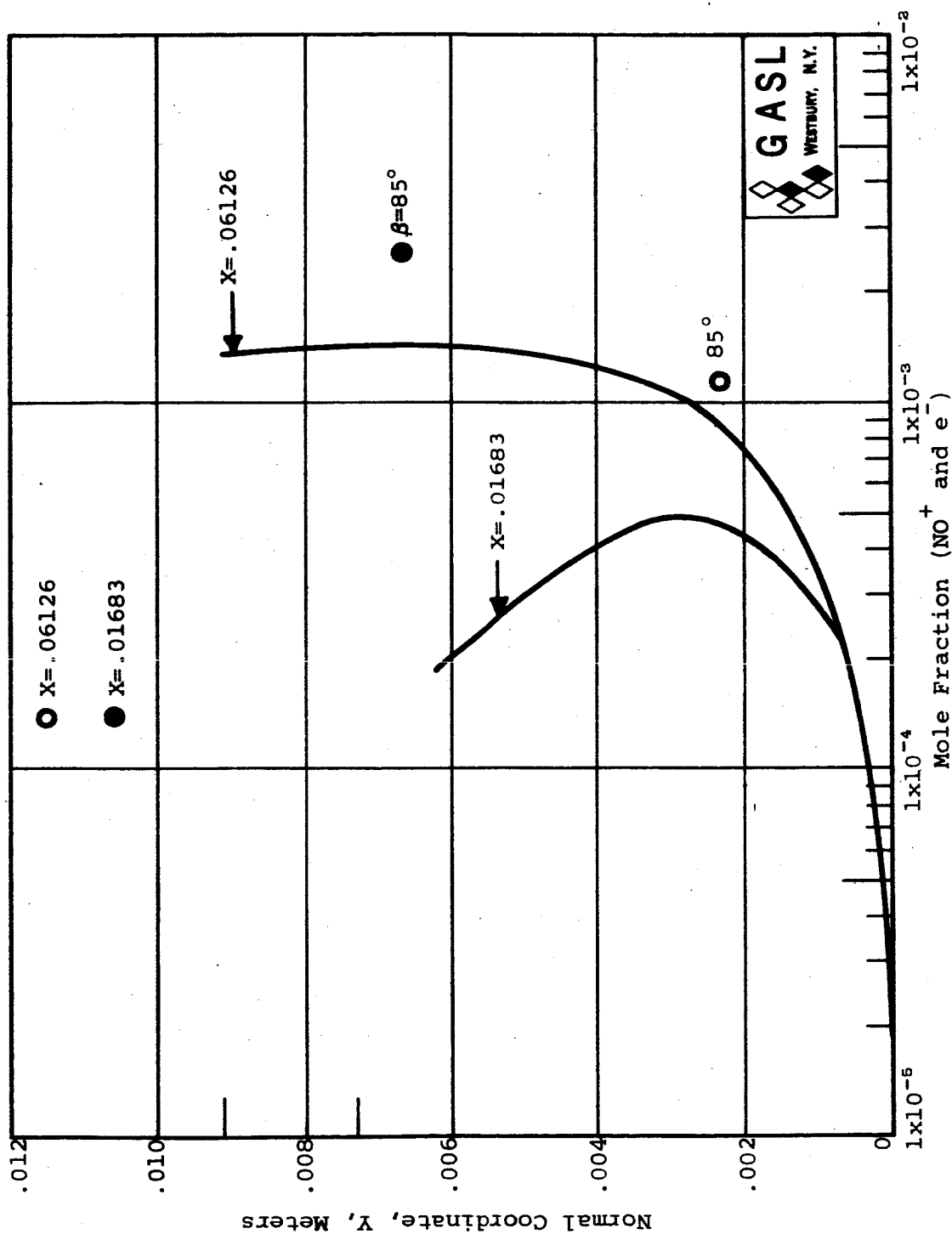X=1.309 METERS, ALTITUDE = 71,000
METERS

FIG. 106. SPECIE PROFILES (NO$^+$ AND e$^-$) AT SURFACE COORDINATE
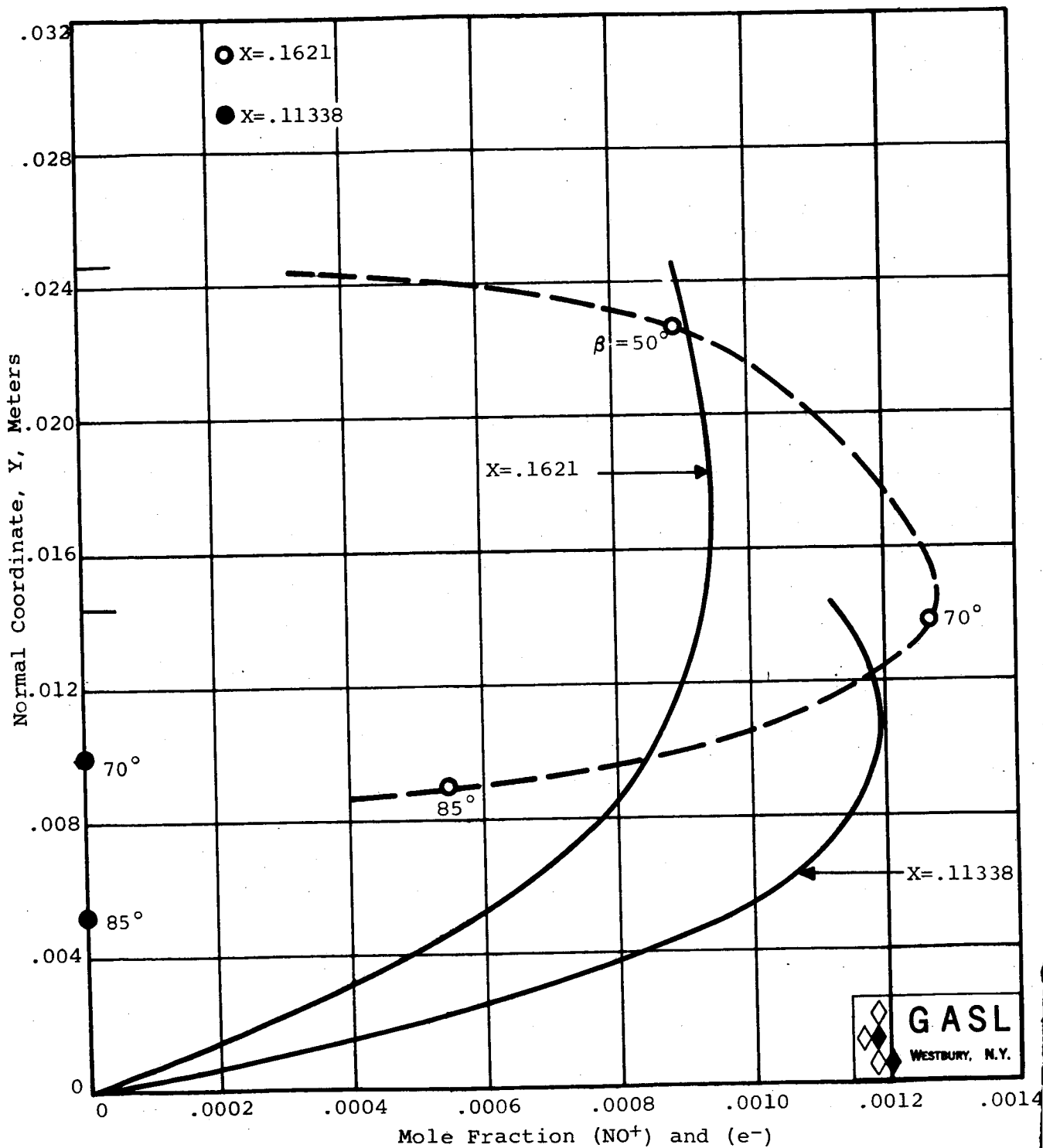LOCATIONS X=.06126 AND X=.01683 METERS,
ALTITUDE = 71,000 METERS

FIG. 107. SPECIE PROFILES (NO$^+$) AND (e$^-$) AT SURFACE
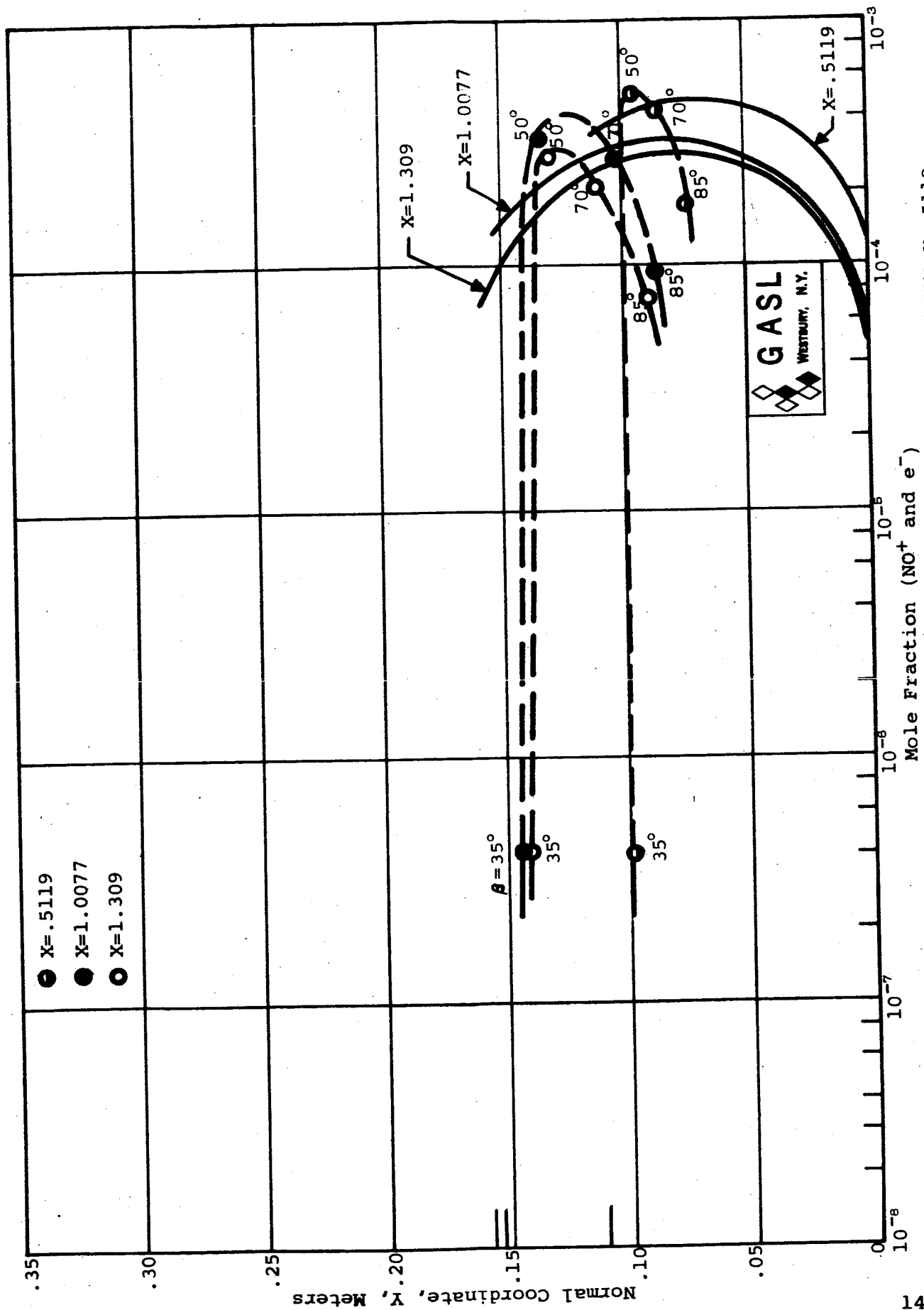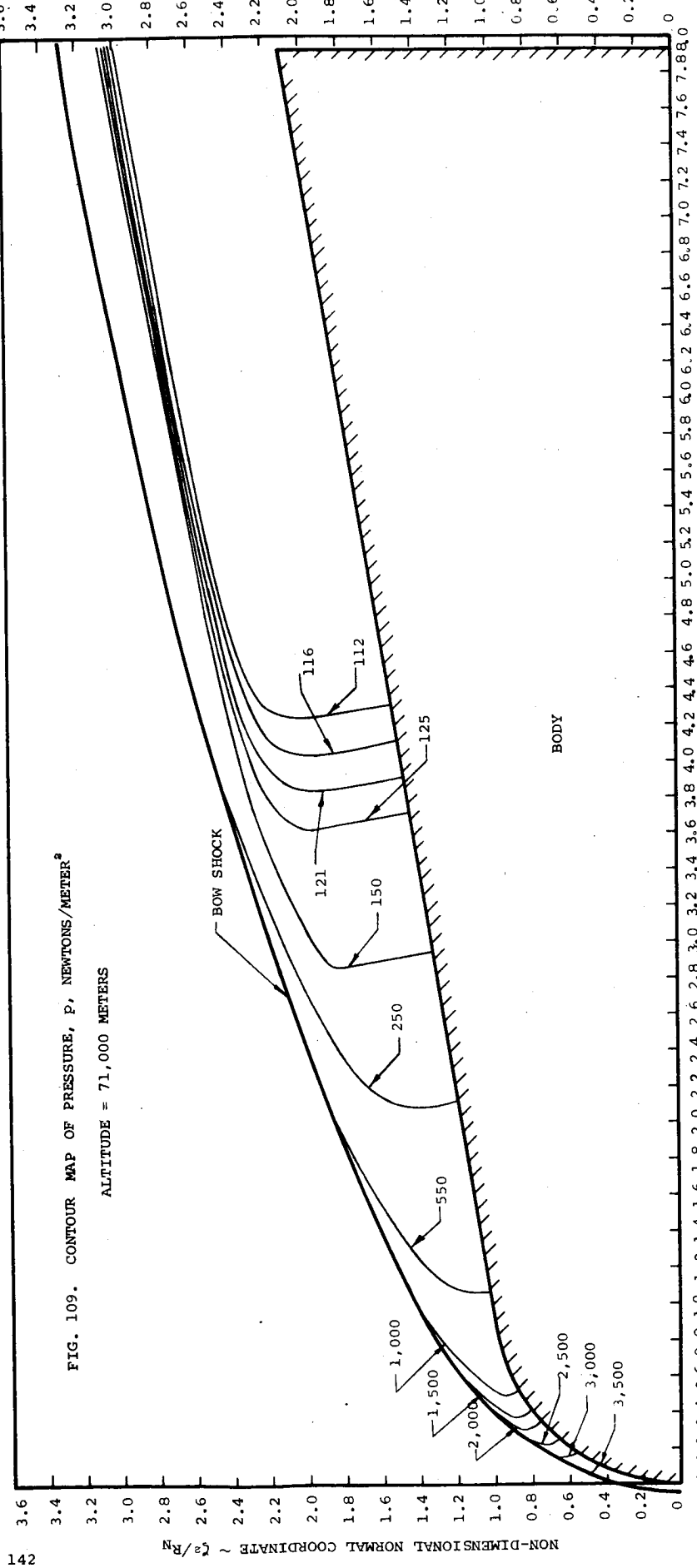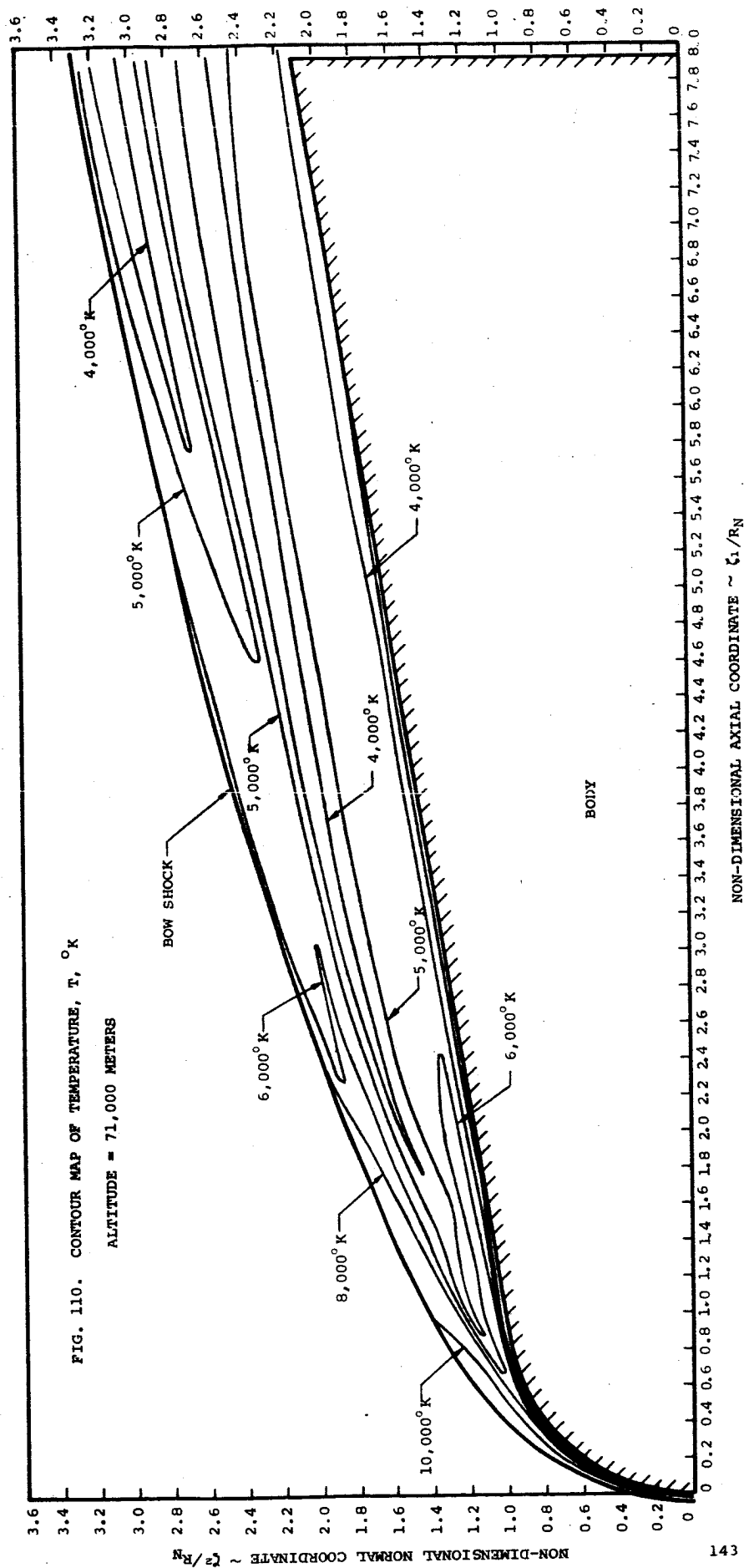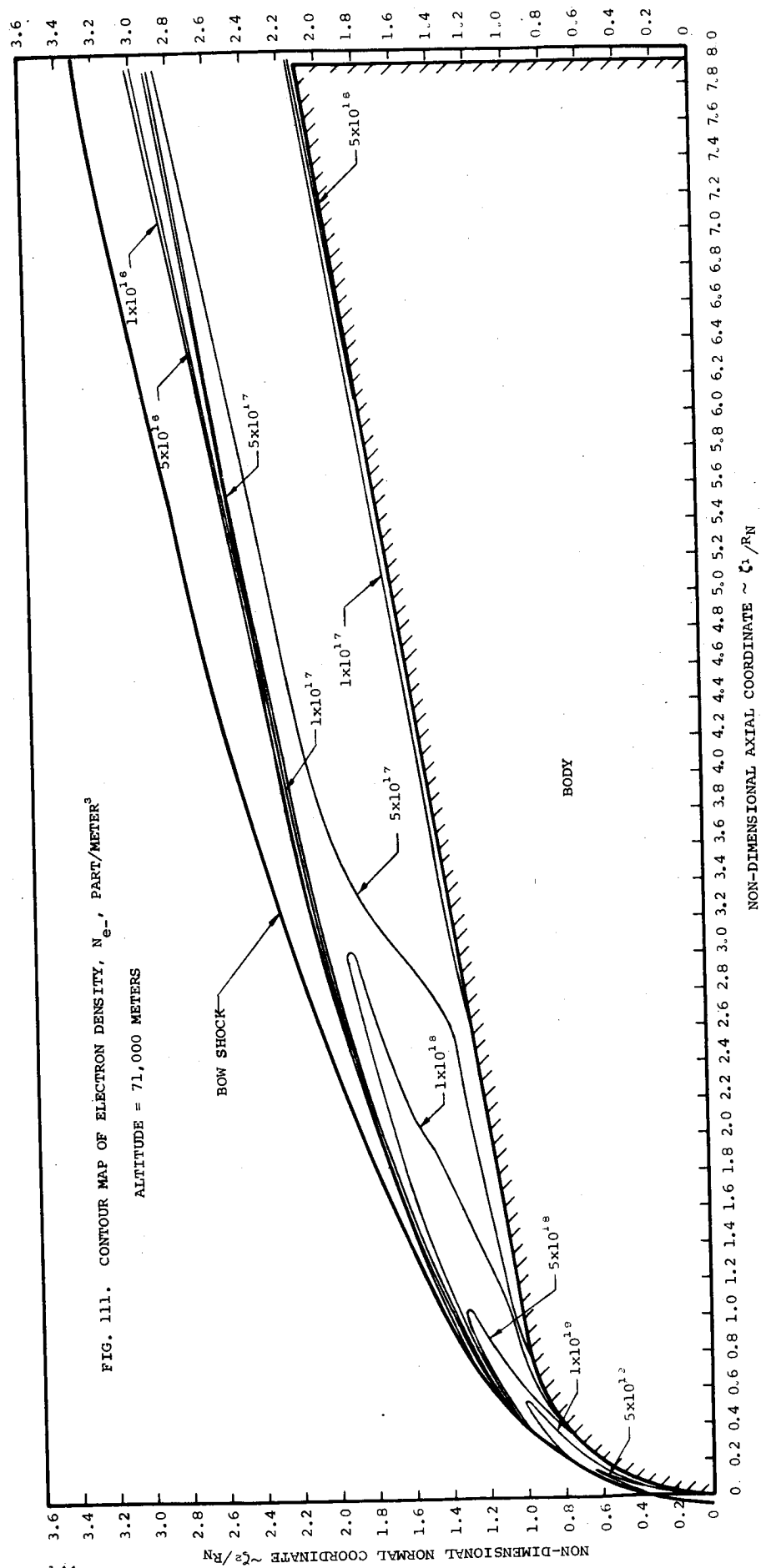COORDINATE LOCATION X=.1621 AND X=.11338
METERS, ALTITUDE = 71,000 METERS

FIG. 108. SPECIE PROFILES (NO+ AND e−) AT SURFACE COORDINATE LOCATIONS X=.5119,
X=1.0077, AND X=1.309 METERS, ALTITUDE = 71,000 METERS

141

FIG. 109. CONTOUR MAP OF PRESSURE, p, NEWTONS/METER^2

ALTITUDE = 71,000 METERS

142

FIG. 110.   CONTOUR MAP OF TEMPERATURE, T, °K

ALTITUDE = 71,000 METERS

NON-DIMENSIONAL AXIAL COORDINATE ~ ζ_1/R_N

NON-DIMENSIONAL NORMAL COORDINATE ~ ζ_2/R_N

143

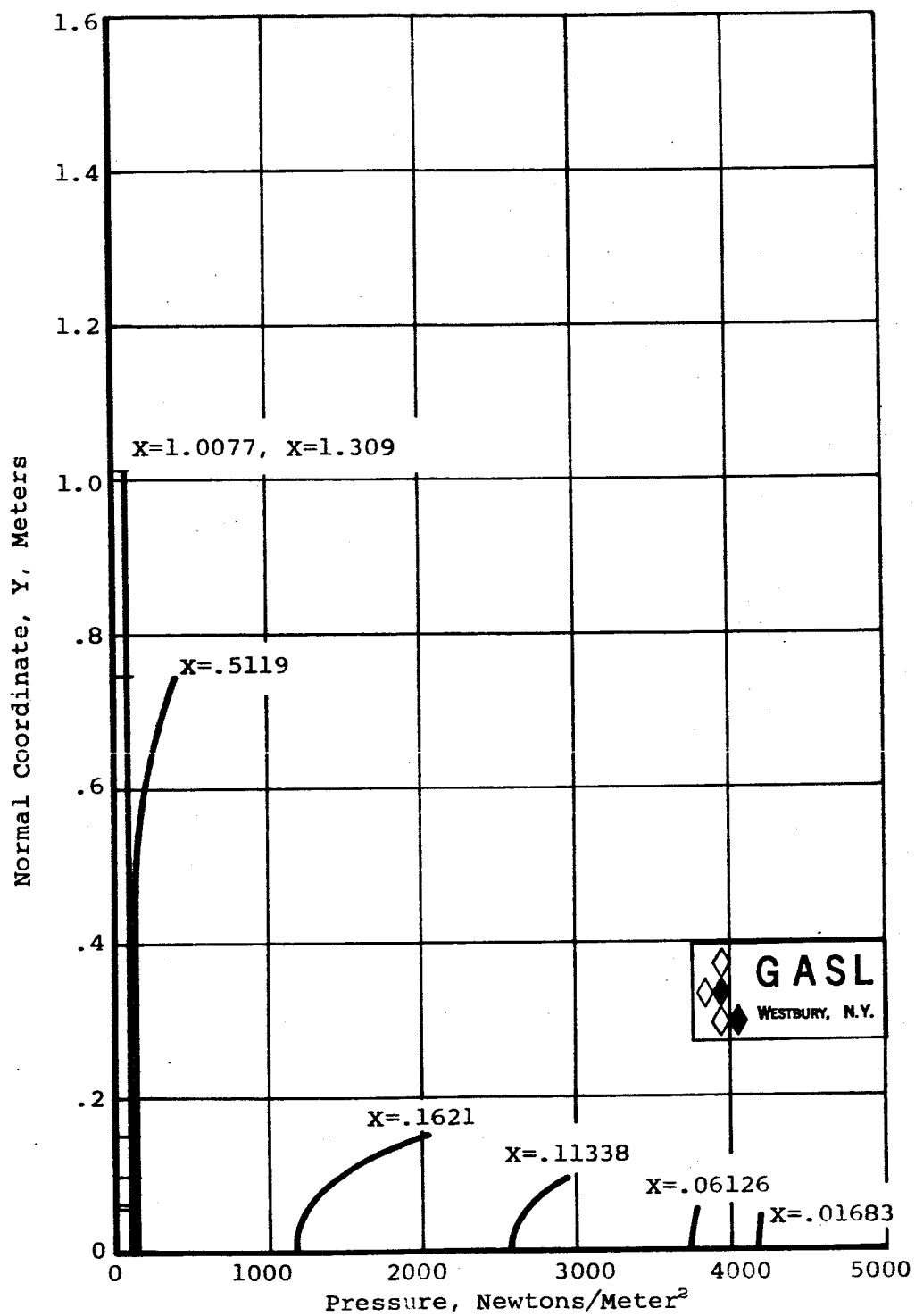FIG. 111.   CONTOUR MAP OF ELECTRON DENSITY, N_{e^-}, PART/METER^3

ALTITUDE = 71,000 METERS

FIG. 112. PRESSURE PROFILES AT SURFACE COORDINATE
LOCATIONS X=.01683, X=.06126, X=.11338,
X=.1621, X=.5119, X=1.0077, AND X=1.309
METERS, ALTITUDE = 71,000 METERS

145